"STUDIES OF THE DEFECTS IN CAESIUM IODIDE"

Thesis

Submitted for the Degree of

DOCTOR OF PHILOSOPHY

of the

University of Glasgow

by

Brian D. McNicol B.Sc.

September 1966.

ProQuest LLC.
789 East Eisenhower Parkway
P.O. Box 1346
Ann Arbor, MI 48106 – 1346

ACKNOWLEDGEMENTS.

I would like to thank my supervisor, Dr. I.M. Hoodless, for suggesting the research problem and for his untiring help and advice during the last three years.

My thanks are also due to Messrs. Connolly, Pitt and Leon for construction of glassware and to Messrs. MacQuarrie and Ritchie for technical assistance.

I wish to acknowledge a maintenance grant from the Science Research Council.

Finally I would like to thank my wife, Janet, for typing the manuscript and for her encouragement during the three years of research.

Brian D. McNicol.

ABSTRACT.

The ionic conductivity and Cs^+ self-diffusion have been measured in "pure", melt-grown and solution-grown single crystals of CsI over the temperature range 150-600°C. Conductivity measurements have been made on aliovalent cation and anion doped single crystals, both melt-grown and solution-grown. The Cs^+ self-diffusion has also been measured in aliovalent cation doped crystals.

The Cs^+ self-diffusion in both solution and melt-grown "pure" CsI crystals showed one diffusion region extending over the temperature range 250-500°C. This diffusion can be represented by;

$$D_{(cm^2 sec^{-1})} = 2.25 \times 10^2 \exp.(-1.74 eV/kT).$$

and this has been interpreted as due to movement of the Cs^+ ion via intrinsic defects.

Conductivity studies on "pure" crystals showed two temperature ranges. A low temperature region (< 300°C) was not reproducible and depended on the history of the specimen studied. Above 300°C the conductivity was reproducible and was associated with an intrinsic property of the crystal and this conductivity may be represented by

$$\sigma_{(ohm^{-1} cm^{-1})} = 8.48 \times 10^4 \exp.(-1.37 eV/kT)$$ for melt-grown crystals

and $$\sigma_{(ohm^{-1} cm^{-1})} = 6.04 \times 10^4 \exp.(-1.37 eV/kT)$$ for solution-grown crystals.

A comparison of the intrinsic conductivity and total diffusion using the Nernst-Einstein relationship was made and the results indicated that the conductivity was ionic with Schottky defects predominating.

Conductivity measurements on aliovalent cation impurity-doped crystals over the temperature range 150-600°C showed essentially the same features as "pure" crystals. There was no appreciable variation in the low temperature range with impurity content and the high temperature range was the same as in "pure" crystals. The impurity seemed to be relatively insoluble in the CsI lattice.

High temperature annealing under vacuum produced an increase in conductivity in "pure" crystals both in the intrinsic and low temperature regions. This increase in the intrinsic range did not seem to be due to a change in the defect nature of the crystal since there was no apparent change in activation energy. The change in the magnitude of σ is believed to be due to a surface area change brought about by the annealing under vacuum.

Vacuum annealing produced marked changes in the ionic conductivity of aliovalent cation doped crystals. The low temperature conductivity was increased and in some cases was prefaced by a region of very low activation energy. This range is interpreted in terms of contributions from ionic and electronic conductivity. A sharp change in the slope of the conductivity/reciprocal temperature curve occurred above the low temperature range and a region of conductivity which was reproducible from sample to sample was observed. This range which had a higher magnitude of conductivity than the intrinsic range is interpreted in terms of cation impurity dissolution in the crystal lattice, the "average" enthalpy of solution being 1.34 ± 0.22eV.

Immediately following the "solubility" range the conductivity/reciprocal temperature curve shows a decrease in activation energy and in this region the conductivity was impurity dependent. This region is believed to be associated with the movement of free cation vacancies created by the dissolved aliovalent impurity. On this assumption U_+, the activation energy for mobility of a cation vacancy is approximately 0.90eV. Diffusion regions corresponding to "solubility" and impurity vacancy movement have been observed in Cs^+ self-diffusion in aliovalent cation-doped melt-grown crystals.

If Schottky defects predominate in this system then from the value of U_+ and the Cs^+ diffusion activation energy the heat of formation W has been estimated at 1.70eV and this is compared with theoretical estimates.

Conductivity measurements have also been made on divalent anion doped CsI crystals between 150-600°C and the results indicated the apparent insolubility of this impurity even after quenching from high temperatures to liquid N_2 temperature, or after high temperature annealing. Possible reasons for the relatively easier solubility of aliovalent cations over anions have been given in terms of polarisation effects.

CONTENTS.

CHAPTER 1.

INTRODUCTION.

1.1 GENERAL INTRODUCTION.

The most stable state of a crystal at the absolute zero of temperature is one in which there is complete order. At temperatures above the absolute zero the crystal structure still approaches closely a regular lattice, but deviations from this complete order are possible. It is the presence of these defects i.e. disorder, and their ability to migrate which accounts for many of the physical and chemical properties of solids.

Defects in pure crystals can be considered to be of three main types:

1. Thermal vibrations.
2. Point or lattice defects.
3. Surface and line defects.

The most fundamental defect is associated with the quantum excitation of vibrational modes within a real crystal. The forces holding atoms in position in a crystal are not strong enough to produce a rigid lattice: the thermal energy of the atoms is sufficient to cause them to be displaced from equilibrium. On the assumption that the neighbours to a given atom are fixed, the frequency of vibration can be calculated. This is not however valid, for, in a real crystal, the neighbouring atoms will also be in motion. Moreover there will be interaction between different vibrational planes which produces appreciable anharmonic components. Thus when all possible motions of atoms or groups of atoms are considered, a range of frequencies is found to exist. Each separate mechanical oscillation at a given frequency is known as a phonon. The displacement of an atom in a solid is calculated by summing over all the phonons. These thermal vibrations of atoms in a solid, though important in themselves, do not seriously disturb the perfection of the crystal since on the average the atom or ion is in its

proper position. However the other types of lattice defect involve the presence of physical lattice imperfections.

Point defects are associated with disorder involving isolated lattice positions. They may exist as vacancies in the lattice, i.e. lattice sites where atoms or ions are missing, or alternatively atoms or ions may be displaced from their normal lattice positions to interstitial positions. The introduction of these point defects greatly increases the entropy of the crystal and at high enough temperatures this compensates to a large extent for the energy of formation of the defect.

Surface and line defects, on the other hand, are imperfections which involve the misalignment of relatively large numbers of atoms or ions. Surface defects are of two types, external and internal. The external type is simply the disorder represented by the discontinuity at the surface while the internal type occurs when the crystal lattice changes from one orientation to another i.e. misorientation of two adjacent crystal grains. The volume around the junction of the two grains is associated with a high degree of disorder. The line defects, as their name implies, have an appreciable extension in one dimension. It is this latter type of defect, generally referred to as a dislocation, which is particularly important in determining the mechanical properties of the solid.

A more detailed discussion of these defects, with special reference to ionic crystals, is given in the following sections.

1.2. POINT DEFECTS IN IONIC CRYSTALS.

In 1926 Frenkel[1] proposed that as a result of thermal vibrations some ions receive sufficient energy to move from their lattice positions to interstitial positions, thereby creating lattice vacancies, Fig.1. Under further thermal excitation the interstitial ion can move from one interstitial position to another until it eventually meets a vacancy and

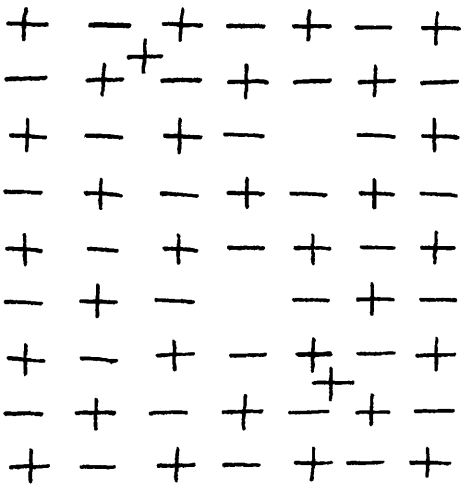

FIG. 1. FRENKEL DEFECTS.

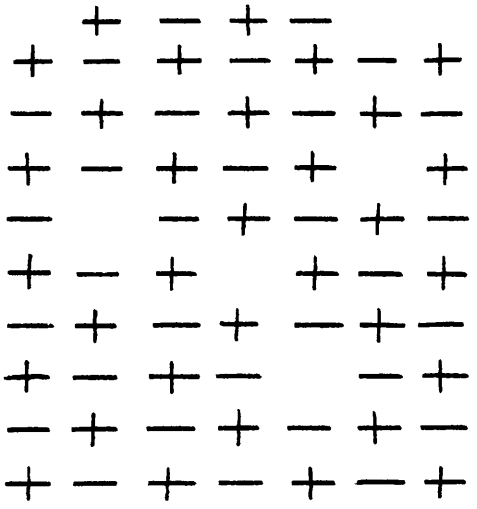

FIG. 2. SCHOTTKY DEFECTS.

drops back into a normal lattice position. Frenkel disorder is generally associated with the cation lattice since, on the grounds of ionic size, formation of an interstitial anion would be energetically unlikely.

Another method for the formation of lattice vacancies was suggested by Schottky[2]. He proposed that equal numbers of anions and cations could be removed from their lattice positions to form additional ionic layers at internal or external surfaces. The process would create equal numbers of anion and cation vacancies in the lattice, Fig.2. It is also possible that equal numbers of anion and cation vacancies could be formed by the presence of equal numbers of interstitial anions and cations. However this has not been found in ionic crystals since, for the reasons discussed above, the formation of interstitial anions is unlikely.

The presence of point defects increases the configurational entropy of the crystal to a large extent; therefore, although their formation requires a considerable amount of energy, at elevated temperatures the free energy of the crystal may be reduced. The concentration of point defects as a function of temperature can readily be calculated from normal thermodynamic considerations. For example, consider a crystal containing N anions and cations and suppose there are n Schottky defects, i.e. n cation vacancies and n anion vacancies, present at a particular temperature T. The presence of these Schottky defects increases the crystal's entropy, according to the Boltzmann relationship, by an amount,

$$\Delta S = k.\ln \left[\frac{N!}{(N-n)!\, n!} \right]^2 \qquad \text{----------(1)}$$

The increase in internal energy is nW, where W is the energy to form a Schottky defect, and the change in free energy is given by

$$\Delta F = nW - T\Delta S \qquad \text{----------(2)}$$

and from (1)

$$\Delta F = nW - kT.\ln\left[\frac{N!}{(N-n)!n!}\right]^2 \qquad \text{---------- (2a)}$$

Minimising ΔF with respect to n and by applying Stirling's approximation, equation (2a) becomes,

$$\left(\frac{\partial(\Delta F)}{\partial n}\right)_T = W - kT.\ln\left[\frac{N-n}{n}\right]^2 = 0 \qquad \text{---------- (3)}$$

$$\left(\frac{N-n}{n}\right)^2 = \exp.\left(\frac{W}{kT}\right) \qquad \text{---------- (4)}$$

Since the extent of Schottky disorder is usually small, i.e. $N-n \approx N$, equation (4) reduces to

$$\left(\frac{n}{N}\right)^2 = \exp.\left(-\frac{W}{kT}\right) \qquad \text{---------- (5)}$$

$$\text{or } n = N \exp.\left(-\frac{W}{2kT}\right) \qquad \text{---------- (6)}$$

A similar type of derivation for Frenkel disorder gives,

$$n = (NN_i)^{\frac{1}{2}} \exp.\left(-\frac{W}{2kT}\right) \qquad \text{---------- (7)}$$

where N_i is the total number of interstitial positions per unit volume.

The derivation is simplified since it has not taken into account thermal expansion of the crystal or changes in vibrational frequency of the ions due to the presence of the defects. As the temperature rises thermal expansion leads to a decrease in W and this can be written:

$$W_T = W_o + \alpha V_o T\,(dW/dV) \qquad \text{---------- (8)}$$

where W_o and V_o are respectively the energy to form the defects and the volume of the crystal at 0^oK and α is the crystal thermal expansion coefficient.

The correction for differing vibrational frequencies introduces a pre-exponential factor, γ, which is given by,

$$\gamma = \left(\frac{v}{v'}\right)^{\chi} \qquad \text{---------- (9)}$$

where v is the normal lattice frequency at the particular temperature, v' is the frequency of an ion adjacent to a defect and χ is the number of nearest neighbour ions around

the defect.

The modified equation for the concentration of Schottky defects is then,

$$n = \gamma BN \exp.\left(-\frac{W}{2kT}\right) \qquad \text{---------- (10)}$$

where $B = \exp.\left(-\alpha\frac{V_o}{2k} \cdot \frac{dW}{dV}\right)$

In ionic crystals the pre-exponential factor, γ, can lie between 10 and 10^4 for Schottky defects but is several orders of magnitude smaller for Frenkel defects[3].

It should be noted that under constant temperature conditions equation (10) can be represented by,

$$x_1 x_2 = \text{constant} = x_o^2 \qquad \text{---------- (11)}$$

where x_1 and x_2 are the mole fractions $\frac{n}{N}$ of cation and anion vacancies, which, in a pure crystal will be identical and equal to x_o.

1.3. CALCULATION OF POINT DEFECT FORMATION ENERGIES.

Although both Frenkel and Schottky defects will be present in any ionic crystal, their energies of formation (W) are usually sufficiently different in any particular crystal for one type of defect to predominate. Calculations of defect formation energies are very detailed and in this section the problem will be discussed qualitatively.

The calculation is based on the classical Born[4] theory of ionic crystals, and in this approach the lattice energy of an ionic crystal is given by,

$$W_L = \frac{Ae^2}{a_o}\left(1 - \frac{1}{n}\right) \qquad \text{---------- (12)}$$

where W_L is the lattice energy

A is the Madelung constant

e is the electronic charge

a_o is the interionic distance

n is the Born exponent.

Since these calculations have been mostly applied to the alkali halides no account is taken of Van der Waal's and

and zero point energies.

Let us consider the energy involved in the formation of a positive ion vacancy, W_+. If the positive ion was removed from the interior of the crystal to infinity, while the charge distribution in the crystal is kept the same as it was, then the energy involved in this step would be W_L, the lattice energy. However the ion is only transferred to a surface of the crystal (for a Schottky defect) so that in bringing the ion back from infinity to the crystal surface a gain in energy of $\frac{1}{2} W_L$ would result. Therefore the overall energy involved in the formation of the positive ion vacancy would be $\frac{1}{2} W_L$ and the energy required for the formation of the Schottky defect would be W_L. In the alkali halides the lattice energy varies between 6 and 11eV approximately and so the formation of these defects would be energetically unfeasible except at very high temperatures i.e. near the melting point.

However Jost[5] was the first to point out the importance of the polarisation of the lattice which results from the formation of a vacancy or interstitial. The removal of a positive ion, for example, will affect the neighbouring ions in such a way that an adjustment takes place by which energy is gained. The removal of the positive ion will have the net effect of adding an extra negative charge at the lattice site. Consequently the surrounding material will become polarised. The polarisation consists in the formation of dipoles induced in the ions by the Coulombic field of the missing ion and secondly in a small ionic displacement of the surrounding ions, Fig.3. Because of the long range of Coulombic forces, the polarisation effects will be spread over large distances in the crystal and hence the calculation of the polarisation energy is complicated. Jost [5] simplified the calculation by assuming that the vacant lattice site could be treated as a spherical cavity (radius R) in a continuous medium of dielectric constant ϵ. The gain

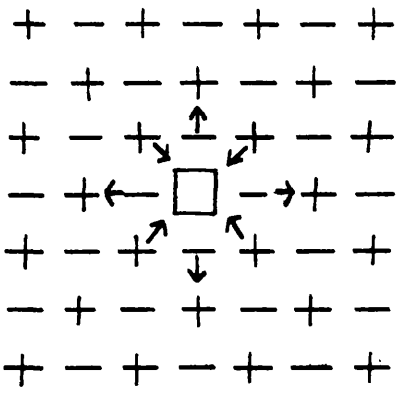

FIG. 3. POLARISATION OF SURROUNDINGS CAUSED BY A VACANCY.

in energy from polarisation is then given by

$$P = \frac{e^2}{2R}\left(1 - \frac{1}{\epsilon}\right) \qquad \text{---------- (13)}$$

Hence the energy of formation of a Schottky defect is given by,

$$W = W_L - P_+ - P_- \qquad \text{---------- (14)}$$

The difficulty in this particular calculation is in assigning values of R_+ and R_-, the radii of positive ion and negative ion vacancies. As a result of more accurate calculations[6] it has been suggested that for the alkali halides,

$$R_+ = 0.6a_o, \quad R_- = 0.9a_o \qquad \text{---------- (15)}$$

It is possible from the above treatment to indicate the crystal conditions which favour particular types of point defects. An interstitial ion is generally much closer to its neighbours than a normal ion and since the repulsive interactions between ions varies as r^{-n} (n varies from 5 to 12), the repulsive forces will favour Schottky as opposed to Frenkel defects. However where there is an appreciable difference in size between cations and anions there will be more room for an interstitial cation and there will also be a large gain in polarisation energy from the incorporation of a small cation in an interstitial position. From equation (13) it is apparent that in a medium of high dielectric constant the gain in polarisation energy associated with Frenkel disorder can offset the increase in repulsion energy. It is for these reasons that Schottky defects predominate in the alkali halides while in AgCl and AgBr Frenkel defects are important.

The above simplified treatment of defect formation energies has been refined in several ways.[6,7,8,9,10] The continuum model for the calculation of polarisation energy is replaced by a more detailed model based on the actual ionic picture. The electronic dipole moment and the positional displacement

of the neighbouring ions are estimated and these values are used in the calculation of the polarisation energy. The repulsion energy term is also modified to take into account these ionic displacements and non-nearest neighbour interactions. The results of these calculations for the energy of formation of a Schottky defect in the alkali halides are in fairly good agreement with experimental determinations, Table 1.

Table 1

	W(eV) Calc.[6]	W(eV) Exp.
NaCl	1.86	2.02 [11] 2.09 [12]
KCl	2.08	2.4 [13] 2.1 [14]
KBr	1.92	1.99 [15]

A detailed review of these types of calculation is to be found in an article by Lidiard [16].

1.4. THE ROLE OF POINT DEFECTS IN IONIC MIGRATION.

The presence of point defects in an ionic lattice provides a route for ion movement. In a crystal exhibiting Schottky defects, the ions can move through the crystal via the vacancies, Fig.4a. In crystals exhibiting Frenkel defects two mechanisms for ion movement are possible; an interstitial ion can move from one interstitial position to another (Fig. 4b), or it may move through the crystal by pushing one of the neighbouring ions into an interstitial position and itself occupying the vacant lattice site, Fig.4c.

The most common experimental methods for the investigation of ion movement involve the use of tracer methods to measure diffusion, the random movement of ions through the crystal, and in the measurement of ionic conductivity, which is, in effect, diffusion under an applied electric field.

In a crystal containing Schottky defects the ionic

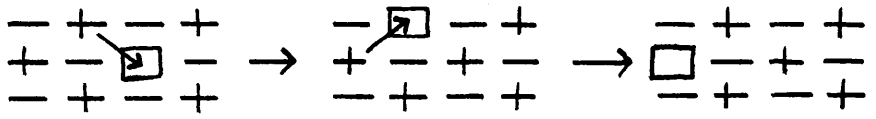

(a) VIA VACANCIES.

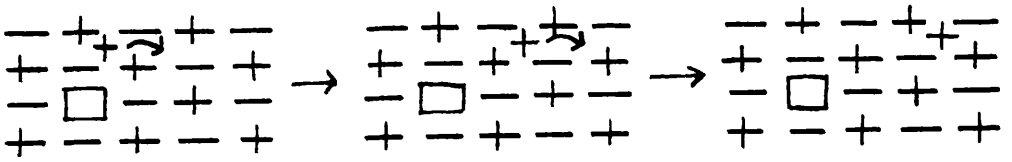

(b) VIA INTERSTITIAL POSITIONS.

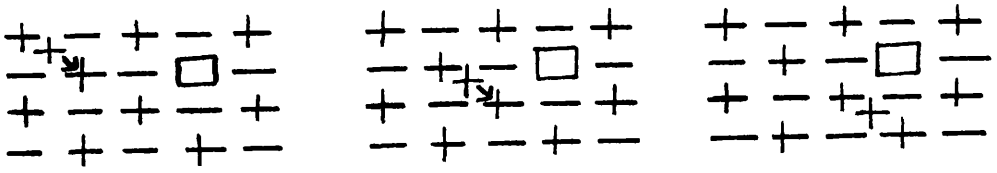

(c) VIA INTERSTITIAL POSITIONS
AND LATTICE SITES.

FIG. 4. MODES OF ION MIGRATION.

conductivity, σ, can be represented by

$$\sigma = n_1 q \mu_1 + n_2 q \mu_2 \qquad \text{---------- (16)}$$

where n_1 and n_2 are the number of charge carriers per cm^3 i.e. n_1 and n_2 are respectively the number of cation and anion vacancies per cm^3, q is charge on the ions and μ_1 and μ_2 are respectively the cation and anion mobilities, i.e. the rate of movement under unit field.

This relationship, equation (16), between the conductivity and the number of vacancies has led to ionic conductivity studies being widely used in studies of the defect nature of solids. Experimentally the total conductivity of the ionic crystal can be measured but it is frequently useful to determine the component contributions of the anion and cation. Transport number determinations[17] have shown that for a number of alkali halides, e.g. LiCl, NaCl and KCl, the conductivity is almost exclusively cationic except at temperatures near the melting point. In these cases equation (16) may be approximated by

$$\sigma = n_1 q \mu_1 \qquad \text{---------- (17)}$$

The equation may be expanded by introducing the expression for the mobility[18],

$$\mu = \left(\nu a^2 \frac{Cq}{kT}\right) \exp. \left(\frac{-U}{kT}\right) \qquad \text{---------- (18)}$$

where ν is the vibrational frequency of the ion,

a is the distance between the ions

and C is a thermal expansion correction to the height of the energy barrier for mobility (U).

Substitution of this expression of mobility and the expression for vacancy concentration (eqn. (10)) in equation (17) gives

$$\sigma = \left(\frac{\gamma_{BCN} \nu a^2 q^2}{kT}\right) \exp. \left(-\frac{(U + W/2)}{kT}\right) \qquad \text{---------- (19)}$$

The corresponding expression for the diffusion coefficient, D, is given by

$$D = \gamma BC\sqrt{a^2} \exp.\left(-\frac{(U + W/2)}{kT}\right) \qquad \text{---------- (20)}$$

It can be seen from equations (19) and (20) that if the same type of defect is responsible for both ionic conduction and diffusion, and this will generally be the case, then

$$\frac{\sigma}{D} = \frac{Nq^2}{kT} \qquad \text{---------- (21)}$$

The above equation is known as the Nernst-Einstein relationship.

In the systems under discussion e.g. LiCl, NaCl and KCl where the conductivity is essentially cationic, the self-diffusion coefficient D is that of the cation. However in systems where both anion and cation contribute to the conductivity, equation (16) can be expanded in the same way as we have shown for equation (17). The modified expressions for σ and D then contain the sum of two exponential terms. The Nernst-Einstein equation is still valid but now D represents the sum of the anion and cation self-diffusion.

Experimentally the self-diffusion coefficients are determined using radiotracer techniques since these tracer ions are distinguishable from the host ions of the crystal and furthermore since they are generally employed in small concentrations, statistical correlations between the directions of successive jumps of the tracer ion may occur. The Nernst-Einstein equation is modified to make allowance for these correlation effects.

$$\frac{\sigma f}{D_{tracer}} = \frac{Nq^2}{kT} \qquad \text{---------- (22)}$$

For vacancies in NaCl-type lattices f is 0.7815 while for CsCl-type lattices f is 0.6555[19].

1.5. THE ROLE OF LINE DEFECTS IN ION MIGRATION.

Line defects or dislocations are more complicated than point defects in that they are not confined to any one lattice point but are extensive in the crystal. Dislocations also

contrast with point defects in that they are fundamentally non-equilibrium states, although they may be formed under near equilibrium conditions. There are two extreme types of line defect, namely the screw dislocation and the edge dislocation.

The screw dislocation consists of a line of atoms (or ions) each of which has the correct number of atoms co-ordinating it but the co-ordination polyhedron is distorted. The dislocation may be thought of as being produced by displacing one part of the crystal, usually one atomic spacing, relative to the remainder of the crystal, the displacement terminating within the crystals, Fig.5. Atoms near the centre of the dislocation are in regions of high distortion and this distortion decreases the further they are away from the dislocation. The presence of the screw dislocation transforms successive atom planes into the surface of a helix and hence they are of extreme importance in the growth of crystals from the vapour or solution; the dislocation provides a "continuous" step for deposition of atoms.

The edge dislocation consists of a line of atoms, each of which has one less atom co-ordinating it than is required by the crystal structure. The dislocation is formed by the slip of one crystal section one atomic distance with respect to the other section of the crystal, Fig.6(a). Alternatively the dislocation may be regarded as being formed by the insertion of an extra plane of atoms part way into the crystal, Fig.6(b). The dislocation line, which is the internal boundary of this extra plane of atoms, need not be a straight line but can jump to an adjacent slip plane; the point at which the jump is made is called a "jog". In ionic crystals the structure of the edge dislocations are essentially governed by the condition of charge neutrality in the crystal. In particular the jogs in edge dislocations

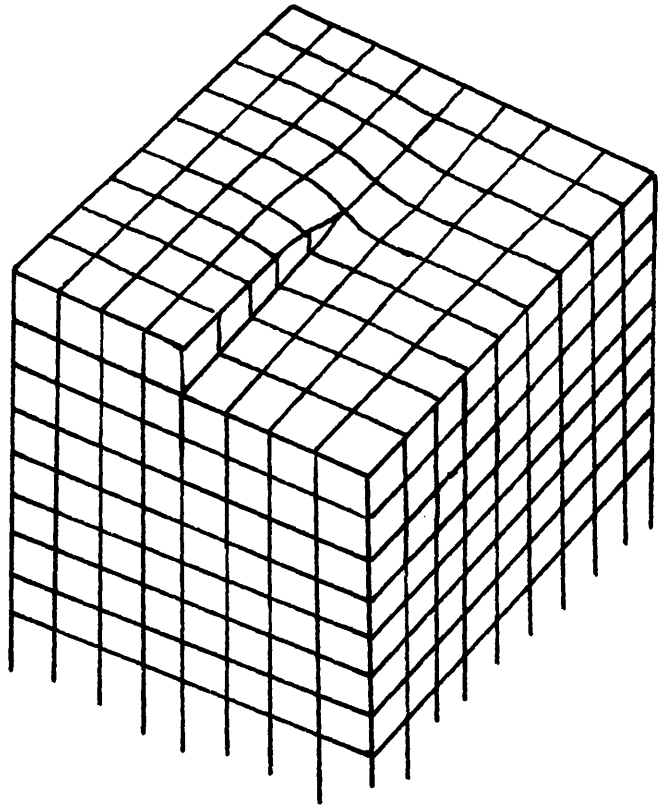

FIG. 5. THE SCREW DISLOCATION.

(a)

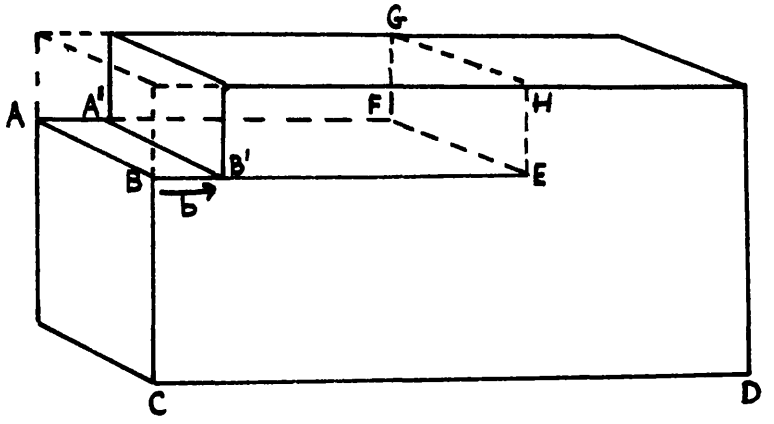

EF is edge dislocation line.

(b)

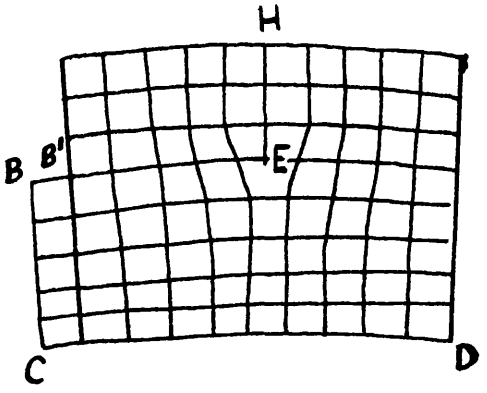

FIG. 6. THE EDGE DISLOCATION.

may be charged[20] and this determines to a large extent the properties of the dislocation.

The presence of dislocations in ionic crystals influences the ion mobility only to a very small extent since the moving ions, because of their large mass, are only slightly scattered when they meet a dislocation. However the dislocations can have a very important influence on the concentrations of point defects.

The edge dislocations can move in the crystal in two distinct ways. The first is movement in the slip plane and is a relatively easy process. The second type of movement involves the climbing of the dislocation from plane to plane and will generally only occur at elevated temperature. In metals the movement of dislocations generally increases the concentrations of vacancies or interstitial atoms[21]. In ionic crystals the charged nature of the dislocation jogs restricts the types of movement and to retain charge neutrality a moving dislocation produces Schottky defects i.e. equal numbers of anion and cation vacancies, in the crystal.

A stationary dislocation can also affect the local concentration of point defects in that they can act as a source or sink for point defects. Schottky or Frenkel defects can be formed at surfaces, grain boundaries and at dislocation jogs and since the energy of formation of the two oppositely charged components of such a defect pair are unequal, the thermal equilibrium concentrations will be unequal[22,23]. For example in NaCl the sodium ion vacancies are more easily formed than chlorine ion vacancies. Hence when the temperature is raised from absolute zero the sodium ion vacancies will be emitted into the crystal leaving a net positive charge on the surface. This resulting space charge discourages the emission of more sodium ion vacancies and encourages the emission of chlorine ion vacancies into the crystal. The net result is that there will be a space charge layer associated with each edge dislocation arising from the

excess of anion vacancies in the neighbourhood of the dislocation and these are balanced by an excess of cation vacancies penetrating some distance into the crystal. The magnitude and width of the space charge layer will depend on the temperature and on the difference in the formation energies of anion and cation vacancies. For NaCl the width of the space charge layer is estimated to be 2.2×10^{-5}cm at $600^{o}K$ and 1.3×10^{-6}cm at $900^{o}K$[22]. It is therefore to be expected that line defects could be of extreme significance in ionic migration, particularly at low temperatures.

1.6. EXPERIMENTAL INVESTIGATIONS OF ION MIGRATION IN ALKALI HALIDES OF THE SODIUM CHLORIDE-TYPE STRUCTURE.

Transport number measurements[17] have shown that the conduction in the lithium halides and sodium and potassium chlorides is exclusively ionic and that cation transport is the predominant contribution in conduction. Only at temperatures near the melting point is there a significant contribution from the chloride ion. The ionic conductivity as a function of temperature should be given by equation (19). A single range of conduction should be observed, the activation energy being U + W/2.

In practice two main ranges of conduction are observed. The high temperature range is an intrinsic property of the crystal. The conduction in this range is explicable in terms of the theory given in section 1.4; the conduction is due to thermally created Schottky defects. The low temperature range is not reproducible, the activation energy in this region is much lower and the magnitude of the conductivity is critically dependent on the history of the crystal specimen.

Three possible mechanisms have been suggested for the low temperature conductivity; (a) frozen-in defects[24] (b) surface and grain boundary conductivity[25] (c) effects of aliovalent impurity ions in the crystal lattice[26]. It is this latter effect which is of prime importance in the low temperature conduction.

Even the most "pure" crystals contain small quantities of impurity and these impurities can have significant effects if they are aliovalent, i.e. of different valency to the host lattice, and if they are substitutionally dissolved in the lattice. If, for example, the NaCl crystal contains some Cd^{2+} ions substitutionally incorporated in lattice positions then in order to retain electroneutrality one cation vacancy must be formed for each Cd^{2+} present in the lattice. These impurity created vacancies will be particularly important at low temperatures where the concentrations of thermally created Schottky defects will be low. Under these conditions the conductivity equation will no longer contain an exponential factor for the heat of formation of the defect and therefore the activation energy for conduction will be U.

The earlier treatment of conduction (section 1.4) can be modified to take into account impurity effects.

From equation (11)

$$\chi_1\chi_2 = \text{constant} = \chi_o^2$$

and suppose the concentration of divalent cation impurity is c. Then for electroneutrality

$$\chi_1 = \chi_2 + c \qquad \text{----------} \quad (23)$$

Equation (11) then becomes

$$\chi_1(\chi_1 - c) = \chi_o^2$$

$$\text{or} \quad \chi_1 = \frac{c}{2}\left\{1 + (1 + 4\chi_o^2/c^2)^{\frac{1}{2}}\right\} \qquad \text{----------} \quad (24)$$

This relationship shows the change from intrinsic conduction at high temperatures where $\chi_o \gg c$, to impurity controlled conduction at low temperatures where $\chi_o \ll c$. The validity of this approach has been shown by conductivity measurements on alkali halides which have been deliberately doped with divalent cation impurity e.g. $CdCl_2$ + NaCl[11], $CaCl_2$ + NaCl[27],

$SrCl_2$ + KCl[28]. Divalent anions are relatively insoluble in these lattices e.g. K_2O + KCl[29], K_2SO_4 + KCl[30].

Comparison of cation self-diffusion and ionic conductivity in NaCl[12] and KCl[31] establishes the validity of the Nernst-Einstein relationship in the high temperature (intrinsic) region. In the low temperature range the measured cation self-diffusion is always greater than that calculated on the basis of ionic conductivity measurements. This difference between the calculated and measured diffusion coefficients has been ascribed to the presence in the crystal of essentially uncharged defects which can contribute to diffusion but not to the ionic conductivity.

One possible neutral defect is known as the vacancy pair. A cation vacancy has an effective negative charge and an anion vacancy an effective positive charge. There will thus be an electrostatic attraction between the two defects leading to the formation of a double vacancy Fig.7(a). The concentration of these vacancy pairs, $\mathcal{K}_p$, in a sodium chloride type lattice is given by[32],

$$\mathcal{K}_p = 6 \exp. (-g/kT) \qquad \text{----------} \quad (25)$$

where g is the free energy of formation of a vacancy pair. One important aspect of vacancy pairs is that their concentration is dependent only on the product concentrations of anion and cation vacancies i.e. $\mathcal{K}_1 . \mathcal{K}_2$. Hence, at any one temperature, the concentration of vacancy pairs is unaffected by changes in $\mathcal{K}_1$ and $\mathcal{K}_2$ brought about by the presence of aliovalent impurities.

The significance of vacancy pairs in cation transport in these crystals is doubtful. It had been supposed that the uncharged nature of the defect would enable it to have a high mobility in ionic crystals. However it has been shown by theoretical calculation[33] that the activation energy for

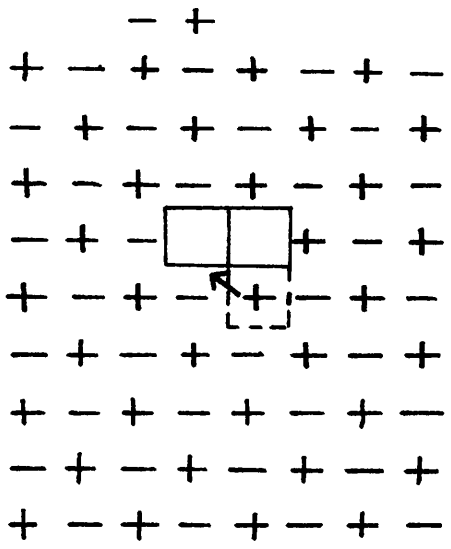

(a). VACANCY-PAIR AND ITS MOVEMENT.

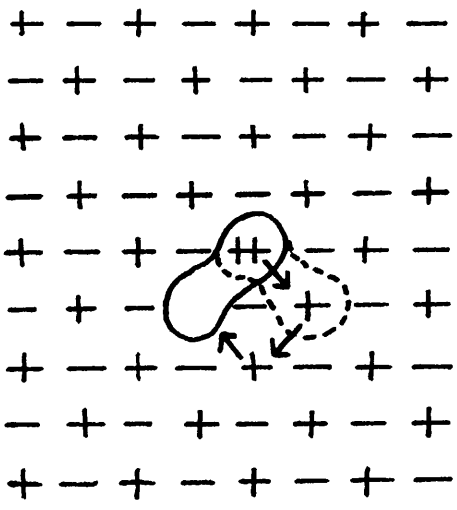

(b). IMPURITY-VACANCY COMPLEX AND ITS MOVEMENT.

FIG. 7. NEUTRAL COMPLEXES.

ionic movement via vacancy pairs is greater than the energy for movement via single cation vacancies. The role of the vacancy pair in cation transport in these crystals is of minor importance.

The discrepancy between the calculated and measured diffusion coefficients is usually ascribed to the presence of aliovalent impurity-vacancy complexes which contribute to diffusion but not to conductivity. The association of a divalent impurity cation with a cation vacancy, which bears an effective negative charge, will result in the formation of a neutral complex, Fig. 7b. If all but nearest neighbour interactions are neglected the equilibrium between the complexes (concentration χ_c), impurity cations and free cation vacancies is given by[16]

$$\frac{\chi_c}{\chi_1(c-\chi_c)} = z_c \exp.(W_a/kT) \qquad \text{----------} \quad (26)$$

where W_a is the free energy of association (excluding configurational entropy) and z_c is the number of distinct orientations of the complex. Hence these complexes will be formed in appreciable concentrations at low temperatures. Lidiard[16] has given a theory of ionic conductivity taking into account these impurity-vacancy complexes and good agreement between theory and experiment is observed e.g. $CdCl_2$ + NaCl[11], $SrCl_2$ + KCl[28]. The energies of association, W_a, thus obtained are in good agreement with theoretical estimates[8,34]. Other information on impurity-vacancy complexes has been obtained from studies of dielectric relaxation[35], electron spin resonance[36] and nuclear magnetic resonance[37].

Conductivity measurements[38] on NaCl over the temperature range 20°C to the melting point actually show four ranges of conduction, Fig.8. Ranges I and II are respectively the intrinsic and the structure sensitive ranges which have been discussed above. Range III is interpreted as being due to

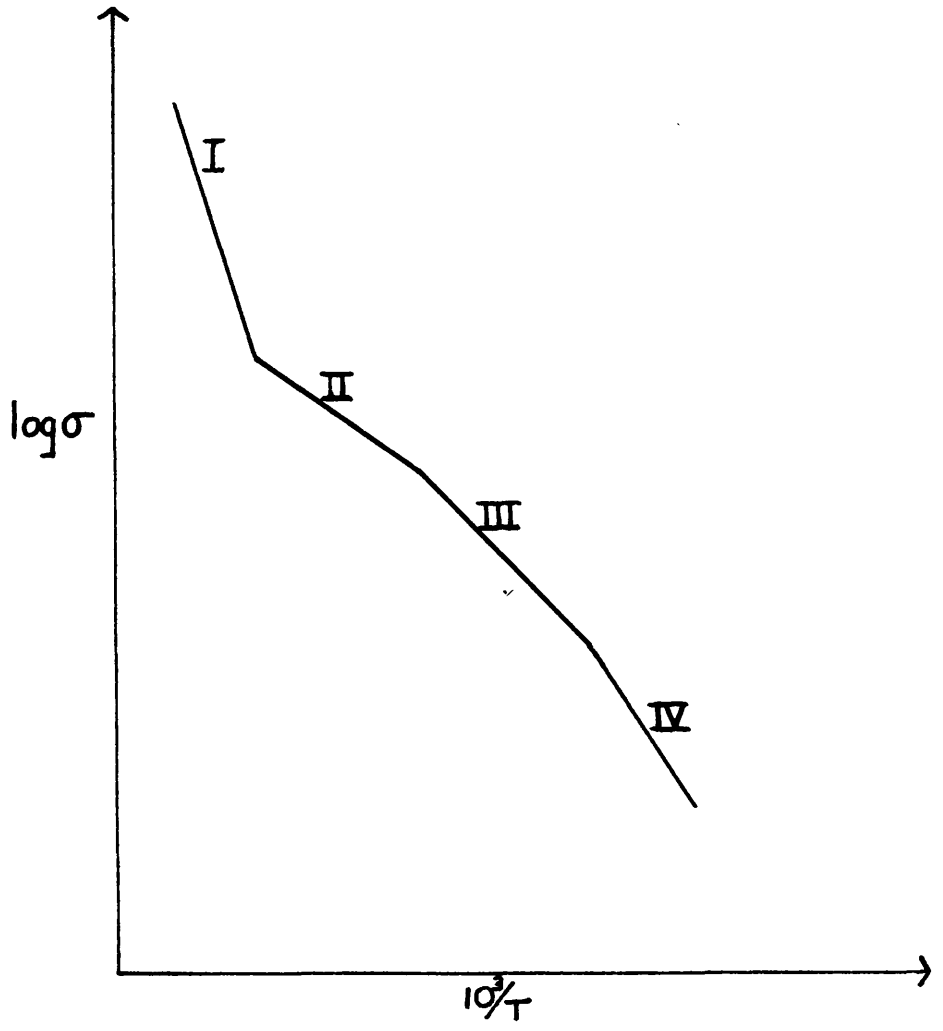

FIG. 8. CONDUCTIVITY/TEMPERATURE RELATIONSHIP FOR SODIUM CHLORIDE.

the impurity-vacancy association reaction and the activation energy should be $U + \frac{1}{2} W_a$. These association complexes are generally precursers to precipitation of the impurity from the lattice and range IV is associated with this precipitation phenomena.

The principal role of line defects in ionic conductivity and cation self-diffusion in these crystals is in their ability to act as centres for precipitation[39,40]. However in chloride ion diffusion in NaCl-type crystals dislocations are important particularly at low temperatures[41]. The space charge on the dislocations will favour chloride ion diffusion in these regions. The effect of divalent cation impurity would be to reduce the space charge[23] and although the anion diffusion is reduced in divalent cation doped crystals the reduction is essentially independent of impurity content[42]. It has been found that while at lower temperatures the anion diffusion is undoubtedly dependent upon the dislocation density in the crystals, within the temperature range 450°-700°C diffusion is probably proceeding via single anion vacancies and vacancy pairs [42,43,44].

Relatively few ionic conductivity and diffusion studies in crystals of the bromides and iodides of sodium and potassium have been made. In these crystals the anion mobility is large enough at high temperatures to make a significant contribution to the conductivity. Rolfe[45] has made a detailed study of KBr doped with either Ca^{2+} or CO_3^{2-} ions. The simple impurity-vacancy association theory was adequate to describe the results for the Ca^{2+} -doped crystals but the divalent anion was only soluble in the lattice at high temperatures. These results will be considered in more detail in the discussion.

1.7. INVESTIGATIONS OF ION TRANSPORT IN ALKALI HALIDE CRYSTALS OF THE CAESIUM CHLORIDE-TYPE STRUCTURE.

Self-diffusion studies [46, 47, 48] have shown that in crystals of the above structure, the anion is the more mobile species. However there is not the marked difference in anion and cation diffusion coefficient which was found in the majority of the alkali halides. Both the anions and cations in CsCl, CsBr and CsI make a significant contribution to the ionic conductivity. The simple expression for the conductivity, equation (19), is no longer adequate and the conductivity must be calculated in terms of equation (16),

$$\sigma = n_1 q \mu_1 + n_2 q \mu_2$$
$$= Nq (x_1 \mu_1 + x_2 \mu_2)$$

Few detailed studies of ionic transport have been made in the caesium halides. Ubbelohde et al[49] have measured the conductance of polycrystalline specimens and have interpreted the conduction in terms of significant electronic contributions[50]. They propose that the presence of dissolved oxide ions in the lattice produces excess anion vacancies and also some caesium ions are present in the divalent state. The electronic conduction arises from the process,

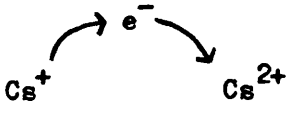

Rossel et al[51] have investigated the conductance in zone-refined CsI. They observed two ranges of conduction with activation energies similar to those reported by Ubbelohde et al[49]. However the low temperature range is interpreted in terms of aliovalent impurity effects and in a more recent publication[52] they report only one range of conduction below 420°C.

The first detailed study of ionic transport in these systems was carried out by Lynch[47] who investigated conductivity and self-diffusion in single crystals of

CsBr and CsI. The results are interpreted in terms of movement via Schottky defects and the approximate satisfaction of the Nernst-Einstein relationship indicates that conductivity is nearly completely ionic. He has also postulated that there is possibly an additional contribution to anion or cation movement by diffusion via vacancy pairs. The same type of investigation[48] in single crystals of CsCl (low temperature form) has given results which compare favourably with those of Lynch[47] but do not indicate anion or cation movement via vacancy pairs. The results of all the ionic transport investigations are summarised in Tables 2 and 3.

Although the investigations of Lynch[47] indicate a reasonable agreement between self-diffusion and ionic conductivity in the higher temperature regions, there are some anomalies at lower temperatures. The single crystals of CsBr and CsI contained significant concentrations of aliovalent impurities (approximately 1×10^{-4} mole fraction), and a low temperature, low activation energy (0.58 eV), conduction range observed in many of the samples was attributed to impurity created cation vacancies. A similar conduction range was observed in a CsBr crystal supersaturated with Ba^{2+}. However in the self-diffusion studies there was no evidence of cation diffusion via impurity created vacancies; a single range of diffusion was observed. It has been suggested[47] that the impurity controlled CsI conductivity is electronic in nature, yet the activation energy is very close to that for CsBr in which there is no evidence of electronic conductivity. Further investigation of this low temperature region is required.

TABLE 2.

Experimentally determined conduction parameters ($\sigma = \sigma_0 \exp.(-E/kT)$).

Reference	Material	Temperature range (°C)	σ_0 ($ohm^{-1}\ cm^{-1}$)	E (eV)
	CsCl.			
Ubbelohde[49]	polycrystalline.	200 - 469	50	1.04
Harvey[48]	single crystals.	230 - 469	1.64×10^5	1.395
	CsBr.			
Ubbelohde[49]	polycrystalline.	340 - 623	1.0×10^3	1.15
Lynch[47]	single crystals.	300 - 475	2.51×10^4	1.285
		475 - 590	2.48×10^5	1.435
	CsI.			
Ubbelohde[49]	polycrystalline.	340 - 500	8	0.87
		530 - 600	3×10^4	1.37
Rossel et al[51]	zone-refined CsI.	200 - 420	-	1.00
		> 420	1.0×10^6	1.49
Rossel et al[52]	zone-refined CsI.	200 - 420	-	1.33
		> 420	-	~1.60
Lynch[47]	single crystals.	300 - 480	1.38×10^4	1.25
		480 - 595	2.21×10^5	1.43

TABLE 3.

Experimentally determined diffusion parameters ($D = D_o \exp. (- E/kT)$).

Reference	Material	Tracer	Temp. range (°C)	D_o ($cm^2\ sec^{-1}$)	E (eV)
Laurent & Benard[46]	CsCl powder compacts.	Cs^{137}	below 465	1.0×10^{-5}	0.70
		Cl^{36}	below 465	1.3×10^{-3}	0.87
Harvey[48]	CsCl single crystals.	Cs^{137}	290 - 470	25.3	1.54
		Cl^{36}	290 - 470	2.1	1.30
Lynch[47]	CsBr single crystals.	Cs^{134}	320 - 550	15.1	1.54
		Br^{82}	330 - 415	0.441	1.29
		Br^{82}	415 - 530	3.92	1.42
Lynch[47]	CsI single crystals.	Cs^{134}	320 - 550	14.24	1.53
		I^{131}	300 - 410	0.487	1.28
		I^{131}	410 - 540	2.05	1.37

1.8. AIMS OF THE PRESENT INVESTIGATION.

It is proposed to investigate ionic transport in single crystals of caesium iodide with particular reference to the effects of divalent impurities. It is intended to pursue this research along two main lines.
(a) The measurement of ionic conductivity in single crystals of CsI doped with divalent impurities.

Investigations of conductivity in impurity-doped systems in which both the anion and cation are significantly mobile are few but they should be of considerable importance. An analysis of the conductance results in such systems has been proposed by Lidiard[16] and the method of treatment is outlined below.

The ionic conductance in this system is given by equation (16),

$$\sigma = Nq\,(x_1\mu_1 + x_2\mu_2)$$

and in a crystal doped with c mole fraction of divalent cations from equation (24),

$$x_1 = \frac{c}{2}\left\{1 + (1 + 4\,x_o^2/c^2)^{\frac{1}{2}}\right\}$$

Substitution of this in (16) gives,

$$\sigma = Nq\,x_o(\mu_1 + \mu_2)\left[\left\{\left(\frac{c}{2x_o}\right)^2 + 1\right\}^{\frac{1}{2}} - \frac{c}{2x_o}\cdot\frac{\phi - 1}{\phi + 1}\right] \text{ --- (27)}$$

where $\phi = \frac{\mu_2}{\mu_1}$

The term $Nqx_o\,(\mu_1 + \mu_2) = \sigma_o$ will be the intrinsic conductivity in an ideally pure crystal. Hence equation (27) becomes,

$$\frac{\sigma}{\sigma_o} = \left[\left(\frac{c}{2x_o}\right)^2 + 1\right]^{\frac{1}{2}} - \frac{c}{2x_o}\cdot\frac{\phi - 1}{\phi + 1} \qquad \text{-------- (28)}$$

When $c \gg \chi_o$ the isotherm becomes linear,

$$\frac{\sigma}{\sigma_o} = \frac{c}{\chi_o(1 + \phi)} \qquad \text{---------- (29)}$$

When $c \ll \chi_o$ the initial gradient of the isotherm is

$$\frac{d(\sigma/\sigma_o)}{dc}_{\text{as } c \to 0} = \frac{1 - \phi}{2\chi_o(1 + \phi)} \qquad \text{---------- (30)}$$

This is positive for $\phi < 1$ and negative for $\phi > 1$. There will thus be a minimum in the σ versus c curve at

$$c_{min} = \frac{\chi_o(\phi - 1)}{\phi^{\frac{1}{2}}} \qquad \text{---------- (31a)}$$

$$\left(\frac{\sigma}{\sigma_o}\right)_{min.} = \frac{2\phi^{\frac{1}{2}}}{1 + \phi} \qquad \text{---------- (31b)}$$

This minimum will be of particular interest when $\phi > 1$ which is the case in CsI where $D_I - > D_{Cs^+}$.

It was therefore proposed to measure the conductivity of single crystals of CsI doped with divalent cation impurity. The principal impurity cation chosen was Ba^{2+} since its ionic size is the nearest of any divalent ion to the Cs^+ ion ($R(Cs^+) = 1.69\text{Å}$, $R(Ba^{2+}) = 1.35\text{Å}$[53]). Analysis of the results in terms of the above treatment should give information on the relative ion mobilities, and on the concentration of intrinsic defects, equations 31a and b. It should also be possible to determine the activation energy for mobility of a cation vacancy, U_+, and to decide whether the low temperature range previously observed[47] is due to these impurity created cation vacancies. Some investigations of conductivity are also to be made in divalent anion-doped crystals. The impurity ion chosen in this case is the SO_4^{2-} ion since earlier work on CsCl[48] indicated the solubility of this impurity ion in the CsCl-type lattice.

(b) The measurement of diffusion in single crystals of CsI doped with divalent impurities.

The conductivity studies are to be supplemented by investigations of cation self-diffusion in these crystals. The diffusion measurements at low temperatures should be useful in determining the role of impurity created cation vacancies in the transport processes and in the possible significance of vacancy pairs in the cation diffusion. It is also thought necessary to determine the cation self-diffusion at high temperatures since Ubbelohde et al[49] and Rossel et al[52] have observed a significant increase in the activation energy for conduction at high temperatures. The latter authors have interpreted the increase in terms of thermally created cation vacancy contributions and this would suggest a much higher activation energy for cation self-diffusion than has been observed[47].

It was also proposed to make some measurements on anion diffusion in these crystals. Because of the short half-life of the tracer I^{131} ($t_{\frac{1}{2}}$ = 8.05 days) and the long diffusion times required at low temperatures, Cl^{36} ($t_{\frac{1}{2}} = 3.2 \times 10^5$ years) was used as the tracer ion. It is unlikely that the magnitude and activation energy for chloride ion diffusion will be substantially different from the iodide ion [54] and moreover the anion diffusion results were intended only to investigate qualitatively the effects of impurity-doping.

CHAPTER 2.

EXPERIMENTAL TECHNIQUE.

2.1. CRYSTALS.

The crystals used in these experiments were obtained from several sources. Some of the crystals of pure caesium iodide were supplied by Mervyn Instruments Limited and by Lights Limited. The usual dimensions of these crystals were 10 x 10 x 5 mm. and they were cut to the required size, generally 5 x 5 x 1 mm., and polished before being used in the experiments. The doped crystals and some of the pure crystals were grown in this laboratory.

2.1.(a) GROWTH FROM AQUEOUS SOLUTION.

Several methods of crystal growth from solution were attempted. Initially the crystals were grown by slow cooling of a saturated solution of caesium iodide. The solution was cooled from 70°C to room temperature over a period of 72 hours. Although this method has been shown to be effective for caesium chloride[48], the results obtained for caesium iodide were, in general, unsatisfactory. The crystals were usually too small for use in the experiments and variations in the cooling rates, from hours to weeks, did little to improve the size or the quality of the crystals. Attempts to promote crystal growth by seeding the solution with a small single crystal of caesium iodide were seldom successful.

It was found that crystals of a reasonable size and quality could be obtained by suspending a saturated solution (~20 ml.) of caesium iodide in a petri-dish over a desiccant in a desiccator. Initially the desiccant used was concentrated sulphuric acid and good crystals were obtained within a few days. The use of concentrated sulphuric acid could possibly lead to the incorporation of small amounts of bisulphate or sulphate ion in the crystals and so it was later decided to use anhydrous calcium chloride as the desiccant. The latter was not as efficient as sulphuric acid and it required a period of at least two weeks of crystal growth

before the specimens were large enough to be used in the conductivity and diffusion studies. The crystals were removed from the solution by filtering under vacuum and they were then stored in desiccators over silica-gel until required.

2.1.(b) THE GROWTH-HABIT OF THE SOLUTION-GROWN CRYSTALS.

The crystals, grown by the above methods, were hexagonal in shape and exhibited marked growth patterns. Their crystal structure was determined by X-ray diffraction. The Debye-Scherrer[55] powder method was used and the diffraction pattern is shown in Plate 1. The results for the lattice spacings determined by this method are compared with the literature values[56] in Table 4.

Table 4.

X-ray powder photograph data and literature values.

θ^{o}	d (Å)	$h^2 + k^2 + l^2$	$a_{meas.}$ (Å)	$a_{lit.}$ (Å)
13.75	3.25	2	4.59	4.57
19.75	2.28	4	4.56	4.58
24.38	1.87	6	4.57	4.56
28.50	1.62	8	4.57	4.58

These results show that the crystals have the normal simple interpenetrating cubic structure.

The effect of impurities on the growth habit was studied. The incorporation of Ca^{2+}, Sr^{2+} and Ba^{2+} ions in solution gave the same result as the "pure" solution, the crystals being hexagonal platelets. However incorporation of Pb^{2+} ions resulted in the crystal showing typical cubic symmetry.

2.1.(c) PRETREATMENT OF SOLUTION-GROWN CRYSTALS.

The infra-red spectra of these crystals showed peaks at 1600 and 3500 cm^{-1}. These peaks are generally associated with the occlusion of water in crystals[57]. Two methods were employed for its removal. The crystals were either

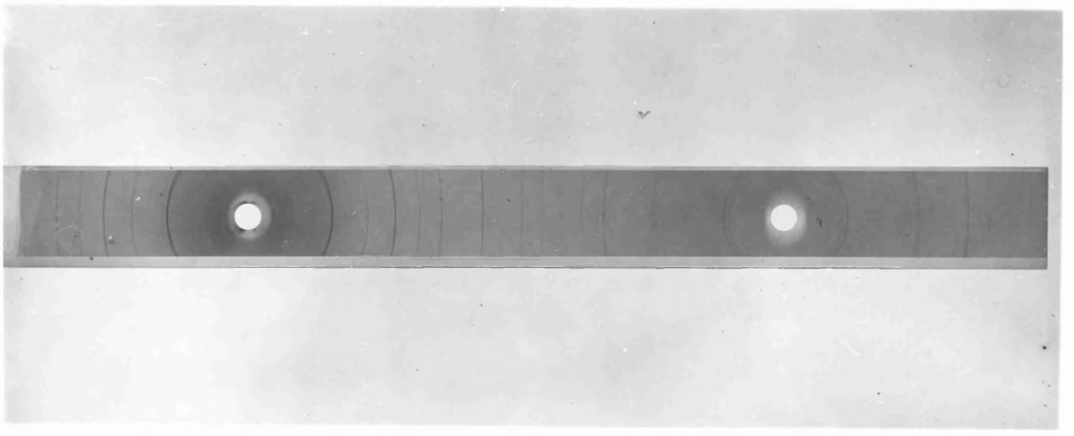

PLATE 1.

heated for twelve hours at 150°C in an atmosphere of dry nitrogen or were dried at 150°C in vacuum for two hours. Subsequent results proved to be independent of the method of pretreatment employed. Prior to the conductivity and diffusion measurements the crystal faces were polished in a small amount of absolute alcohol on a ground glass plate.

2.1.(d) GROWTH OF CRYSTALS FROM THE MELT.

The crystals were grown by a modified Stockbarger[58] technique; the apparatus is shown in Fig.9. 20g. samples of caesium iodide were sealed under vacuum in the silica vessel S. The vessel was suspended in the furnace, F, whose dimensions were 6 inches internal diameter by 12 inches in length. A temperature gradient was maintained in the furnace, 640°C at the lower end and 600°C at the upper end. The silica vessel, with the caesium iodide molten, was raised through the furnace at a rate of 4 inches per hour. After growth, the crystal was cooled slowly to room temperature over a period of thirty hours.

In general the centre of the boule of caesium iodide was polycrystalline but the outer portion, approximately 1 cm. in thickness, was a single crystal. Specimens for conductivity and diffusion were cut from this portion using a clean, moist razor blade. These single crystal pieces were then polished in absolute alcohol on a ground glass plate.

2.1.(e) IMPURITY-DOPING OF CRYSTALS.

Doped crystals of caesium iodide were prepared from both aqueous solutions and from the melt. The divalent cation impurities, Ba^{2+}, Mg^{2+} and Ca^{2+} were added to the solution or melt in the form of the Analar reagent grade chlorides, since it was not possible to obtain high purity iodides. The divalent anion impurity was added in the form of the Analar reagent grade potassium sulphate.

2.1.(f) ANNEALING STUDIES.

Annealing of the crystals was carried out either under

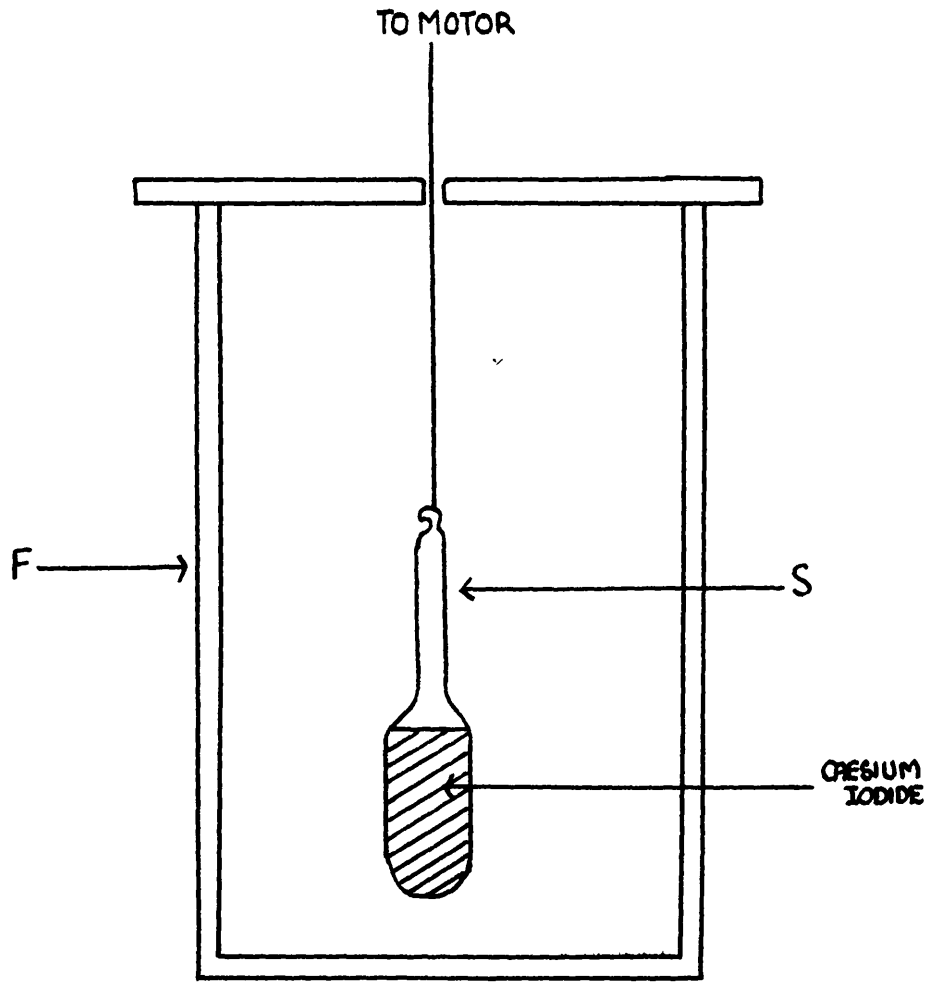

FIG. 9. APPARATUS FOR CRYSTAL GROWTH FROM THE MELT.

vacuum or under a pressure of dry nitrogen. The crystals were sealed in pyrex cells and annealed at 550°C for periods up to 400 hours. On cooling it was frequently observed that the crystals were coloured. This colouration was not homogeneous but consisted of blackened regions in the crystals and was particularly marked in crystals annealed under vacuum. In order to investigate this effect further, several crystals were annealed in iodine vapour. A CsI crystal and a small crystal of iodine were placed in a pyrex cell and sealed under vacuum. The annealing procedure was as above. A detailed discussion of these observations will be given in a later section.

2.2. CONDUCTIVITY.

An a.c. bridge technique was used to measure the conductivity of the single crystals of CsI over the temperature range 20-580°C.

2.2.(a) THE BRIDGE.

The conductivity was measured at 1592 c/s on a Wayne-Kerr B221 Universal bridge. The bridge is based on the transformer ratio-arm technique and reads out directly the reciprocal resistance and capacitance. In some crystals, polarisation phenomena and dielectric loss were investigated and for these measurements a Wayne-Kerr S121 audio signal generator and a Wayne-Kerr A321 waveform analyser were incorporated in the circuit. This allowed measurements to be made over the frequency range 20 c/s to 20 ko/s.

2.2.(b) THE CONDUCTIVITY CELL.

A diagram of the conductivity cell is shown in Fig.10. The electrodes (B) were rectangular platinum face plates, 0.30 x 0.50 inches, silver soldered through brass discs, 0.60 inches in diameter and 0.20 inches in height, to thick copper wire leads (W). The latter provided the connection to the Wayne-Kerr bridge. The electrodes were enclosed in a silica

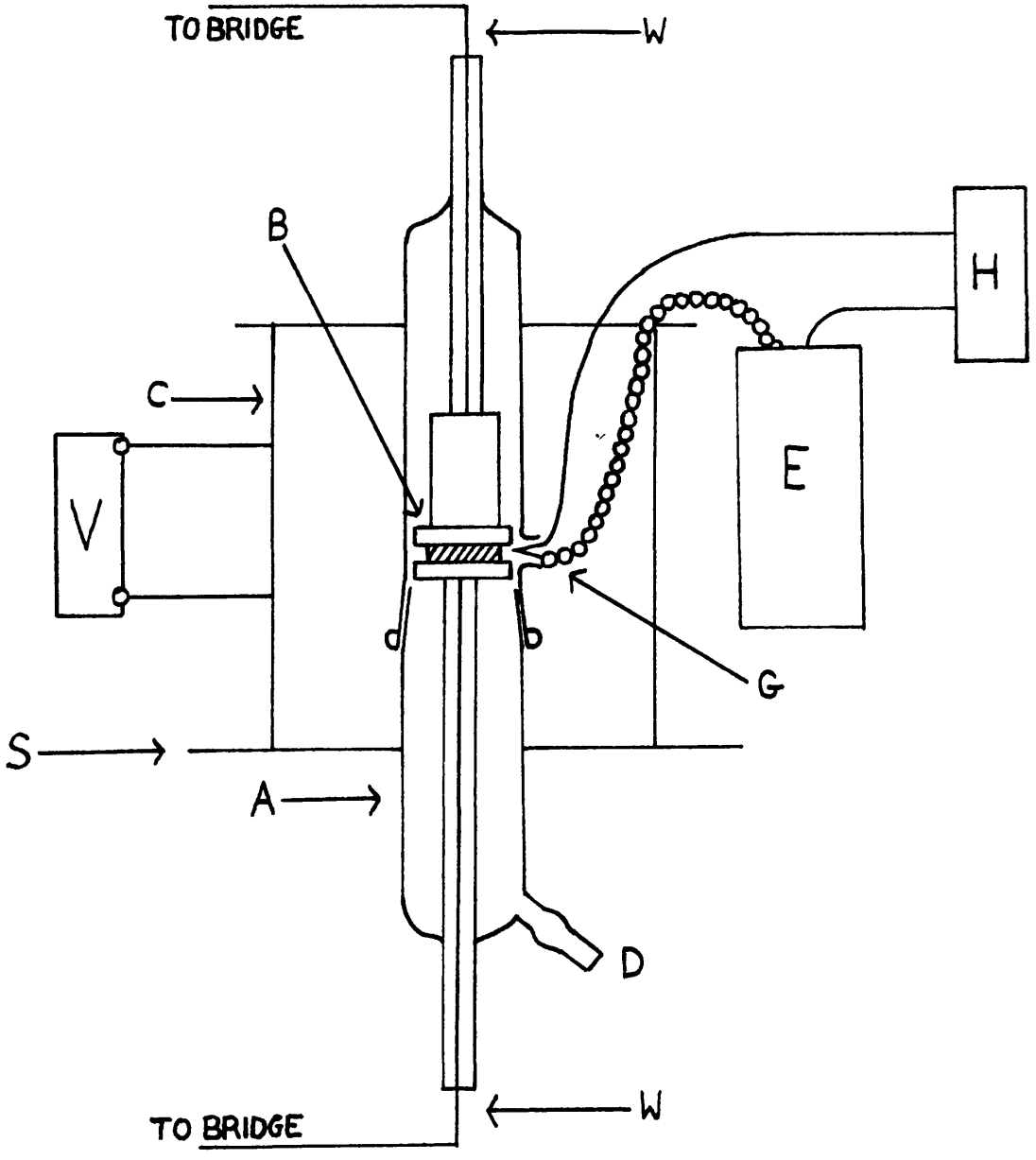

FIG. 10. CONDUCTIVITY APPARATUS.

vessel (A) comprising a B24 cone and socket with two capilliary bore tubes acting as electrode supports to minimise electrode movement during the measurements. The cell was clamped in position through a hole in a piece of Sindanyo board(s), whose dimensions were 4 x 4 x 0.4 inches.

The silica vessel was fitted with two side-arms, one acting as an inlet for the supply of nitrogen gas (D) and the other, situated level with the crystal position, acted as an inlet for the thermocouple (G). The silica vessel was surrounded by a furnace (C). The latter consisted of a cylindrical copper tube, 4 inches in height and 3 inches in diameter, which was covered with layers of asbestos paper and Nichrome wire (resistance 10 ohms per yard) wound thereon giving a total resistance of 90 ohms at room temperature. The windings were well lagged with asbestos tape and asbestos string and finally with a coating of thermal cement. The top of the furnace was carefully lagged with asbestos sheeting to reduce temperature fluctuations due to external draughts. Power to the furnace was controlled by a variac (V).

The crystal temperature was measured by a platinum - platinum - 13% rhodium thermocouple, the "hot" end being as near to the crystal as possible and the "cold" end being immersed in an ice bath in a Dewar flask (E). The thermocouple potential was determined on a Doran thermocouple potentiometer, type E4225, (H) and converted to degrees centigrade by means of the standard calibration tables[59]. The thermocouple was frequently checked by comparing its readings with those of another thermocouple or thermometer placed in the crystal position. It is estimated that the thermocouple temperature is within 2^{o} of the actual crystal temperature.

2.2.(c) PROCEDURE DURING CONDUCTIVITY RUN.

The platinum face plates and the upper and lower faces of the crystal were coated with "DAG" electrode paint. The "DAG" is a colloidal suspension of graphite in alcohol and it was found to be much more satisfactory than silver electrode paint. The latter was satisfactory at low temperatures but at temperatures above 400°C there was considerable diffusion of the electrode coating into the crystal. The "DAG" coating ensures good electrical contact between the crystal and the electrodes.

The crystal was clamped between the electrodes, and nitrogen, dried by passing through B.P.H_2SO_4 and then anhydrous $CaCl_2$, was continuously passed through the cell. The temperature was then slowly raised until the reciprocal resistance of the crystal was greater than 1×10^{-10} mhos, the minimum conductance reading on the Wayne-Kerr bridge. The temperature was allowed to stabilise and then the reciprocal resistance and capacitance were measured by the bridge and the thermocouple potential noted. The variac was then adjusted to give a rise in temperature in the furnace of 10 - 20°, the system again allowed to stabilise and further readings of the reciprocal resistance, capacitance and temperature taken. This procedure was continued up to temperatures of approximately 600°C.

2.2.(d) CALCULATION OF CONDUCTIVITY.

The resistance of a conductor varies directly as its length (d cm) and inversely as its cross-sectional area (A cm^2). Hence

$$R = \rho \frac{d}{A} \qquad \text{---------- (32)}$$

where ρ is the specific resistance i.e. the resistance between the opposite faces of a 1 cm. cube of the material.

The specific conductivity, σ , is defined as the reciprocal of the specific resistance and from equation (32),

$$\sigma = \frac{1}{\rho} = \frac{1}{R} \cdot \frac{d}{A} \qquad \text{---------- (33)}$$

The factor $\frac{d}{A}$, known as the cell constant, was obtained from the crystal dimensions. The thickness of the crystal, d, was measured with a micrometer screw gauge calibrated to thousandths of a centimetre. A, the cross-sectional area, was determined by weighing the crystal, prior to the electrode coating, and dividing the weight by the density of CsI (4.51 $g.cm^{-3}$) and thickness of the crystal.

$$A = \frac{\text{Volume}}{d} = \frac{\text{Weight}}{\text{density x } d} \qquad \text{---------- (34)}$$

Thus by multiplying the bridge reading, i.e. 1/R, by the cell constant d/A, the specific conductivity, in $ohm^{-1}\ cm^{-1}$, was calculated.

2.3. MEASUREMENT OF DIFFUSION.

The diffusion coefficients of Cs^+ and Cl^- in CsI were measured over the temperature range 250 - 500°C using the radioactive isotopes Cs^{137} and Cl^{36} as tracers.

There are three available methods for the determination of diffusion coefficients using radioactive tracers,

(a) Sectioning or grinding techniques,

(b) Isotope exchange techniques

and (c) Surface decrease technique.

2.3.(a) SECTIONING AND GRINDING TECHNIQUES.

In this method a thin layer of the salt, containing the tracer, is evaporated on to one face of the crystal. After allowing diffusion to take place the tracer will have penetrated some depth into the crystal. The solution of Fick's[60] second law of diffusion for this particular case is given by,

$$C = C_o\ (\pi Dt)^{-\frac{1}{2}} \exp.\ (-x^2/4Dt) \qquad \text{---------- (35)}$$

where C is the concentration of the tracer at a penetration depth x, after a diffusion time, t. D is the diffusion coefficient.

The concentration of the tracer as a function of the penetration depth can be determined by measuring the tracer activity in layers of the crystal which are removed by either sectioning with a microtome[12, 46, 54] or grinding[61].

2.3.(b) THE ISOTOPE EXCHANGE METHOD.

This method depends upon the rate of exchange between a radiotracer isotope incorporated in the crystal and a corresponding inactive gas being determined by the rate of the tracer diffusion in the crystal. It is particularly suited to studies of chloride ion diffusion in alkali metal chlorides where the diffusion coefficient at low temperatures is very small.

The method was used by Harrison, Morrison and Rudham[62] in the determination of chloride ion diffusion in NaCl. Cl^{36} was incorporated in the NaCl lattice and the rate of exchange of the isotope between the solid and the surrounding chlorine gas was measured. The solution of Fick's law[63] in this case is given by,

$$n^2 = (2Ac_o)^2 \quad Dt/\pi \qquad \text{---------- (36)}$$

where n is the amount exchanged in a time t, and A is the surface area of the specimen.

The advantage of this method is that diffusion measurements over a series of ascending temperatures can be made on the same crystal[64]. However it is restricted to situations where the parent element of the ion can be obtained in a gaseous form under reasonable temperature conditions or to systems where solid-solution exchange is possible e.g. AgI - $AgNO_3$[65].

2.3.(c) THE SURFACE DECREASE METHOD.

The surface decrease (or absorption) method involves the determination of the surface radioactivity before and after diffusion. Diffusion of an α or β - emitting isotope into the crystal will result in a decrease in count rate at the surface because of the absorption of the α or β particles by the intervening crystal layers. The solution of the diffusion equation for this situation is given by[66],

$$A_t/A_o = \left\{1 - \text{erf}\,(\mu^2 Dt)^{\frac{1}{2}}\right\} \exp.\,(\mu^2 Dt) \quad \text{------} \quad (37)$$

where A_o and A_t are the surface count rates at zero time and after a time t, μ is the absorption coefficient of the isotope radiation in the crystal and erf ( ) is the error function[67].

In this research it was decided to measure the anion and cation diffusion by methods (a) and (c). However method (a) has been subject to serious experimental difficulties, which will be discussed in more detail in section 2.3.(g). The majority of diffusion results have therefore been obtained by method (c).

2.3.(d) PREPARATION OF RADIOACTIVE MATERIAL.

1. Caesium - 137

Cs^{137} is a β^- emitter (0.52 MeV) and γ emitter (0.66 MeV) and has a half-life of 30 years.

The isotope was obtained from the Radiochemical Centre at Amersham as $Cs^{137}Cl$ in 1N HCl; the specific activity was ~1c/gCs. This solution was neutralised with 1N NaOH and some inactive CsI added. The resultant solution was then slowly evaporated to dryness in a beaker in a fume cupboard. The resulting solid was then placed in a large desiccator over silica-gel until required.

2. Chlorine - 36.

Cl^{36} is a β^- (0.714MeV) emitter and has a half-life of 3.2×10^5 years. The isotope was obtained from Amersham as 3.55N HCl^{36}, specific activity 50uc/gCl, and this solution was placed in a small beaker and neutralised by the addition of the appropriate amount of solid Cs_2CO_3, thereby forming $CsCl^{36}$ according to the equation

$$2HCl + Cs_2CO_3 = 2CsCl + H_2O + CO_2$$

The solution was then slowly evaporated to dryness in a fume cupboard and the resulting solid $CsCl^{36}$ stored in a desiccator over silica-gel until required.

3. Method of Evaporation.

A large cell (Fig.11), was designed consisting of a B55 pyrex cone (A), the base of which had a small protrusion (B) of diameter 0.50 inches and depth 0.50 inches. The top half (C) of the cell was a B55 socket with two side-arms, one to air and the other to a rotary pump via a liquid nitrogen cold trap (E). The total length of the cell was 8.00 inches.

The radioactive material was placed in the protrusion in the base and the crystal holder inserted. This consisted of a pyrex ring (F), 1.50 inches in diameter and 0.50 inches high, and an aluminium disc (G) which covered the ring. This disc had eight small holes, each 0.13 inches in diameter, drilled in it. A crystal was then placed over each hole and the B55 joint greased with Silicone high vacuum grease. The taps on the side-arms were greased with Apiezon N vacuum grease and the top and bottom halves connected.

The rotary pump was switched on and the cold trap inserted into a Dewar flask containing liquid nitrogen and the tap to pump opened slowly. The system was left

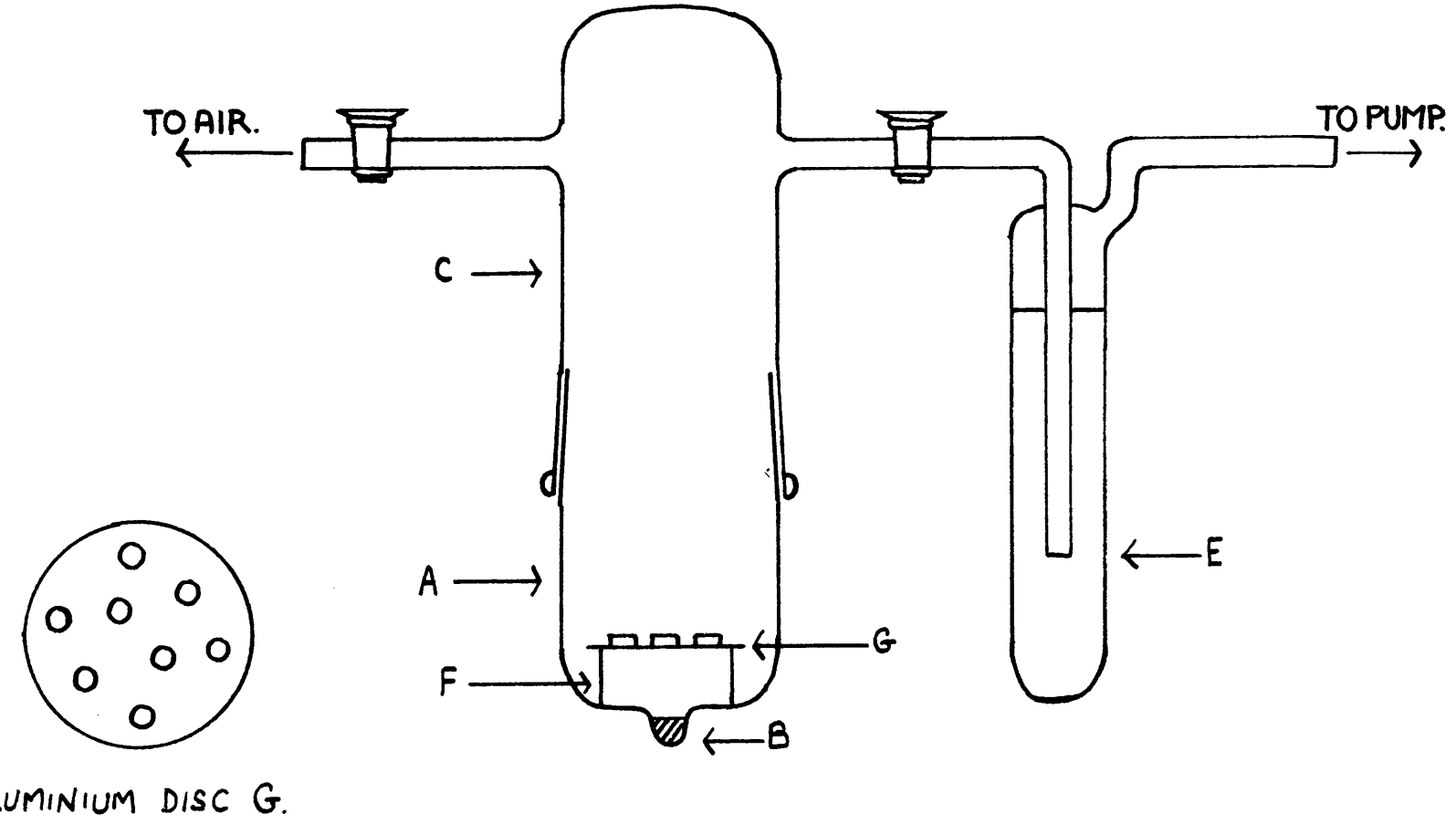

FIG. 11. EVAPORATION APPARATUS.

pumping for one hour and then the tap to pump closed. The protrusion in the base containing the radioactive material was then heated gently with a small bunsen flame until evaporation had taken place. This usually took about five minutes of gentle, uniform heating. Care was taken not to heat the base too strongly. The system was then allowed to cool under vacuum. After cooling the vacuum was released, the cell opened and the crystals removed and counted. The crystals were stored in a desiccator over silica-gel until required.

A uniform deposit of 0.13 inches diameter was obtained on each crystal, the surface activity being in the range of 500 - 3000 cpm.

2.3.(e) COUNTING PROCEDURE.

Crystals were counted in a G-M thin end window counter of thickness 3.75 $mg.cm^{-2}$ and working voltage 700 volts. It is essential that the positioning of the crystals on the counting set-up is reproducible and so a brass plate fitted with an L-shaped bracket in the centre was used as crystal holder. The crystal was marked and placed in the bracket, Fig.12.

In Cl^{36} diffusion, the plate (P) containing the crystal was placed in the second shelf of the lead castle (L) which contained a small crucible of anhydrous calcium chloride (C) as desiccant, Fig.13.

A total count of 10000 was taken on each sample to ensure a 1% statistical accuracy. A Cs^{137} standard source specially prepared on a brass plate of the same dimensions as that used for counting the crystal, was then counted in order to enable any correction for counter fluctuations to be made. The count rates were corrected for dead-time losses and background counting rate. This procedure was repeated after the diffusion had taken place.

For the Cs^{137} diffusion the procedure was slightly different.

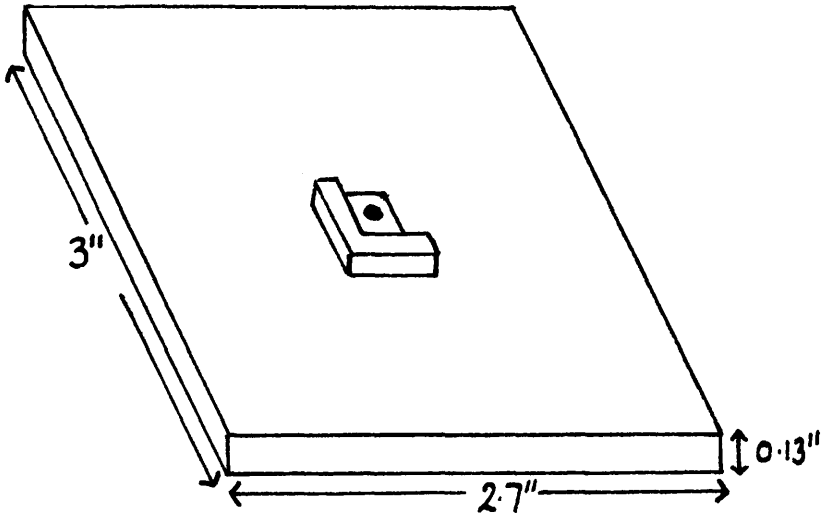

FIG. 12. COUNTING TRAY.

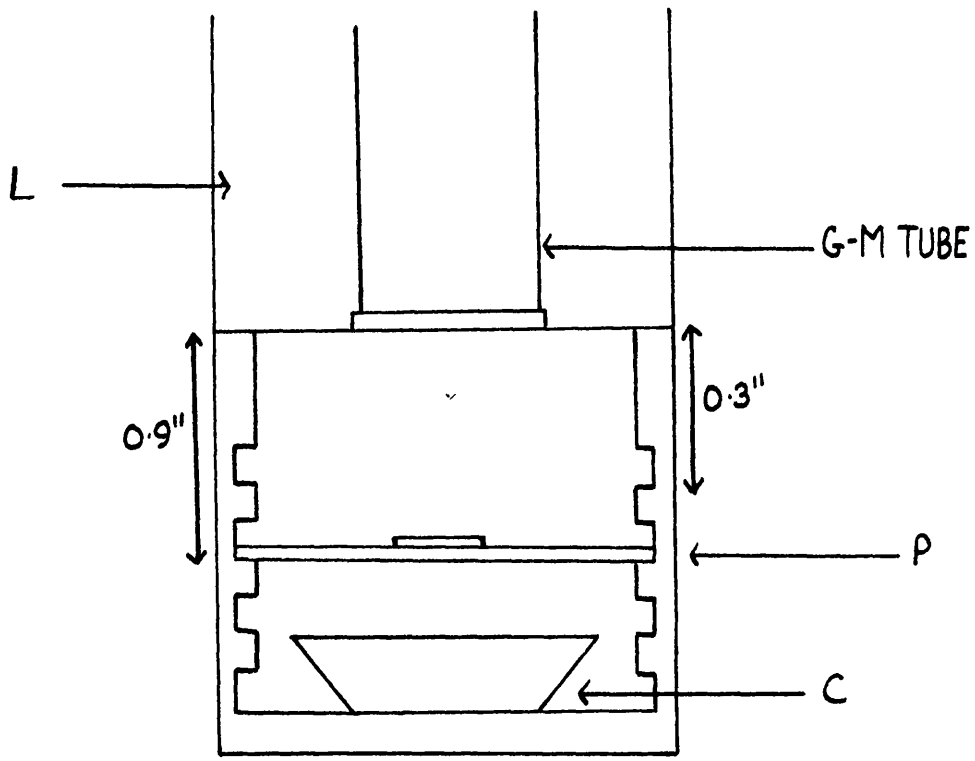

FIG. 13 COUNTING SYSTEM.

The plate containing the crystal was again placed in the second shelf of the counter castle and 10000 counts taken. An aluminium absorber (98 $mg.cm^{-2}$) capable of cutting out all the β- radiation was then placed on the top shelf of the castle and the count rate again measured. This enabled the count rate due to the γ radiation to be calculated. The γ count rate was subtracted from the total enabling the β count rate to be obtained. Corrections were again applied for dead-time losses, background, and any change in the Cs^{137} standard. Also if any evaporation occurred during diffusion this could be allowed for since there would be a significant drop in the γ counting rate. This procedure was repeated after diffusion had taken place.

2.3.(f) ABSORPTION COEFFICIENT CALCULATIONS FOR Cl^{36} and Cs^{137} IN CAESIUM IODIDE.

In using the surface decrease method for diffusion it was necessary to calculate the absorption coefficient, μ, for each isotope in caesium iodide.

1. Calculation of μ for Cl^{36} in CsI.

Since it was impossible to prepare thin enough sections of CsI for this experiment, standard Aluminium absorbers were used and the corresponding absorption in CsI calculated by comparison of the densities of Al and CsI.

A crystal of CsI was prepared with a deposit of $CsCl^{36}$ on one face. The absorption was determined by measuring the activity with varying thicknesses of Al absorber between the crystal and the G-M counter in the apparatus described in the previous section. The count rates were corrected for dead-time losses, window thickness (3.75 $mg.cm^{-2}$), air absorption (1.27 $mg.cm^{-2}$) and background counting rate. A plot of log activity (cpm) versus absorber thickness ($mg.cm^{-2}$) was drawn and the half-thickness $d_{\frac{1}{2}}$ calculated from the curve. The half-thickness is that weight

per square centimetre of absorber which would be required to halve the counting rate. The curve and table of results for this determination are shown in Fig. 14 and Table 5 respectively.

The absorption coefficient μ is then calculated in the following way. The absorption of radiation in matter is given by[68]:

$$\frac{A_d}{A_o} = \exp.(-\mu d) \qquad \text{---------- (38)}$$

where A_o is initial activity

A_d is activity with absorber of thickness d $mg.cm^{-2}$

d is absorber thickness in $mg.cm^{-2}$

μ is the absorption coefficient.

$$\mu = \frac{2.303}{d} \cdot \log \frac{A_d}{A_o} \qquad \text{---------- (39)}$$

$$= \frac{2.303}{d_{\frac{1}{2}}} \cdot \log 2$$

$$= \frac{0.693}{d_{\frac{1}{2}}} \ mg.cm^{-2} \ Al$$

and converting to cm^{-1} in CsI (density of CsI = 4510 $mg.cm^{-3}$)

$$\mu = \frac{0.693 \times 4510}{d_{\frac{1}{2}}} \ cm^{-1} \ CsI.$$

$$= 72.70 \ cm^{-1} \text{ for } Cl^{36} \text{ radiation in CsI.}$$

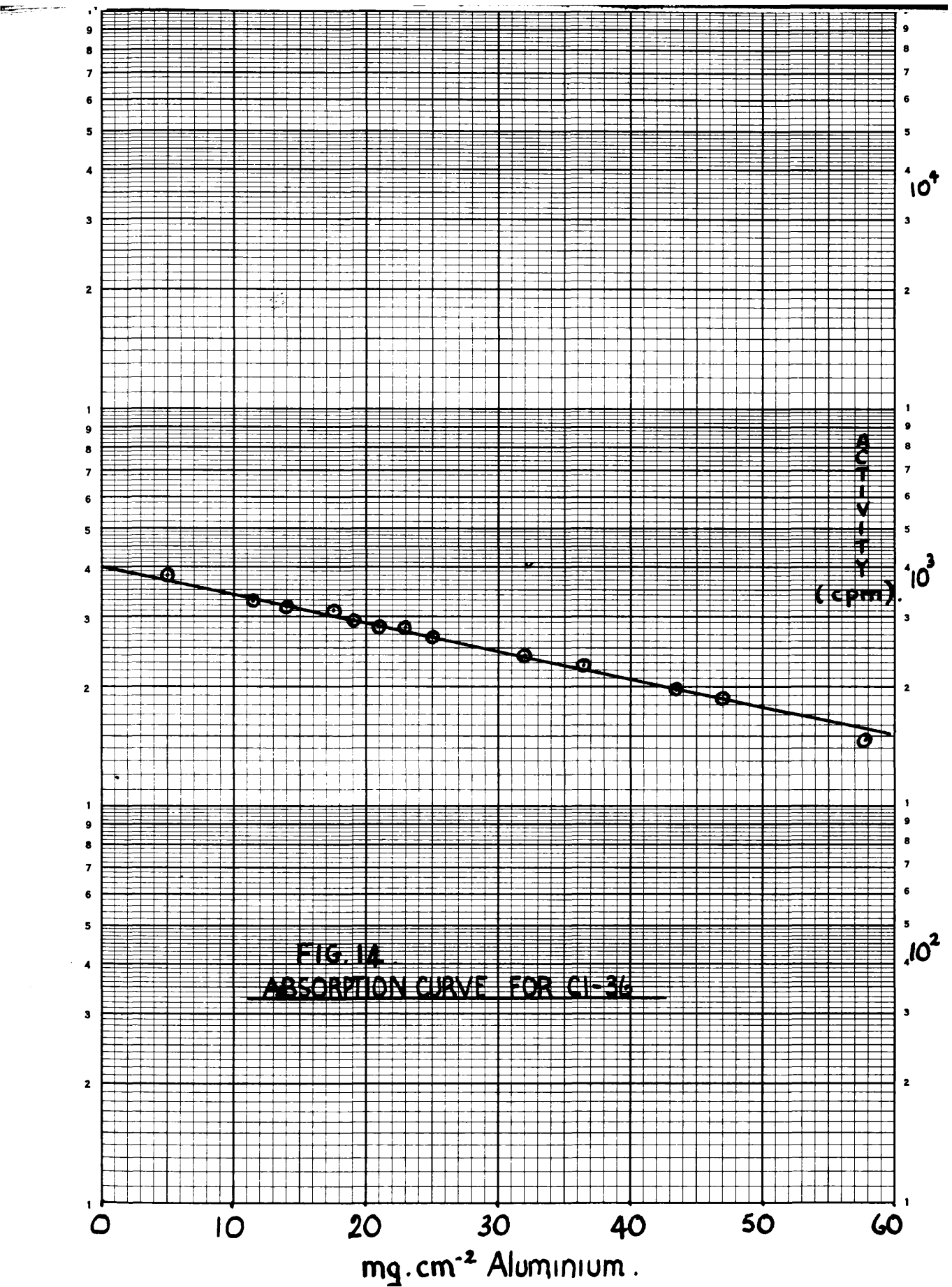

FIG. 14.
ABSORPTION CURVE FOR Cl-36

TABLE 5.

Absorption coefficient data for Cl^{36} in CsI.

Corrected Activity (cpm.)	Absorber Thickness ($mg.cm^{-2}$)
3785	5.02
3353	11.62
3164	14.12
3085	17.52
2950	19.02
2858	20.92
2823	23.02
2644	25.12
2361	31.92
2281	36.57
1936	43.72
1875	46.97
1467	57.82

The activity/absorber thickness relationship is shown in Fig. 14. From this $d_{\frac{1}{2}}$ is found to be 43 $mg.cm^{-2}$ Al. This leads to the value of 72.70 cm^{-1} for the absorption coefficient μ for Cl^{36} radiations in CsI.

2. Calculation of μ for Cs^{137} in CsI.

The procedure here is similar to that used for Cl^{36}. The curve this time contains two distinct portions, Fig. 15. The first portion is due to both β and γ components and the second portion to the γ component only. The latter portion is extrapolated to zero thickness of absorber and the corresponding γ - activity subtracted from the total activity for various thicknesses of absorber, thus giving the β - activities. A graph of log β activity versus absorber thickness in $mg.cm^{-2}$ was plotted (Fig. 15), and the half-thickness calculated. The results are shown in Table 6. The absorption coefficient μ, which was calculated as in the previous section, was found to be 211 cm^{-1}.

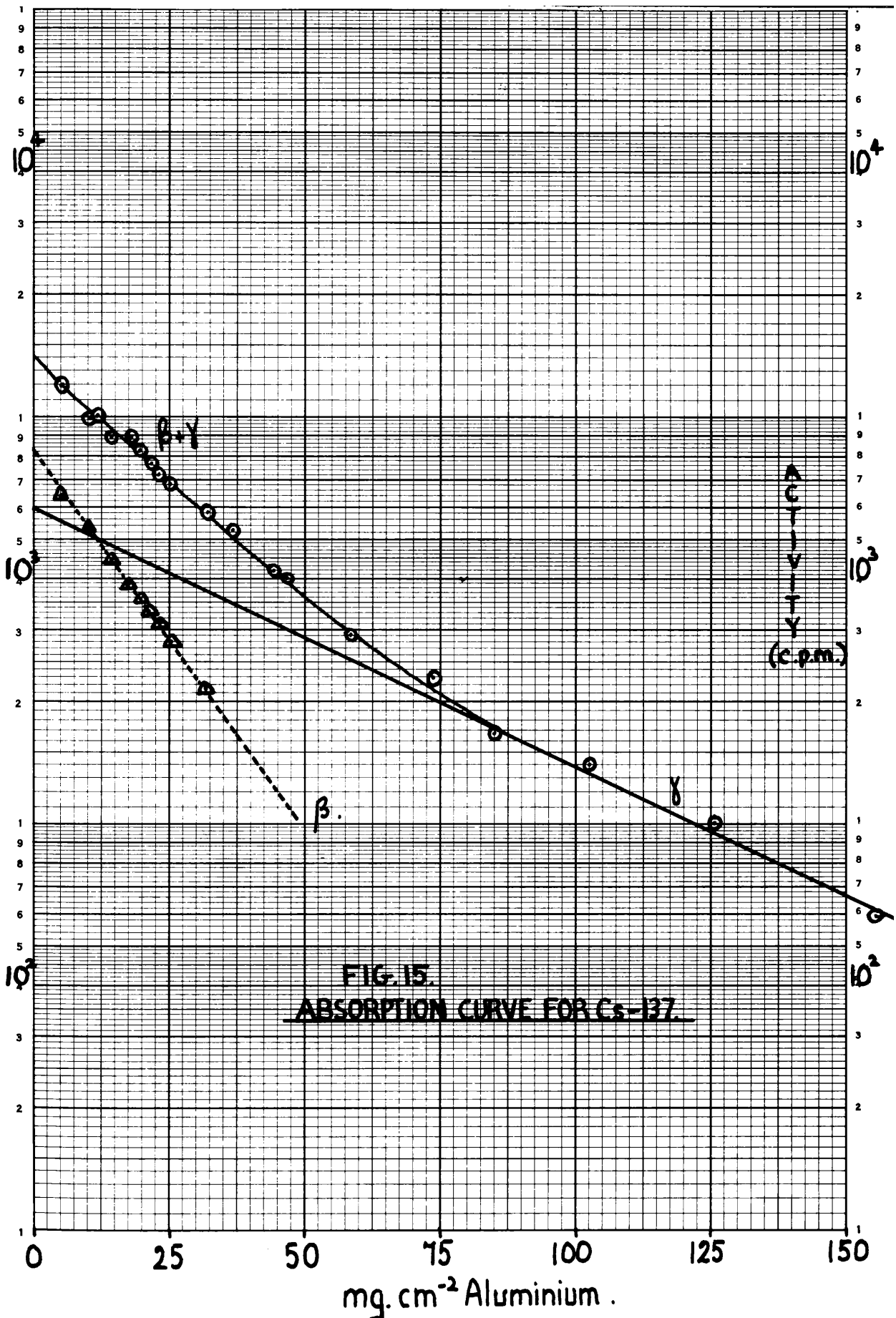

FIG. 15.
ABSORPTION CURVE FOR Cs-137.

TABLE 6.

Absorption coefficient data for Cs^{137} in CsI.

Total Corrected Activity (cpm.)	β - activity.	Absorber thickness ($mg.cm^{-2}$).
11,900	6400	5.02
9900	5300	10.12
9998	4900	11.62
8900	4450	14.12
8820	3850	17.52
8185	3600	19.02
7620	3350	20.92
7190	3130	23.02
6800	2800	25.12
5865	2175	31.92
5300		36.57
4410		43.72
4027		46.97
2912		57.82
2310		74.12
1675		84.32
1399		103.02
1020		126.02
590		155.02

The absorption coefficient for Cs^{137} radiation in CsI was found to be 211 cm^{-1}.

2.3.(g) THE CRYSTAL MICROTOME.

The accuracy of the sectioning method for the determination of diffusion coefficients using a microtome is critically dependent on the alignment of the knife with the crystal face and on the collection of all the sectioned material in a reproducible pattern. The error introduced in the diffusion coefficient due to misalignment of the specimen can be estimated[69].

In this research an MSE 9010 freezing microtome was used. The crystal, after diffusion, was fixed to a wooden block with Araldite adhesive and the block then clamped in the microtome chuck. The angular adjustment of the chuck is limited and alignment of the crystal face with the knife, which moves in an arc over the crystal face, was achieved by inserting metal "spacers" of appropriate thickness around the wooden block. The minimum section thickness which can be removed with this microtome is 5×10^{-4} cm.

The collection of the sectioned material proved extremely difficult. It is usually collected on an adhesive tape but in this work it was found that small amounts of material always adhered to the blade. This error is not too significant when using large crystals ($\sim$1 cm), but in these experiments the area of the crystal face was usually less than 0.25 cm^2. Several types of adhesive tape have been used but in all cases the amount of material left on the blade caused large errors in the diffusion measurements. Collection of the sectioned material was considerably improved by embedding the crystal in paraffin wax but the wax was not a rigid support and movement of the crystal occurred during the microtoming.

Some diffusion measurements have been possible using this microtome when the tracer has a fairly energetic γ - emission. In these cases the sectioned material is not

collected and counted, but the γ - activity remaining in the crystal after each cut is determined by scintillation counting. This necessitates the removal of the crystal from the microtome for counting and so extreme care is needed in repositioning the crystal in the microtome. Since the extent of absorption of the γ -rays in the diffusion length in the crystal is small, the difference in crystal counts before and after sectioning can be taken as the γ -activity of the section. Recently a comparison[57] of this method with the surface decrease method for Na^{22} diffusion (E_γ for Na^{22} = 1.27 MeV) in NaCl has given diffusion coefficients which agree within a factor of two.

It has therefore been found in this experimental work that the available microtome was not satisfactory for the study of Cl^{36} diffusion. Some results have been obtained for Cs^{137} diffusion, but the absorption of Cs^{137} γ-radiation in CsI is sufficient to introduce significant errors in the determination. The diffusion coefficients have consequently been measured mainly by the surface decrease method.

2.3.(h) THE DIFFUSION FURNACE.

It is essential for accurate diffusion results that good temperature control must be maintained over long periods of time. It has been found in this work that this can only be achieved by using a furnace with two heating coils. In furnaces with a single set of windings the switching off and on of the power at the desired temperature causes considerable fluctuations in the temperature stability. It was therefore necessary to use a furnace with two sets of windings, one set supplying the major part of the power to bring and maintain the temperature near the desired value, and the second set, which supplies a much smaller amount of power, acting as a "fine control" for the

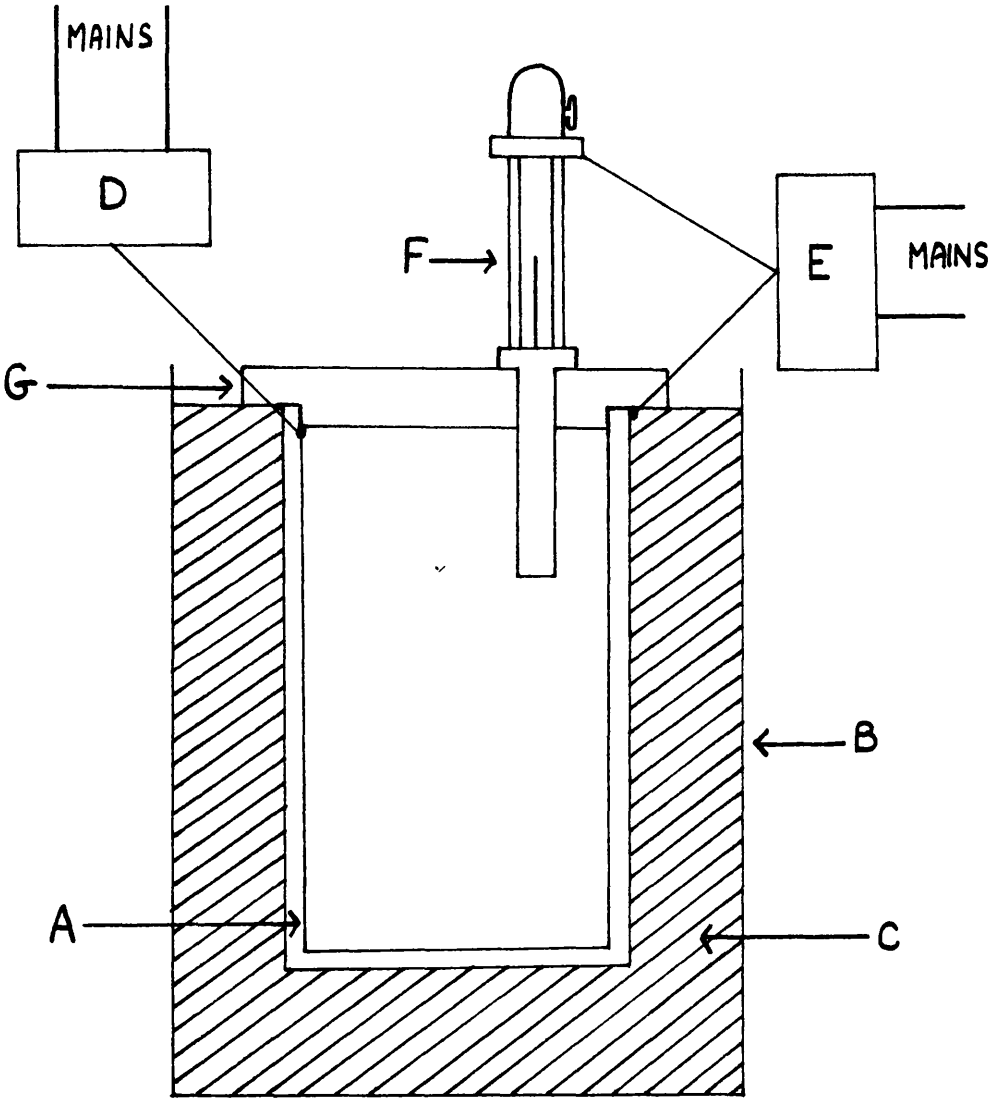

FIG.16. DIFFUSION FURNACE AND CIRCUIT.

temperature. The construction of this furnace is described below.

A furnace core (A), Fig.16, of length 12.00 inches and diameter 4.00 inches and thickness 0.38 inches was obtained and wound with Nichrome resistance wire, of resistance 10 ohms per yard to give a total resistance of 100 ohms. This was then well lagged with asbestos paper. Another length of resistance wire was wound round to give a resistance of 300 ohms. This furnace was also well lagged with asbestos paper and then asbestos string. The whole core was then placed in a metal container (B) and lined with magnesia pipeclay lagging (C).

The inner core leads were connected to the mains via a Variac (D) and the outer core leads to the mains via a Jumo GKT 15-0 thermoregulator (E) and a Jumo MS6.62 Mercury Relay Switch (F). The relay switch was contained in the top of the furnace which was covered with a thick Sindanyo board lid (G). The inner core furnace was taken up to within twenty degrees of the required temperature and the thermoregulator in conjunction with the pre-set relay switch provided the additional heating. The furnace was allowed to stabilise out for a day before using. Temperature control of $\pm$ 2°C was obtained over long periods.

2.3.(i) DIFFUSION CELLS.

All the diffusion experiments were carried out in dry nitrogen atmospheres. For long diffusion times i.e. $>$ 14 hours the large furnace already described was used. The diffusion cell and crystal holder which were made of pyrex glass are shown in Fig.17. The crystals, after counting, were placed on small triangular trays in the crystal holder and the holder placed in the cell. A 0 - 540°C thermometer, previously calibrated against a platinum-platinum - 13% rhodium thermocouple, was placed in the cell beside the stand. The B 29 joint was greased with Silicone high vacuum grease and the taps with Apiezon N vacuum grease and the cell closed. The cell was then evacuated to a pressure of

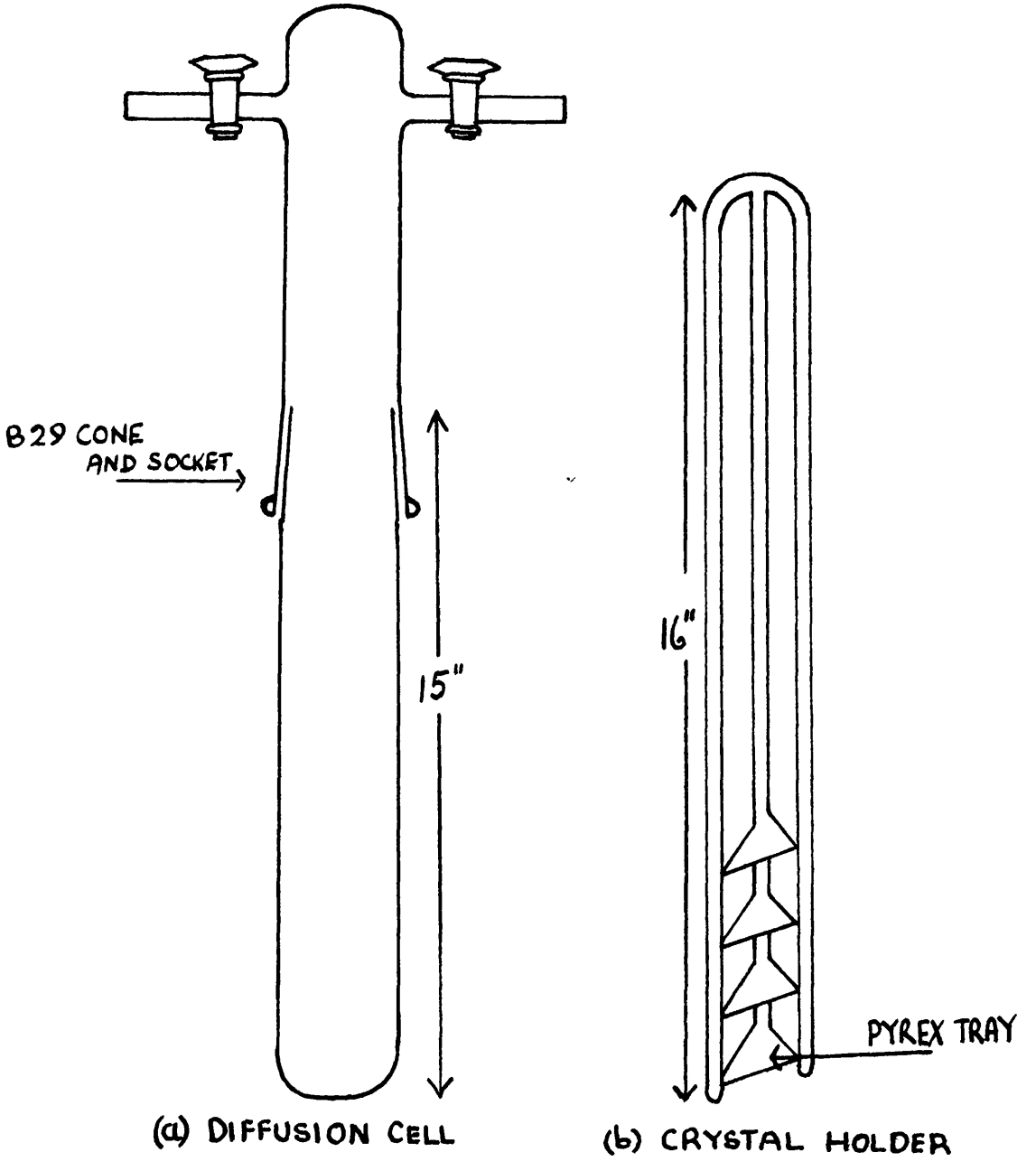

FIG. 17. LARGE DIFFUSION CELL
AND CRYSTAL HOLDER.

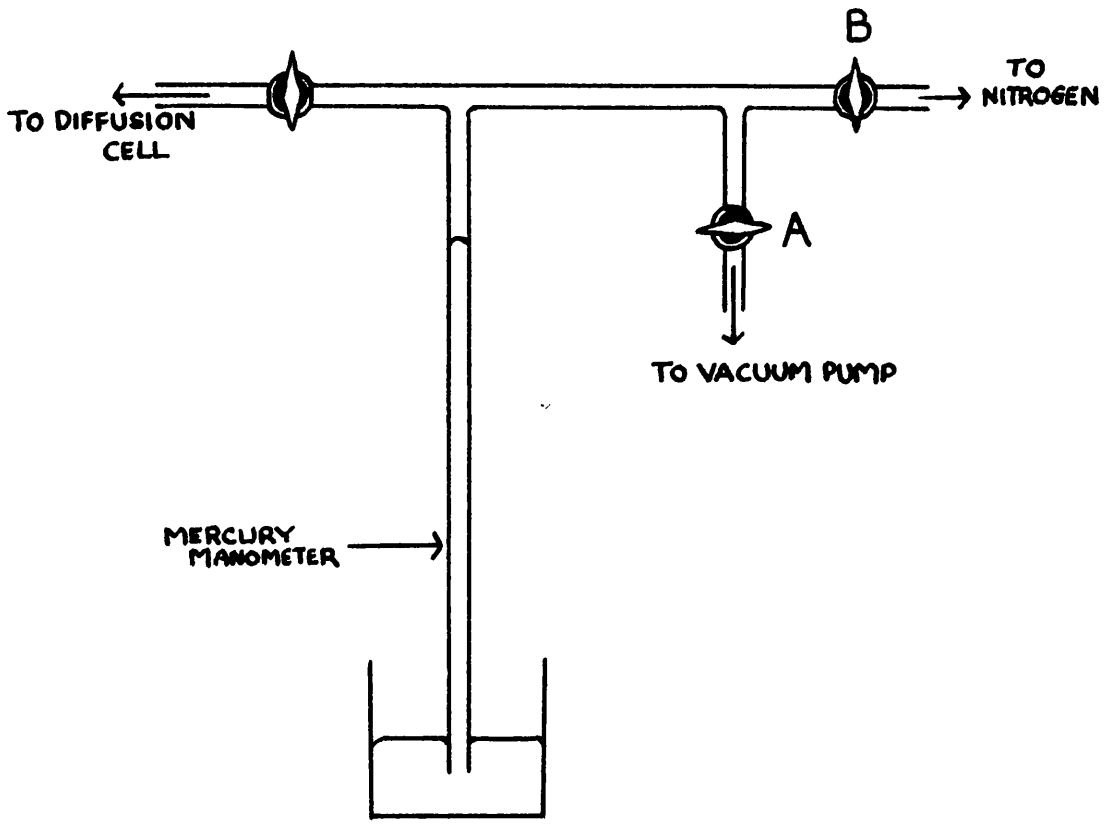

FIG. 18. SIMPLE VACUUM SYSTEM.

1×10^{-2} cm Hg using a simple vacuum system incorporating a mercury manometer, Fig. 18. Tap A was then closed and tap B opened and dry nitrogen allowed in to flush out the system. Tap B was then closed and tap A opened and the system was again evacuated. Tap A was closed again and tap B opened, and dry nitrogen was allowed into the system until the required pressure was reached (76 cm of N_2 at the temperature of the experiment). The cell was then placed in a copper block which had a hole bored in it of diameter and depth convenient to take the diffusion cell and this system then transferred to the furnace which was pre-heated to the desired diffusion temperature. Usually the diffusion cell had attained the required temperature within twenty minutes after placing it in the furnace.

For diffusion times of less than 14 hours another smaller cell was designed, Fig. 19. This was used when a constant observation of the temperature was able to be maintained. A small furnace, (A), as in the conductivity experiments, was used and this was again connected to a variac. The temperature was measured using a platinum-platinum - 13% rhodium thermocouple (B) in the crystals' position. A constant flow of dry nitrogen was maintained through the cell during the experiment. The top of the furnace was covered with pieces of asbestos sheeting.

The crystals were contained in a pyrex cell (C) comprising a B 29 cone and socket, with a side-arm (D) for entry of nitrogen, and an inner tube of 0.25 inches pyrex tubing with a pyrex plate of diameter 1.00 inches at the top. A small hole of diameter 0.25 inches and length 0.25 inches was made for accommodation of the thermocouple. The whole cell was clamped through a piece of Sindanyo board (E) of dimensions 4.00 x 4.00 x 0.40 inches with a hole in the centre through which the cell could just pass. The crystal holder (F) consisted of a pyrex plate of diameter

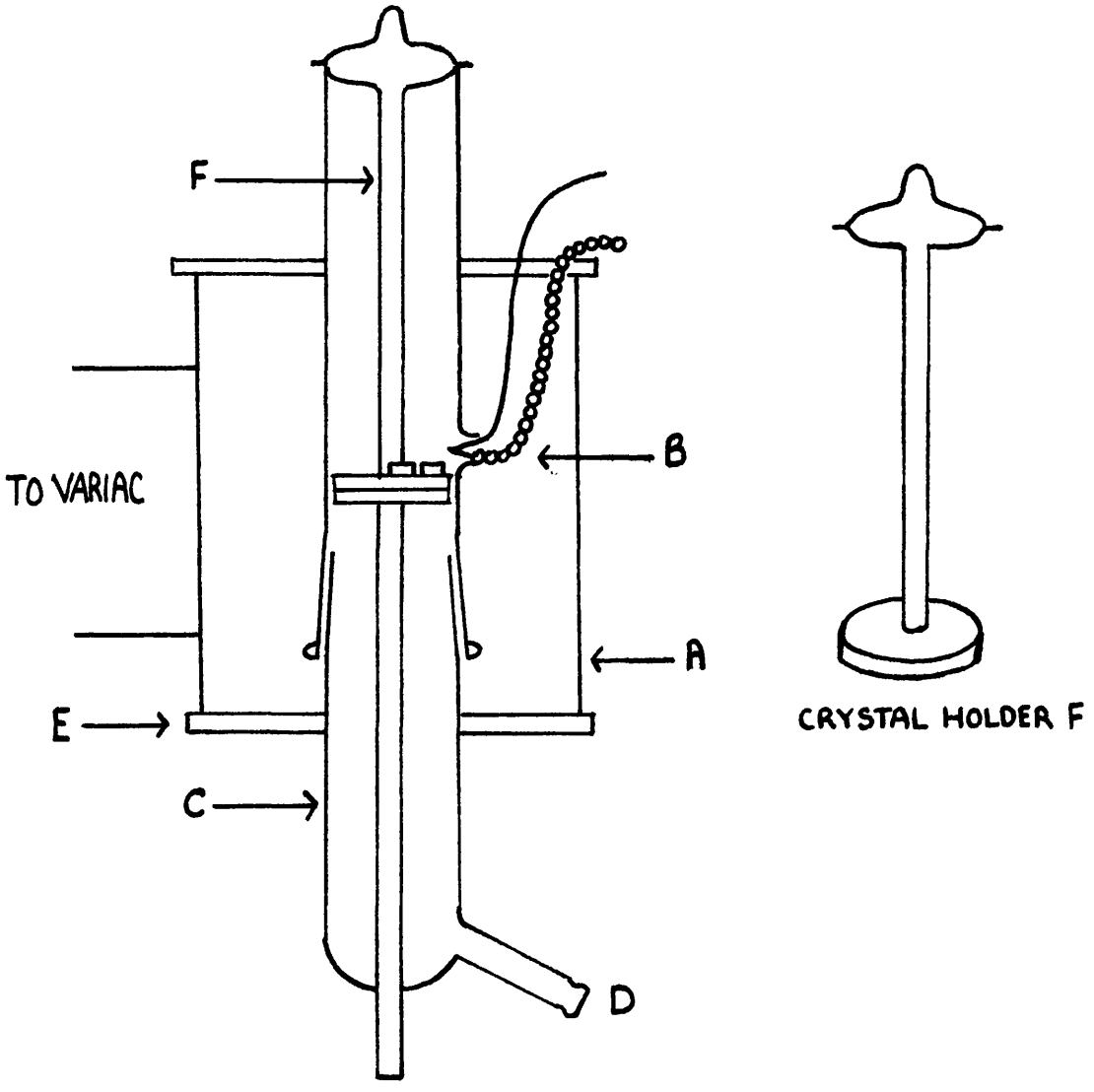

FIG. 19. SMALL DIFFUSION CELL
AND CRYSTAL HOLDER.

1.00 inches connected to a glass stopper by a length of 0.25 inches pyrex tubing. The crystals were placed in this tray and inserted into the cell in the furnace. About five minutes were required for the crystals to attain the experiment temperature. A temperature control of $\pm$ 2°C was again obtained during the time of the experiment.

2.4. ANALYSIS.

In any research project involving conductivity and diffusion experiments on both pure and impurity-doped specimens it is necessary that a reasonably accurate method of analysis of the specimens is available. It is obvious that a quantitative treatment of the results of such measurements is only possible where analytical data on the specimens used can be obtained. In this research several standard methods of analysis were attempted, and they are described in the following section.

2.4.(a) ANALYTICAL METHODS USED.

1. Spectrophotometric Titration.

Analyses of traces of alkaline-earth elements present in a large excess of an alkali-halide have been performed successfully using the large absorbance in the ultra-violet at 222 mμ of EDTA (ethylenediaminetetra-acetic acid)[70]. This involves a spectrophotometric titration of a buffered solution of the sample under examination with EDTA. Initially the change in absorbance at 222 mμ is small due to the preliminary formation of the alkaline-earth EDTA complex. However, once all the alkaline-earth ion has been complexed, there is a marked rise due to the large absorbance of the alkali-EDTA complex. Extrapolation of the two linear portions of the absorbance/ml.EDTA graph gives the end point of the titration.

This method of analysis was found to be admirable for the alkali chlorides of the NaCl-type structure[70]

and also for CsCl[48]. However this was not suitable for traces of alkaline-earth metals in CsI since there is a large masking absorbance in the u.v. due to I^-, over the wavelength used for the titration.

A preliminary removal of the alkaline-earth metal ions using a cation-exchange resin was attempted. This would have eliminated the problem of I^- absorption. However the experimental technique involved too many sources of error for accurate quotations of analyses figures.

2. Flame Photometry.

A flame photometric technique[71] for the determination of Barium was investigated. This involved the precipitation of the Ba^{2+} in a CsI crystal as $BaSO_4$ from an acidic solution. The resultant precipitate of $BaSO_4$ was then dissolved in a solution of ammonium ethylenediaminetetra-acetate. An E.E.L. flame photometer, model A, was set to the zero using ammonium ethylenediamine-tetra-acetate solution, and to full-scale deflection using a solution containing a known concentration of $BaSO_4$ dissolved in the ammonium - EDTA complex. The unknown sample was then analysed.

This method required the use of large samples i.e. large amounts of CsI. The crystals used in our investigations weighed approximately 0.15 - 0.50 g., and for successful operation of this method a number of crystals had to be analysed together, which, of course, was not of any use since the impurity content of each individual crystal was required. The alternative to this was the addition of known amounts of Ba^{2+} to the crystal solution prior to precipitation as $BaSO_4$. However this did not give consistent results.

3. Atomic Absorption Spectrophotometry.

Trials using standard solutions of alkaline-earth doped CsI employing a Unicam SP 90 atomic absorption spectrophotometer, showed that solutions containing large amounts of CsI caused blocking of the burner. As a result of this, very dilute solutions ($\sim 5\%$) had to be used. The limits of accuracy for CsI were thus: 500 ppm Ba, 20 ppm Sr and 10 ppm Ca. Since in this research the main impurity dopant was Ba, obviously atomic absorption spectrophotometry was not really accurate enough.

4. Spectrographic Analysis.

A preliminary complete spectrographic analysis of a solution-grown crystal of CsI by Messrs Johnson, Matthey & Co., Limited showed that there were traces of iron and copper in addition to alkaline-earth metal ions in the crystal. It was decided therefore as a result of this, and also due to the lack of success with the three methods of analysis described above, to have complete spectrographic analyses done on the crystals by Johnson, Matthey & Co., Limited.

The analysis results for each crystal analysed are given in mole-fraction divalent impurity in the summary of results accompanying each conductivity/temperature relationship (Results Section). It was found that those crystals, grown from a solution of B.D.H. Limited CsI, showed the largest concentrations of impurity other than alkaline-earth metals. The accuracy quoted by Johnson, Matthey is $\pm$ 30%.

CHAPTER 3.

RESULTS SECTION.

3.1. CONDUCTIVITY.

From equation (19) already discussed,

$$\sigma = \sigma_0 \exp.(-E/kT) \qquad \text{---------- (40)}$$

where σ is the specific conductivity in $ohm^{-1}cm^{-1}$

σ_0 is a constant ($ohm^{-1}cm^{-1}$)

E is the activation energy for the process (eV).

k is the Boltzmann Constant.

T is the absolute temperature (^oA),

and so a graph of log σ versus 1/T should be a straight line of slope -E/k, and intercept σ_0. The conductivity results have been analysed in terms of equation (40).

3.1.(a) SUMMARY OF OBSERVATIONS.

Several ranges of conduction have been observed depending on the pretreatment of the crystal. It was decided to designate the regions of conductivity as Ranges I to III, and it will be proposed in the discussion that Range I is associated with ionic and electronic contributions to the conduction; Range I (a) is due to cation impurity dissolution in the lattice; Range I (b) is associated with conduction due to free cation vacancies with possible contributions from dissociation of complexes; Range II is controlled by the movement of thermally created anion vacancies in the crystal and Range III possibly arises from the increasing significance of the thermally created cation defect at high temperatures.

3.1.(b) METHOD OF PRESENTATION.

The conductivity results are presented in the form of graphs of log σ versus $10^3/T(^oA)$, with a tabulated summary of the salient features of each graph on the succeeding page. The graphs are presented in the following order,

Untreated "Pure" CsI, Figs. 20-24.

Vacuum annealed "Pure" CsI, Figs. 25-26.

Untreated cation-impurity doped CsI, Figs.27-37.

Vacuum annealed cation-impurity doped CsI, Figs. 38-47.

Other treatments on "Pure" and doped crystals Figs. 48-53.

Magnified Range 1(b) and 1(a), Fig.54.

Divalent anion doped CsI, Figs. 55-56.

Polarisation effects and dielectric loss have been investigated at temperatures below 300°C in annealed and untreated crystals of CsI. It has been pointed out that the presence of divalent impurities in alkali-halide crystals[72] can cause appreciable polarisation effects. These effects are indicated by changes in capacitance with frequency - the capacitance rises with decreasing frequency, the charge carriers causing "blocking" at the electrodes. This effect would be expected to be most significant in samples doped with aliovalent impurities[72]. Also dielectric loss experiments have been used widely in the investigation of association of impurity-vacancy complexes and anion-cation vacancy pairs[35,73,74]. Thus investigations were made of these effects in Range I, the lowest temperature range, where the impurity effects should be most pronounced. The results of the investigations on two annealed and unannealed crystals of CsI are summarised in a graph of the dielectric loss, tan δ , versus frequency in cycles/sec, Fig. 57, and tables of capacitance, frequency and tan δ , tables (43) - (46).

3.1.(c) THE CONDUCTIVITY RESULTS.

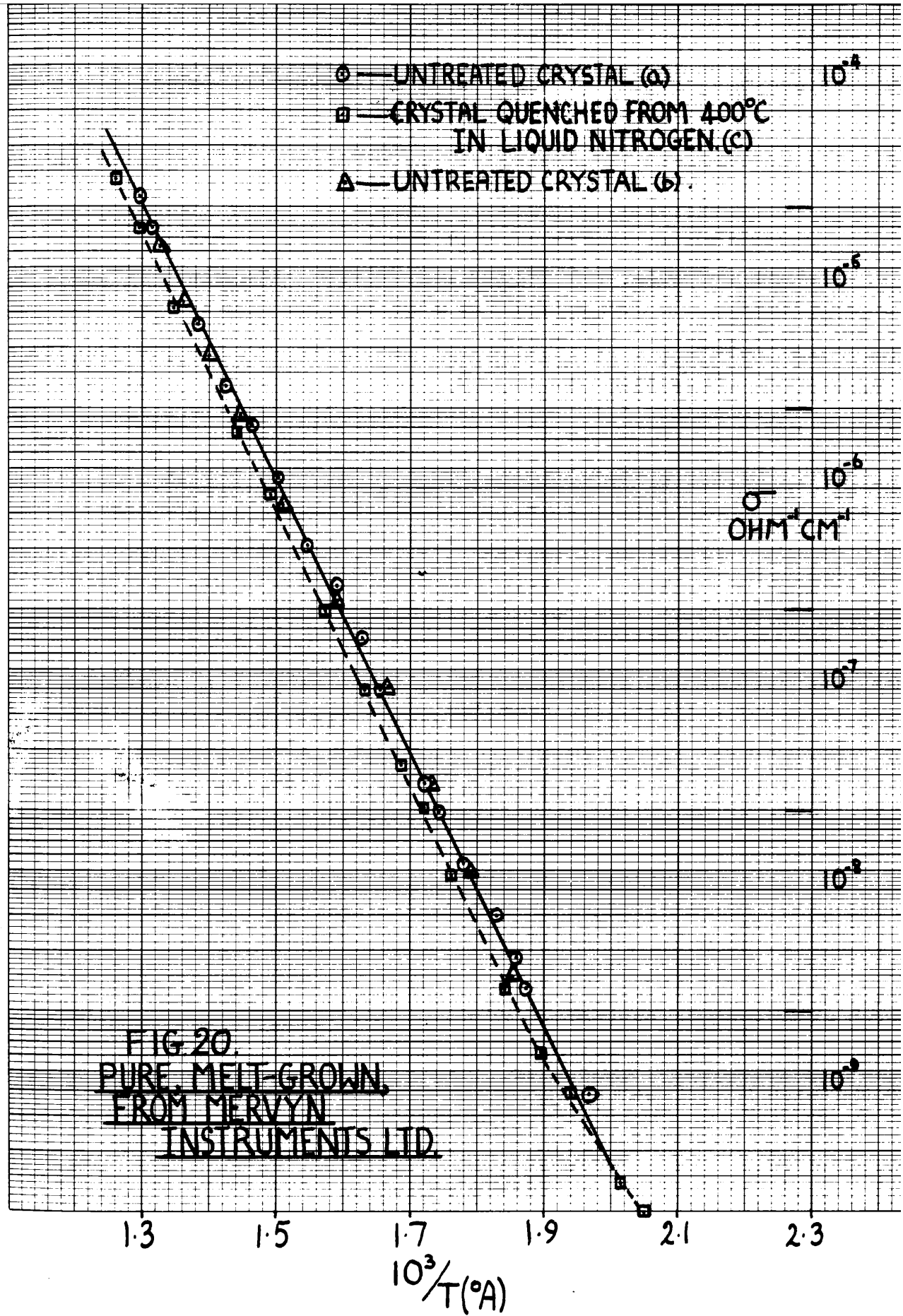

FIG. 20.
PURE, MELT-GROWN, FROM MERVYN INSTRUMENTS LTD.

TABLE 7 (Fig.20)

Pure CsI, melt-grown, from Mervyn Instruments Limited.

Pretreatment:- Crystals (a) and (b) were untreated, crystal (c) was quenched from 400°C in liquid N_2.

	Heating.		
	Crystal (a)	Crystal (b)	Crystal (c)
Range I (°C)	-	-	215-256
E_A(eV)	-	-	1.04
$\sigma_{2.0\ R.T.U.}$ ($ohm^{-1}cm^{-1}$)	-	-	1.7×10^{-9}
Range II (°C)	235-497	265-479	256-520
E_A(eV)	1.37	1.37	1.36
$\sigma_{1.4\ R.T.U.}$ ($ohm^{-1}cm^{-1}$)	2.1×10^{-5}	2.1×10^{-5}	1.5×10^{-5}

Impurity Content of Mervyn Crystals.

$< 2.3 \times 10^{-5}$ m.f. Fe.

$< 5 \times 10^{-6}$ m.f. alkaline-earth metal.

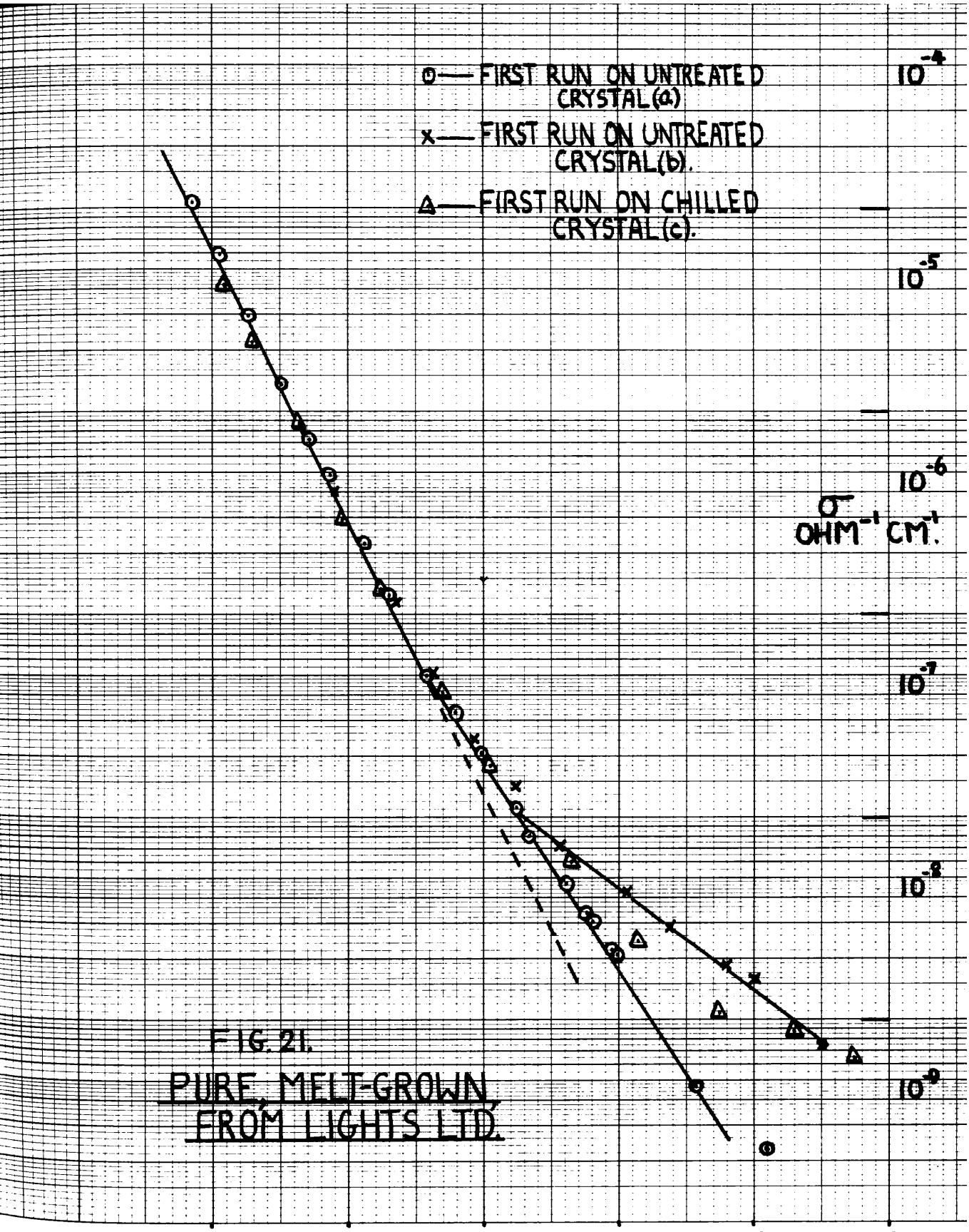

FIG. 21.

PURE, MELT-GROWN, FROM LIGHTS LTD.

TABLE 8 (Fig. 21)

Pure CsI, melt-grown, from Lights Limited.

Pretreatment:- Crystals (a) and (b) were untreated. Crystal (c) was chilled from room temperature in liquid N_2.

Heating.

	Crystal (a)	Crystal (b)	Crystal (c)
Range I (°C)	217-344	182-298	173-302
E_A(eV)	1.01	0.50	immeasurable
$\sigma_{2.0\ R.T.U.}$ ($ohm^{-1}cm^{-1}$)	5.3×10^{-9}	2.4×10^{-8}	$\sim 1.4\times10^{-8}$
Temperature Range (°C)	217-344	298-344	302-344
E_A(eV)	1.01	1.00	1.00
$\sigma_{1.7\ R.T.U.}$ ($ohm^{-1}cm^{-1}$)	1.85×10^{-7}	1.85×10^{-7}	1.85×10^{-7}
Range II (°C)	344-514	344-402	344-485
E_A(eV)	1.33	1.33	1.30
$\sigma_{1.4\ R.T.U.}$ ($ohm^{-1}cm^{-1}$)	1.4×10^{-5}	-	1.3×10^{-5}

Impurity Content of Lights Crystals.

$< 2.05 \times 10^{-5}$ m.f. Cu.

$< 1.0 \times 10^{-5}$ m.f. alkaline-earth metal.

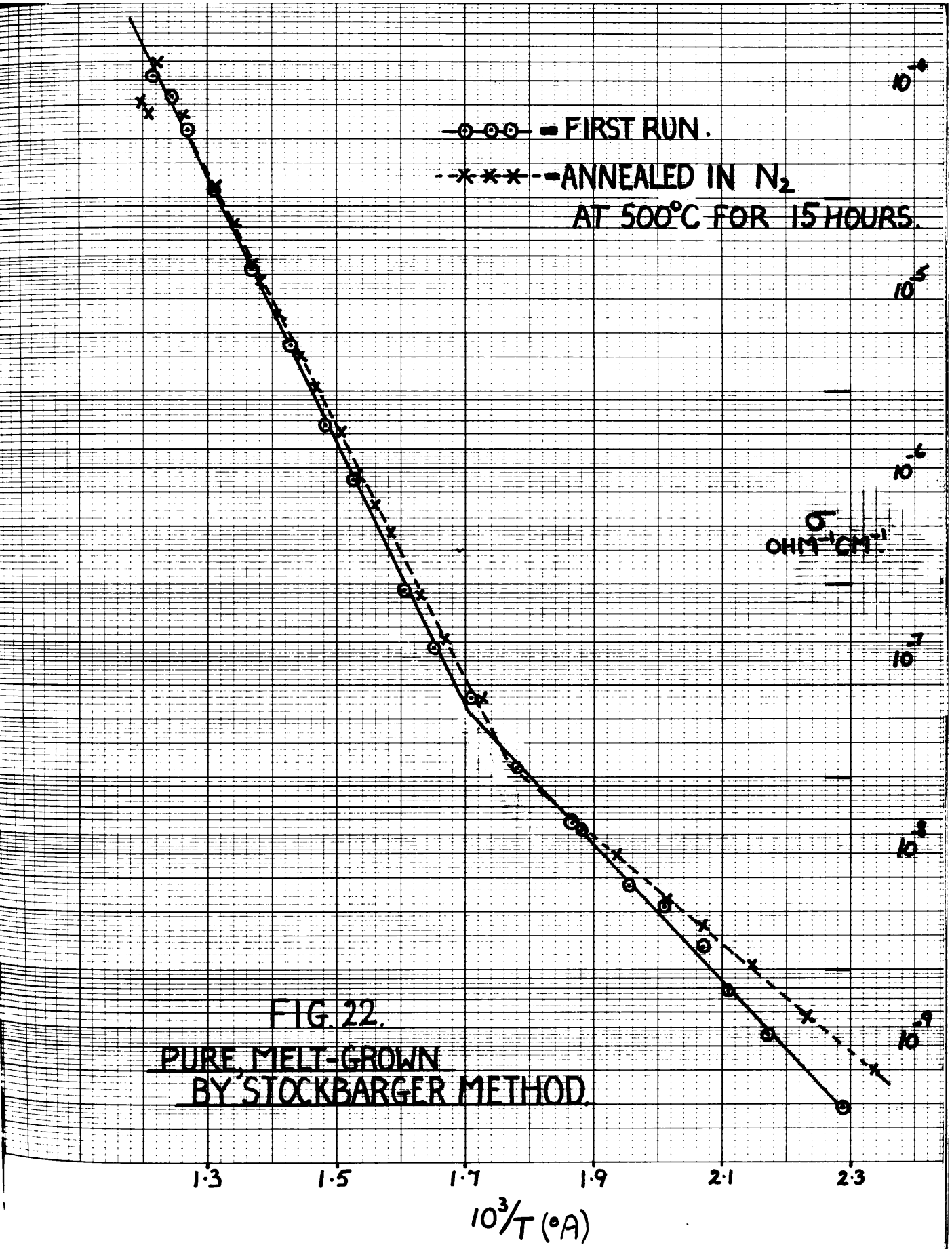

FIG. 22.
PURE, MELT-GROWN BY STOCKBARGER METHOD.

TABLE 9 (Fig.22)

Pure CsI, melt-grown by Stockbarger Method.

Pretreatment:- Untreated for first run, then annealed in dry N_2 for 15 hours at 500°C before the second run.

	Heating.	
	First Run.	Seoond Run.
Range I (°C)	162-315	158-295
E_A(eV)	0.71	0.56
$\sigma_{2.0\ R.T.U.}$ ($ohm^{-1}cm^{-1}$)	1.95×10^{-8}	2.6×10^{-8}
Range II (°C)	315-560	295-560
E_A(eV)	1.36	1 .32
$\sigma_{1.4\ R.T.U.}$ ($ohm^{-1}cm^{-1}$)	2.6×10^{-5}	2.9×10^{-5}

Impurity Content.

2.00×10^{-4} m.f. Cu.

5×10^{-6} m.f. alkaline-earth metal.

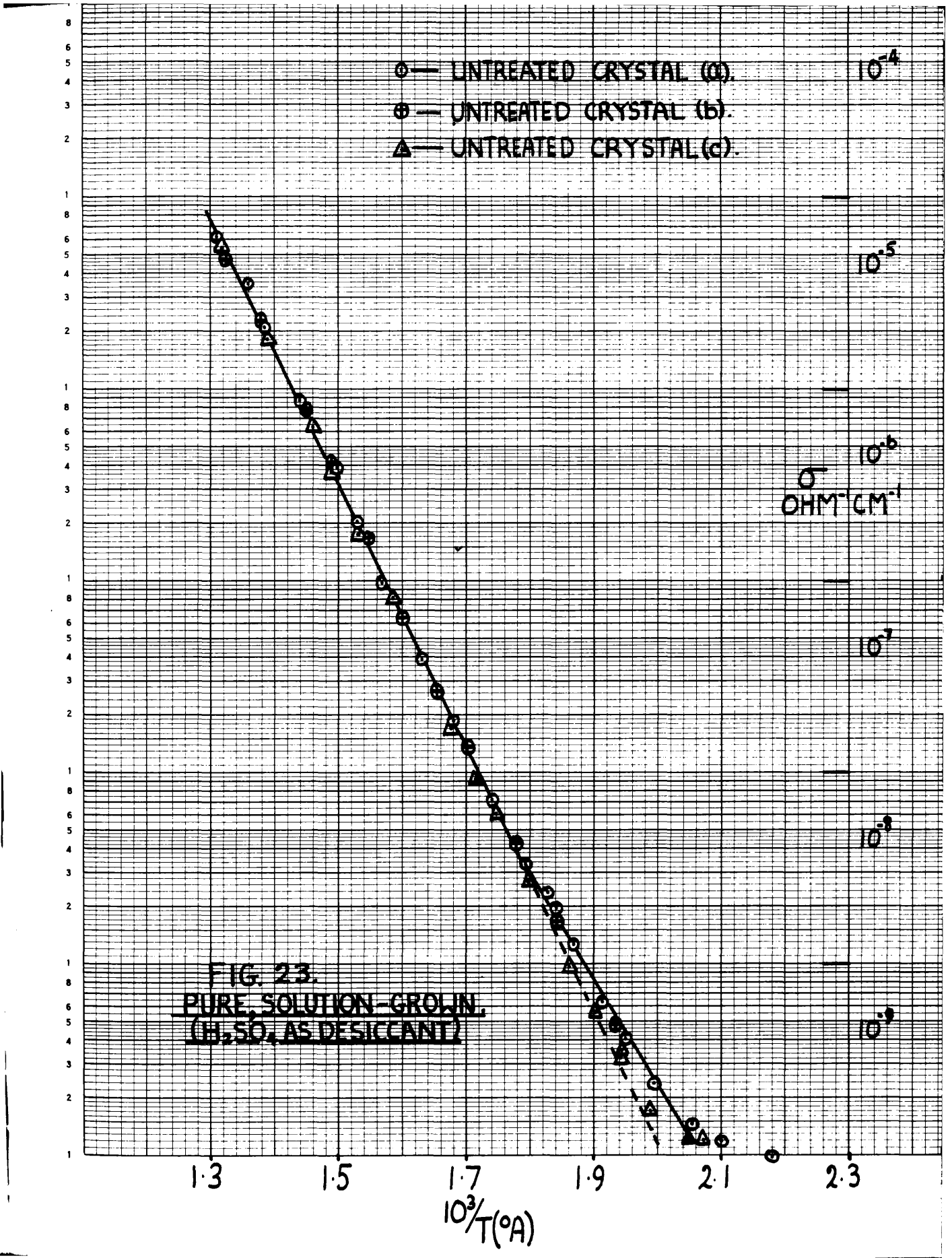

FIG. 23.
PURE, SOLUTION-GROWN.
(H_2SO_4 AS DESICCANT)

TAPLE 10 (Fig. 23).

Pure CsI, solution-grown. (H_2SO_4 as desiccant).

Pretreatment:- Untreated, apart from vacuum drying.

	Heating.		
	Crystal (a).	Crystal (b).	Crystal(c).
Range I (°C)	217-283	245-289	-
E_A(eV)	1.13	1.13	-
$\sigma_{2.0\ R.T.U.}$($ohm^{-1}cm^{-1}$)	$2.4x10^{-9}$	-	-
Range II (°C)	283-496	289-479	227-496
E_A(eV)	1.37	1.37	1.37
$\sigma_{1.4\ R.T.U.}$($ohm^{-1}cm^{-1}$)	$1.55x10^{-5}$	$1.55x10^{-5}$	$1.55x10^{-5}$

Impurity Content.

(a) Hopkins and Williams CsI.

$< 2x10^{-5}$ m.f. Ca

(b) and (c) B.D.H. Limited CsI.

$1-3x10^{-4}$ m.f. alkaline-earth metals (Sr and Ba).

$0.1-1x10^{-4}$ m.f. Fe and Cu.

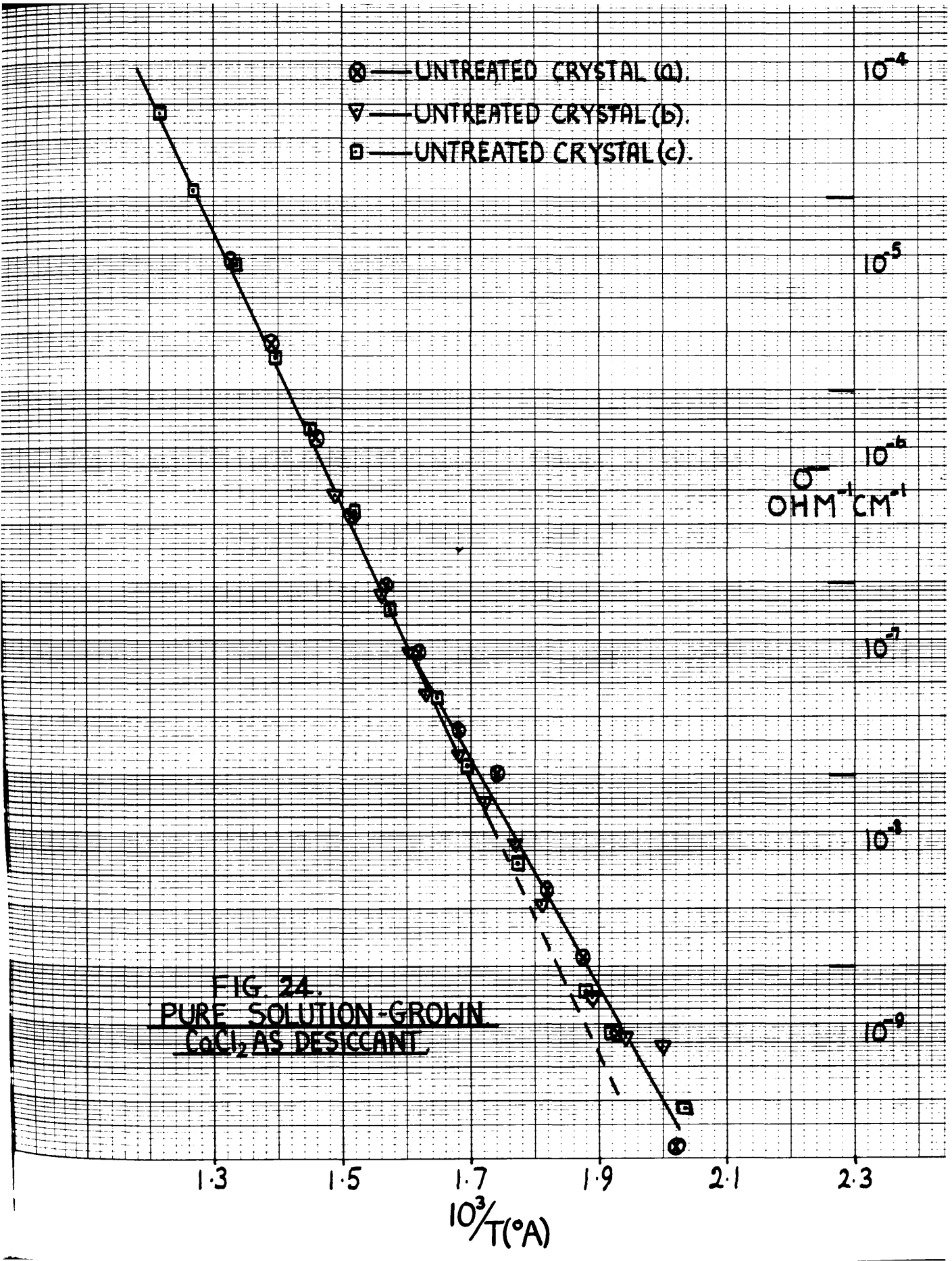

FIG. 24.
PURE SOLUTION-GROWN $CoCl_2$ AS DESICCANT.

TABLE 11 (Fig. 24)

Pure CsI, solution-grown ($CaCl_2$ as desiccant).

Pretreatment:- Untreated, apart from vacuum drying.

	Heating.		
	Crystal (a)	Crystal (b)	Crystal (c)
Range I (°C)	248-352	242-315	248-308
E_A(eV)	1.18	1.18	1.18
$\sigma_{2.0\ R.T.U.}$($ohm^{-1}cm^{-1}$)	2.0×10^{-9}	2.0×10^{-9}	1.5×10^{-9}
Range II (°C)	352-484	315-398	308-560
E_A(eV)	1.40	1.41	1.41
$\sigma_{1.4\ R.T.U.}$($ohm^{-1}cm^{-1}$)	1.3×10^{-5}	-	1.3×10^{-5}

Impurity Content of (a), (b) and (c) grown from B.D.H. Ltd. CsI.

$1\text{-}3 \times 10^{-4}$ m.f. alkaline-earth metal (Ba and Sr).

$0.1\text{-}1 \times 10^{-4}$ m.f. Cu and Fe.

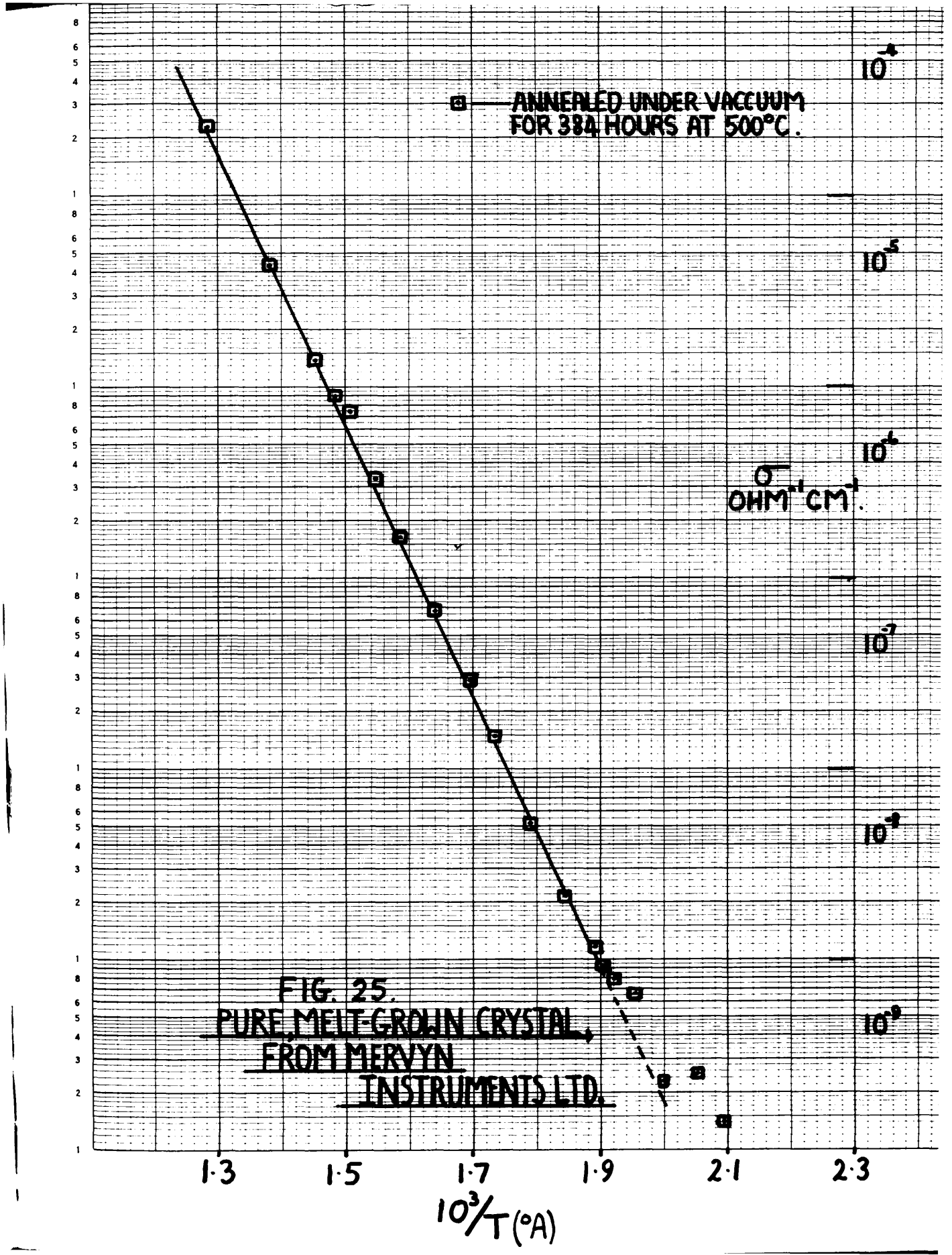

FIG. 25.
PURE MELT-GROWN CRYSTAL
FROM MERVYN
INSTRUMENTS LTD.

TABLE 12 (Fig.25)

Pure CsI, melt-grown, from Mervyn Instruments Limited.

Pretreatment:- Annealed under vacuum at 500°C for 384 hours.

	First Run - Heating.
Range I (°C)	203 - 253
E_A(eV)	immeasurable
$\sigma_{2.0\ R.T.U.}$ ($ohm^{-1}cm^{-1}$)	$\sim 4.0 \times 10^{-9}$
Range II (°C)	253 - 500
E_A(eV)	1.40
$\sigma_{1.4\ R.T.U.}$ ($ohm^{-1}cm^{-1}$)	3.2×10^{-5}

Impurity Content.

$< 5 \times 10^{-6}$ m.f. alkaline-earth.

$< 2.3 \times 10^{-5}$ m.f. Fe.

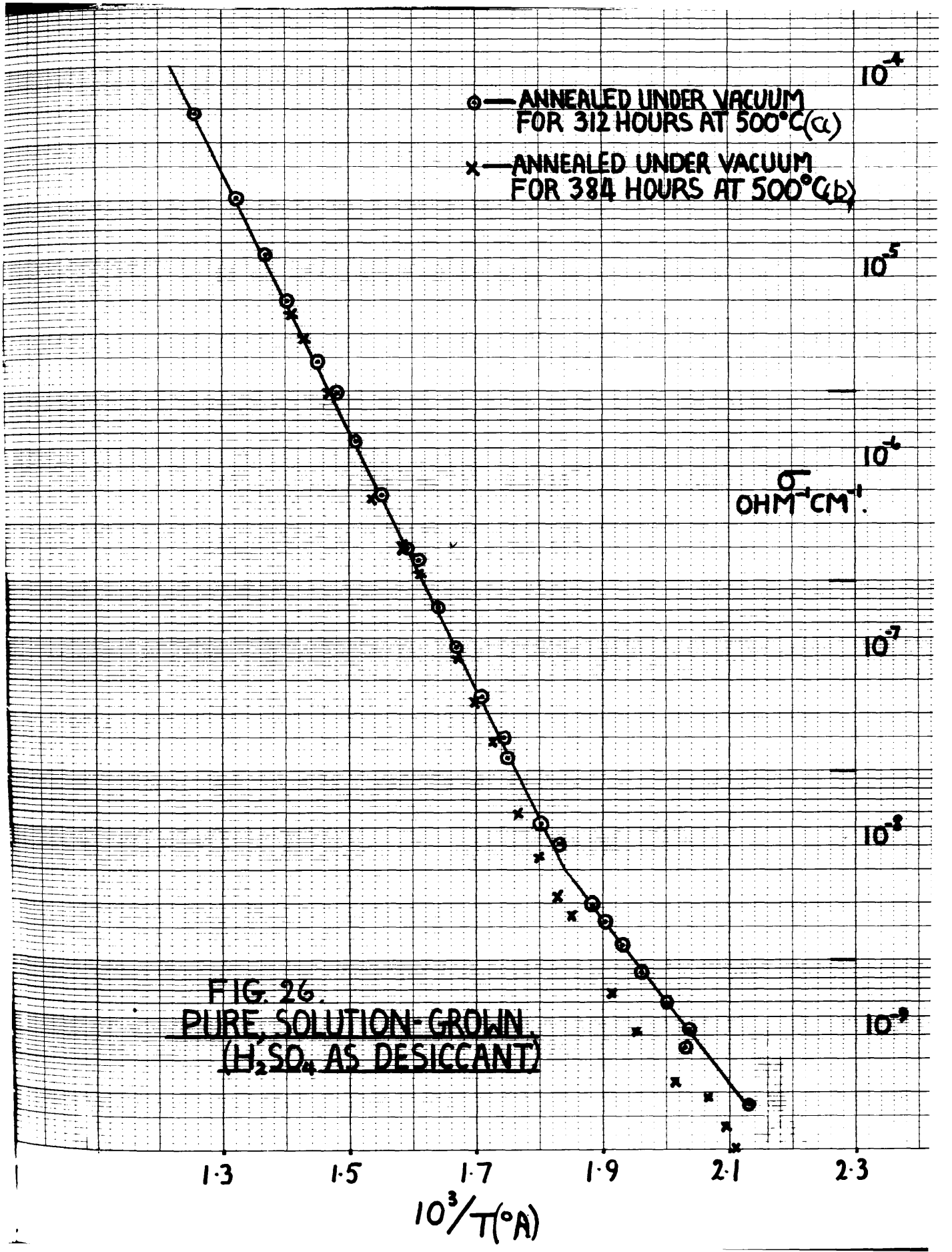

FIG. 26.
PURE, SOLUTION-GROWN.
(H_2SO_4 AS DESICCANT)

TABLE 13 (Fig.26)

Pure CsI, solution-grown (H_2SO_4 as desiccant).

Pretreatment:- Crystals (a) and (b) were annealed for 312 and 384 hours respectively, under vacuum at 500°C.

	Heating	
	Crystal (a)	Crystal (b)
Range I (°C)	199-302	199-300
E_A(eV)	0.86	0.90
$\sigma_{2.0\ R.T.U.}$($ohm^{-1}cm^{-1}$)	6.0×10^{-9}	2.8×10^{-9}
Range II (°C)	302-550	300-441
E_A(eV)	1.37	1.37
$\sigma_{1.4\ R.T.U.}$($ohm^{-1}cm^{-1}$)	2.9×10^{-5}	2.9×10^{-5}

Impurity Content of Crystals grown from B.D.H. Ltd. CsI.

$1 - 3 \times 10^{-4}$ m.f. alkaline-earth (Ba and Sr).

$0.1 - 1 \times 10^{-4}$ m.f. Cu and Fe.

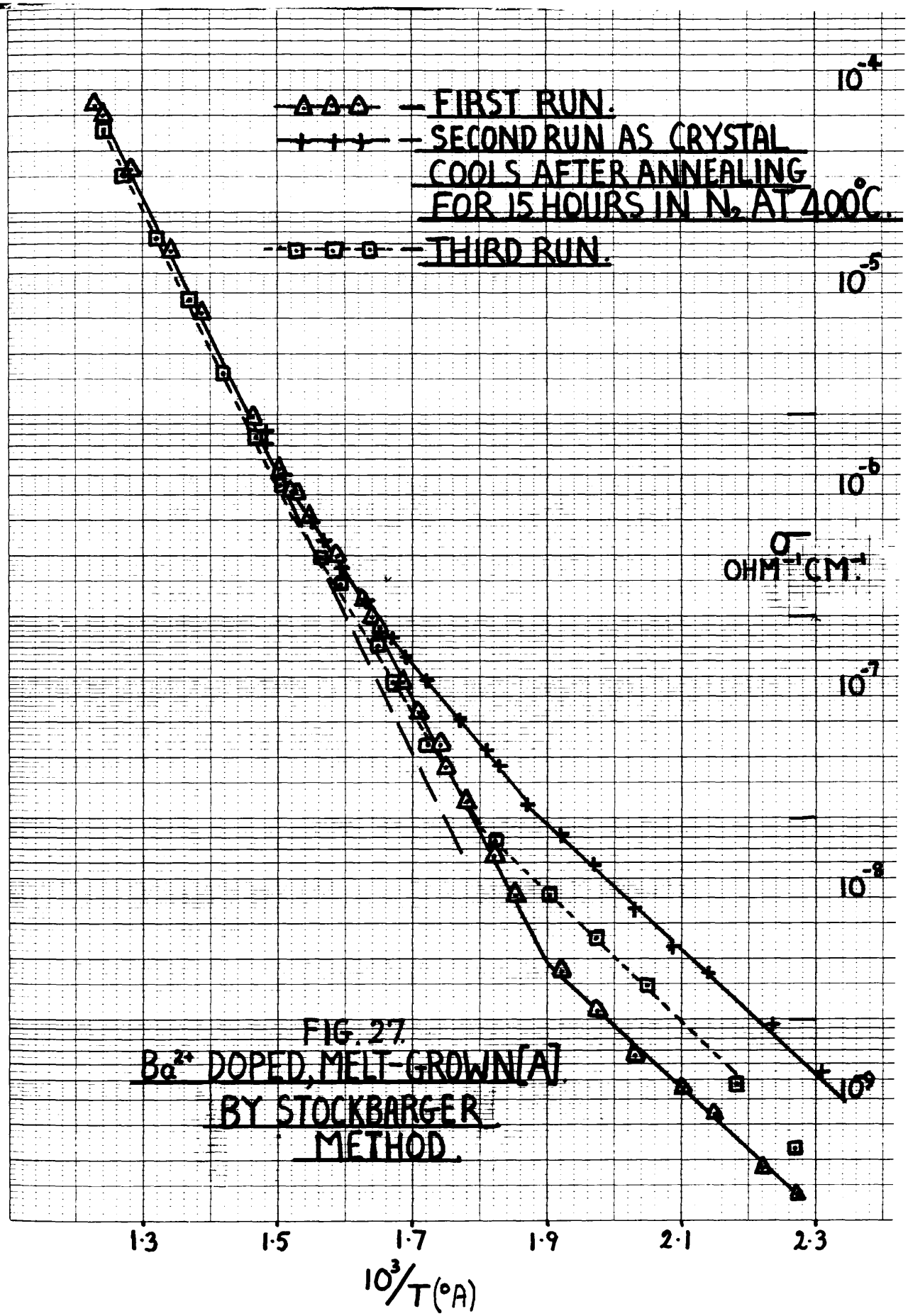

FIG. 27.
Ba^{2+} DOPED, MELT-GROWN [A] BY STOCKBARGER METHOD.

TABLE 14 (Fig. 27)

Ba^{2+}-doped CsI, melt-grown by Stockbarger Method.

Specimen (A).

Pretreatment:- No pretreatment for first run, but left for 15 hours at 400°C in dry nitrogen atmosphere before second run.

	First Run (Heating)	Second Run (Cooling)	Third Run (Heating)
Range I (°C)	162-253	162-262	183-283
E_A(eV)	0.61	0.61	0.64
$\sigma_{2.0\ R.T.U.}(ohm^{-1}cm^{-1})$	9.0×10^{-9}	4.6×10^{-8}	2.0×10^{-8}
Temperature Range (°C)	-	262 -333	283-394
E_A(eV)	-	0.81	1.12
$\sigma_{1.7\ R.T.U.}(ohm^{-1}cm^{-1})$	-	5.8×10^{-7}	3.3×10^{-7}
Range I (a) (°C)	253-333	-	-
E_A(eV)	1.31	-	-
$\sigma_{1.7\ R.T.U.}(ohm^{-1}cm^{-1})$	3.9×10^{-7}	-	-
Range I (b) (°C)	333-389	333-400	-
E_A(eV)	1.00	1.00	-
$\sigma_{1.55\ R.T.U.}(ohm^{-1}cm^{-1})$	3.1×10^{-6}	3.1×10^{-6}	-
Range II (°C)	389-533	-	394-533
E_A(eV)	1.35	-	1.35
$\sigma_{1.4\ R.T.U.}(ohm^{-1}cm^{-1})$	2.4×10^{-5}	-	2.1×10^{-5}

Impurity Content of Crystal from same boule.

7.6×10^{-5} m.f. Ba.

4.8×10^{-5} m.f. Ca.

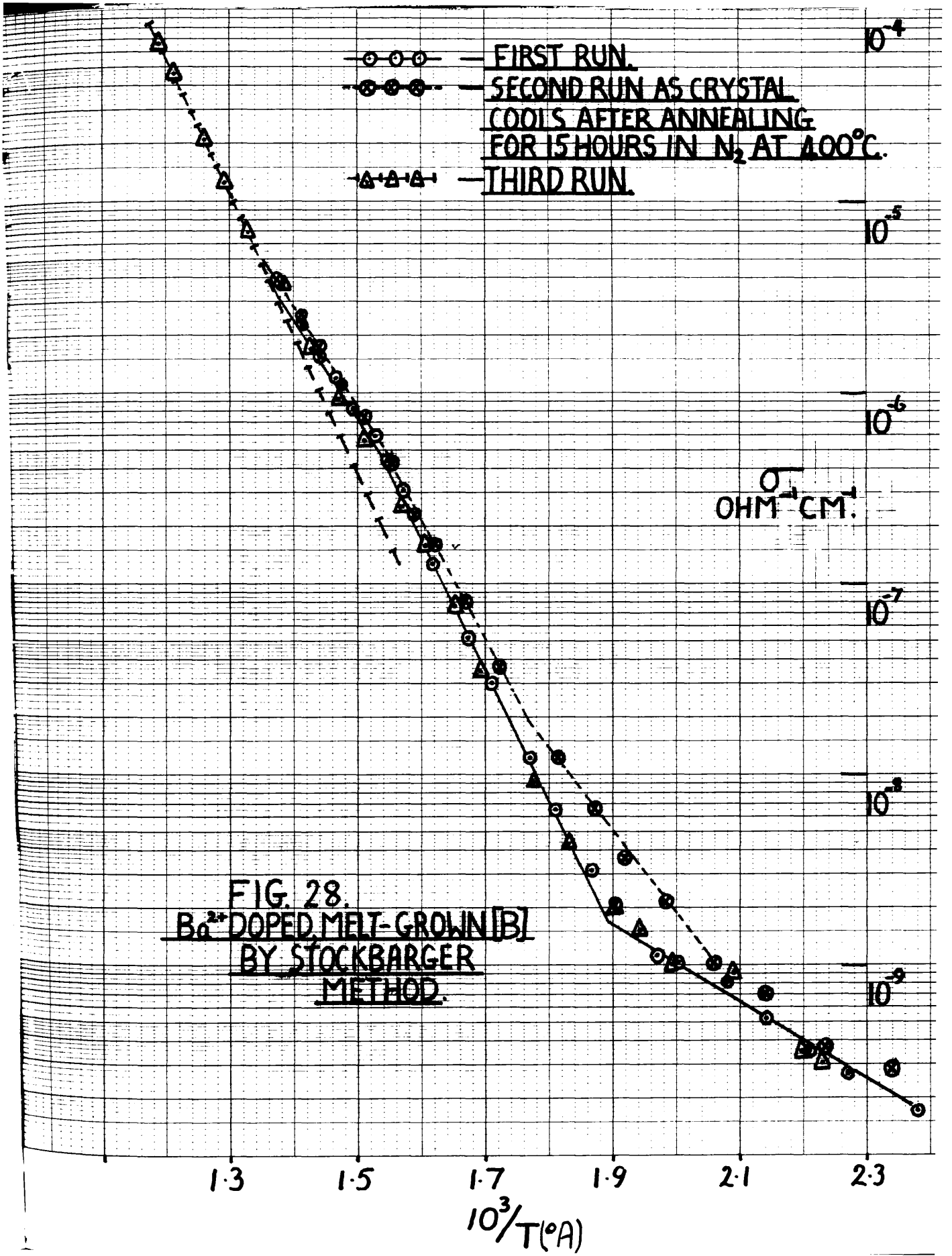

FIG. 28.
Ba^{2+} DOPED MELT-GROWN [B] BY STOCKBARGER METHOD.

TABLE 15 (Fig. 28)

Ba^{2+}-doped CsI, melt-grown by Stockbarger Method.

Specimen (B).

Pretreatment:- No pretreatment for first run, but left for 15 hours at 400°C in dry nitrogen before second run.

	First Run (Heating)	Second Run (Cooling)	Third Run (Heating)
Range I (°C)	147-256	295-213	< 256
E_A(eV)	0.42	0.85	-
$\sigma_{2.0\ R.T.U.}$($ohm^{-1}cm^{-1}$)	$1.0x10^{-8}$	$1.9x10^{-8}$	$1.0x10^{-8}$
Range I (a) (°C)	256-368	376-295	256-368
E_A(eV)	1.38	1.26	1.38
$\sigma_{1.7\ R.T.U.}$($ohm^{-1}cm^{-1}$)	$3.5x10^{-7}$	$5.0x10^{-7}$	$3.5x10^{-7}$
Range I (b) (°C)	368-421	457-376	368-467
E_A(eV)	0.99	1.01	0.99
$\sigma_{1.55\ R.T.U.}$($ohm^{-1}cm^{-1}$)	$4.8x10^{-6}$	$4.8x10^{-6}$	$4.2x10^{-6}$
Range II (°C)	-	-	467-575
E_A(eV)	-	-	1.42
$\sigma_{1.4\ R.T.U.}$($ohm^{-1}cm^{-1}$)	-	-	$2.4x10^{-5}$

Impurity Content.

5.7×10^{-5} m.f. Ba.
2.0×10^{-4} m.f. Cu.
1.4×10^{-5} m.f. Fe.

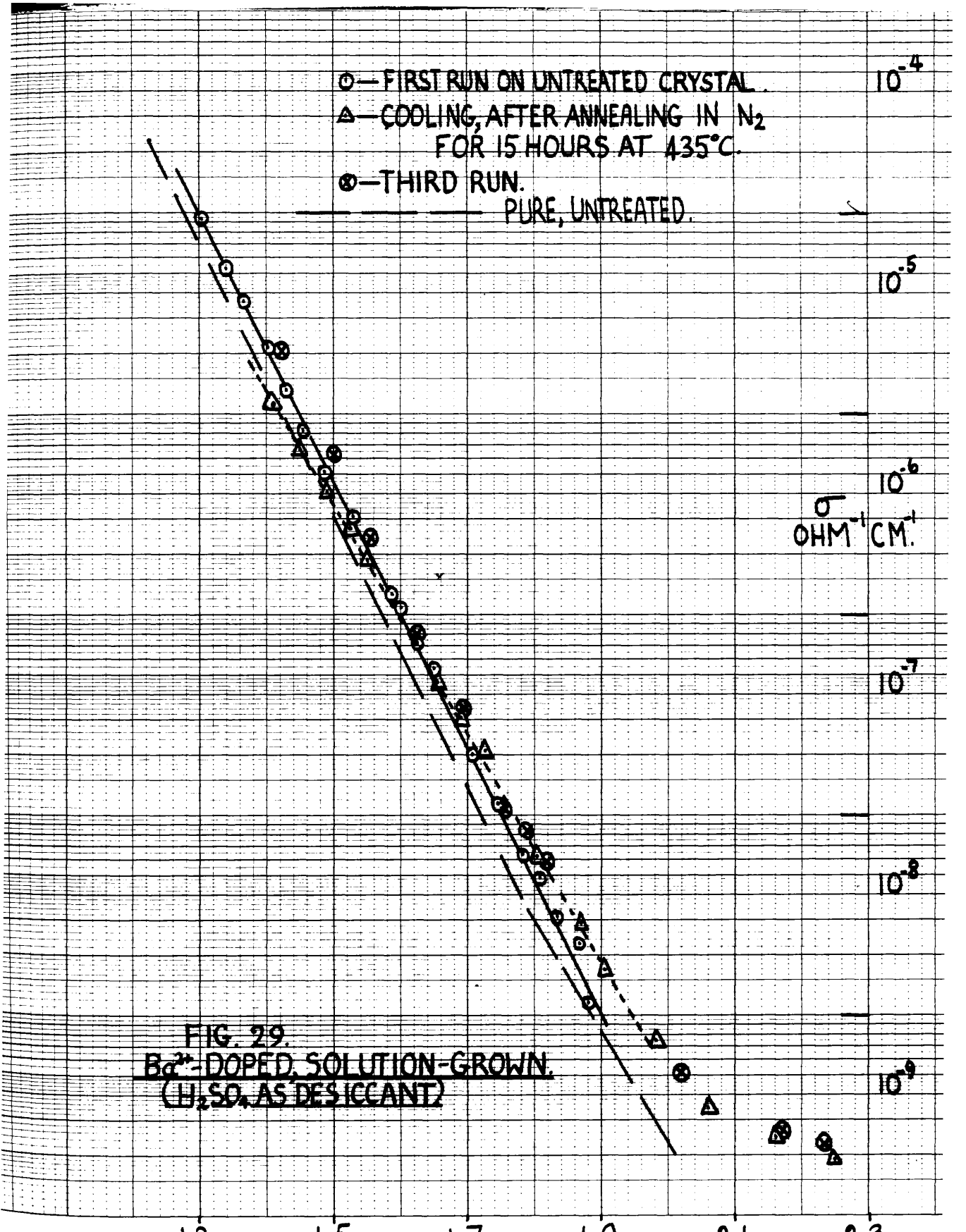

FIG. 29.
Ba^{2+}-DOPED, SOLUTION-GROWN.
(H_2SO_4 AS DESICCANT)

TABLE 16 (Fig.29)

Ba^{2+}-doped CsI, solution-grown (H_2SO_4 as desiccant).

Pretreatment:- First run untreated; second run, cooling after anneal in dry N_2 for 15 hours at 435°C.

	First Run (Heating).	Second Run (Cooling)	Third Run (Heating)
Range I (°C)	-	-	222-298
E_A(eV)	-	-	1.00
$\sigma_{2.0\ R.T.U.}$($ohm^{-1}cm^{-1}$)	-	-	5.0×10^{-9}
Temperature Range (°C)	-	253-435	-
E_A(eV)	-	1.15	-
$\sigma_{1.4\ R.T.U.}$($ohm^{-1}cm^{-1}$)	-	1.3×10^{-5}	-
Range (II) (°C)	253-496	-	298-431
E_A(eV)	1.34	-	1.36
$\sigma_{1.4\ R.T.U.}$($ohm^{-1}cm^{-1}$)	2.1×10^{-5}	-	2.7×10^{-5}

The second run on this crystal may be in error due to oxidation of the electrode paint during the anneal prior to the run.

Impurity Content (Grown from Hopkins and Williams CsI).

1.95×10^{-5} m.f. Ba.
4.6×10^{-5} m.f. Fe.

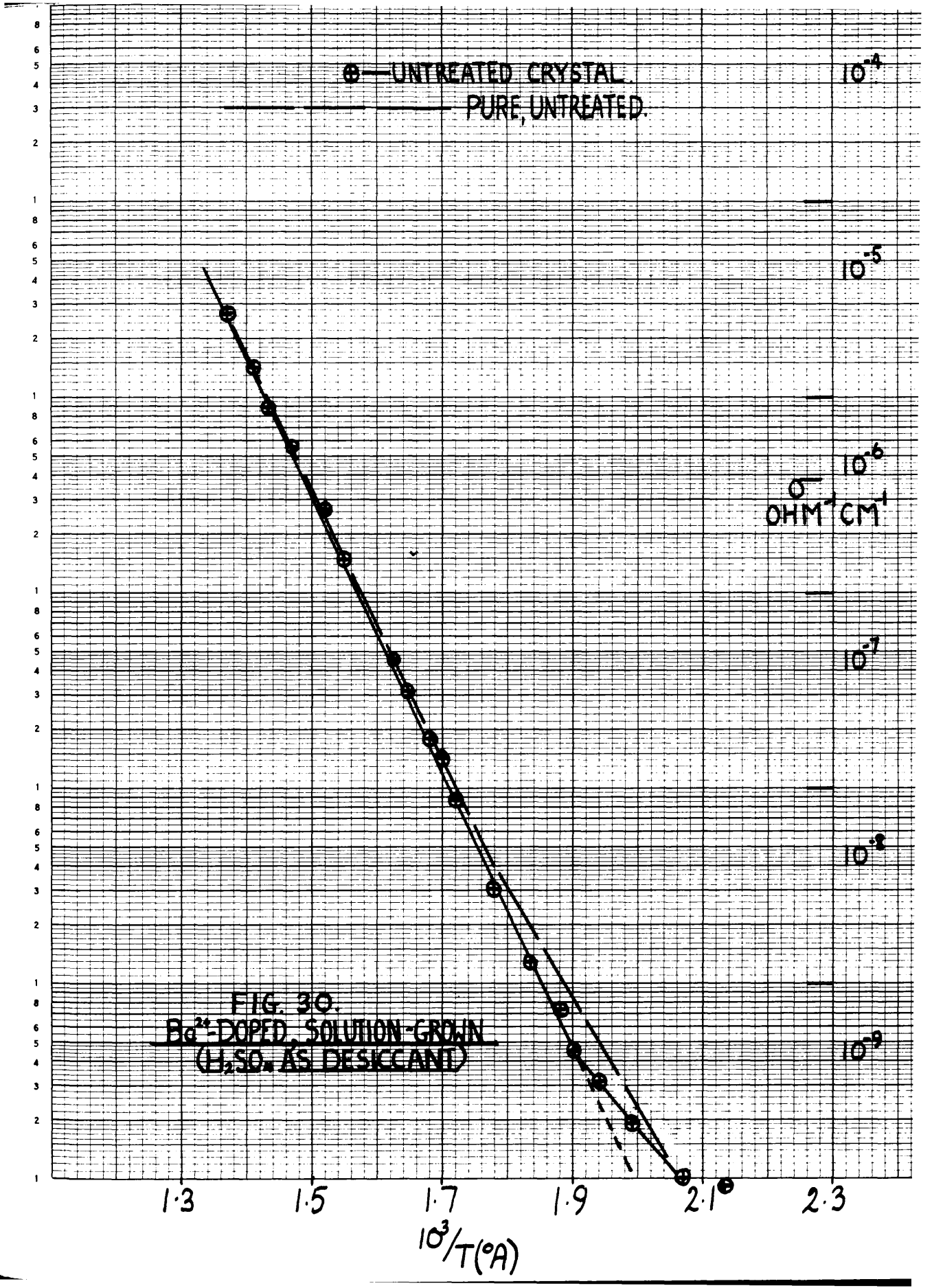

FIG. 30.
Ba^{2+}-DOPED, SOLUTION-GROWN (H_2SO_4 AS DESICCANT)

TABLE 17 (Fig.30)

Ba^{2+}-doped CsI, solution-grown (H_2SO_4 as desiccant).

PRETREATMENT:- Untreated apart from vacuum drying.

	First Run - Heating.
Range I (°C)	205–253
E_A(eV)	0.79
$\sigma_{2.0\ R.T.U.}$($ohm^{-1}cm^{-1}$)	1.8×10^{-9}
Range II (°C)	253–457
E_A(eV)	1.40
$\sigma_{1.4\ R.T.U.}$($ohm^{-1}cm^{-1}$)	1.55×10^{-5}

Impurity Content - Unknown.

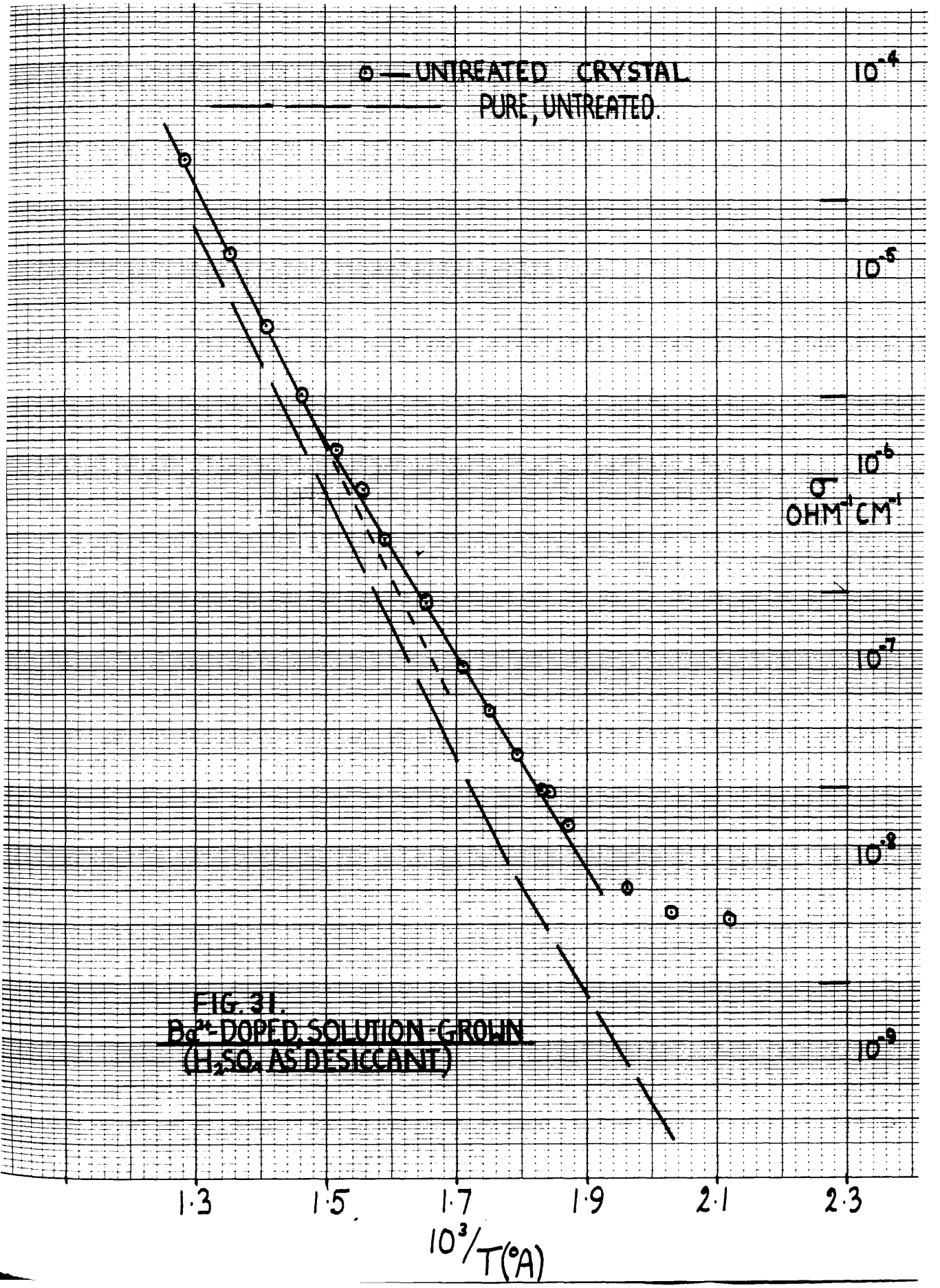

FIG. 31.
Pb^{2+}-DOPED, SOLUTION-GROWN
(H_2SO_4 AS DESICCANT)

TABLE 18 (Fig. 31)

Ba^{2+}-doped CsI, solution-grown (H_2SO_4 as desiccant).

Pretreatment:- Untreated, apart from being vacuum dried.

	First Run - Heating.
Range I (°C)	253-402
E_A(eV)	1.09
$\sigma_{2.0\ R.T.U.}$($ohm^{-1}cm^{-1}$)	1.2×10^{-8}
Range II (°C)	402-508
E_A(eV)	1.34
$\sigma_{1.4.\ R.T.U.}$($ohm^{-1}cm^{-1}$)	2.5×10^{-5}

Impurity Content - Unknown.

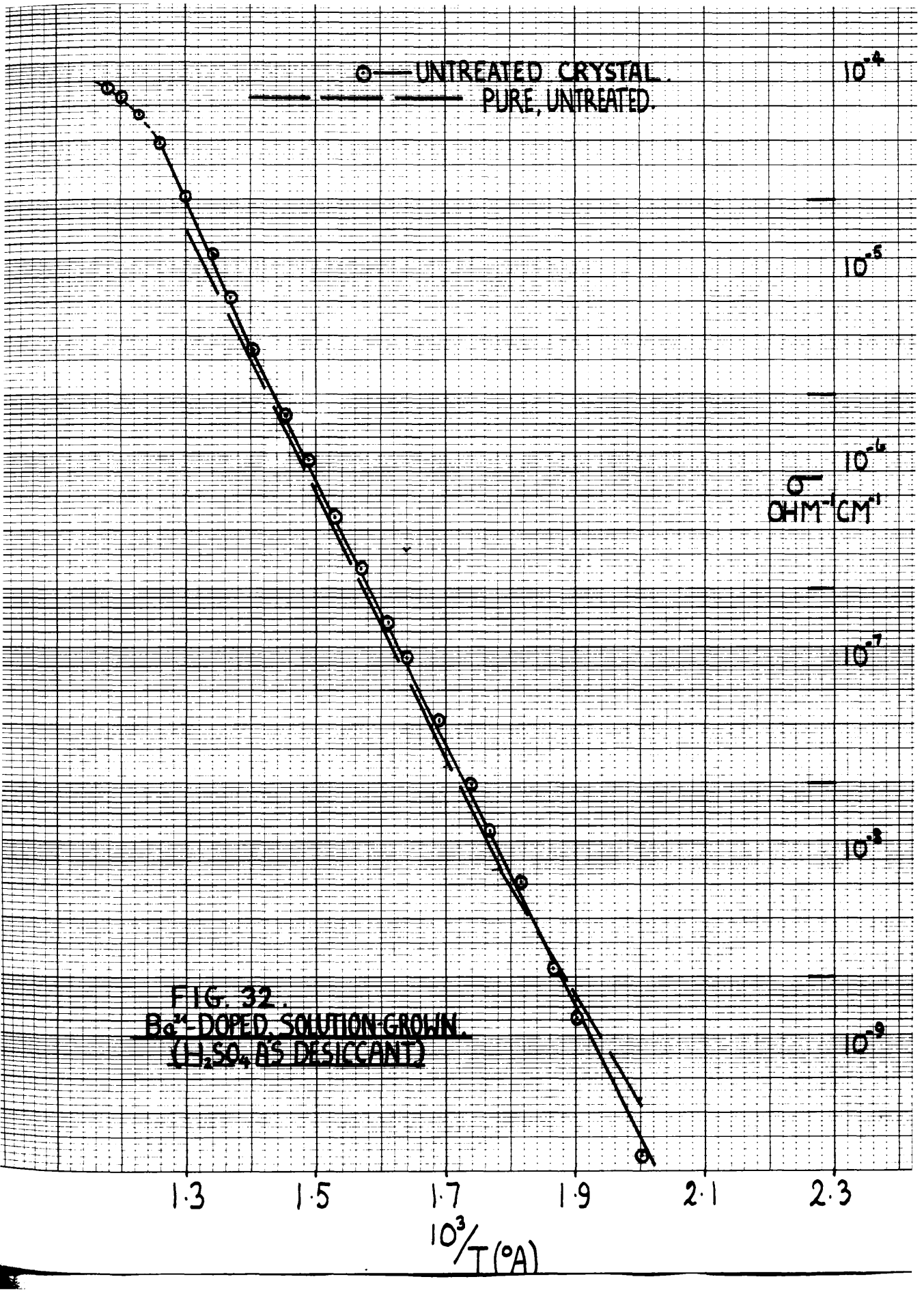

FIG. 32.
Ba^{++}-DOPED, SOLUTION-GROWN.
(H_2SO_4 AS DESICCANT)

TABLE 19 (Fig.32)

Ba^{2+}-doped CsI, solution-grown (H_2SO_4 as desiccant).

Pretreatment:- Untreated, apart from being vacuum dried.

First Run - Heating.

Range II (°C)	222-442
E_A(eV)	1.36
$\sigma_{1.4\ R.T.U.}$ ($ohm^{-1}cm^{-1}$)	1.7×10^{-5}
Range III (°C)	442-521
E_A(eV)	1.56
$\sigma_{1.25\ R.T.U.}$ ($ohm^{-1}cm^{-1}$)	2.3×10^{-4}

Impurity Content (Grown from Hopkins and Williams CsI).

5.7×10^{-4} m.f. Ba.

1.95×10^{-5} m.f. Cu.

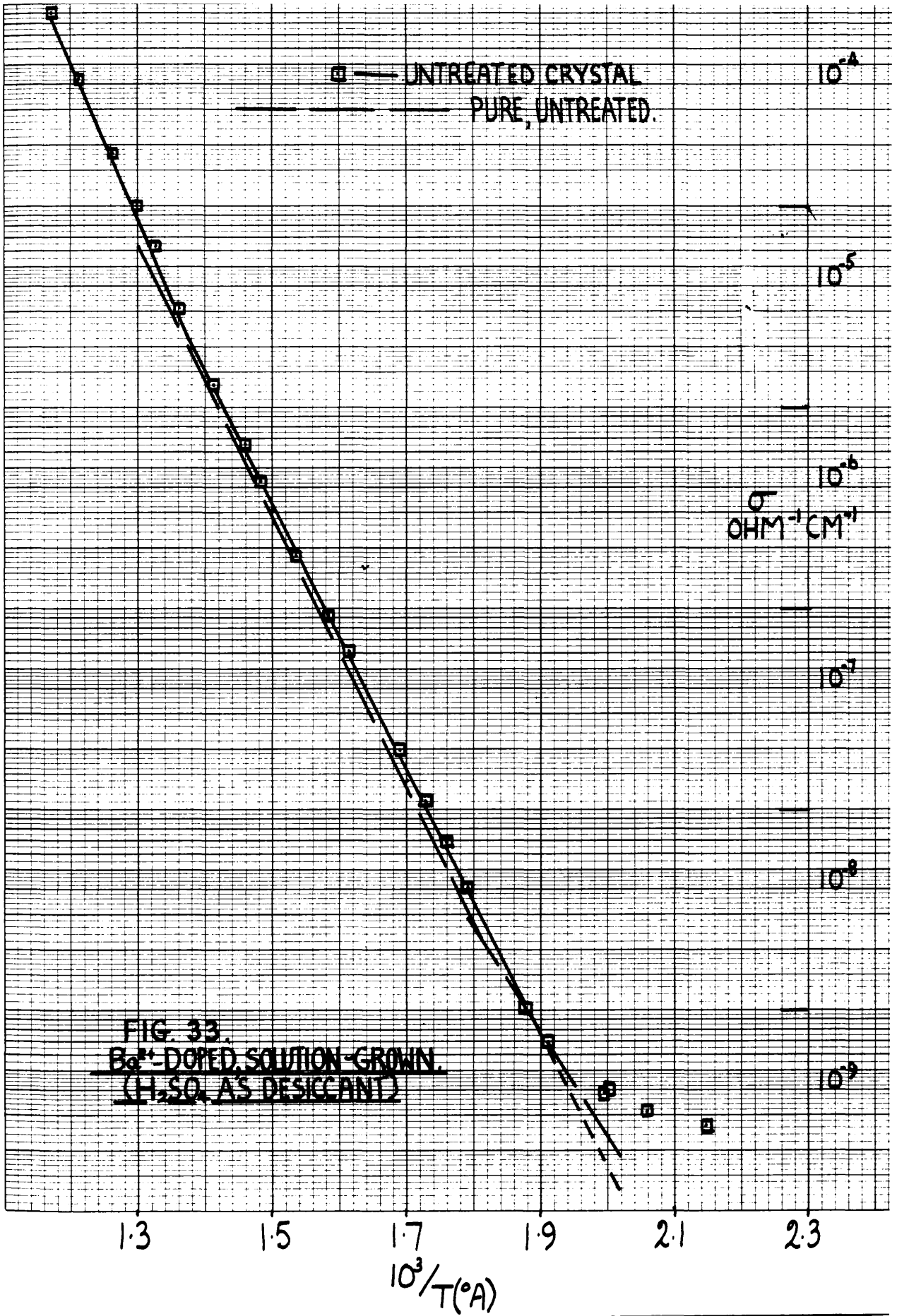

FIG. 33.
Be^{2+}-DOPED, SOLUTION-GROWN.
(H_2SO_4 AS DESICCANT)

TABLE 20 (Fig. 33)

Ba^{2+}-doped CsI, solution-grown (H_2SO_4 as desiccant).

Pretreatment:- Untreated, apart from being vacuum dried.

	First Run - Heating.
Range II (°C)	248-457
E_A(eV)	1.33
$\sigma_{1.4\ R.T.U.}$($ohm^{-1}cm^{-1}$)	1.5×10^{-5}
Range III (°C)	457-582
E_A(eV)	1.57
$\sigma_{1.25\ R.T.U.}$($ohm^{-1}cm^{-1}$)	2.1×10^{-4}

Impurity Content (Grown from Hopkins and Williams CsI).

1.9×10^{-4} m.f. Ba.

6.5×10^{-5} m.f. Ca.

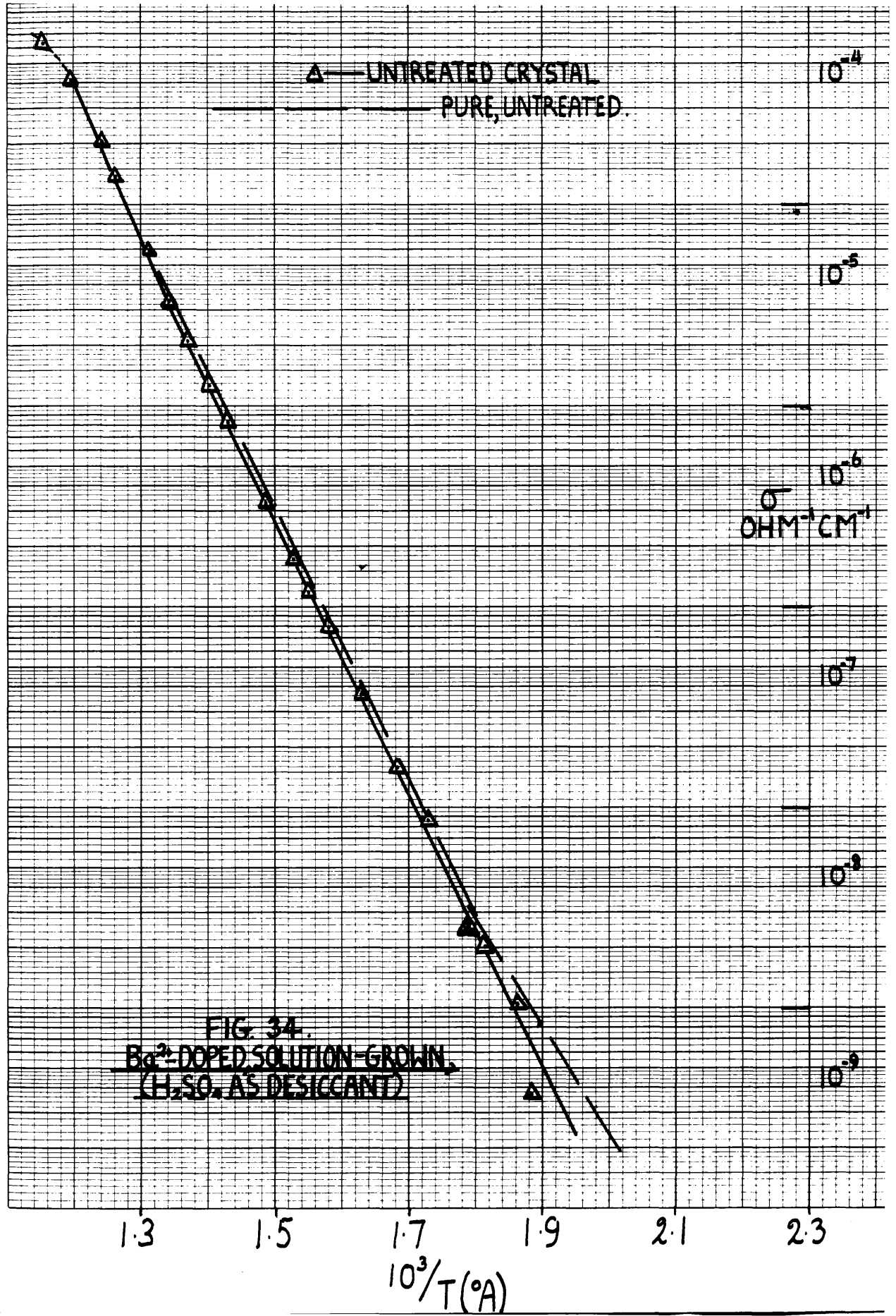

FIG. 34.
Ba^{2+}-DOPED SOLUTION-GROWN
(H_2SO_4 AS DESICCANT)

TABLE 21 (Fig. 34)

Ba^{2+}-doped CsI, solution-grown (H_2SO_4 as desiccant).

Pretreatment:- Untreated, apart from being vacuum dried.

	First Run - Heating.
Range II (°C)	253-473
E_A(eV)	1.35
$\sigma_{1.4\ R.T.U.}$(ohm^{-1}cm^{-1})	1.3×10^{-5}
Range III (°C)	473-560
E_A(eV)	1.55
$\sigma_{1.25\ R.T.U.}$(ohm^{-1}cm^{-1})	1.65×10^{-4}

Impurity Content (Grown from Hopkins and Williams CsI).

1.9×10^{-3} m.f. Ba.

3.3×10^{-5} m.f. Ca.

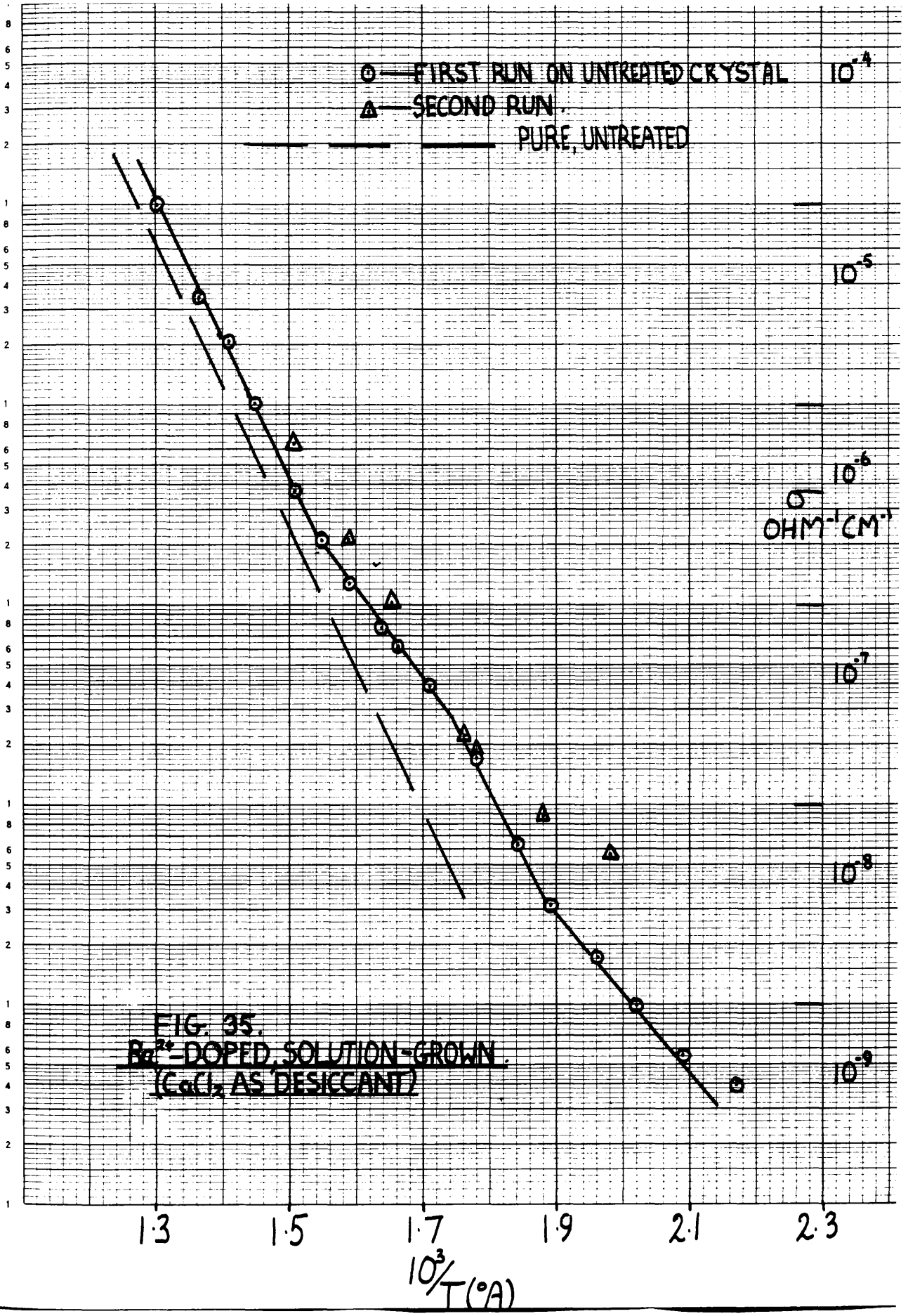

FIG. 35.
Ba^{2+}-DOPED, SOLUTION-GROWN.
($CaCl_2$ AS DESICCANT)

TABLE 22 (Fig. 35)

Ba^{2+}-doped CsI, solution-grown ($CaCl_2$ as desiccant).

Pretreatment:- Untreated, apart from being vacuum dried.

First Run - Heating.

Range I (°C)	203-256
E_A(eV)	0.78
$\sigma_{2.0\ R.T.U.}$ ($ohm^{-1}cm^{-1}$)	1.1×10^{-8}
Range I (a) (°C)	256-299
E_A(eV)	1.28
$\sigma_{1.7\ R.T.U.}$ ($ohm^{-1}cm^{-1}$) estimated.	5.6×10^{-7}
Range I (b) (°C)	299-376
E_A(eV)	0.89
$\sigma_{1.55\ R.T.U.}$ ($ohm^{-1}cm^{-1}$)	2.0×10^{-6}
Range II (°C)	376-496
E_A(eV)	1.40
$\sigma_{1.4\ R.T.U.}$ ($ohm^{-1}cm^{-1}$)	2.2×10^{-5}

Impurity Content (Grown from B.D.H. Ltd. CsI).

1.9×10^{-4} m.f. Ba.

5.94×10^{-4} m.f. Sr.

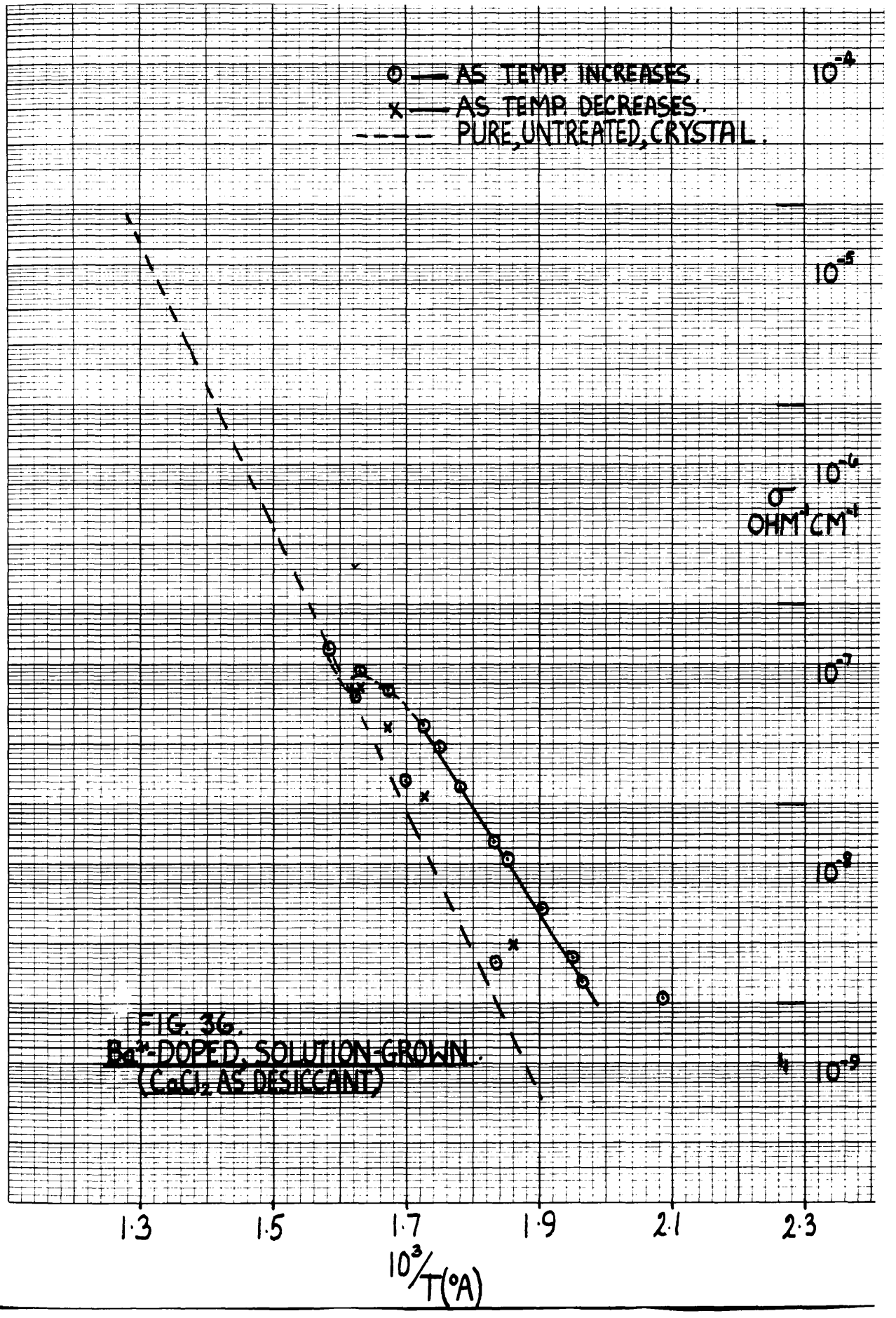

FIG. 36.
Ba^{++}-DOPED, SOLUTION-GROWN.
($CaCl_2$ AS DESICCANT)

TABLE 23 (Fig.36)

Ba^{2+}-doped CsI, solution-grown ($CaCl_2$ as desiccant).

Pretreatment:- Untreated, apart from being vacuum dried.

	First Run - Heating.
Range I (°C)	232-315
E_A(eV)	1.06
$\sigma_{2.0\ R.T.U.}$($ohm^{-1}cm^{-1}$)	8.8×10^{-9}

There was a maximum in the conductivity/temperature graph at 341°C.
The value of σ at the maximum was:

$$\sigma_{max.} = 4.5 \times 10^{-7}\ ohm^{-1}cm^{-1}.$$

Impurity Content (Grown from B.D.H. Ltd. CsI).

1.9×10^{-4} m.f. Ba.
2.97×10^{-4} m.f. Sr.

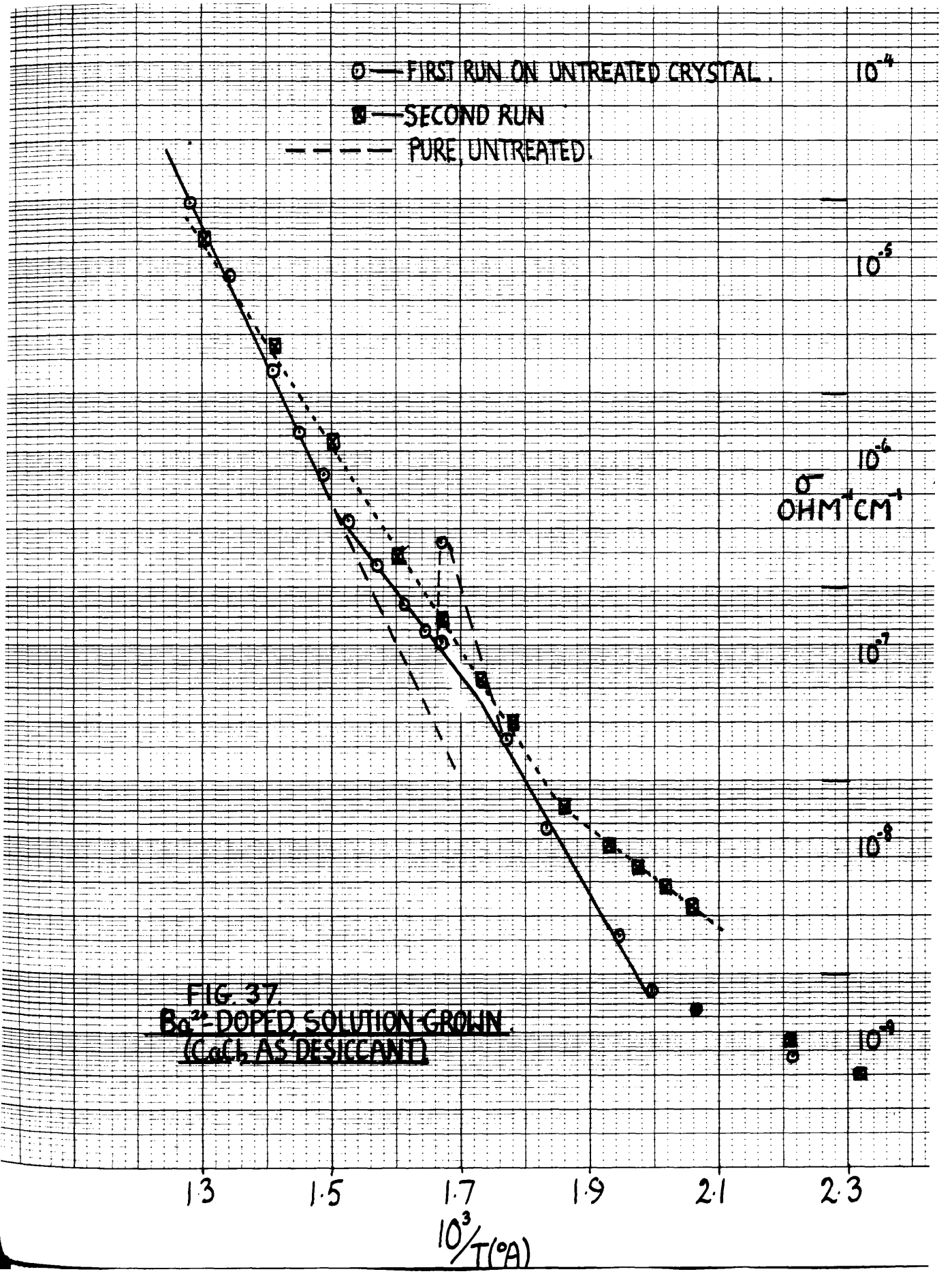

FIG. 37.
Ba^{2+}-DOPED, SOLUTION-GROWN.
($CaCl_2$ AS DESICCANT)

TABLE 24 (Fig. 37)

Ba^{2+}-doped CsI, solution-grown ($CaCl_2$ as desiccant).

Pretreatment:- Untreated, apart from being vacuum dried.

	First Run (Heating)	Second Run (Heating).
Range I (°C)	-	203-265
E_A(eV)	-	0.52
$\sigma_{2.0\ R.T.U.}$($ohm^{-1}cm^{-1}$)	-	3.1×10^{-8}
Range I (a) (°C)	229-308	-
E_A(eV)	1.18	-
$\sigma_{1.7\ R.T.U.}$($ohm^{-1}cm^{-1}$)	4.0×10^{-7}	-
Range I (b) (°C)	308-394	-
E_A(eV)	0.88	-
$\sigma_{1.55\ R.T.U.}$($ohm^{-1}cm^{-1}$)	1.55×10^{-6}	-
Temperature Range (°C)	-	265-497
E_A(eV)	-	1.05
$\sigma_{1.55\ R.T.U.}$($ohm^{-1}cm^{-1}$)	-	2.9×10^{-6}
Range II (°C)	394-502	-
E_A(eV)	1.40	-
$\sigma_{1.4\ R.T.U.}$($ohm^{-1}cm^{-1}$)	1.4×10^{-5}	-

Impurity Content (Grown from B.D.H. Ltd. CsI).

1.9×10^{-4} m.f. Ba.

2.97×10^{-4} m.f. Sr.

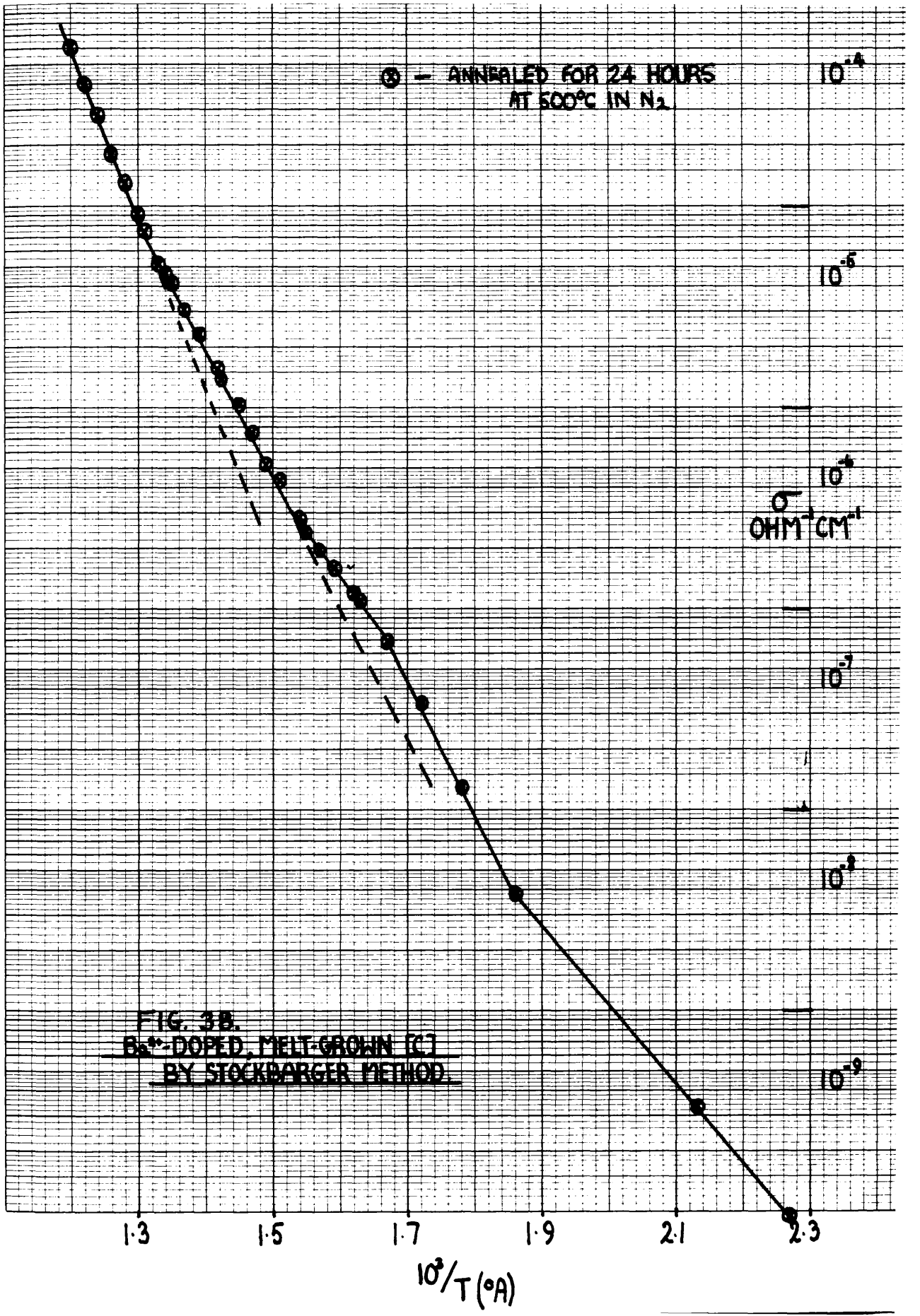

FIG. 3B.
B_{2}^{+}-DOPED, MELT-GROWN [C] BY STOCKBARGER METHOD.

TABLE 25 (Fig. 38)

Ba^{2+}-doped CsI, melt-grown by Stockbarger Method.

Specimen (C).

PRETREATMENT:- Annealed for 24 hours at 500°C in N_2.

	First Run - Heating.
Range I (°C)	168-265
E_A(eV)	0.80
$\sigma_{2.0\ R.T.U.}$($ohm^{-1}cm^{-1}$)	1.0×10^{-8}
Range I (a) (°C)	265-326
E_A(eV)	1.34
$\sigma_{1.7\ R.T.U.}$($ohm^{-1}cm^{-1}$)	4.3×10^{-7}
Range I (b) (°C)	326-376
E_A(eV)	0.90
$\sigma_{1.55\ R.T.U.}$($ohm^{-1}cm^{-1}$)	2.4×10^{-6}
Range II (°C)	376-496
E_A(eV)	1.26
$\sigma_{1.4\ R.T.U.}$($ohm^{-1}cm^{-1}$)	1.9×10^{-5}
Range III (°C)	496-560
E_A(eV)	1.73
$\sigma_{1.25\ R.T.U.}$($ohm^{-1}cm^{-1}$)	2.2×10^{-4}

Impurity Content.

1.9×10^{-4} m.f. Ba.
6.5×10^{-5} m.f. Ca.
2.0×10^{-4} m.f. Cu.
9.2×10^{-5} m.f. Fe.

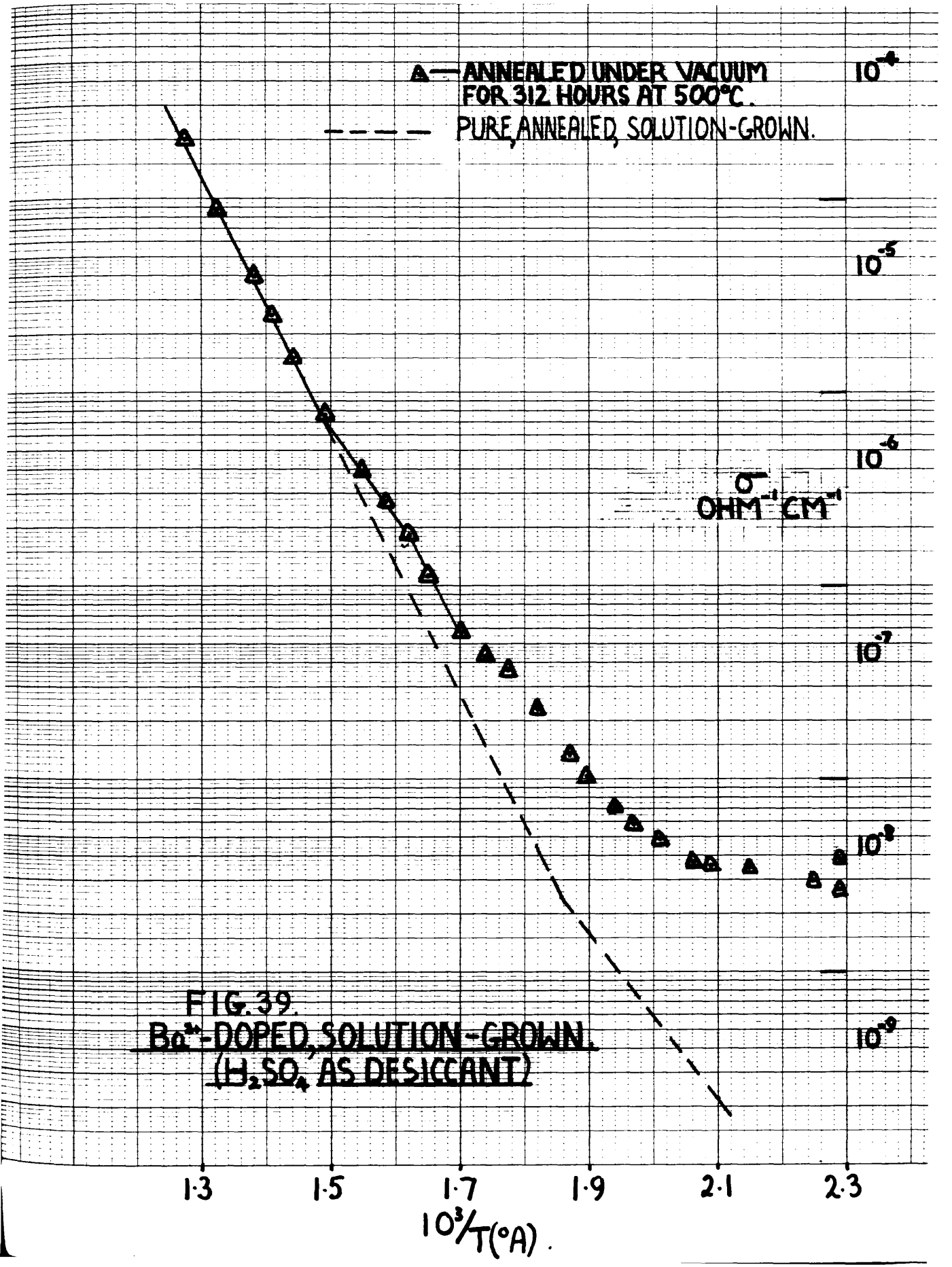

FIG. 39.
Ba^{2+}-DOPED, SOLUTION-GROWN. (H_2SO_4 AS DESICCANT)

TABLE 26 (Fig. 39)

Ba^{2+}-doped CsI, solution-grown (H_2SO_4 as desiccant).

Pretreatment:- Annealed under vacuum for 312 hours at 500°C.

First Run - Heating.

Range I (°C)	160-315
E_A(eV)	curved
$\sigma_{2.0\ R.T.U.}$($ohm^{-1}cm^{-1}$)	5.0×10^{-8}
Range I (a) (°C)	315-344
E_A(eV)	1.28
$\sigma_{1.7\ R.T.U.}$($ohm^{-1}cm^{-1}$)	5.7×10^{-7}
Range I (b) (°C)	344-398
E_A(eV)	0.92
$\sigma_{1.55\ R.T.U.}$($ohm^{-1}cm^{-1}$)	3.9×10^{-6}
Range II (°C)	398-514
E_A(eV)	1.34
$\sigma_{1.4\ R.T.U.}$($ohm^{-1}cm^{-1}$)	2.8×10^{-5}

Impurity Content (Grown from Hopkins and Williams CsI).

3.8×10^{-4} m.f. Ba.
6.5×10^{-5} m.f. Ca.
8×10^{-6} m.f. Cu.
7.0×10^{-5} m.f. Fe.

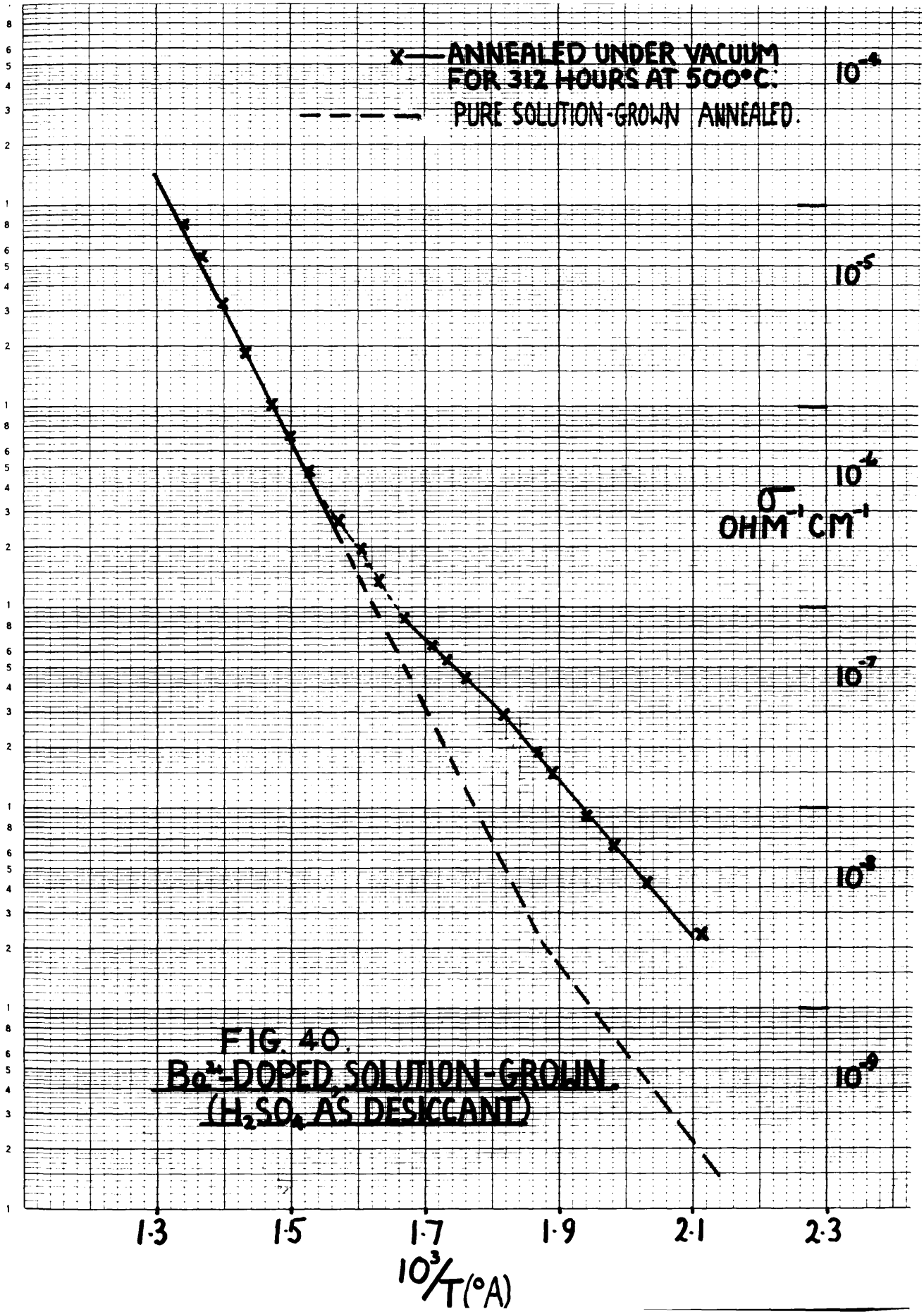

FIG. 40.
Ba^{++}-DOPED SOLUTION-GROWN
(H_2SO_4 AS DESICCANT)

TABLE 27 (Fig. 40)

Ba^{2+}-doped CsI, solution-grown (H_2SO_4 as desiccant).

Pretreatment:- Annealed under vacuum for 312 hours at 500°C.

First Run - Heating.

Range I (°C)	203-280
E_A(eV)	0.90
$\sigma_{2.0\ R.T.U.}$(ohm^{-1}cm^{-1})	5.5×10^{-8}
Temperature Range (°C)	280-326
E_A(eV)	0.64
$\sigma_{1.7\ R.T.U.}$(ohm^{-1}cm^{-1})	6.8×10^{-7}
Temperature Range (°C)	326-372
E_A(eV)	curved
Range II (°C)	372-473
E_A(eV)	1.33
$\sigma_{1.4\ R.T.U.}$(ohm^{-1}cm^{-1})	3.0×10^{-5}

Impurity Content (Grown from Hopkins and Williams CsI).

5.2×10^{-5} m.f. Ca.
2.05×10^{-5} m.f. Cu.
4.65×10^{-5} m.f. Fe.

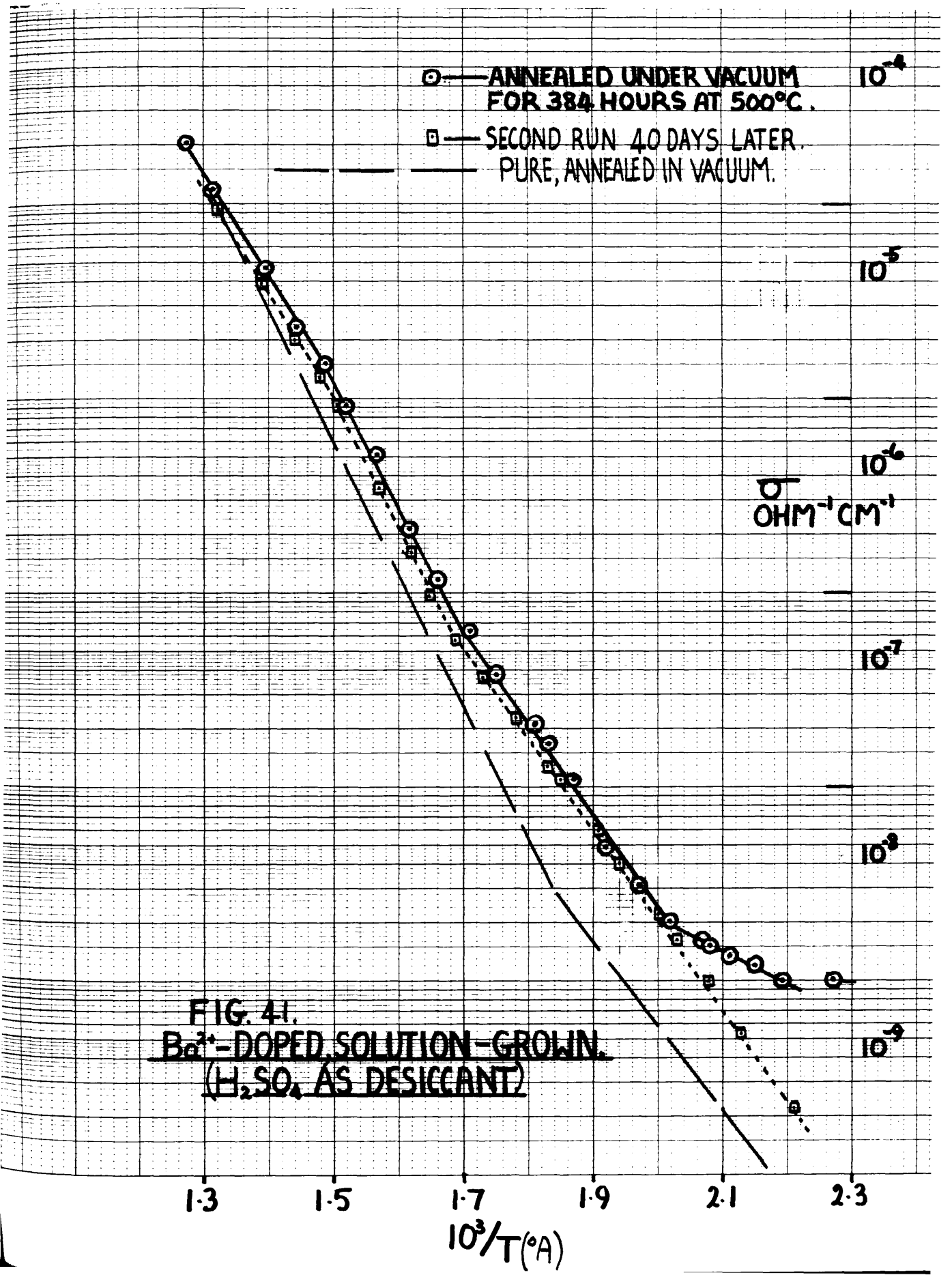

FIG. 41.
Ba^{2+}-DOPED, SOLUTION-GROWN.
(H_2SO_4 AS DESICCANT)

TABLE 28 (Fig. 41)

Ba^{2+}-doped CsI, solution-grown (H_2SO_4 as desiccant)

Pretreatment:- Annealed under vacuum for 384 hours at 500°C.

	First Run (Heating)	Second Run, 40 days later. (Heating)
Temperature Range (°C)	177-224	—
E_A(eV)	0.33	—
$\sigma_{2.2\ R.T.U.}$($ohm^{-1}cm^{-1}$)	8.5×10^{-9}	—
Range I (°C)	224-315	179-319
E_A(eV)	0.93	0.93
$\sigma_{2.0\ R.T.U.}$($ohm^{-1}cm^{-1}$)	2.4×10^{-8}	2.1×10^{-8}
Range I (a) (°C)	315-398	319-394
E_A(eV)	1.30	1.32
$\sigma_{1.7\ R.T.U.}$($ohm^{-1}cm^{-1}$)	6.0×10^{-7}	5.0×10^{-7}
Range I (b) (°C)	398-514	394-496
E_A(eV)	1.07	1.06
$\sigma_{1.55\ R.T.U.}$($ohm^{-1}cm^{-1}$)	7.5×10^{-6}	6.0×10^{-6}

Impurity Content (Grown from B.D.H. Ltd. CsI).

1.9×10^{-4} m.f. Ba.
5.94×10^{-4} m.f. Sr.
2.0×10^{-5} m.f. Ca.
4.1×10^{-5} m.f. Cu.
4.65×10^{-5} m.f. Fe.

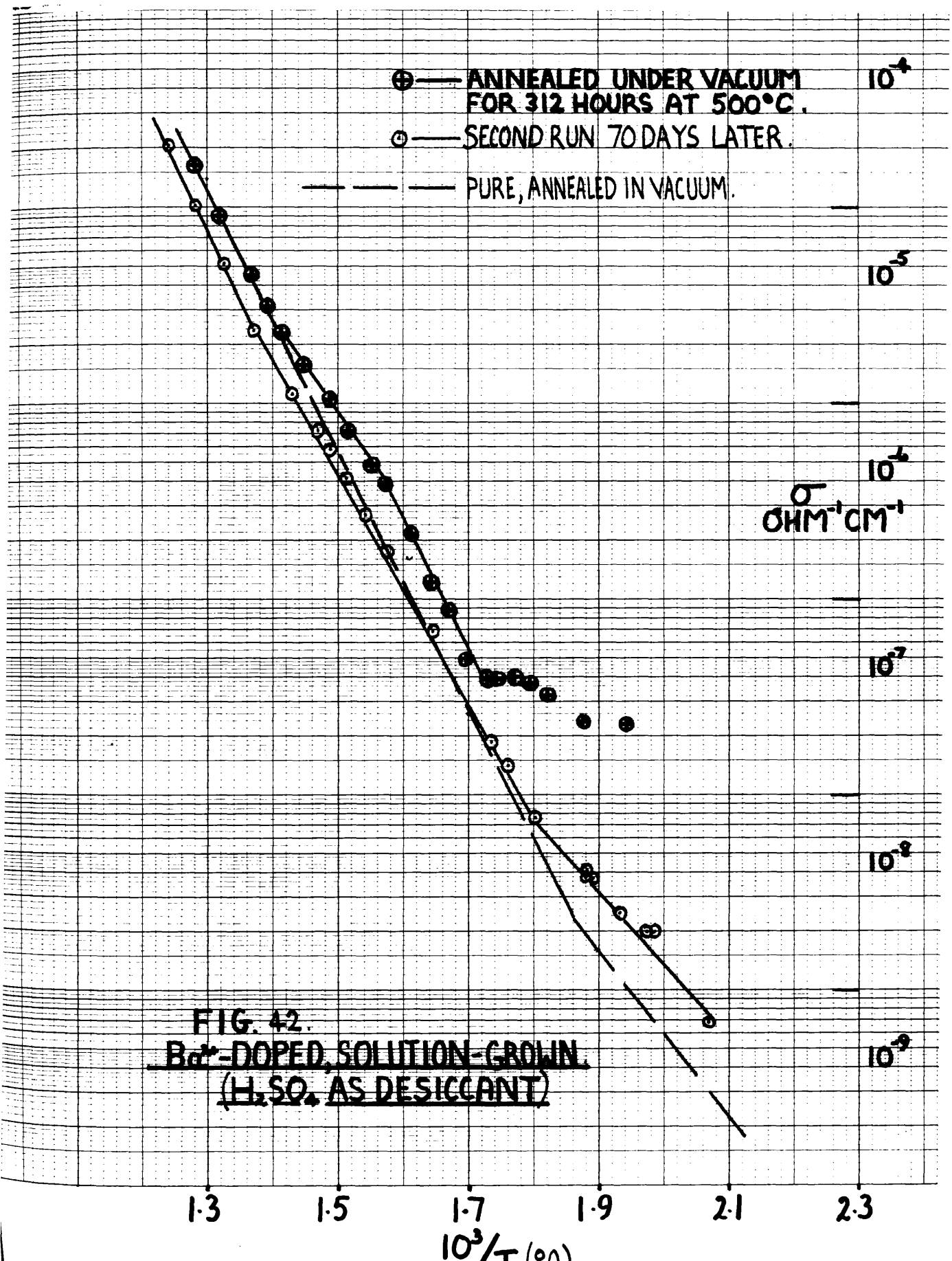

FIG. 42.
Ba^{++}-DOPED, SOLUTION-GROWN.
(H_2SO_4 AS DESICCANT)

TABLE 29 (Fig.42).

Ba^{2+}-doped CsI, solution-grown. (H_2SO_4 as desiccant).

Pretreatment:- Annealed in vacuum for 312 hours at 500°C.

	First Run (Heating)	Second Run, 70 days later (Heating).
Range I (°C)	<305	208-283
E_A(eV)	curved	0.75
$\sigma_{2.0.\ R.T.U.}$($ohm^{-1}cm^{-1}$)	-	1.35×10^{-8}
Temperature Range (°C)	-	283-457
E_A(eV)	-	1.18
$\sigma_{1.7\ R.T.U.}$($ohm^{-1}cm^{-1}$)	-	2.8×10^{-7}
Range I (a) (°C)	305-360	-
E_A(eV)	1.33	-
$\sigma_{1.7\ R.T.U.}$($ohm^{-1}cm^{-1}$)	5.5×10^{-7}	-
Range I (b) (°C)	360-436	-
E_A(eV)	0.96	-
$\sigma_{1.55\ R.T.U.}$($ohm^{-1}cm^{-1}$)	5.3×10^{-6}	-
Range II (°C)	436-508	457-533
E_A(eV)	1.32	1.41
$\sigma_{1.4\ R.T.U.}$($ohm^{-1}cm^{-1}$)	2.6×10^{-5}	1.5×10^{-5}

Impurity Content (Grown from Hopkins and Williams CsI).

1.9×10^{-4} m.f. Ba.
1.95×10^{-5} m.f. Ca.
4.1×10^{-5} m.f. Cu.
9.3×10^{-5} m.f. Fe.

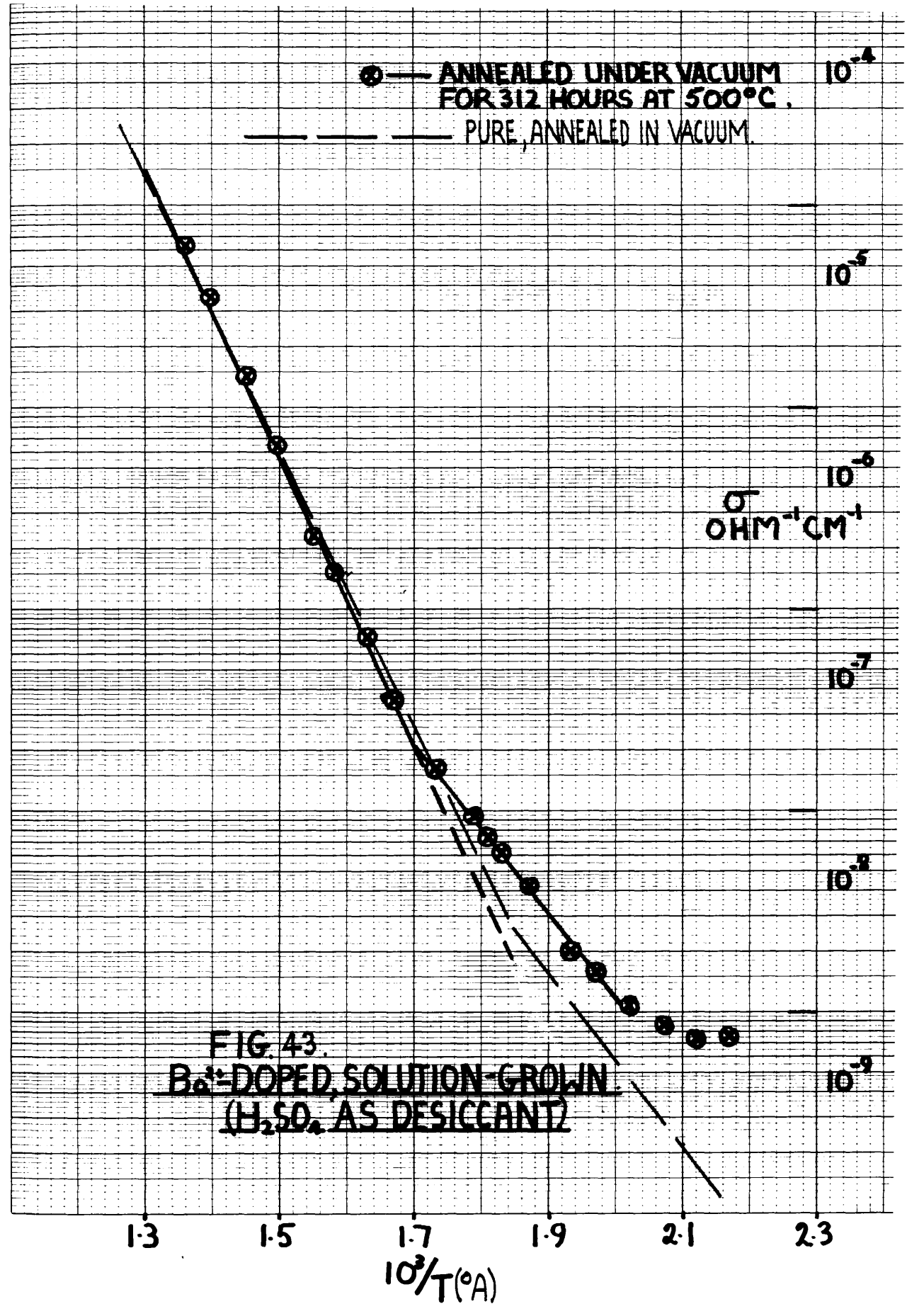

FIG. 43.
B_2^{3+}-DOPED, SOLUTION-GROWN
(H_2SO_4 AS DESICCANT)

TABLE 30 (Fig. 43)

Ba^{2+}-doped CsI, solution-grown (H_2SO_4 as desiccant).

Pretreatment:- Annealed under vacuum for 312 hours at 500°C.

	First Run - Heating.
Range I (°C)	222-315
E_A(eV)	0.85
$\sigma_{2.0\ R.T.U.}$ ($ohm^{-1}cm^{-1}$)	1.15×10^{-8}
Range II (°C)	315-462
E_A(eV)	1.43
$\sigma_{1.4\ R.T.U.}$ ($ohm^{-1}cm^{-1}$)	2.8×10^{-5}

Impurity Content (Grown from Hopkins and Williams CsI).

5.2×10^{-5} m.f. Ca.
2.05×10^{-5} m.f. Cu.
1.86×10^{-4} m.f. Fe.

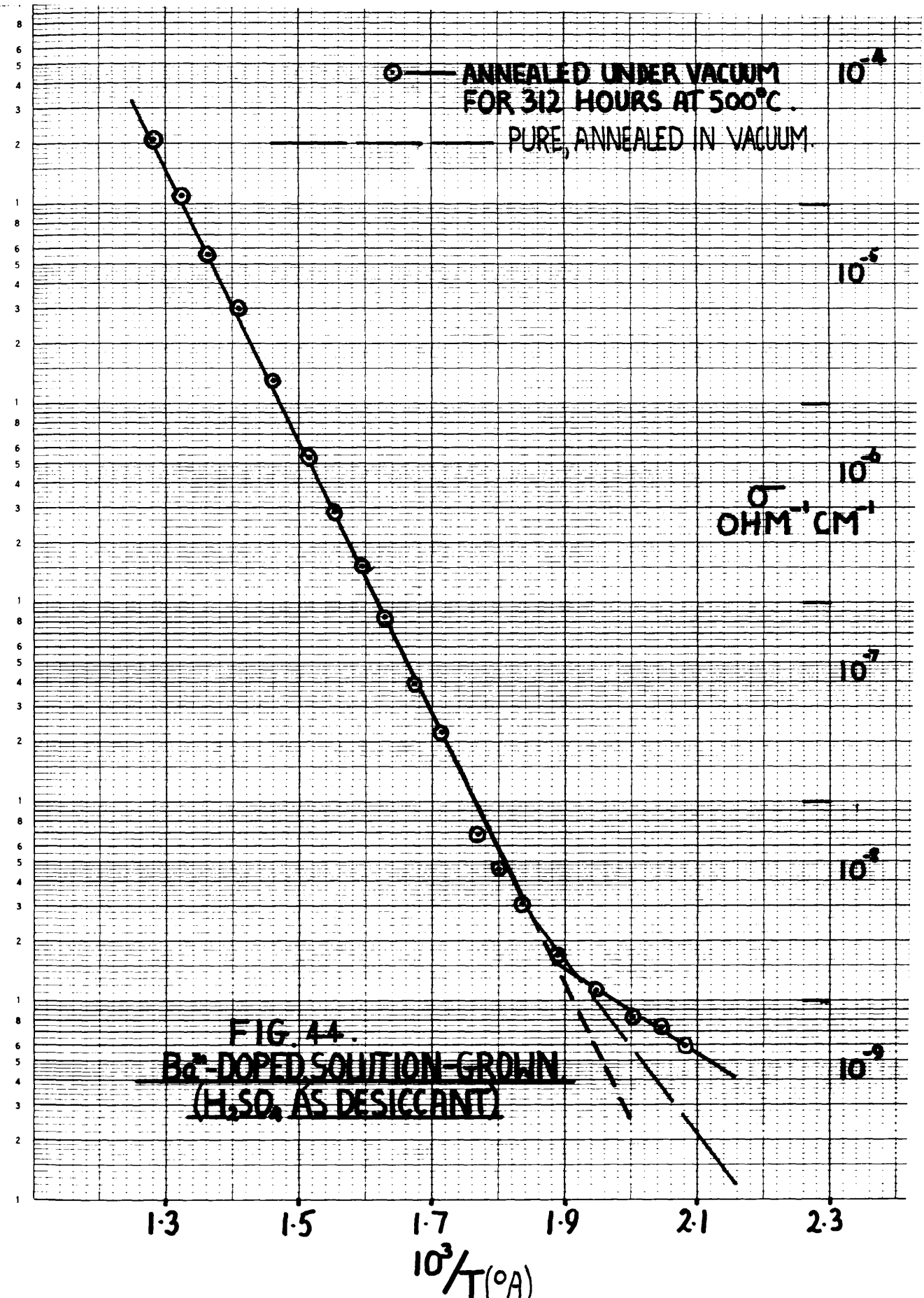

FIG. 4.4.
Ba^{++}-DOPED SOLUTION-GROWN
(H_2SO_4 AS DESICCANT)

TABLE 31 (Fig. 44)

Ba^{2+}-doped CsI, solution-grown (H_2SO_4 as desiccant).

Pretreatment:- Annealed under vacuum for 312 hours at 500°C.

First Run - Heating.

Range I (°C)	208-259
E_A(eV)	0.43
$\sigma_{2.0\ R.T.U.}$ ($ohm^{-1}cm^{-1}$)	8.9×10^{-9}
Range II (°C)	259-508
E_A(eV)	1.35
$\sigma_{1.4\ R.T.U.}$ ($ohm^{-1}cm^{-1}$)	3.0×10^{-5}

Impurity Content (Grown from Hopkins and Williams CsI).

$> 1 \times 10^{-3}$ m.f. Ba.

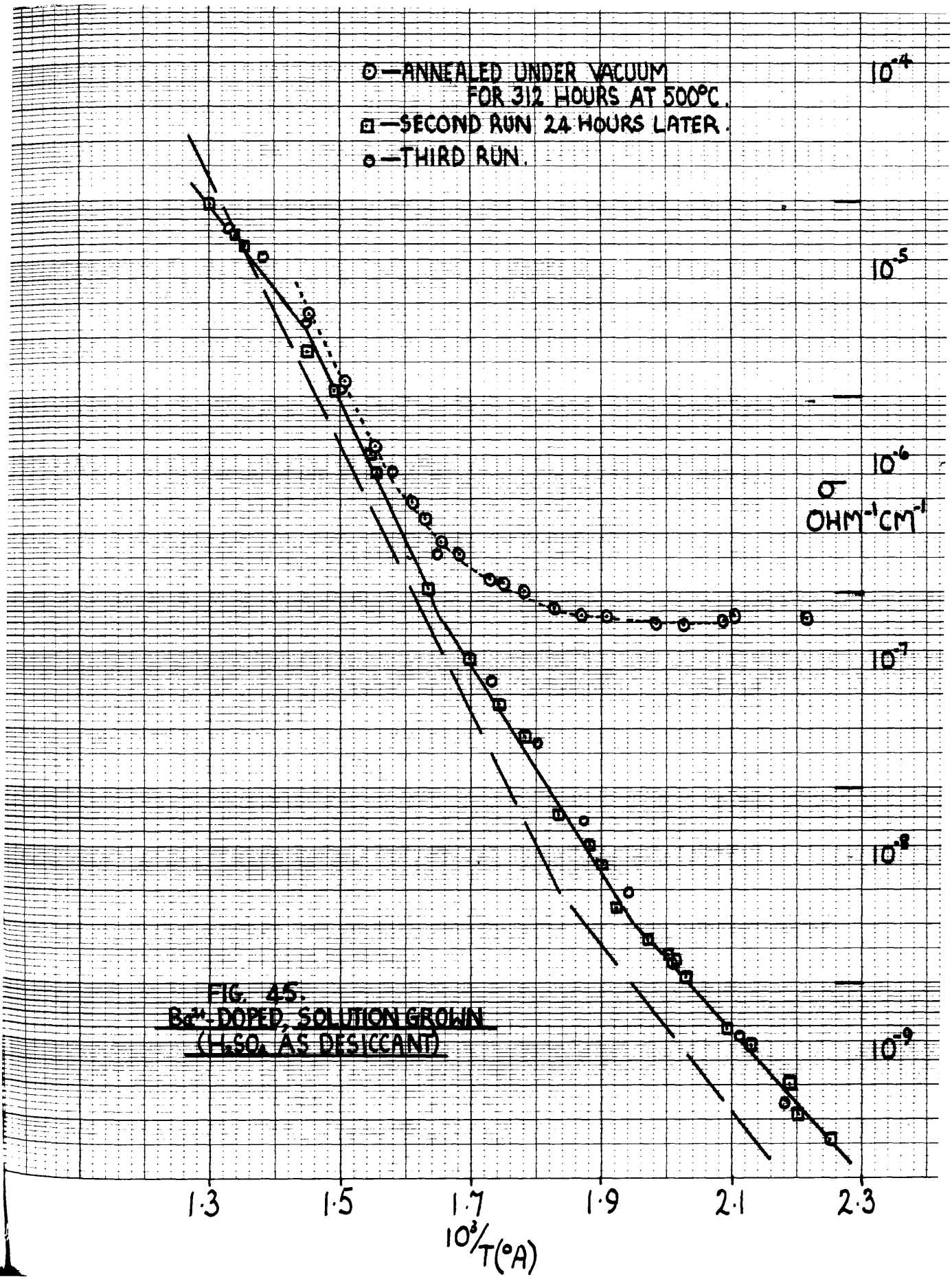

FIG. 45.
Ba⁺⁺-DOPED, SOLUTION GROWN
(H_2SO_4 AS DESICCANT)

TABLE 32 (Fig. 45)

Ba^{2+}-doped CsI, solution-grown (H_2SO_4 as desiccant).

Pretreatment:- Annealed under vacuum for 384 hours at 500°C.

	First Run (Heating)	Second Run, 24 hours later. (Heating).
Range I (°C)	177-360	162-240
E_A(eV)	curved	0.70
$\sigma_{2.0\ R.T.U.}$($ohm^{-1}cm^{-1}$)	7.0×10^{-7}	1.35×10^{-8}
Temperature Range (°C)	-	240-333
E_A(eV)	-	1.07
$\sigma_{1.7\ R.T.U.}$($ohm^{-1}cm^{-1}$)	-	4.2×10^{-7}
Range I (a) (°C)	360-417	333-417
E_A(eV)	1.34	1.39
$\sigma_{1.7\ R.T.U.}$($ohm^{-1}cm^{-1}$) estimated.	5.5×10^{-7}	3.8×10^{-7}
Range I (b) (°C)	-	417-496
E_A(eV)	-	0.86
$\sigma_{1.55\ R.T.U.}$($ohm^{-1}cm^{-1}$) estimated.	-	8.0×10^{-6}

A third run on this crystal gave the same conduction as the second heating.

Impurity Content (Grown from B.D.H. Ltd. CsI).

9.5×10^{-4} m.f. Ba.
5.94×10^{-4} m.f. Sr.
1.3×10^{-5} m.f. Ca.
1.2×10^{-5} m.f. Cu.
2.3×10^{-5} m.f. Fe.

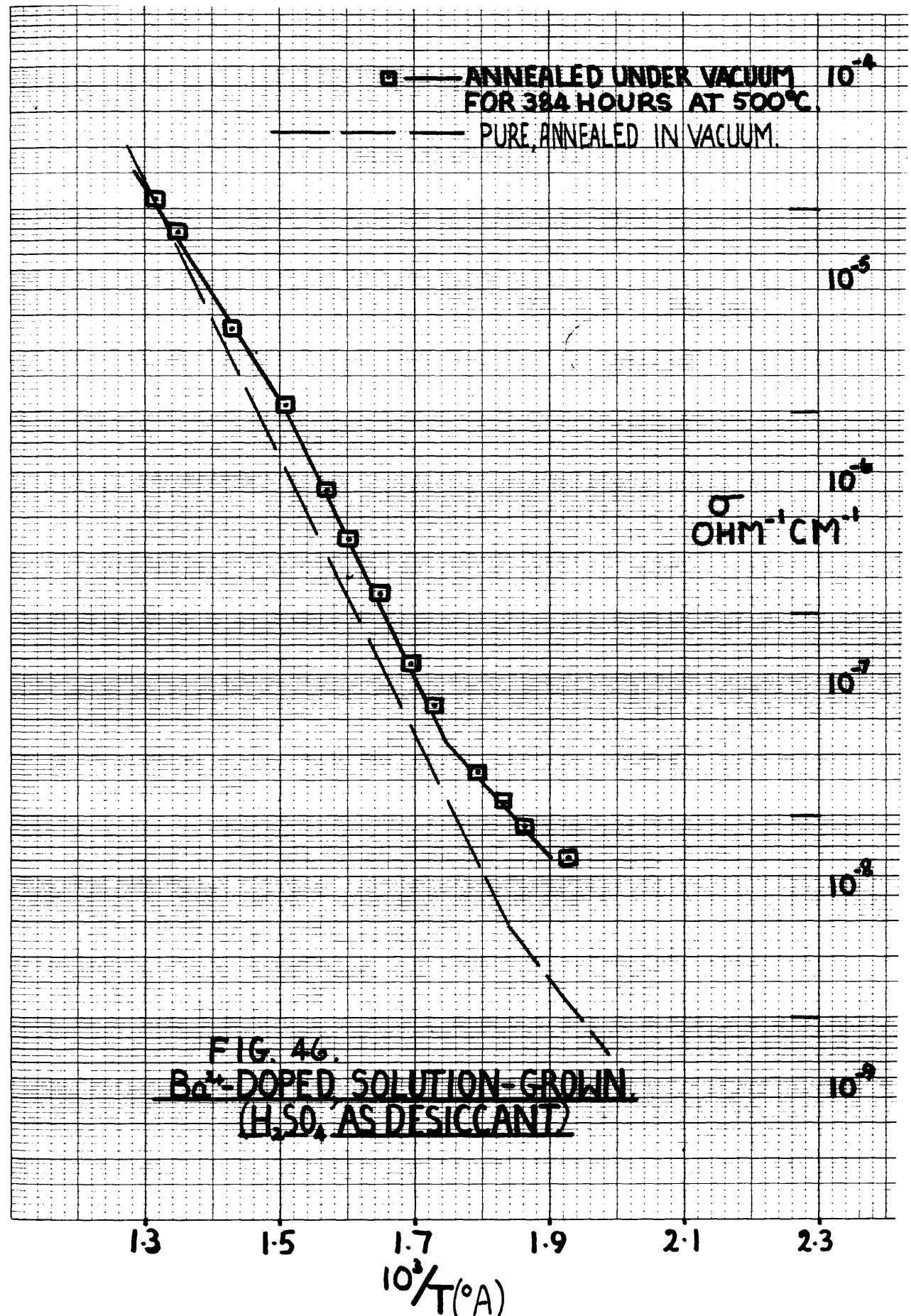

FIG. 46.
Ba^{++}-DOPED, SOLUTION-GROWN
(H_2SO_4 AS DESICCANT)

TABLE 33 (Fig. 46)

Ba^{2+}-doped CsI, solution-grown (H_2SO_4 as desiccant).

Pretreatment:- Annealed under vacuum for 384 hours at 500°C.

	First Run - Heating.
Range I (°C)	253-302
E_A(eV)	0.75
$\sigma_{2.0\ R.T.U.}$ ($ohm^{-1}cm^{-1}$) estimated.	2.6×10^{-8}
Range I (a) (°C)	302-394
E_A(eV)	1.38
$\sigma_{1.7\ R.T.U.}$ ($ohm^{-1}cm^{-1}$)	4.9×10^{-7}
Range I (b) (°C)	394-497
E_A(eV)	1.04
$\sigma_{1.55\ R.T.U.}$ ($ohm^{-1}cm^{-1}$) estimated.	6.5×10^{-6}

Impurity Content (Grown from B.D.H. Ltd. CsI).

5.7×10^{-4} m.f. Ba.
8.91×10^{-4} m.f. Sr.
1.9×10^{-5} m.f. Ca.
4.1×10^{-5} m.f. Cu.
4.65×10^{-5} m.f. Fe.

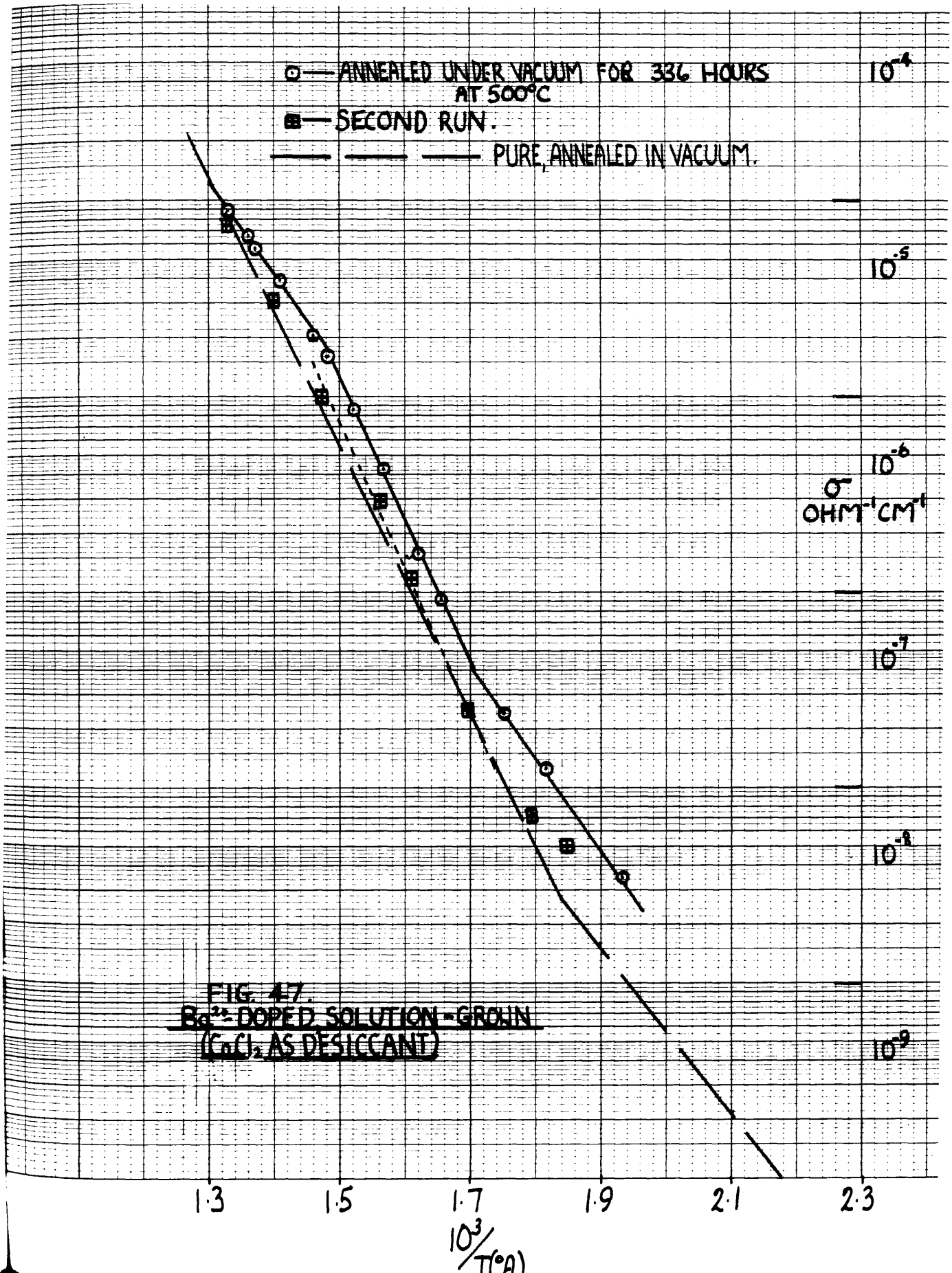

FIG. 47.
Ba^{2+}-DOPED SOLUTION-GROWN $CaCl_2$ (AS DESICCANT)

TABLE 34 (Fig. 47)

Ca^{2+}-doped CsI, solution-grown ($CaCl_2$ as desiccant).

Pretreatment:- Annealed under vacuum for 336 hours at 500°C.

First Run - Cooling.

Range I (°C)	242-315
E_A(eV)	0.93
$\sigma_{2.0\ R.T.U.}$($ohm^{-1}cm^{-1}$)	1.65×10^{-8}
Range I (a) (°C)	315-400
E_A(eV)	1.44
$\sigma_{1.7\ R.T.U.}$($ohm^{-1}cm^{-1}$)	4.4×10^{-7}
Range I (b) (°C)	400-496
E_A(eV)	0.92
$\sigma_{1.55\ R.T.U.}$($ohm^{-1}cm^{-1}$) estimated.	8.0×10^{-6}

A second run was done on this crystal but not enough observations were made to justify quotation of activation energies. However, the conductivity showed a significant decrease from the first run.

Impurity Content (Grown from B.D.H. Ltd. CsI).

1.9×10^{-4} m.f. Ba.
5.94×10^{-4} m.f. Sr.

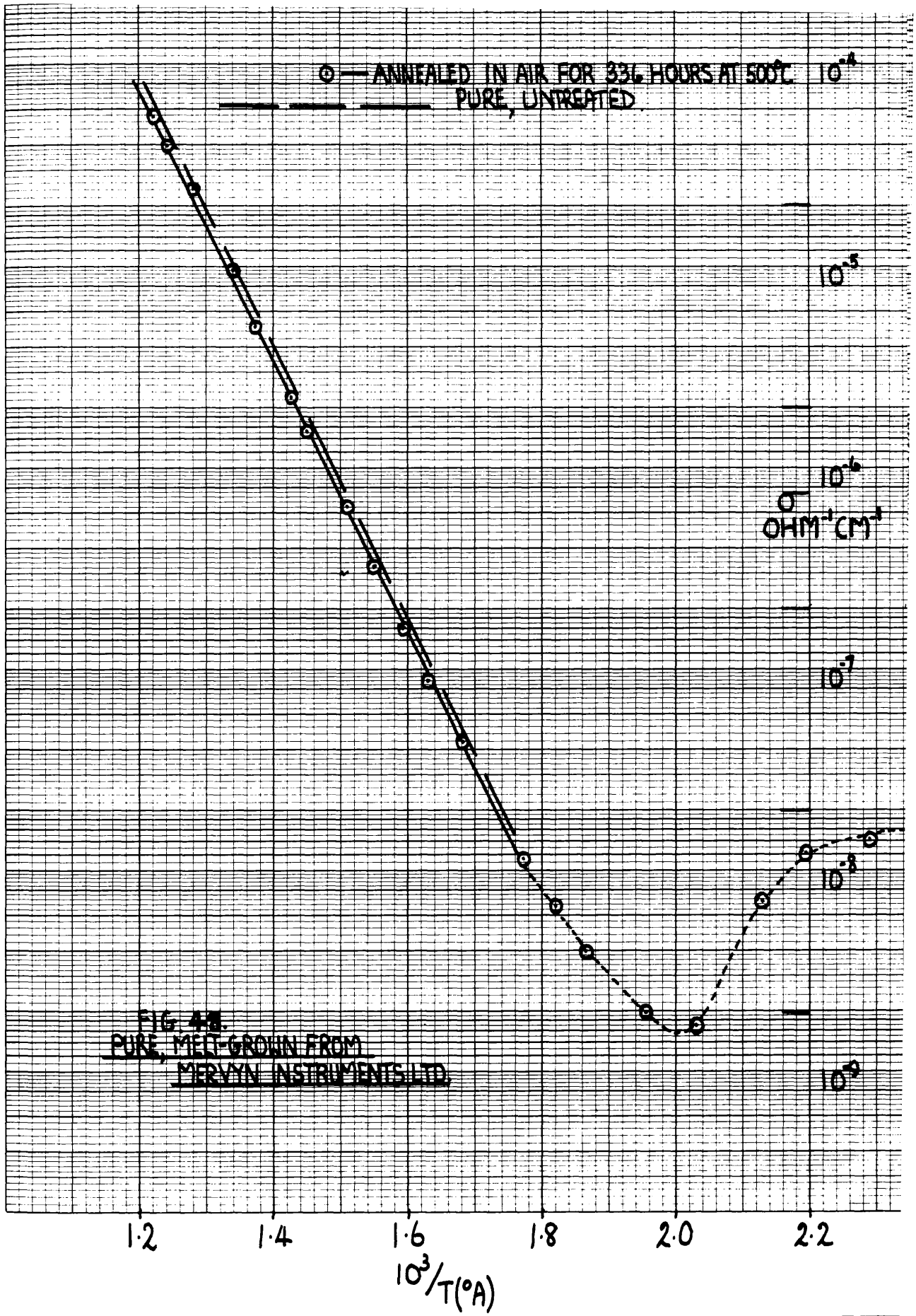

FIG. 4B.
PURE, MELT-GROWN FROM
MERVYN INSTRUMENTS LTD.

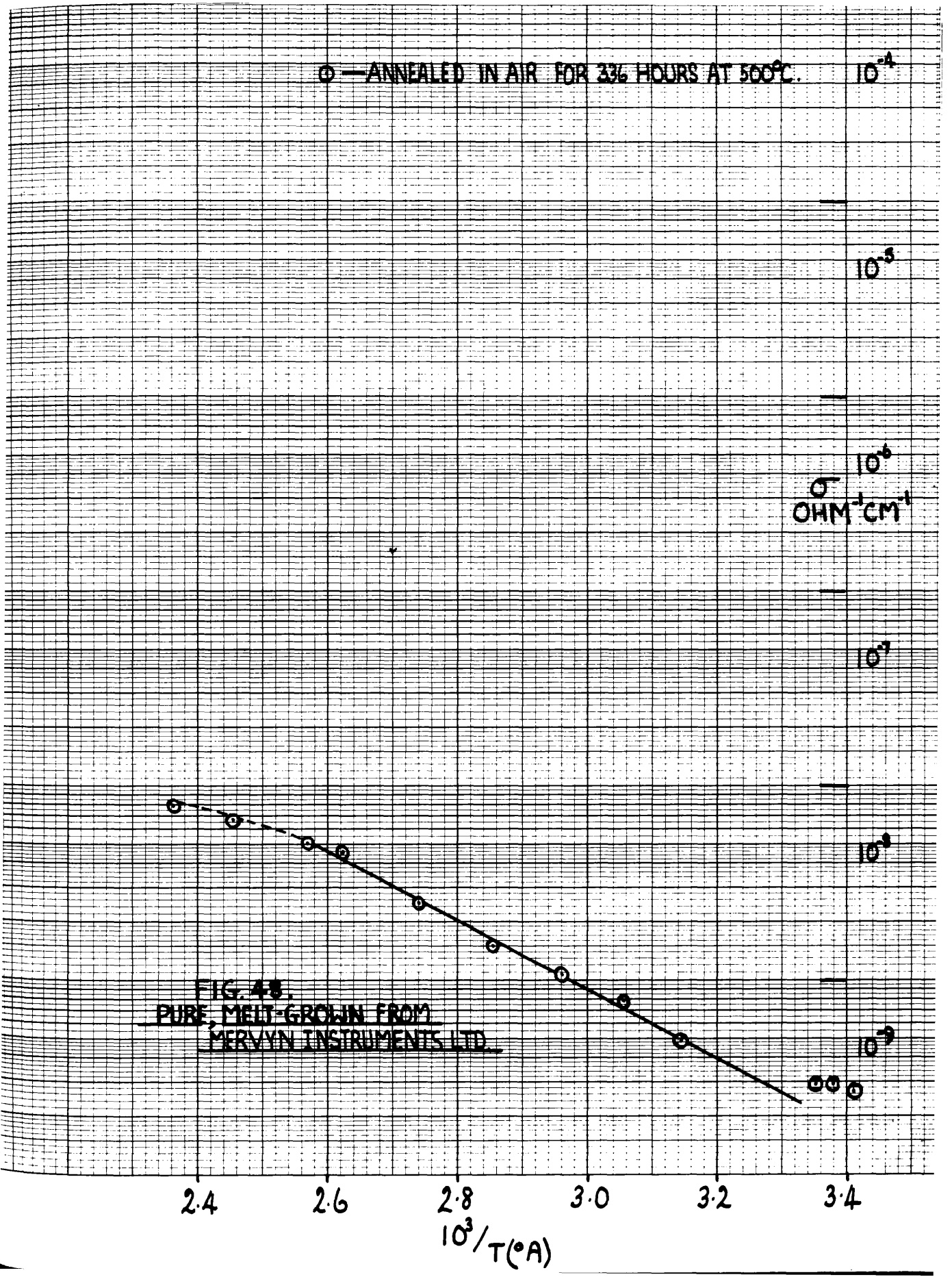

FIG. 48.
PURE, MELT-GROWN FROM
MERVYN INSTRUMENTS LTD.

TABLE 35(Fig.48)

Pure CsI, melt-grown, from Mervyn Instruments Limited.
Pretreatment:- Annealed in air at 500°C for 336 hours.
Free iodine was evident in the crystal after the anneal.

	First Run - Heating.
Temperature Range (°C)	30 - 118
E_A(eV)	0 .35
$\sigma_{3.0\ R.T.U.}$ ($ohm^{-1}cm^{-1}$)	8.0×10^{-9}
Temperature Range (°C)	118 - 227
E_A(eV)	Fall in σ
$\sigma_{max.}$ ($ohm^{-1}cm^{-1}$)	9.0×10^{-8}
$\sigma_{min.}$ ($ohm^{-1}cm^{-1}$)	7.9×10^{-9}
Range I (°C)	227 - 292
E_A(eV)	0.82
$\sigma_{2.0\ R.T.U.}$($ohm^{-1}cm^{-1}$)	$\sim 6.0 \times 10^{-9}$
Range II (°C)	292 - 560
E_A(eV)	1.34
$\sigma_{1.4\ R.T.U.}$($ohm^{-1}cm^{-1}$)	1.7×10^{-5}

Impurity Content.

$< 5 \times 10^{-6}$ m.f. alkaline-earth metal.
$< 2.3 \times 10^{-5}$ m.f. Fe.

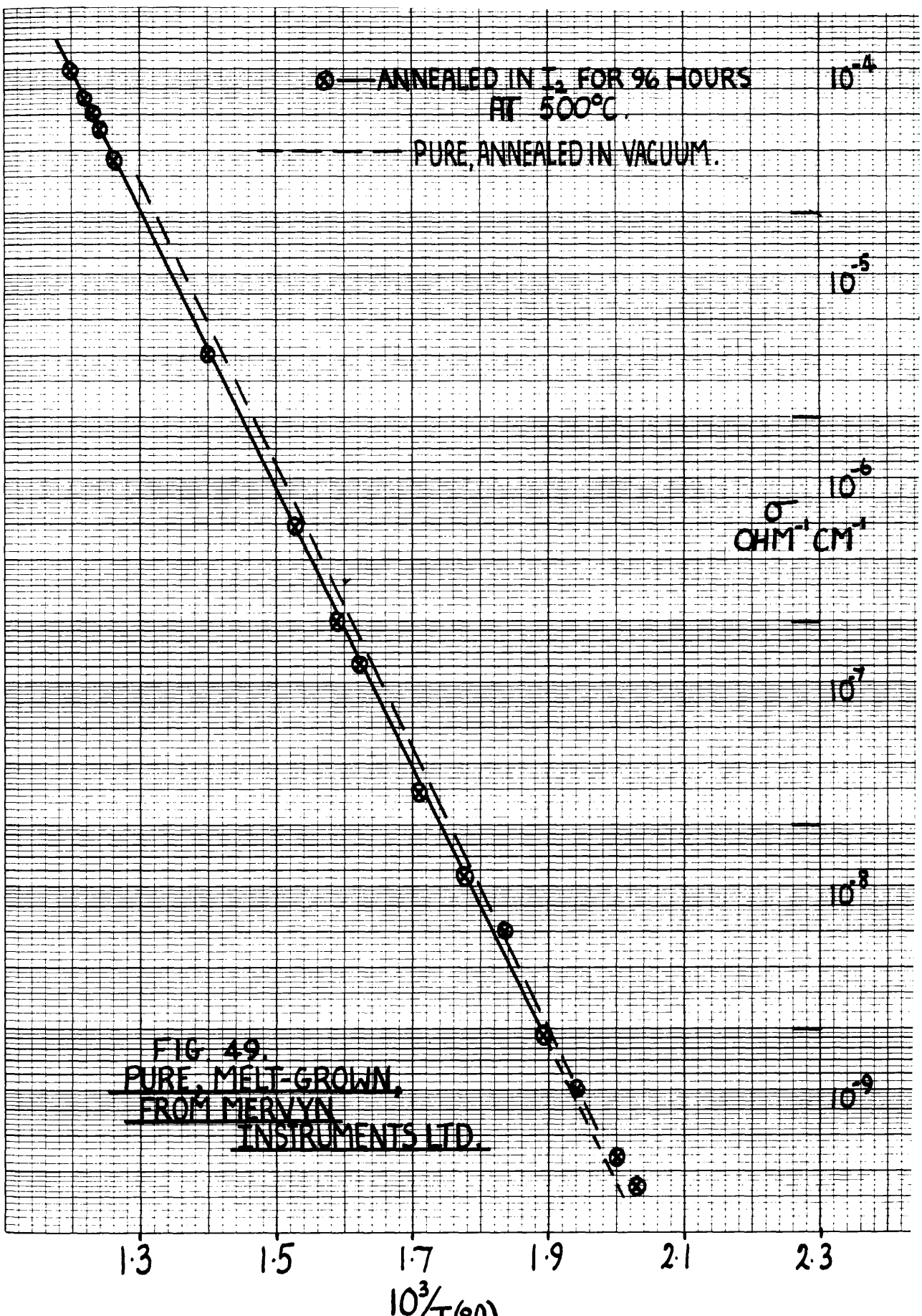

FIG. 49.
PURE, MELT-GROWN, FROM MERVYN INSTRUMENTS LTD.

TABLE 36(Fig.49)

Pure CsI, melt-grown, from Mervyn Instruments Limited.

Pretreatment:- Annealed in I_2 for 96 hours at 500°C.

	First Run - Heating.
Range II (°C)	227 - 560
E_A(eV)	1.37
$\sigma_{1.4\ R.T.U.}$ ($ohm^{-1}cm^{-1}$)	2.1×10^{-5}

Impurity Content.

$< 5 \times 10^{-6}$ m.f. alkaline-earth metal.

$< 23 \times 10^{-6}$ m.f. Fe.

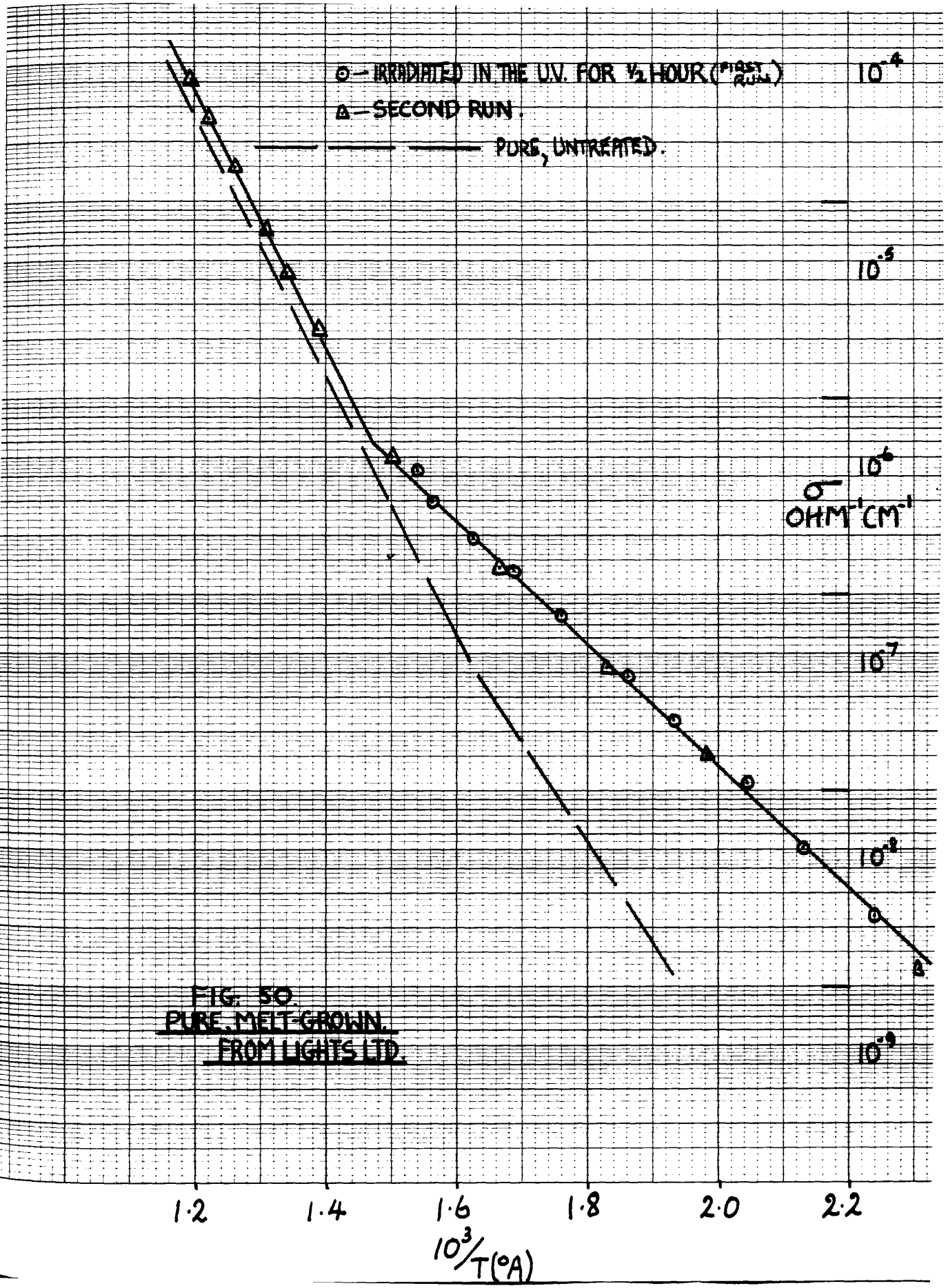

FIG. 50.
PURE, MELT-GROWN,
FROM LIGHTS LTD.

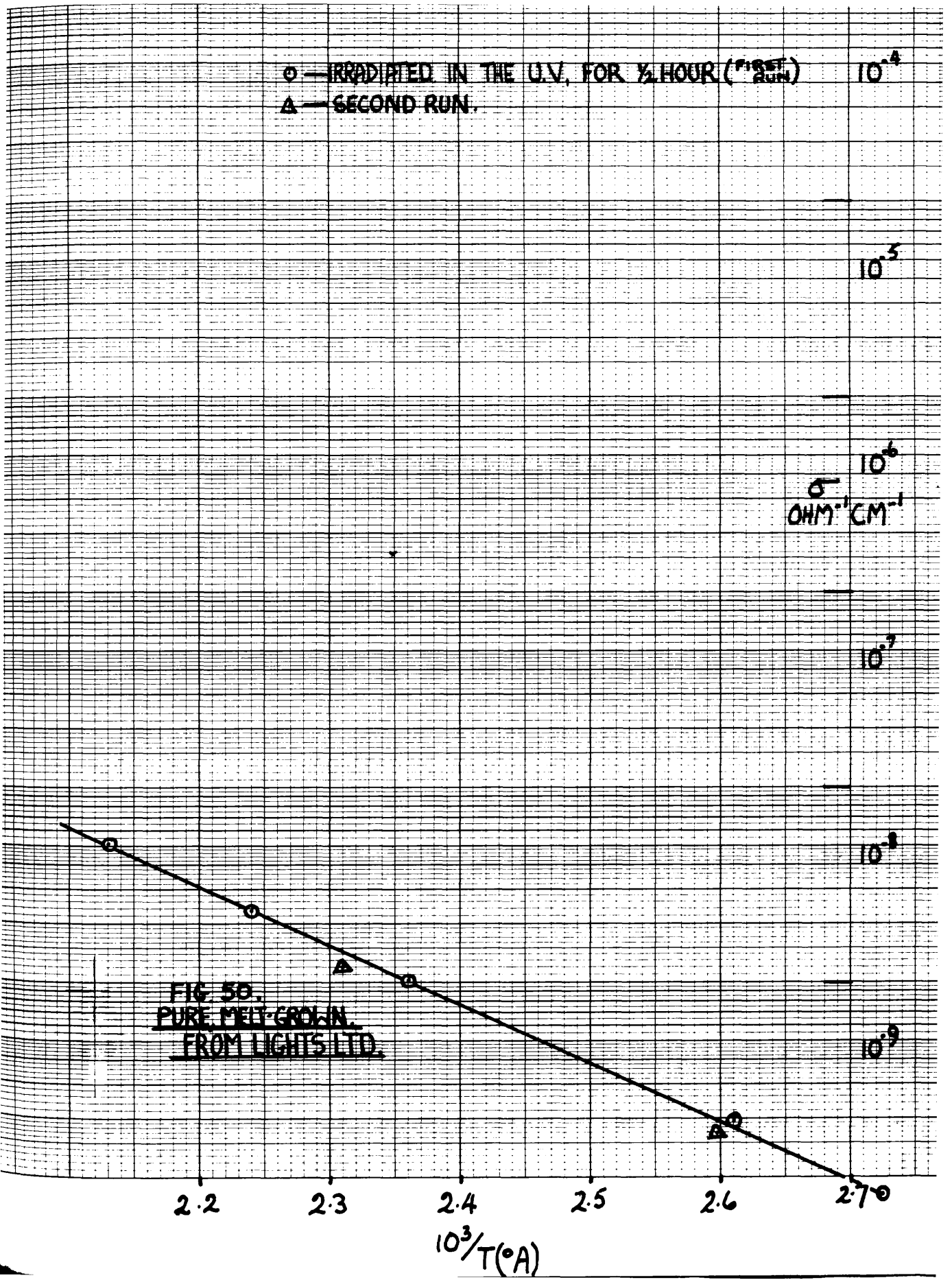

FIG 50.
PURE MELT-GROWN.
FROM LIGHTS LTD.

TABLE 37 (Fig. 50)

Pure CsI, melt-grown, from Lights Limited.

Pretreatment:- Irradiated in the ultra-violet for 30 minutes.

	Heating.	
	First Run	Second Run
Range I (°C)	91-376	112-407
E_A(eV)	0.62	0.62
$\sigma_{2.0\ R.T.U.}$($ohm^{-1}cm^{-1}$)	1.33×10^{-7}	1.33×10^{-7}
Range II (°C)	-	407-560
E_A(eV)	-	1.34
$\sigma_{1.4\ R.T.U.}$($ohm^{-1}cm^{-1}$)	-	1.8×10^{-5}

Impurity Content.

$< 1.0 \times 10^{-5}$ m.f. alkaline-earth metal.

$< 2.05 \times 10^{-5}$ m.f. Cu.

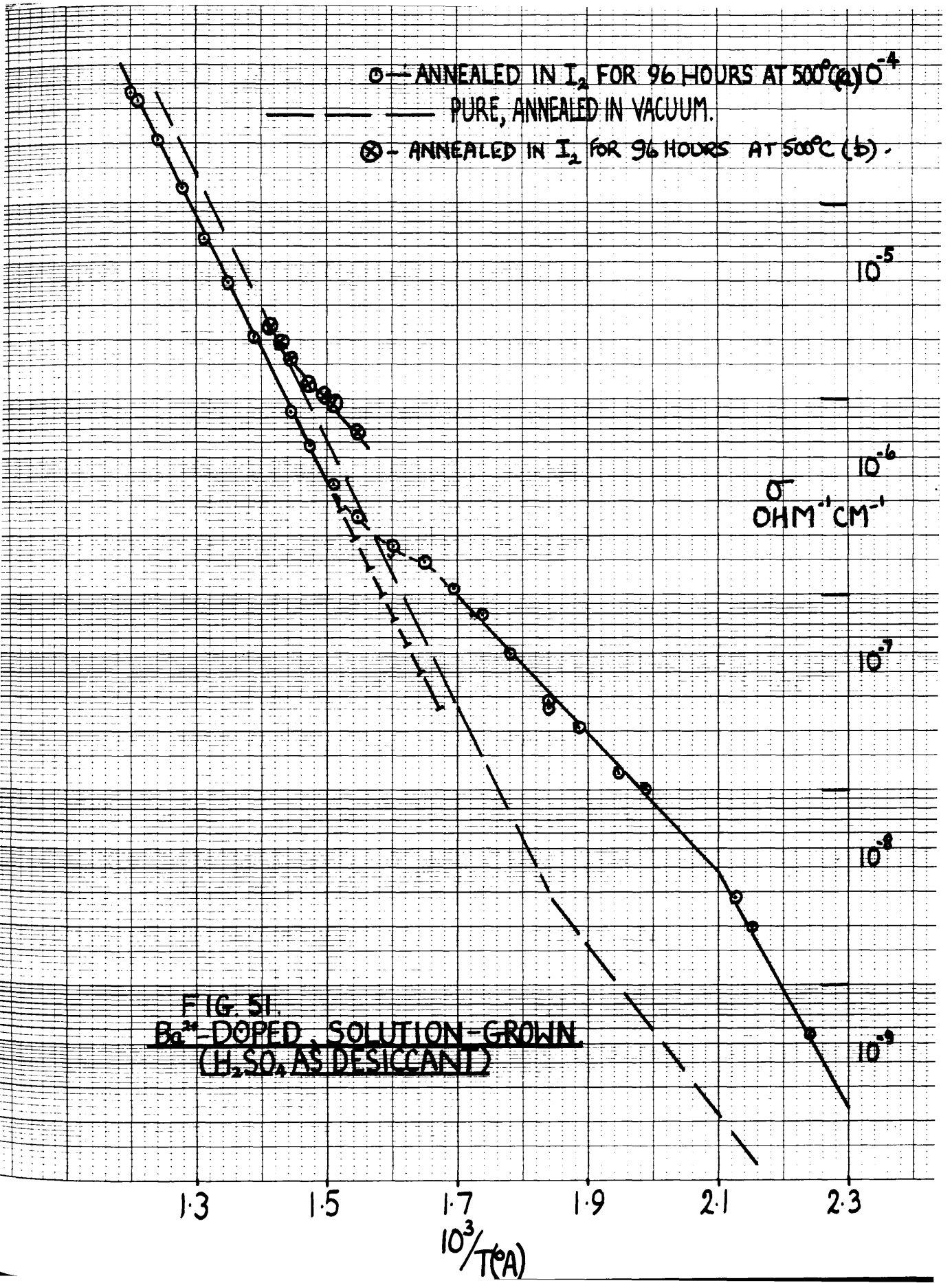

FIG. 51.
Ba^{++}-DOPED, SOLUTION-GROWN.
(H_2SO_4 AS DESICCANT)

TABLE 38 (Fig. 51)

Ba^{2+}-doped CsI, solution-grown (H_2SO_4 as desiccant).

Pretreatment:- Annealed in I_2 for 96 hours at 500°C.

	Crystal (a) (Heating).	Crystal (b) (Heating).
Temperature Range (°C)	173-203	-
E_A(eV)	1.20	-
$\sigma_{2.2\ R.T.U.}$($ohm^{-1}cm^{-1}$)	9.4×10^{-9}	-
Range I (°C)	203-394	-
E_A(eV)	0.71	-
$\sigma_{2.0\ R.T.U.}$($ohm^{-1}cm^{-1}$)	8.5×10^{-8}	-
Range I (b) (°C)	-	372-441
E_A(eV)	-	0.76
$\sigma_{1.55\ R.T.U.}$($ohm^{-1}cm^{-1}$)	-	6.5×10^{-6}
Range II (°C)	394-560	-
E_A(eV)	1.36	-
$\sigma_{1.4\ R.T.U.}$($ohm^{-1}cm^{-1}$)	1.85×10^{-5}	-

Impurity Content (Grown from B.D.H. Ltd. CsI).

Crystal (a)	Crystal (b)
5.7×10^{-5} m.f. Ba.	1.9×10^{-4} m.f. Ba.
2.3×10^{-5} m.f. Fe.	8.9×10^{-5} m.f. Sr.

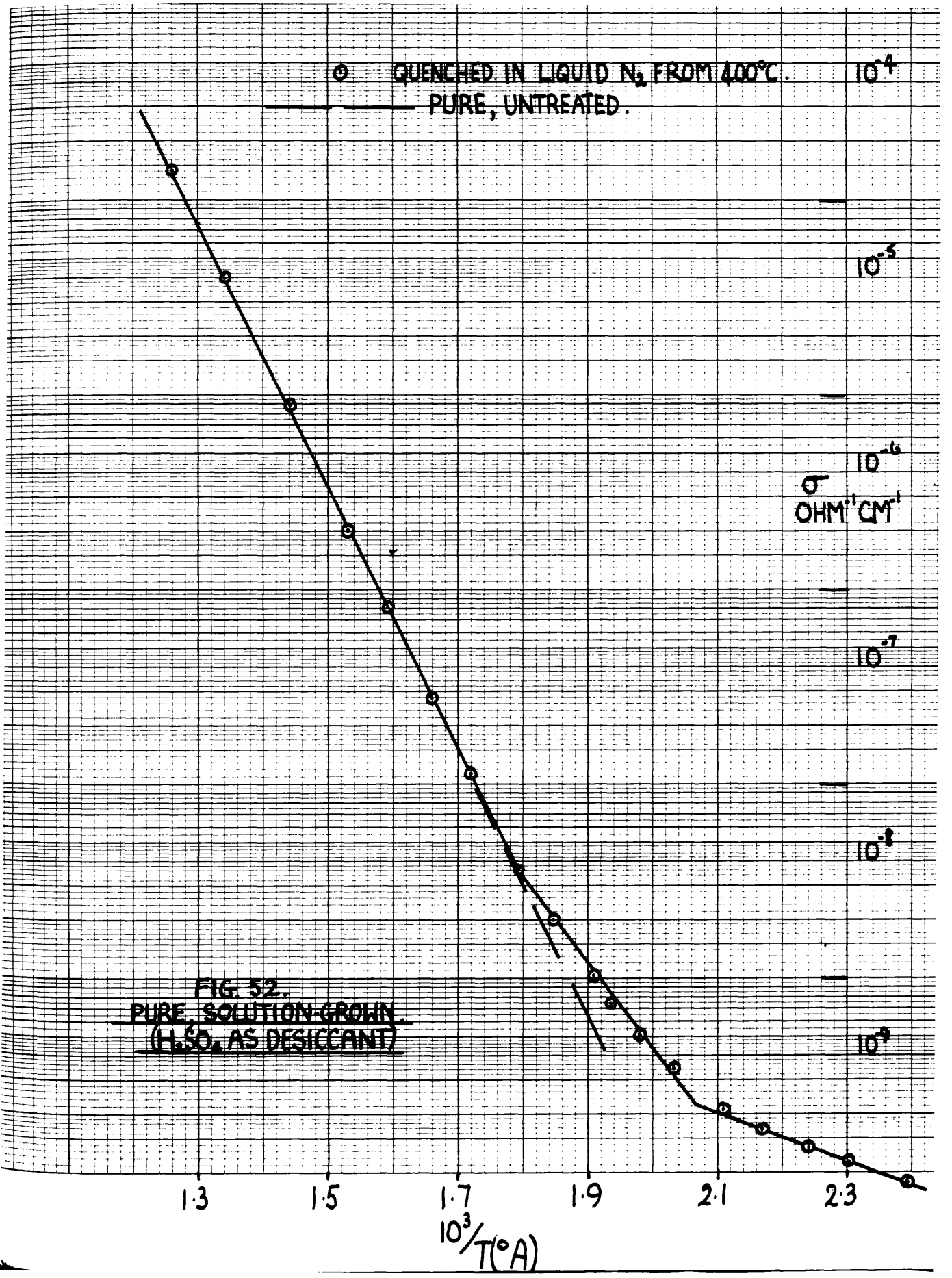

FIG. 52.
PURE, SOLUTION-GROWN.
(H_2SO_4 AS DESICCANT)

TABLE 39 (Fig.52)

Pure CsI, solution-grown (H_2SO_4 as desiccant).

Pretreatment:- Quenched in liquid N_2 from 400°C.

	First Run - Heating.
Temperature Range (°C)	103-212
E_A(eV)	0.24
$\sigma_{2.3\ R.T.U.}$ ($ohm^{-1}cm^{-1}$)	1.15×10^{-9}
Range I (°C)	212-289
E_A(eV)	0.88
$\sigma_{2.0\ R.T.U.}$ ($ohm^{-1}cm^{-1}$)	4.3×10^{-9}
Range II (°C)	289-521
E_A(eV)	1.33
$\sigma_{1.4\ R,T.U.}$ ($ohm^{-1}cm^{-1}$)	1.55×10^{-5}

Impurity Content (Grown from B.D.H. Ltd. CsI).

$1 - 3 \times 10^{-4}$ m.f. alkaline-earth metal (Ba and Sr).

$0.1 - 1 \times 10^{-4}$ m.f. Fe and Cu.

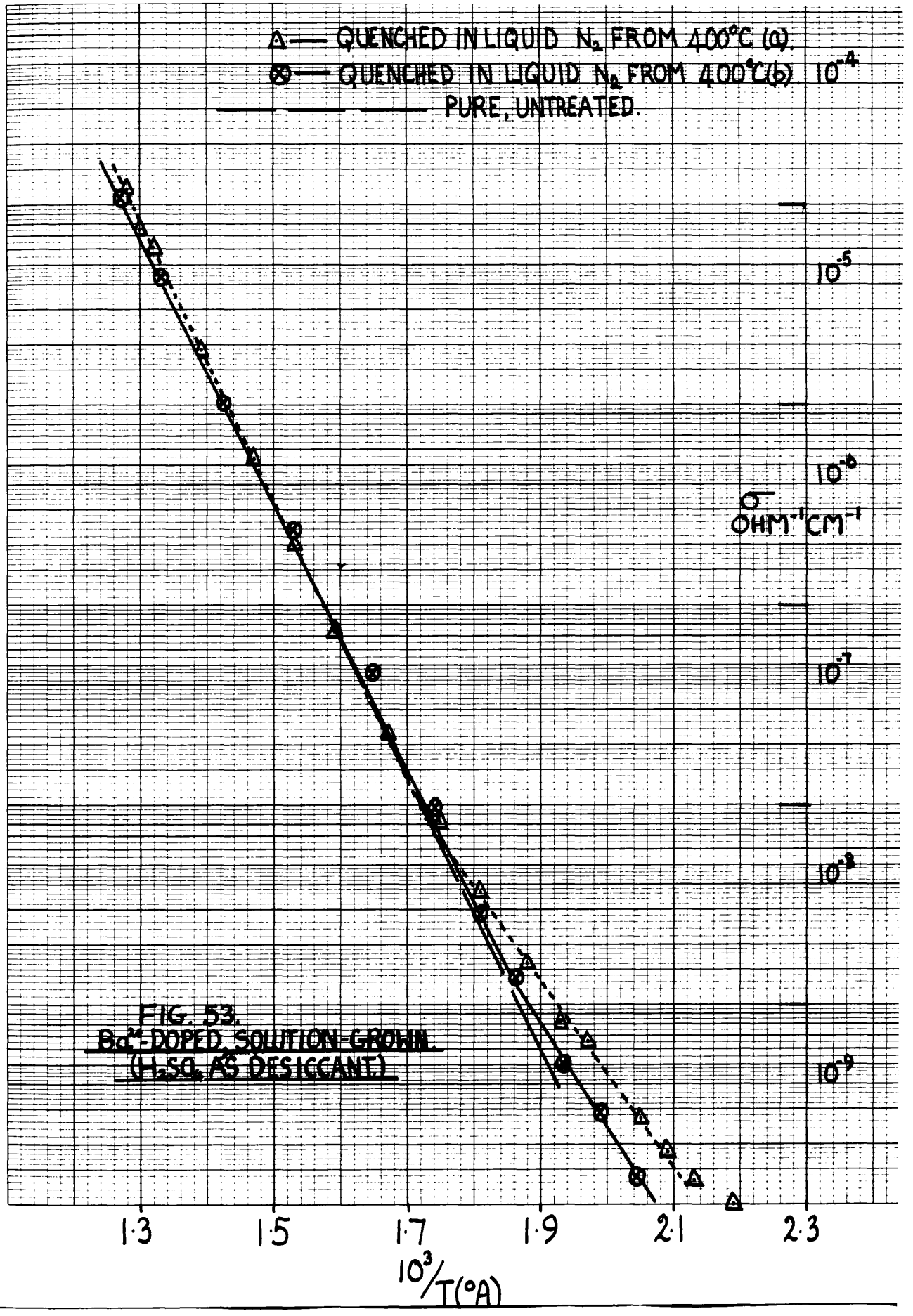

FIG. 53.
Ba^{++}-DOPED SOLUTION-GROWN
(H_2SO_4 AS DESICCANT.)

TABLE 40 (Fig. 53)

Ba^{2+}-doped CsI, solution-grown (H_2SO_4 desiccant).

Pretreatment:- Quenched in liquid N_2 from 400°C.

	Crystal (a) (Heating).	Crystal (b) (Heating).
Range I (°C)	200-265	203-302
E_A(eV)	1.03	0.94
$\sigma_{2.0\ R.T.U.}$($ohm^{-1}cm^{-1}$)	2.4×10^{-9}	4.5×10^{-9}
Range II (°C)	265-508	302-508
E_A(eV)	1.33	1.41
$\sigma_{1.4\ R.T.U.}$($ohm^{-1}cm^{-1}$)	1.4×10^{-5}	1.65×10^{-5}

Impurity Content - Unknown.

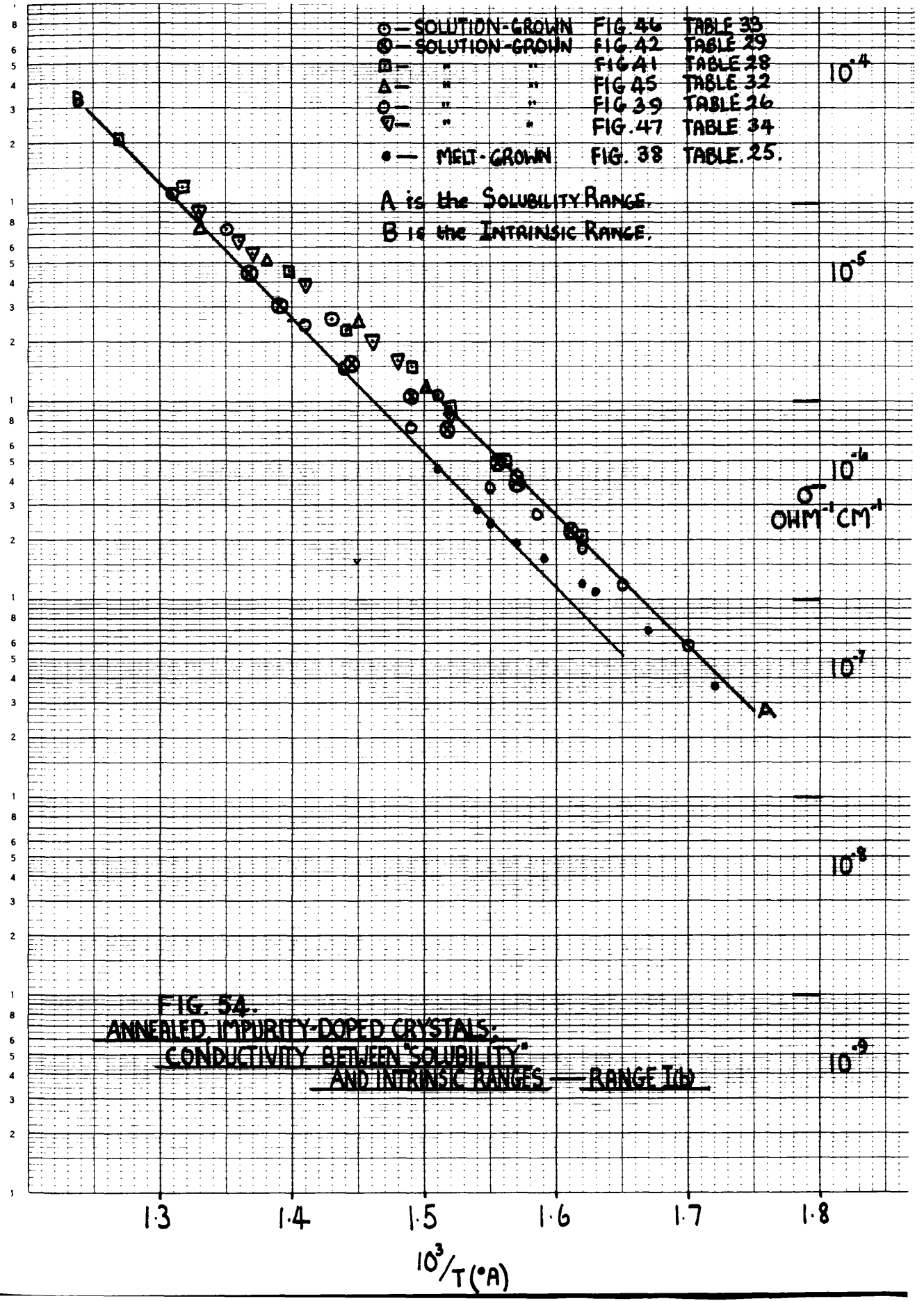

FIG. 54.
ANNEALED IMPURITY-DOPED CRYSTALS:
CONDUCTIVITY BETWEEN SOLUBILITY AND INTRINSIC RANGES — RANGE Tᵈ

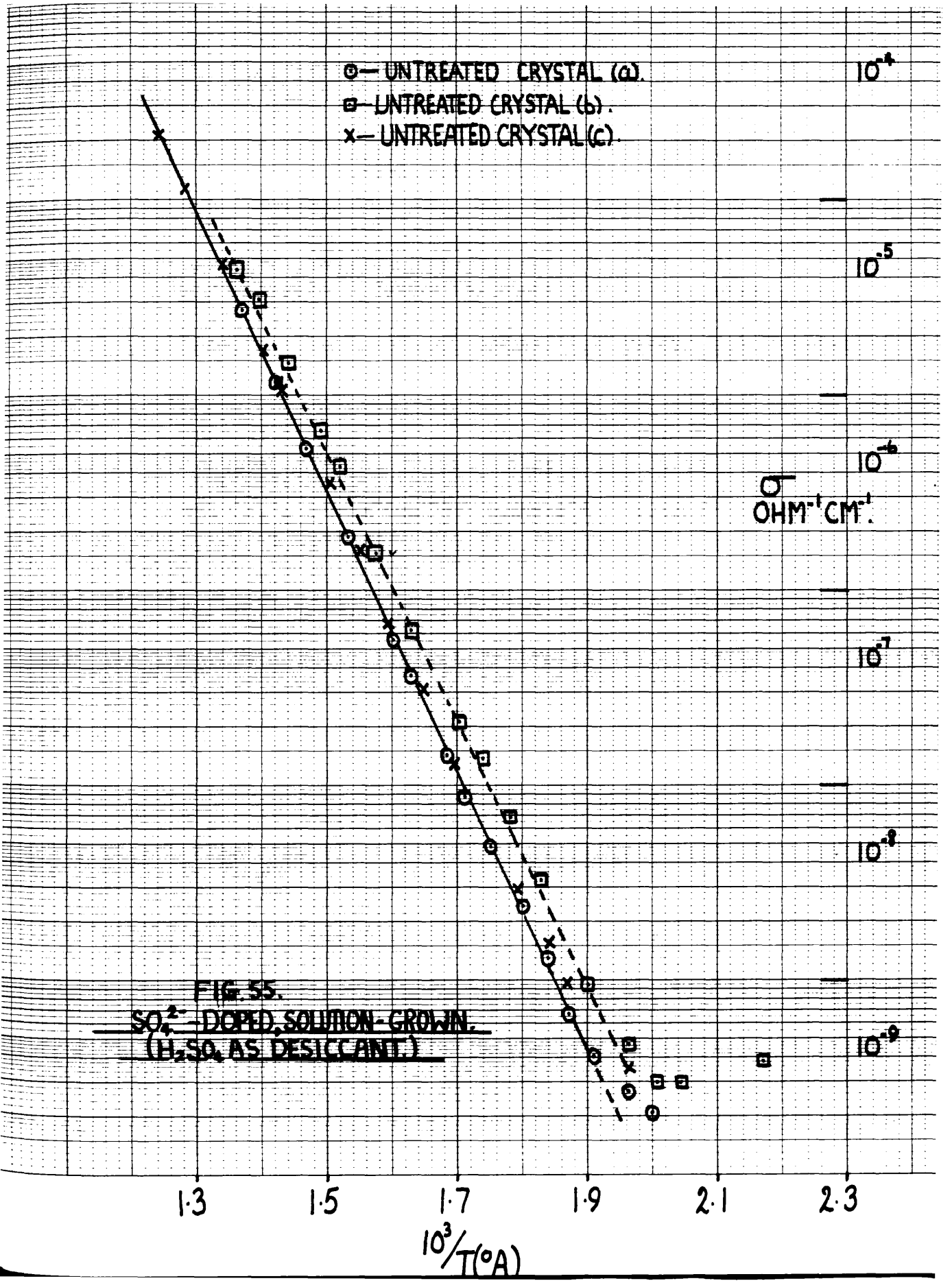

FIG. 55.
SO_4^{2-} – DOPED, SOLUTION-GROWN.
(H_2SO_4 AS DESICCANT.)

TABLE 41 (Fig.55)

SO_4^{2-}-doped CsI, solution-grown (H_2SO_4 as desiccant).

Pretreatment:- Untreated, apart from being vacuum dried.

	Crystal (a) (Heating).	Crystal (b) (Heating).	Crystal (c) (Heating).
Range II (°C)	253-457	237-457	250-533
E_A(eV)	1.42	1.36	1.42
$\sigma_{1.4\ R.T.U.}$($ohm^{-1}cm^{-1}$)	1.65×10^{-5}	2.4×10^{-5}	1.65×10^{-5}

The SO_4^{2-} content of these crystals is unknown.

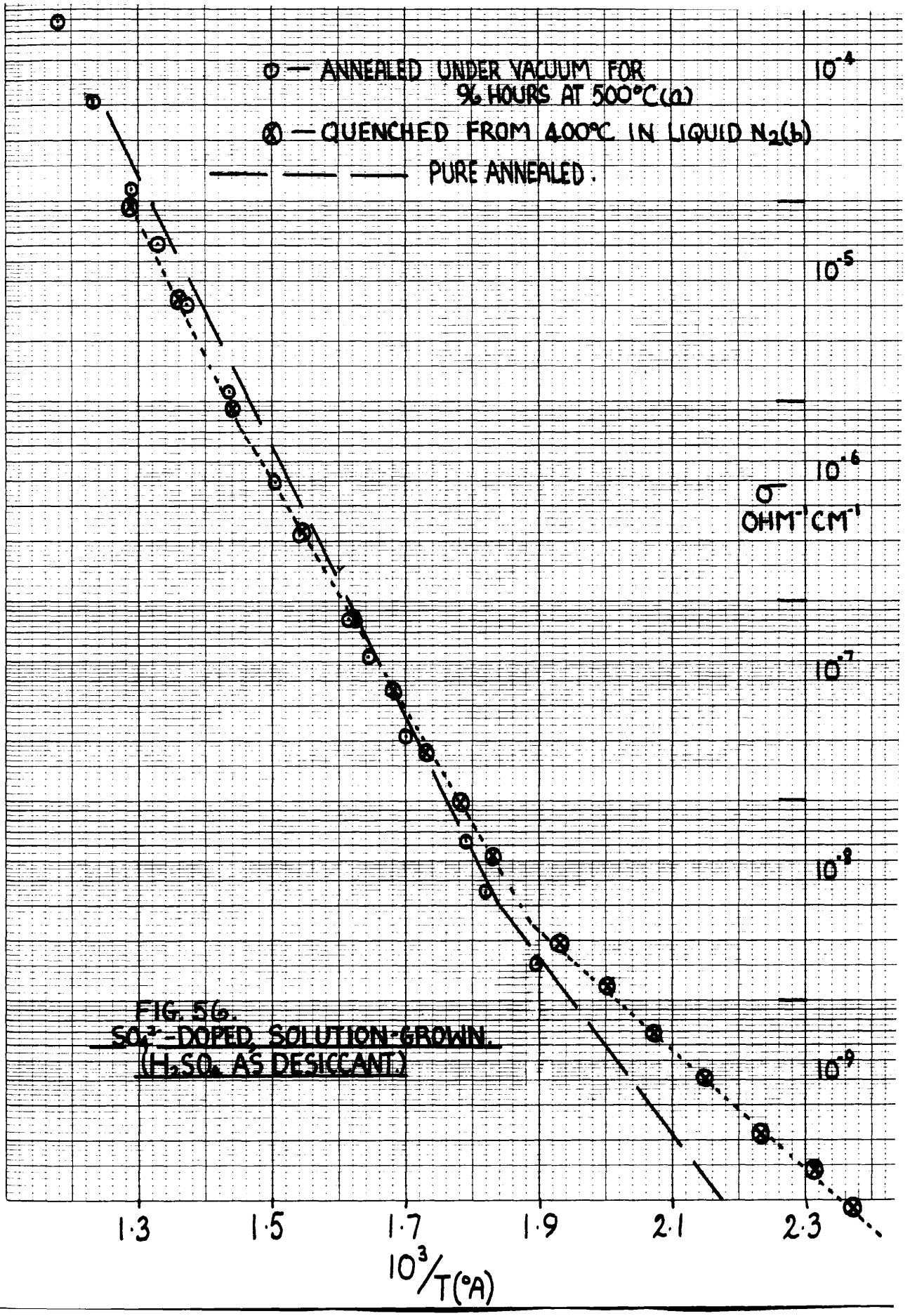

FIG. 56.
SO_4^{2-}-DOPED, SOLUTION-GROWN. (H_2SO_4 AS DESICCANT)

TABLE 42 (Fig.56)

SO_4^{2-}-doped CsI, solution-grown (H_2SO_4 as desiccant).

Pretreatment:- Crystal (a) was annealed under vacuum for 96 hours at 500°C. Crystal (b) was quenched from 400°C in liquid N_2.

	Crystal (a) (Heating).	Crystal (b) (Heating).
Range I (°C)	-	122-259
E_A(eV)	-	0.59
$\sigma_{2.0\ R.T.U.}$($ohm^{-1}cm^{-1}$)	-	1.15×10^{-8}
Temperature Range (°C)	253-421	259-421
E_A(eV)	1.26	1.14
$\sigma_{1.7\ R.T.U.}$($ohm^{-1}cm^{-1}$)	2.2×10^{-7}	2.9×10^{-7}
Range II (°C)	421-575	421-500
E_A(eV)	1.44	1.35
$\sigma_{1.4\ R.T.U.}$($ohm^{-1}cm^{-1}$)	2.0×10^{-5}	1.65×10^{-5}

The SO_4^{2-} impurity content of these crystals is unknown.

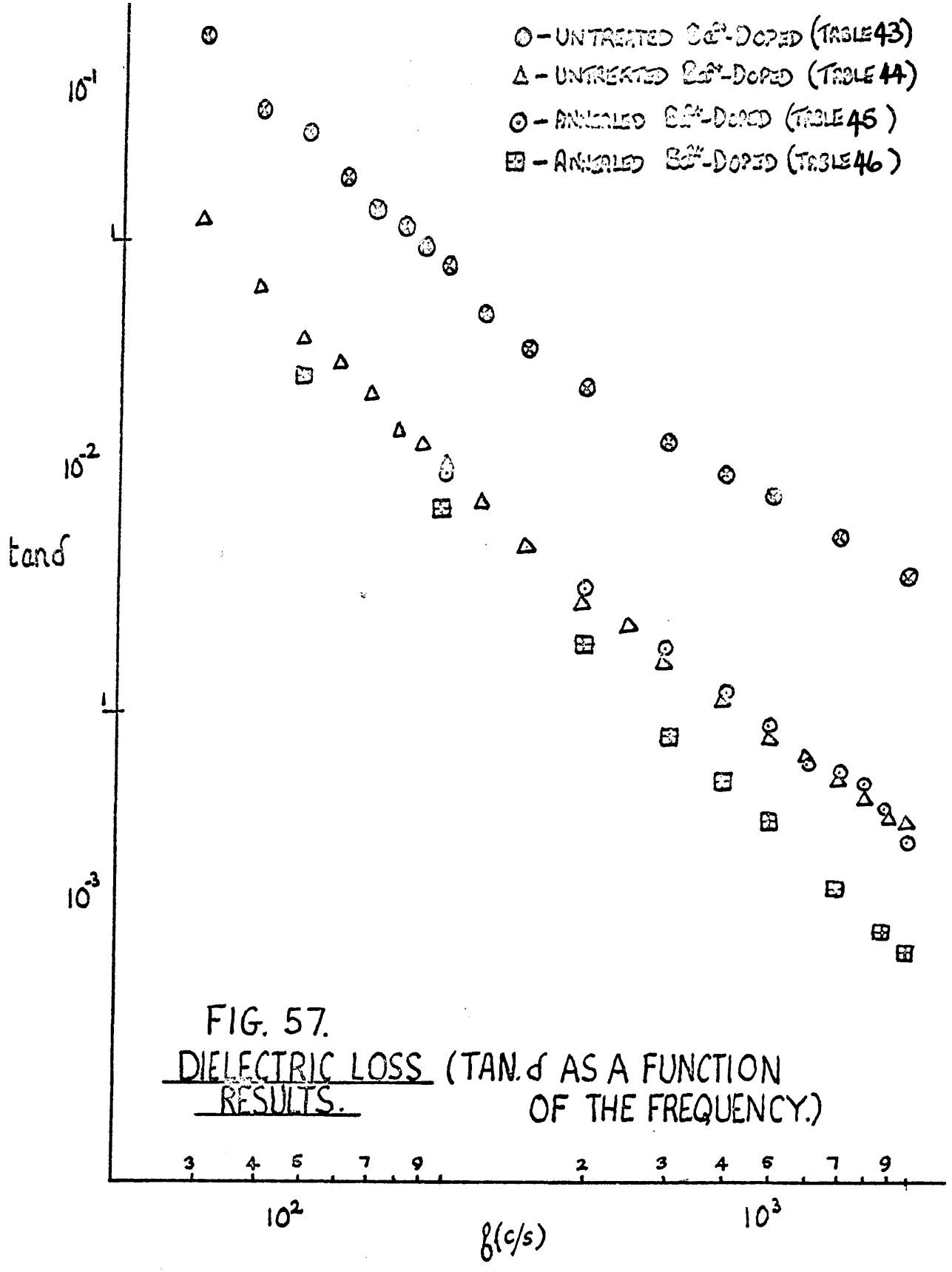

FIG. 57.
DIELECTRIC LOSS RESULTS. (TAN. δ AS A FUNCTION OF THE FREQUENCY.)

POLARISATION AND DIELECTRIC LOSS RESULTS.

Typical results of the above investigations are shown for two vacuum annealed and two untreated Ba^{2+}-doped crystals.

TABLE 43 (Fig. 57)

Untreated Ba^{2+}-doped solution-grown CsI, total cation impurity content $\sim 1 \times 10^{-3}$ m.f.

Capacitance (μμF).	tan δ.	Frequency (c/s).
8.4	0.415	200
8.6	0.278	300
9.4	0.195	400
8.7	0.176	500
9.2	0.140	600
9.1	0.120	700
9.0	0.113	800
9.0	0.100	900
8.8	0.092	1000
9.0	0.073	1200
8.9	0.062	1500
8.6	0.051	2000
8.5	0.039	3000
8.4	0.034	4000
8.2	0.031	5000
8.0	0.025	7000
7.4	0.020	10,000

The temperature at which the above observations were made was $270 \pm 2^{\circ}C$.

TABLE 44 (Fig. 57).

Untreated Ba^{2+}-doped solution-grown CsI, impurity content unknown.

Capacitance (μμF).	tan δ .	Frequency (c/s).
4.7	0.237	200
6.5	0.114	300
6.8	0.082	400
7.0	0.064	500
7.0	0.057	600
7.0	0.0487	700
7.0	0.0400	800
7.0	0.0379	900
7.0	0.0341	1000
7.4	0.0287	1200
7.4	0.0230	1500
7.3	0.0175	2000
7.1	0.0161	2500
7.2	0.0132	3000
7.2	0.0111	4000
7.2	0.0091	5000
7.0	0.0083	6000
7.0	0.0075	7000
7.0	0.0068	8000
7.0	0.0063	9000
7.0	0.0061	10,000

The temperature at which these observations were made was $270 \pm 2^{\circ}C$.

TABLE 45 (Fig. 57).

Vacuum annealed Ba^{2+}-doped solution-grown CsI, total cation impurity content = 8.1×10^{-4} m.f.

Capacitance (μμF).	tan δ.	Frequency (c/s).
6.8	0.0328	1000
6.8	0.0187	2000
6.6	0.0141	3000
6.7	0.0113	4000
6.6	0.0096	5000
6.6	0.0080	6000
6.6	0.0072	7000
6.5	0.0073	8000
6.4	0.0064	9000
6.5	0.0054	10,000

The temperature at which these observations were made was $210 \pm 2^{\circ}C$.

TABLE 46 (Fig. 57).

Vacuum annealed Ba^{2+}-doped solution-grown CsI, total cation impurity content = 1.48×10^{-3} m.f.

Capacitance (μμF).	tan δ.	Frequency (c/s).
9.0	0.0530	500
8.8	0.0276	1000
8.6	0.0143	2000
8.5	0.0091	3000
8.4	0.0074	4000
8.4	0.0060	5000
8.3	0.0044	7000
8.3	0.0035	9000
8.3	0.0032	10,000

The temperature at which these observations were made was $210 \pm 2^{\circ}C$.

3.2. DIFFUSION.

3.2.(a) Cs - 137 Diffusion.

The majority of the diffusion measurements have been made on pure unannealed solution grown and Mervyn vacuum grown crystals. The results for the latter crystals are somewhat anomalous and it is intended, before presentation of the results, to discuss in some detail the surface decrease method for measurement of diffusion.

The surface decrease method is critically dependent both on the reproducibility of the counting arrangement, i.e. crystal position in regard to the counter, and on the decrease in activity at the surface only resulting from the diffusion of the tracer into the crystal. Processes such as evaporation of the tracer from the crystal surface will give rise to large errors in the determination of the diffusion coefficient. It is therefore an advantage in this method to use a tracer which is both a β and γ-emitter. The absorption of the γ-rays in the crystal is very small for short diffusion distances and hence the γ-count rate should remain constant during the diffusion. Any significant drop in γ-count rate would indicate that evaporation of the active deposit had probably taken place.

In the diffusion measurements on the solution grown crystals the γ-count rate remained constant within the experimental error and the diffusion coefficients have been determined as previously described. The results are summarised in Table 47 and a plot of log D against the reciprocal temperature is given in Fig. 58. The reproducibility and the diffusion graph are reasonably satisfactory.

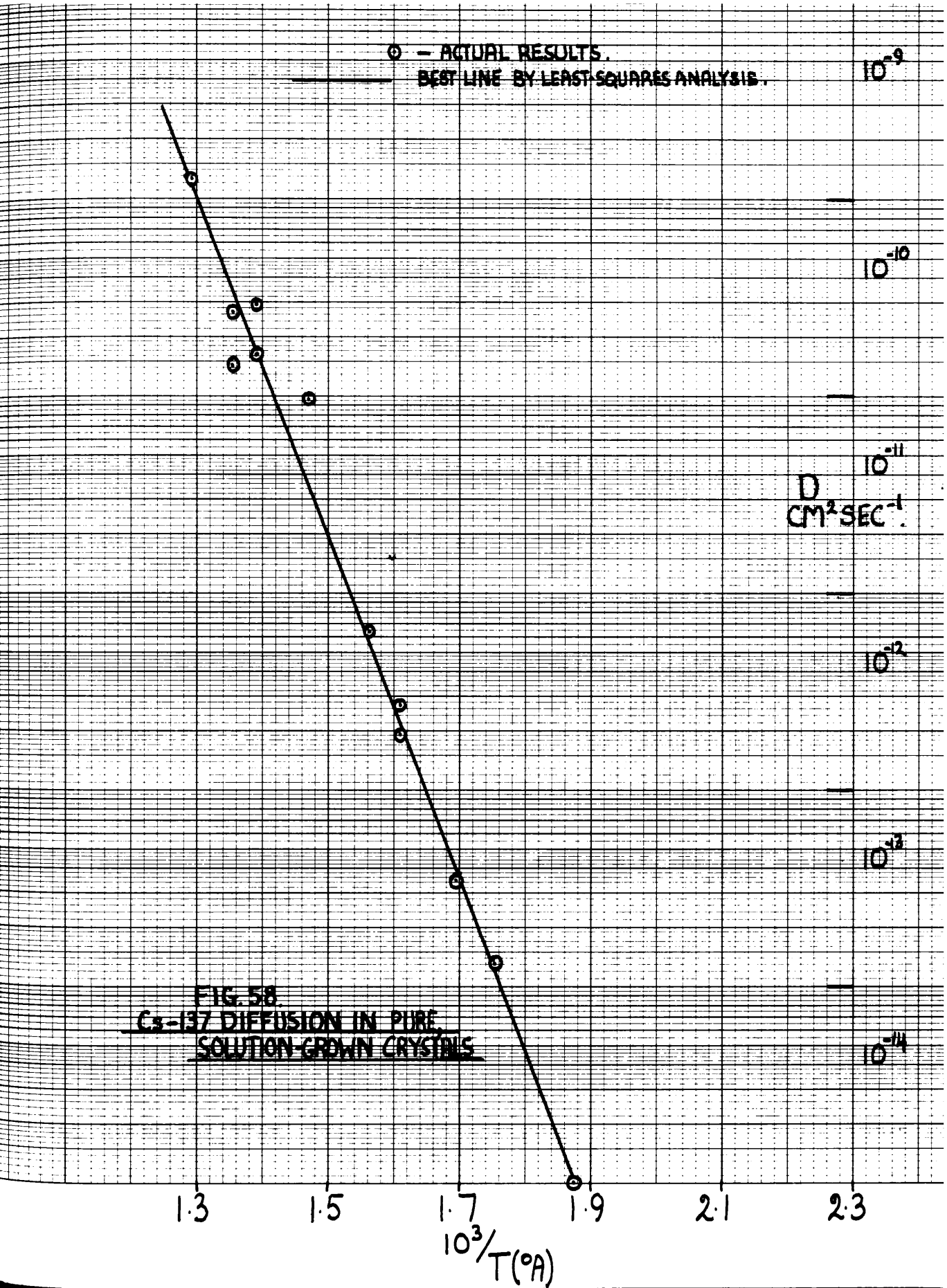

FIG. 58.
Cs-137 DIFFUSION IN PURE, SOLUTION-GROWN CRYSTALS

TABLE 47 (Fig. 58).

Cs^+ diffusion coefficients for pure, untreated, solution-grown crystals of CsI (unpolished).

$10^3/T(^\circ A)$.	$D(cm^2 sec^{-1})$.
1.876	1.00×10^{-14}
1.754	1.30×10^{-13}
1.695	3.51×10^{-13}
1.610	1.90×10^{-12}
1.610	2.70×10^{-12}
1.565	6.32×10^{-12}
1.471	9.50×10^{-11}
1.393	2.93×10^{-10}
1.391	1.63×10^{-10}
1.355	2.68×10^{-10}
1.355	1.44×10^{-10}
1.294	1.27×10^{-9}

Activation energy for diffusion is 1.74 ± 0.08eV.

Typical analyses for these crystals, grown from Hopkins and Williams CsI were $< 2.0 \times 10^{-5}$ m.f. divalent cation impurity (Ca^{2+}).

In the measurements on the Mervyn vacuum grown crystals the count rates increased after the diffusion heating. The increase in γ-count rate varied between 5 and 20% depending on the crystal specimen. There was no obvious correlation between the increase in count rate and either the diffusion time or the diffusion temperature. In other studies where a comparison of surface decrease and microtome techniques have been made there is good agreement between the diffusion coefficients determined by the two methods[75]. In one case, however, (the diffusion of Co - 60 in Ni-Al alloys) increases in β-count rate have been sometimes observed after diffusion. It has been found that this is the result of β-scattering[76]. The β-scattering produces a maximum in the absorption curve. It is unlikely, however, that this is the explanation for the increased count rates in these experiments. The absorption curve has been determined on several occasions and the results are reproducible, Fig. 15. There is no evidence of any maximum in the absorption curve.

Furthermore the absorption measurements are in very good agreement with those of Harvey[48] who used a similar experimental arrangement to study the diffusion of Cs - 137 in single crystals of CsCl. The reproducibility in the diffusion count rates and the diffusion coefficients in this latter work were very satisfactory and no increased count rates were observed after diffusion. It is significant that the CsCl specimens used in these experiments were unpolished, solution-grown crystals. Satisfactory results have been obtained in the present research with the solution-grown crystals (Table 47) which were also unpolished. The Mervyn vacuum grown crystals and all other melt-grown crystals required polishing prior to use in the diffusion and

conductivity experiments. It therefore seems that this anomalous increase in count rate is associated with the polishing of the crystal prior to the diffusion measurements, and this is substantiated by the results for the polished solution-grown crystals which also show increased count rates after diffusion, Appendix(I).

It is suggested that this increase in count rate is due to changes in the counting geometry. It is believed that there is considerable movement of the active deposit in the surface regions of the crystal during diffusion and this results in changes in the counting geometry. Polishing of crystal surfaces frequently produces polycrystallinity in the surface regions[77] and the heating of the crystals during diffusion may produce sintering in these regions. Alternatively the polishing of crystals will certainly produce strain in the surface regions and the release of this strain during heating could lead to deformation of the crystal surface. This has, in fact, been observed in some cases after annealing of polished crystals. It should however be pointed out that the observed increases in some cases are somewhat larger than would be expected on the basis of changes in the counting geometry.

The results for polished crystals have been analysed on the assumption that changes do occur in the counting geometry during diffusion. The efficiency of the counter for β- and γ-rays should not change during diffusion and consequently, if no diffusion occurred, the β/γ count ratio should be essentially independent of small changes in the position of the active deposit with respect to the counter. If diffusion occurred then the β/γ count ratio should decrease and this, in fact, is always observed.

The diffusion coefficients for polished crystals have therefore been calculated using equation 37 but, instead of using only the β-count rate, the initial and final β/γ count ratios are used. The results are summarised in β/γ Tables 48 - 51.

The results for the Cs - 137 diffusion in unannealed Mervyn crystals are shown in Fig.59. The general situation is that although these diffusion results cannot be used for a quantitative argument, the diffusion coefficients for these crystals do show the same qualitative behaviour as the solution-grown crystals. In fact if the diffusion coefficients for the Mervyn crystals are averaged at each temperature then the resulting log D against reciprocal temperature plot is in reasonable agreement with the line for solution-grown crystals, Fig. 60. The results for the polished solution-grown crystals could be taken as justification for the modified method of calculation since the resulting diffusion coefficients agree reasonably with the results for unpolished solution-grown crystals; the difference is less than a factor of two, Fig. 60. Further justification for this method is obtained from the results for three crystals using the microtoming technique described in Chapter 2. The agreement is quite reasonable (microtome results in Appendix(3)).

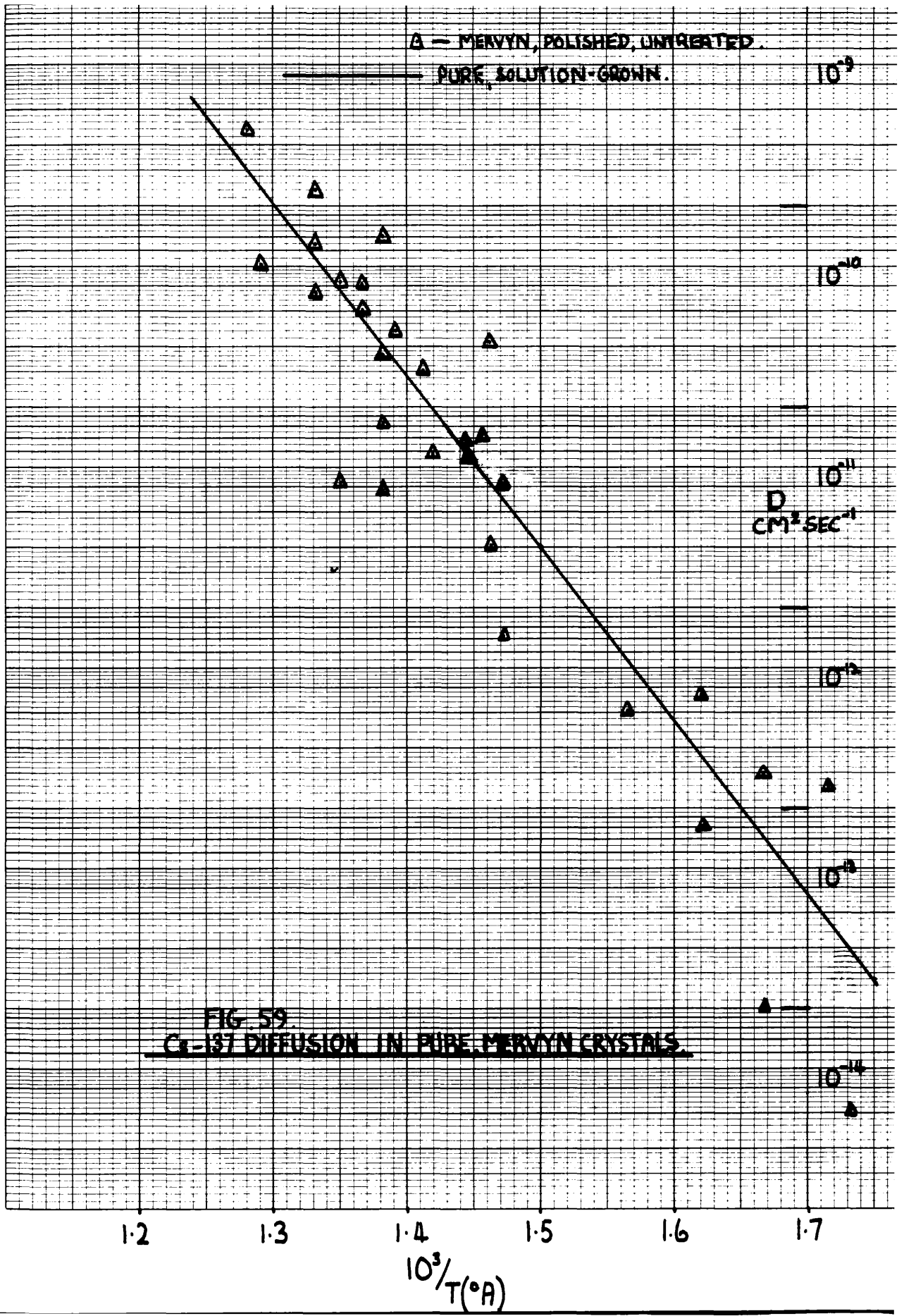

FIG. 59.
Cs^{-137} DIFFUSION IN PURE MERVYN CRYSTALS.

TABLE 48 (Fig. 59).

Cs^+ diffusion coefficients calculated from $(\beta/\gamma)_{\text{before diffusion}}$ and $(\beta/\gamma)_{\text{after diffusion}}$, for polished Mervyn Instruments Limited, untreated CsI crystals.

$10^3/T(^\circ A)$.	$D(cm^2sec^{-1})$.	$10^3/T(^\circ A)$.	$D(cm^2sec^{-1})$.
1.733	3.08×10^{-14}	1.414	1.50×10^{-10}
1.715	1.30×10^{-12}	1.393	2.40×10^{-10}
1.667	1.50×10^{-12}	1.383	1.81×10^{-10}
1.667	1.00×10^{-13}	1.383	7.00×10^{-10}
1.621	8.10×10^{-13}	1.383	8.10×10^{-11}
1.621	3.70×10^{-12}	1.383	3.80×10^{-11}
1.565	3.00×10^{-12}	1.368	4.10×10^{-10}
1.473	4.10×10^{-11}	1.368	3.00×10^{-10}
1.473	7.10×10^{-12}	1.368	1.75×10^{-10}
1.464	2.04×10^{-11}	1.350	4.20×10^{-10}
1.464	2.10×10^{-10}	1.350	4.20×10^{-11}
1.456	7.30×10^{-11}	1.332	6.50×10^{-10}
1.447	5.51×10^{-11}	1.333	3.75×10^{-10}
1.447	6.83×10^{-11}	1.333	1.20×10^{-9}
1.420	5.80×10^{-11}	1.290	5.00×10^{-10}
		1.282	2.40×10^{-9}

Averaged results are shown in Fig. 60.

Typical analyses for Mervyn Instruments Limited crystals showed $< 5\times10^{-6}$ m.f. alkaline-earth impurity and $< 2.3\times10^{-5}$ m.f. Fe.

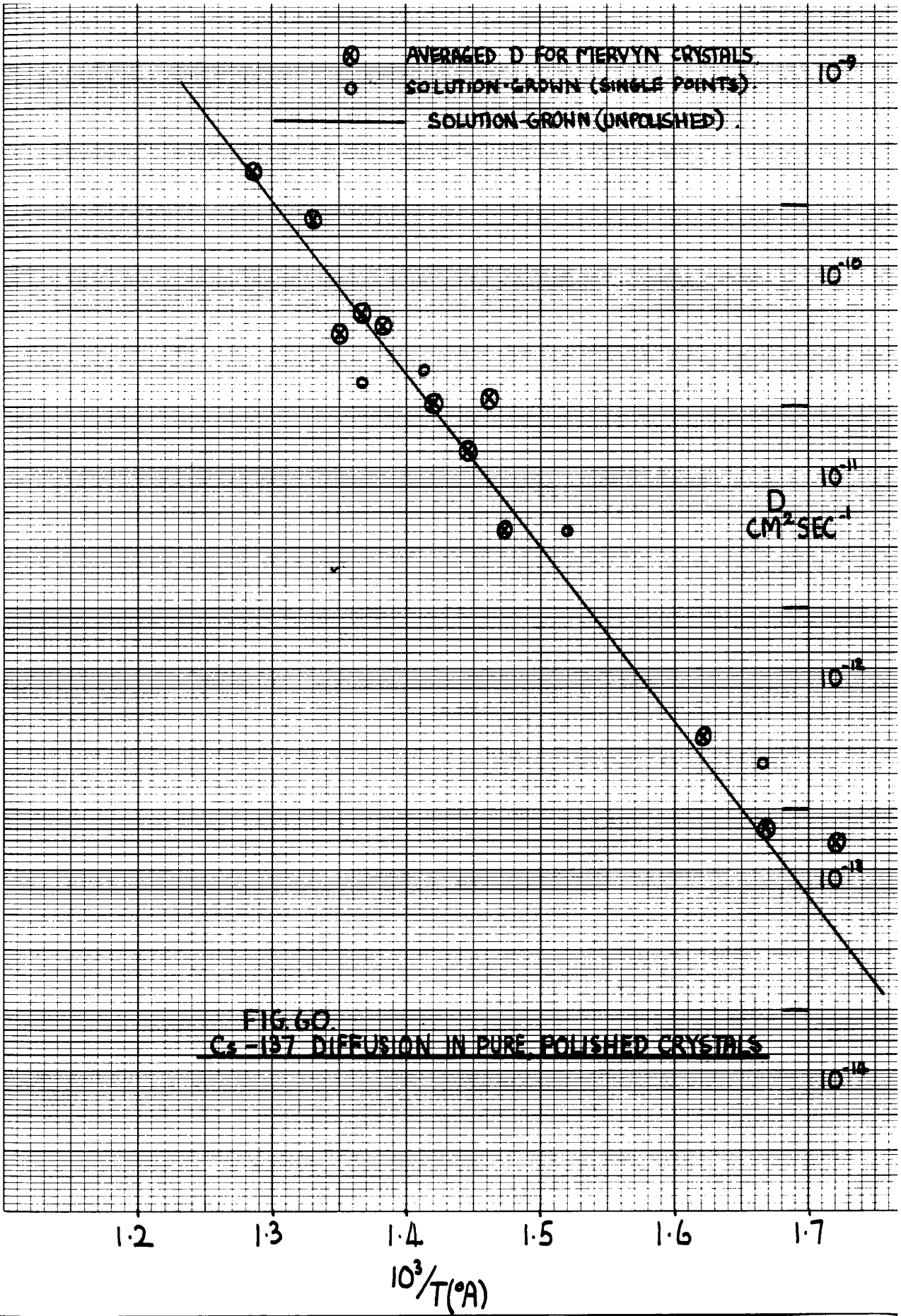

FIG. 60.
Cs-137 DIFFUSION IN PURE POLISHED CRYSTALS

TABLE 49 (Fig. 60).

Cs^+ diffusion coefficients, calculated from $(\beta/\gamma)_{\text{before diffusion}}$ and $(\beta/\gamma)_{\text{after diffusion}}$, for pure, polished, untreated solution-grown crystals of CsI.

$10^3/T(^\circ A)$.	$D(cm^2 sec^{-1})$.
1.667	1.70×10^{-12}
1.522	2.40×10^{-11}
1.414	1.50×10^{-10}
1.366	1.30×10^{-10}

Typical analyses for these crystals, grown from Hopkins and Williams CsI were $< 2.0 \times 10^{-5}$ m.f. divalent cation impurity (Ca^{2+}).

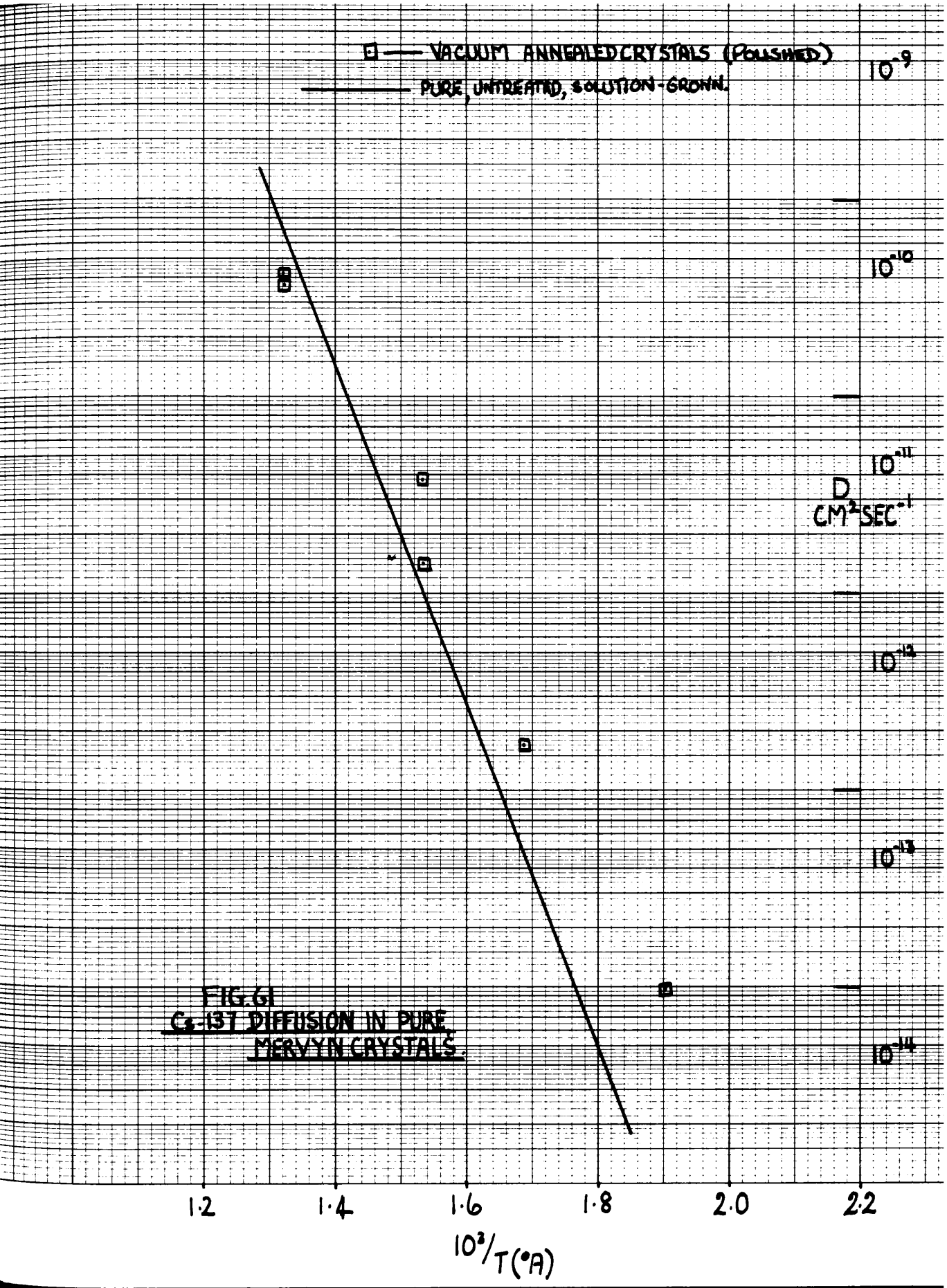

FIG. 61
Cs-137 DIFFUSION IN PURE MERVYN CRYSTALS.

TABLE 50 (Fig. 61).

Cs^+ diffusion coefficients calculated from $(\beta/\gamma)_{\text{before diffusion}}$ and $(\beta/\gamma)_{\text{after diffusion}}$, for vacuum annealed Mervyn Instruments Limited, polished CsI crystals.

$10^3/T(^oA)$.	$D(cm^2sec^{-1})$.
1.905	9.50×10^{-14}
1.686	1.70×10^{-12}
1.527	1.40×10^{-11}
1.527	3.80×10^{-11}
1.321	3.65×10^{-10}
1.321	4.25×10^{-10}

Impurity content same as for other Mervyn crystals.

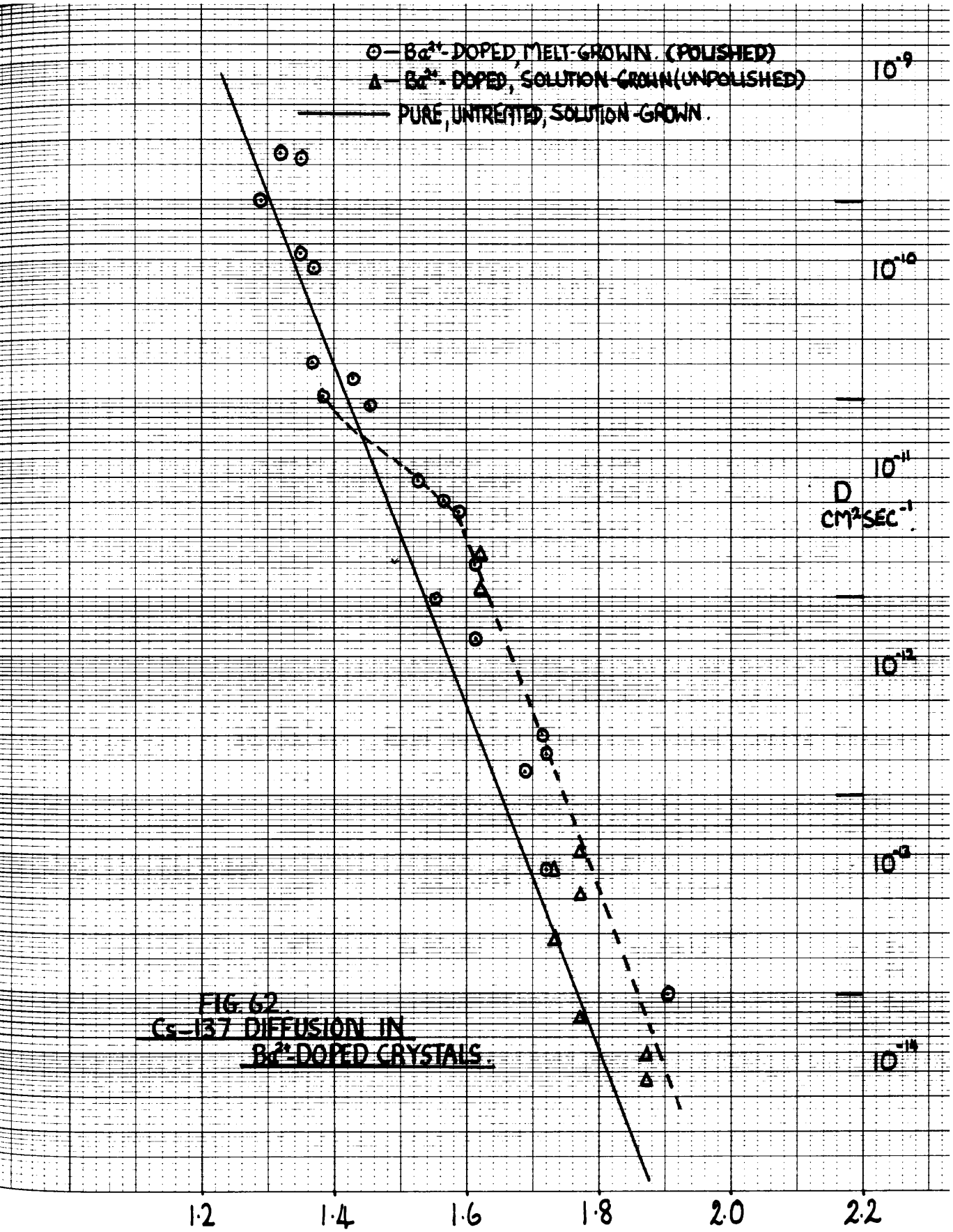

FIG. 62.
Cs-137 DIFFUSION IN
Ba^{2+}-DOPED CRYSTALS.

TABLE 51 (Fig. 62).

Cs^+ diffusion coefficients, calculated from $(\beta/\gamma)_{\text{before diffusion}}$ and $(\beta/\gamma)_{\text{after diffusion}}$, for Ba^{2+}-doped, polished, untreated melt-grown crystals of CsI.

$10^3/T(^\circ A)$.	$D(cm^2sec^{-1})$.	$10^3/T(^\circ A)$.	$D(cm^2sec^{-1})$.
1.905	$9.93x10^{-14}$	1.527	$3.90x10^{-11}$
1.720	$4.26x10^{-13}$	1.456	$9.00x10^{-11}$
1.720	$1.60x10^{-12}$	1.433	$1.28x10^{-10}$
1.715	$2.00x10^{-12}$	1.383	$1.00x10^{-10}$
1.686	$1.30x10^{-12}$	1.368	$1.50x10^{-10}$
1.613	$6.13x10^{-12}$	1.368	$4.50x10^{-10}$
1.613	$1.48x10^{-11}$	1.355	$1.59x10^{-9}$
1.590	$2.70x10^{-11}$	1.355	$5.37x10^{-10}$
1.565	$3.00x10^{-11}$	1.320	$1.70x10^{-9}$
1.548	$9.98x10^{-12}$	1.290	$9.60x10^{-10}$

Impurity Content.

$10^3/T(^\circ A)$.	$D(cm^2sec^{-1})$.	Impurity Content (m.f.)	Metals.
1.686	$1.30x10^{-12}$	$1.43x10^{-4}$	Ba, Cu, Fe.
1.548	$9.98x10^{-12}$	$2.10x10^{-4}$	Ba, Cu, Fe.
1.456	$9.00x10^{-11}$	$1.81x10^{-4}$	Ba, Sr, Fe, Cu.
1.368	$4.50x10^{-10}$	$1.35x10^{-4}$	Ba, Sr, Fe, Cu.
1.383	$1.00x10^{-10}$	$2.10x10^{-4}$	Ba, Cu, Fe.

TABLE 52 (Fig. 62).

Cs^+ diffusion in unpolished, vacuum annealed, Ba^{2+}-doped solution-grown crystals of CsI.

$10^3/T(^\circ A)$.	$D(cm^2 sec^{-1})$.
1.869	3.62×10^{-14}
1.869	4.79×10^{-14}
1.773	3.16×10^{-13}
1.773	5.21×10^{-13}
1.773	7.42×10^{-14}
1.733	4.18×10^{-13}
1.733	1.85×10^{-13}
1.621	2.58×10^{-11}
1.621	1.06×10^{-11}

The impurity content of these crystals is unknown.

3.2.(b). Cl - 36 DIFFUSION.

There was also a large scatter in the diffusion coefficient values in Cl - 36 diffusion. Unfortunately this cannot be corrected for, since Cl - 36 is only a β -emitter. However, we have quoted those results which were reasonably reproducible (Table 53) and have compared them with the interpolated 1.37 eV range observed by Lynch[47], Fig. 63. In cases where reproducibility is good $D_{Cl^-} \approx D_{I^-}$ (Lynch).

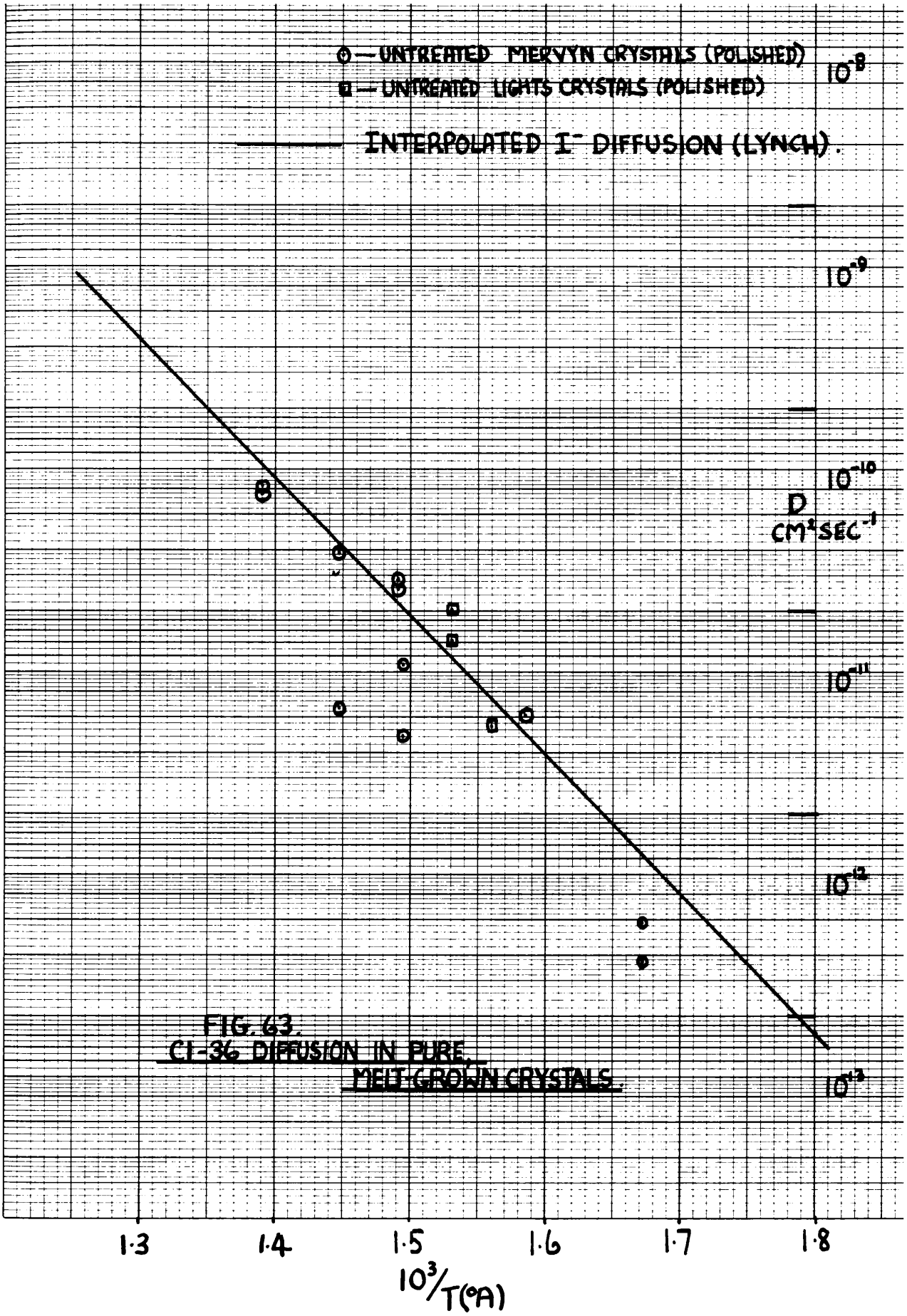

FIG. 63.
CI-36 DIFFUSION IN PURE, MELT-GROWN CRYSTALS.

TABLE 53 (Fig. 63).

Cl^- diffusion coefficients for polished, untreated Mervyn Instruments Limited and Lights Limited CsI single crystals.

$10^3/T(^\circ A)$.	$D(cm^2sec^{-1})$.
1.672	1.85×10^{-12}
1.672	2.90×10^{-12}
1.585	3.05×10^{-11}
1.560	2.70×10^{-11}
1.530	7.00×10^{-11}
1.530	1.00×10^{-10}
1.495	5.40×10^{-11}
1.495	2.50×10^{-11}
1.482	1.40×10^{-10}
1.482	1.30×10^{-10}
1.447	1.90×10^{-10}
1.447	3.35×10^{-11}
1.389	4.10×10^{-10}
1.389	3.95×10^{-10}

Impurity content - same as for other Mervyn and Lights crystals.

CHAPTER 4.

DISCUSSION.

4.1. CONDUCTIVITY IN PURE CRYSTALS.

(a) Untreated Crystals.

Two ranges of conductivity have been observed in undoped crystals over the temperature range 150-600°C. These two regions have been designated Ranges I and II.

Range I is the lower temperature range, generally occurring below 300°C. The conductivity in this range was not reproducible and there is possibly some contribution from impurity effects. A detailed discussion of this range will therefore be given in the section on doped crystals. Range II showed good reproducibility for crystals grown by the same technique though there was a slight difference in the magnitude of conductivity ($\sim$ 1.4 times) between crystals from Mervyn Instruments Limited, and solution-grown crystals, Table 54. However the activation energies were identical. The conductivity equations for Mervyn Instruments Limited, and solution-grown crystals are summarised below.

1. Mervyn Crystals.

$$\underset{(ohm^{-1}cm^{-1})}{\sigma} = 8.48 \times 10^{4} \exp.\ (-1.37\ (eV)/kT) \quad \text{---- (41)}$$

2. Solution-Grown Crystals.

$$\underset{(ohm^{-1}cm^{-1})}{\sigma} = 6.04 \times 10^{4} \exp.\ (-1.37\ (eV)/kT) \quad \text{---- (42)}$$

(b) Annealed Crystals.

The general effect of annealing the crystals under vacuum was to increase the conductivity in Range I: this will be discussed later. The activation energy in Range II was essentially unchanged though the conductivity was raised slightly. The conductivity of all samples in Range II was the same and the conductivity equation can be represented by

$$\underset{(ohm^{-1}cm^{-1})}{\sigma} = 1.13 \times 10^{5} \exp.\ (-1.37(eV)/kT) \quad \text{---- (43)}$$

and a comparison of the results for annealed and untreated crystals in the present research with those of other workers is given in Table 55.

TABLE 54.

Conductivity parameters for "pure" CsI crystals in Range II.

	Crystal Source.	Temperature Range (°C).	E_A(eV).	$\bar{\sigma}_{1.5\ R.T.U.}$ ($ohm^{-1}cm^{-1}$).
1.	Mervyn Instruments	235-497	1.37	4.50×10^{-6}
2.	Mervyn Instruments	265-479	1.37	4.50×10^{-6}
3.	Lights	344-514	1.33	3.00×10^{-6}
4.	Lights	344-502	1.33	3.00×10^{-6}
5.	Stockbarger Techique	315-560	1.36	5.00×10^{-6}
6.	Solution-Grown	283-496	1.37	3.30×10^{-6}
7.	" "	289-479	1.37	3.30×10^{-6}
8.	" "	227-496	1.37	3.30×10^{-6}

TABLE 55.

Conductivity parameters for CsI.

Reference.	Crystal Type.	Temperature Range (°C).	E_A(eV).	$\bar{\sigma}_o$ ($ohm^{-1}cm^{-1}$).
Present Work	Mervyn Untreated	~300-600	1.37	8.48×10^{4}
	" Annealed	~300-600	1.37	1.13×10^{5}
	Solution-grown Untreated	~300-600	1.37	6.04×10^{4}
	Solution-grown Annealed	~300-600	1.37	1.13×10^{5}
Lynch[47]	Melt-grown	~350-480	1.25	1.38×10^{4}
		480-595	1.43	2.21×10^{5}
Ubbelohde et al[49]	Polycrystalline	530-600	1.37	3.00×10^{4}
Rossel et al[51]	Zone-Refined	>400	1.49	$\sim 1.00 \times 10^{6}$
Rossel et al[52]	Zone-Refined	203-420	1.33	-
		>420	1.60	-

The results of the present research compare favourably with those from previous work on CsI. The activation energy for the conduction process in Range II is in good agreement with that reported by Rossel et al[52] (1.33 eV), Ubbelohde et al[49] (1.37 eV) and Lynch[47] (1.43 eV). The 1.37 eV range reported by Ubbelohde et al[49] was interpreted as being due to electronic conductivity. Lynch[47] has discounted electronic conductivity in this range, but postulated that a range of activation energy 1.25 eV between 350-480°C was in fact intrinsic conductivity due to the movement of thermally created defects. However above 480°C Lynch observed a conductivity range of activation energy 1.43 eV which was not discussed in detail. The crystals of CsI used in Lynch's work contained impurities of the order of 0.01% and it could be argued that the conductivity in the range 350-480°C was in fact subject to impurity effects. If this is the case the 1.43eV range would seem to be associated with an intrinsic property of the crystal.

Rossel et al[52] also observed a high temperature range in addition to the 1.33 eV range already mentioned. This second region of conductivity occurred above 420°C and had an activation energy of approximately 1.60eV. Lynch[47] and also Ubbelohde et al[49] observed concavity in their σ / reciprocal temperature plots very near the melting point. It seemed likely that the observed increase in conductivity observed by Lynch and Ubbelohde et al was due to pre-melting phenomena. In the present research a high temperature range was also observed, though this region was not in evidence in pure crystals. This range ($R_a$nge III) will be discussed in the section on doped crystals.

The reproducibility in activation energy in Range II for both annealed and unannealed crystals would suggest that this was in fact the intrinsic range. At any one temperature the difference in the magnitude of σ^- between annealed and unannealed crystals was less than a factor of 2. This, however, was greater than the expected experimental error. This change in conductivity upon annealing does not seem to be associated with any change in the defect nature of the crystal, since any additional conductivity mechanism induced by the annealing process would be expected to manifest itself by a change in activation energy. This was not in fact observed. It should be pointed out that during annealing under vacuum at 500°C, some evaporation did occur from the crystal faces and it may well be that the reason for the change in the magnitude of σ^- is connected with a change in surface area of the crystal, which would lead to a change in conductivity magnitude, but not activation energy. It is significant that annealing in "atmospheres other than vacuum" e.g. I_2 - Fig. 49 and air - Fig. 48 produced no increase in σ^- i.e. Range II was the same as for untreated crystals. For this reason, since our Cs^+ diffusion was carried out in a nitrogen atmosphere and Lynch's I^- diffusion in a helium atmosphere, the comparison of conductivity and diffusion will be made with the untreated crystals.

4.2. DIFFUSION IN PURE CRYSTALS.

A single range of Cs-137 diffusion has been found in solution-grown, untreated crystals of pure CsI over the temperature-range 250-500°C, Fig. 58. Although the results for Mervyn unannealed crystals cannot be regarded as conclusive, they do indicate the same diffusion range as the solution-grown crystals, Figs. 59-60. The diffusion can be represented by

$$D_{(cm^2 sec^{-1})} = 2.25 \times 10^2 \exp.(-1.74(eV)/kT) \qquad \text{------ (44)}$$

The only previous diffusion measurements in this system have been made by Lynch[47] and the results of the present work for Cs^+ diffusion were in disagreement with Lynch's reported data. The magnitude of the Cs^+ diffusion in the present research was lower at low temperatures and a higher activation energy, 1.74eV as opposed to 1.54 eV (Lynch) was obtained. However the magnitude of the diffusion coefficient D was approximately the same in both cases at 500°C.

No measurements of I^- self-diffusion have been made, but the few Cl^- diffusion studies made were in reasonable agreement with Lynch's results for I^- diffusion, Fig. 63. Chemla[54] observed little difference in diffusion between Na^+ and other monovalent positive ions in NaCl. There was also little change in diffusion from the value for Cl^- when Br^- and I^- were examined in NaCl. This would be in agreement with the observations in this research, i.e. Cl^- diffusion of the same magnitude as I^- diffusion in CsI reported by Lynch. It should be mentioned, however, that in a recent publication by Mullen et al[78] on Rb^+ diffusion in NaCl, KCl and RbCl, that there were significant changes in activation energy and diffusion magnitude between Rb^+ and Na^+ in NaCl and Rb^+ and K^+ in KCl. The larger Rb^+ ion showed a higher activation energy and slightly higher diffusion coefficient than the Na^+ ion, for diffusion in NaCl. Similar effects were observed in KCl. However, $R_{Cl^-} < R_{I^-}$, and if one takes Chemla's work into account it is unlikely that this change in ion should appreciably affect the diffusion parameters. Certainly an order of magnitude difference would not be expected and therefore we may be justified in using D_{I^-} (Lynch) and D_{Cs^+} (present work) for comparisons between the diffusion and the conductivity.

4.2.(a) Cs^+ DIFFUSION IN PURE, ANNEALED MERVYN CRYSTALS.

There appeared to be a slight lowering of activation energy for Cs^+ diffusion in pure, Mervyn annealed crystals, Fig. 61, and the diffusion coefficients were slightly higher than in the pure untreated crystals. It is difficult to say whether this increase is of any significance in the light of the unreproducibility associated with polished crystals. Even if this increase is in fact genuine it is too small to account for the increase in σ^- on annealing under vacuum because of the low D_{Cs^+}/D_{I^-} ratio.

4.3. COMPARISON OF σ^- AND D IN PURE CRYSTALS.

If the conductivity in the intrinsic range is purely ionic, and it is the same processes which are responsible for diffusion and conductivity, then a comparison of the results obtained by the two techniques can be made using the Nernst-Einstein relationship (equation 22).

$$\text{i.e.} \quad \frac{\sigma^-}{D_{Cs^+} + D_{I^-}} = \frac{Ne^2}{kT}$$

However, as discussed in the introduction a correlation factor (f) must be included where $f = \frac{D_{Cs^+} + D_{I^-}}{D_{\sigma^-}}$

and where D_{σ^-} is the diffusion calculated from the conductivity using the Nernst-Einstein equation. The evaluation of f can be used as a means of identifying the ionic migration mechanism. For vacancy migration in a CsI lattice $f = 0.6555$,[19] while for movement of interstitials by direct jumps $f = 1$[47].

It is therefore our intention to use our D_{Cs^+} results along with the D_{I^-} results obtained by Lynch and to compare these with the values of D calculated from the conductivity results. We have assumed that the high temperature range of I^- diffusion ($> 410^\circ C$) of

activation energy 1.37eV is in fact associated with intrinsic behaviour, since below 410°C, where Lynch observed a range of I^- diffusion of activation energy 1.28eV, there could be significant impurity effects: the crystals used by Lynch contained ~ 0.01% impurity. Thus the calculation of f has been based on the observed Cs^+ diffusion in this work and the interpolated I^- diffusion (1.37eV) observed by Lynch. However for comparison purposes f derived from the actual I^- diffusion (1.28 and 1.37eV) has been included. The results for solution-grown and Mervyn melt-grown crystals are shown in Tables 56 and 57.

TABLE 56.

Correlation factor f for solution-grown crystals.

$10^3/T(°A)$.	D_{Cs^+} (this work) + D_{I^-} (actual)47 (1) (cm^2sec^{-1}).	D_{Cs^+} (this work) + D_{I^-} (1.37eV) (2) (cm^2sec^{-1}).	$D\sigma$ (cm^2sec^{-1})	f(1).	f(2).
1.8	1.26×10^{-12}	8.72×10^{-13}	8.60×10^{-13}	1.47	1.01
1.7	5.68×10^{-12}	4.38×10^{-12}	4.25×10^{-12}	1.34	1.03
1.6	2.68×10^{-11}	2.23×10^{-11}	2.10×10^{-11}	1.28	1.07
1.5	1.20×10^{-10}	1.13×10^{-10}	1.10×10^{-10}	1.09	1.03
1.4	5.95×10^{-10}	5.95×10^{-10}	5.72×10^{-10}	1.04	1.04
1.3	3.20×10^{-9}	3.20×10^{-9}	2.85×10^{-9}	1.13	1.13

TABLE 57.

Correlation factor f for Mervyn melt-grown crystals.

$10^3/T(^\circ A)$.	D_{total} (1) (cm^2sec^{-1}).	D_{total} (2) (cm^2sec^{-1}).	D_σ (cm^2sec^{-1}).	f(1).	f(2).
1.8	$1.26x10^{-12}$	$8.72x10^{-13}$	$1.15x10^{-12}$	1.10	0.76
1.7	$5.68x10^{-12}$	$4.38x10^{-12}$	$5.91x10^{-12}$	0.96	0.74
1.6	$2.69x10^{-11}$	$2.23x10^{-11}$	$3.00x10^{-11}$	0.89	0.74
1.5	$1.20x10^{-10}$	$1.13x10^{-10}$	$1.55x10^{-10}$	0.78	0.73
1.4	$5.95x10^{-10}$	$5.95x10^{-10}$	$7.74x10^{-10}$	0.77	0.77
1.3	$3.20x10^{-10}$	$3.20x10^{-9}$	$4.16x10^{-9}$	0.77	0.77

The variation in the values of f(1) compared with the constancy of f(2) suggests that our assumption that D_I-(1.37eV) is intrinsic is justified. The value of f(2) lies between the theoretical estimates for Schottky vacancy migration and interstitial movement. However the fact that D_{Cs^+} and D_I- are less than a factor of ten different in this temperature range suggests that Schottky defects are responsible for ionic migration. If Cs^+ had been diffusing by an interstitial mechanism it would be expected that there would be a greater difference between the values of D_{Cs^+} and D_I-[79]. The slightly larger value of f(2) could possibly be due to some diffusion occurring via neutral defects such as anion-cation vacancy pairs. This diffusion would not contribute to ionic conductivity and so D_{total}/D_σ would certainly be larger. Large correlation effects would be expected for diffusion by the interstitialcy mechanism, which was not what was found in this case.

The variation in the f(2) value at 1.30 R.T.U. may be significant. The theoretical calculation of σ from D_{total} predicted an increase in activation energy above 420°C for conductivity (Range III). This activation energy should be about 1.55eV, which would result in a 20% increase in σ at 500°C. This should certainly be observed using the experimental system for conductivity already described. However, the increase has not been observed in pure crystals in this research, though the high temperature range observed by Rossel et al[52], already mentioned, is in agreement with these theoretical predictions. Range III, however, existed in some cation-impurity doped specimens and these will be discussed later.

4.4. CONDUCTIVITY IN DOPED CRYSTALS.

The original intention was to investigate crystals of CsI doped with Ba^{2+}. However, in crystals grown from solution and also some melt-grown crystals there was an appreciable amount of other alkaline-earth impurities (Sr^{2+}, Ca^{2+}). The CsI reagent used for crystal growth was obtained from Messrs. Hopkins and Williams Limited and Messrs. B.D.H. Limited. High purity CsI was not obtainable at the time, though recently OPTRAN high purity CsI has become available. Although the manufacturers' claimed the same source of CsI for their reagents, (and on this basis no special decision was made on the supplier), it has been found that the CsI supplied by Hopkins and Williams Limited is much purer than that of B.D.H. Limited.

4.4(a) UNTREATED CRYSTALS GROWN OVER H_2SO_4 AS DESICCANT.

Two conductivity regions were observed in these crystals corresponding to Ranges I and II in pure crystals. Range I was not reproducible from sample to sample and is discussed in detail later. Range II showed constant values of E_A but there were slight changes in the magnitude of σ varying

between pure, solution-grown unannealed and Mervyn unannealed crystals.

Three of the crystals showed a high temperature conductivity range, corresponding to Range III already mentioned, Figs. 32 - 34. This range occurred in these specimens above 440°C, which is too low for this to be associated with pre-melting phenomena. It is significant that the activation energy shown in this range was 1.55 - 1.57 eV which is very near to that predicted by the diffusion results and it would appear that this range is associated with the increasing significance of the cation defect at these temperatures. The untreated Ba^{2+}-doped crystals, as will be suggested later, contained very little substitutionally dissolved impurity and may be considered to be behaving as "pure" crystals in this range. However it is strange that the pure crystals did not exhibit Range III at all, though Rossel et al[52] working on very pure crystals of CsI did observe this higher activation energy above 420°C. It is apparent that a closer examination of the conductivity and diffusion in this region is required.

4.4.(b) ANNEALED CRYSTALS.

The conductivity of the annealed doped crystals showed significant differences from untreated specimens, Figs. 38 - 47. There existed four ranges of conductivity, Range I and II as before, and in addition Ranges I (a) and I (b) both of which occurred between Ranges I and II.

In Range I (a) the conductivity was reproducible from sample to sample and there was thermal hysteresis in the conductivity on cooling . This behaviour is symptomatic of a region in which impurity dissolution is taking place. Conductivity parameters for this range are shown in Table 58.

TABLE 58.

Conductivity parameters in Range I (a).

Crystal Type.	Alkaline-earth Content (m.f.).	E_A(eV).	σ 1.7 R.T.U. ($ohm^{-1}cm^{-1}$).
Ba^{2+}-doped solution-grown (H_2SO_4 as desiccant)	4.45×10^{-4}	1.28	5.60×10^{-7}
Ba^{2+}-doped solution-grown (H_2SO_4 as desiccant)	8.10×10^{-4}	1.30	5.90×10^{-7}
Ba^{2+}-doped solution-grown (H_2SO_4 as desiccant)	2.10×10^{-4}	1.33	5.50×10^{-7}
Ba^{2+}-doped solution-grown (H_2SO_4 as desiccant)	1.56×10^{-3}	1.34	5.50×10^{-7}
Ba^{2+}-doped solution-grown (H_2SO_4 as desiccant)	1.48×10^{-3}	1.36	4.80×10^{-7}
Ba^{2+}-doped solution-grown ($CaCl_2$ as desiccant)	7.84×10^{-4}	1.44	4.70×10^{-7}
Unannealed Ba^{2+}-doped solution-grown ($CaCl_2$ as desiccant)	4.50×10^{-4}	1.28	5.00×10^{-7}
Unannealed Ba^{2+}-doped solution-grown ($CaCl_2$ as desiccant)	7.84×10^{-4}	1.20	4.00×10^{-7}
Ba^{2+}-doped melt-grown (Unannealed)	-	1.31	4.00×10^{-7}

TABLE 58 (contd.)

Crystal Type.	Alkaline-earth Content (m.f.)	E_A(eV).	σ 1.7 R.T.U. ($ohm^{-1}cm^{-1}$).
Ba^{2+}-doped melt-grown (Unannealed)	5.70×10^{-5}	1.38	3.60×10^{-7}
Ba^{2+}-doped melt-grown (Annealed)	1.96×10^{-4}	1.34	4.40×10^{-7}

There was no correlation between the extent of the "solubility" range and the Ba^{2+}, Sr^{2+} or Ca^{2+} concentrations, nor was there any agreement between the extent of the range and the Cu or Fe content. It would seem logical to assume that the range is due to the alkaline-earth impurity since there was no noticable effect of Fe or Cu in crystals containing only those metals c.f. Mervyn and Stockbarger pure crystals.

Range I (b), in the light of the above proposals, would appear to be due to free cation vacancy movement or to dissociation of cation impurity-vacancy complexes. A more detailed analysis of this range will be given later. Range II, the intrinsic range was in agreement with pure, annealed crystals.

4.4.(c) CRYSTALS GROWN OVER $CaCl_2$ AS DESICCANT.

The untreated Ba^{2+}-doped crystals grown over $CaCl_2$ differed from those grown over H_2SO_4 in that they showed Ranges I (a) and I (b) without annealing but the solubility range showed an anomalously low break temperature.

However, on annealing, the solubility range was extended and agreed with the solubility range observed in annealed crystals grown over H_2SO_4 as desiccant, Table 58.

4.4.(d) CRYSTALS GROWN BY THE STOCKBARGER TECHNIQUE.

These crystals showed the same behaviour as those grown from solution over $CaCl_2$, in that a solubility range with an anomalous break temperature was observed prior to annealing, and this reverted to alignment with the annealed solution-grown crystals after a high temperature anneal, Table 58.

4.4.(e) CONDUCTIVITY IN RANGE I (a) (ALL CRYSTALS).

The conductivity in this range was reproducible from sample to sample and thermal hysteresis was observed on cooling. These characteristics indicate that the conductivity is due to impurity dissolution in the crystal lattice[45]. If this is the case then using the Lidiard notation[16]

$$c(c + \alpha_1) = \exp.\ (- \Gamma_1/kT) \qquad \text{---------- (45)}$$

where c is the cation impurity content in mole fractions (m.f.)

α_1 is the cation vacancy concentration in m.f.

Γ_1 is the free energy of solution.

Where $c \gg \alpha_1$ then,

$$c^2 = \exp.\ (- \Gamma_1/kT) \qquad \text{---------- (46)}$$

$$\text{i.e. } c = \exp.\ (- \Gamma_1/2kT) \qquad \text{---------- (47)}$$

The free energy term can be split into an entropy and enthalpy term in the usual fashion giving

$$c = \exp.\ (\eta_1/2k) \exp.\ (-\chi_1/2kT) \text{---- (48)}$$

Where χ_1 is the enthalpy of solution and η_1 is the entropy of solution.

$$\text{i.e. } c = A \exp.\ (-\chi_1/2kT) \qquad \text{---------- (49)}$$

The solubility range had a higher magnitude than the intrinsic range which would suggest that there was an appreciable concentration of impurity going into solution. For small amounts of impurity the effect would be to depress the thermal anion vacancy concentration which, as has already been discussed, is the main contribution to the conductivity at these temperatures. Therefore the magnitude of the solubility range would tend to suggest that $c \gg \alpha_1$. From equation (49) when $c \gg \alpha_1$ a plot of the solubility range break temperature (i.e. extent) versus $1/T$ should be a straight line of slope $-\gamma_1/2k$. The extent of the solubility range has therefore been examined as a function of mole-fraction alkaline-earth impurity and the results are shown in Fig. 64. A least squares analysis of the data gives a value for $\gamma_1/2$ of 0.67 ± 0.11eV. The heat of solution γ_1 would seem to be of the order 1.35eV and this must be taken as the average heat of solution for alkaline-earth impurity. The 2.10×10^{-4} m.f. alkaline-earth crystal, which is the furthest from the least squares line, seemed to be in error since other analyses on crystals from the same batch gave alkaline-earth impurity contents of the order 5.0×10^{-4} m.f., which would be much more compatible with the other results. The average activation energy in the solubility-range (1.34eV) will not, of course, be equal to $U_+ + \gamma_1/2$, since there will be contributions from thermal anion vacancies in this range. Thus no value of U_+ could be estimated.

It is unlikely that the incorporation of SO_4^{2-} ions from the desiccant would prevent the appearance of a solubility range in untreated crystals grown over H_2SO_4, since there was no effect on the conductivity by the deliberate additions of SO_4^{2-} (or CO_3^{2-}) even upon annealing and

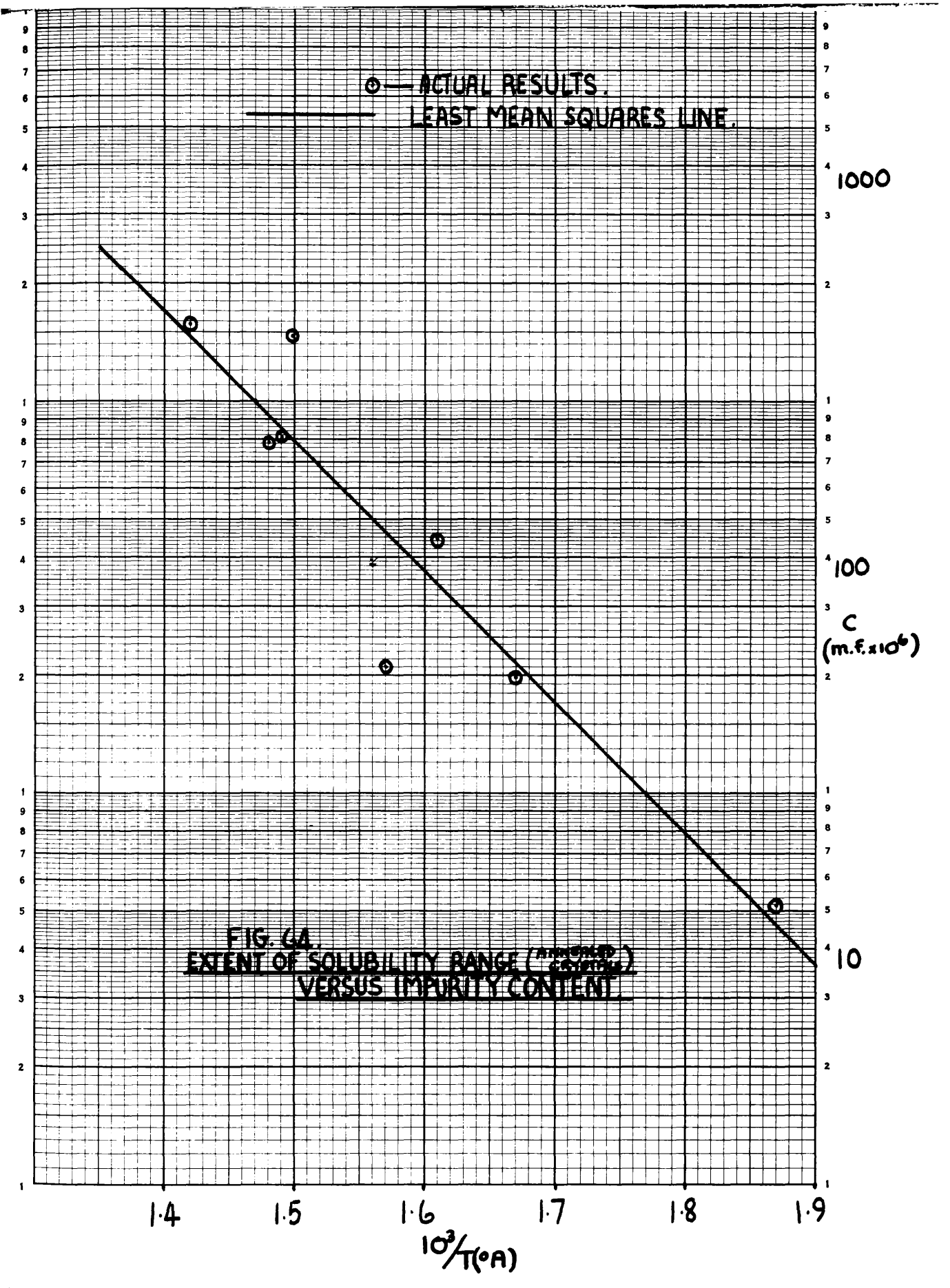

FIG. 6A.
EXTENT OF SOLUBILITY RANGE (ANNEALED SILICON) VERSUS IMPURITY CONTENT.

quenching from high temperatures, Figs. 55 - 56. Also there was no significant difference between the conductivity and diffusion of "pure" crystals grown over H_2SO_4 and $CaCl_2$ as desiccants. The anomaly may be associated with the rate of crystal growth. Generally H_2SO_4 produced faster growth than $CaCl_2$ - less than a week for H_2SO_4 as opposed to weeks for $CaCl_2$. The impurity, which is obviously very insoluble, will probably be present as large "islands" of precipitate in crystals grown over H_2SO_4 and so long periods of annealing are required to break up these "islands" and so produce a more uniform distribution of impurity. Crystals grown over $CaCl_2$ as desiccant will have a slightly more random distribution of impurity and so some can go into solution more readily, but the larger "islands" will still be insoluble. The solubility range break temperature is low because all of the impurity is not dissolved. The crystal requires annealing to produce a completely uniform distribution, and this was confirmed by the comparative agreement between an annealed, doped crystal grown over $CaCl_2$ and the other annealed, doped crystals grown over H_2SO_4, Fig. 47,

The anomalies in the unannealed, melt-grown, doped crystals arise from the non-random distribution of impurity due to the mechanical working and polishing involved in their preparation. The strain introduced by these treatments is removed during the high temperature anneal and the conductivity falls into line with that observed in the annealed crystals.

Further proof of the great insolubility of the cation impurities was obtained by thermal cycling studies. Although there was hysteresis on cooling the crystal from temperatures above the solubility range, further heatings

showed that the impurity had precipitated out at low temperatures on cooling.

4.4.(f) CONDUCTIVITY IN RANGE I (b).

Range I (a) has already been discussed in terms of the dissolution of cation impurity in the crystal lattice. However this solubility range occurred at only a slightly higher magnitude of conductivity than the intrinsic range, and we are therefore faced, in Range I (b), with the experimental limitation of only a small temperature range over which the conductivity can be examined, Fig. 54. It has been suggested that association of impurity with vacancies is a precursor to impurity-dissolution[32]. Vacancy formation due to impurity must reduce the thermal vacancy concentration, and since anion vacancies are the predominant species in conductivity at these temperatures, this would result in a considerable decrease in conductivity due to thermal vacancies. If the impurity vacancies are associated they would not contribute to the conductivity and it would be expected that σ^- would be lower than σ^- (intrinsic). We have observed $\sigma^- > \sigma^-$ (intrinsic) and so the degree of association must be small. If this conductivity range is indeed due to free vacancies, then the activation energy for the process should be U_+, the activation energy for mobility of a positive ion vacancy. The activation energies observed in this range are shown in Table 59.

TABLE 59.

Activation energies for conductivity in Range I (b).

Alkaline-Earth Impurity Content (m.f.).	Crystal Type.	E_A (eV).
4.45×10^{-4}	Solution-grown	0.92
8.10×10^{-4}	" "	1.04
2.10×10^{-4}	" "	0.96
1.56×10^{-3}	" "	0.86
1.48×10^{-3}	" "	1.07
7.84×10^{-4}	" "	0.92
1.96×10^{-4}	Melt-grown (Stockbarger)	0.90

It would seem that U_+ is of the order of 0.90eV, which is considerably higher than the value of 0.58eV proposed for U_+ by Lynch[47].

It should be possible to analyse the results in this range in the manner proposed by Lidiard[16]. In a system where the mobility of the negative ion is greater than that of the positive ion the relative conductivity (σ/σ_o)/impurity content isotherms should show a minimum at positive impurity concentrations. The minimum relative conductivity is given by

$$(\sigma/\sigma_o)_{min} = \frac{2\phi^{\frac{1}{2}}}{1+\phi} \qquad \text{---------- (31b)}$$

and the impurity content at the minimum by

$$c_{min} = \frac{x_o(\phi-1)}{\phi^{\frac{1}{2}}} \qquad \text{---------- (31a)}$$

The above equations and terms have already been discussed in the introduction. The results have been analysed in

this range at 1.55 R.T.U. and 1.50 R.T.U. and the isotherms are shown in Figs. 65 and 66 respectively. A prediction of c_{min} cannot be made since α_o is unknown. However $(\sigma/\sigma_o)_{min}$ can be calculated, as it depends only on the value of ϕ, the mobility ratio μ_2/μ_1, which can be estimated from the self-diffusion results since $\phi = \mu_2/\mu_1 = D_I^-/D_{Cs^+}$. The values of ϕ at 1.55 and 1.50 R.T.U. are 5.33 and 4.50 respectively. These values lead to estimates of $(\sigma/\sigma)_{o\ min}$ at 1.55 and 1.50 R.T.U. respectively, of 0.73 and 0.77 $ohm^{-1}cm^{-1}$. Figs. 65 and 66 show that there is a definite minimum at each temperature, and also the comparative agreement of the magnitude of the minimum with that calculated. It was difficult to estimate with a high accuracy the value of c_{min} from the graphs, since there were few results in the area of the minimum. However, c_{min} at 1.55 R.T.U. appears to be $\sim 1.00 \times 10^{-4}$ m.f. and at 1.55 R.T.U. $\sim 1.50 \times 10^{-4}$ m.f. It is to be stressed that these can only be regarded as estimates; however they are to be used in the calculation of α_o, the concentration of intrinsic defects, at these temperatures.

Substitution of $c_{min} = 1.00 \times 10^{-4}$ in equation (31a) gave a value of 5.33×10^{-5} m.f. for α_o at 1.55 R.T.U. A similar calculation gave $\alpha_o = 9.09 \times 10^{-5}$ m.f. at 1.50 R.T.U. From these values of α_o it was possible to calculate the conductivity at different impurity contents by substitution in equation (28)

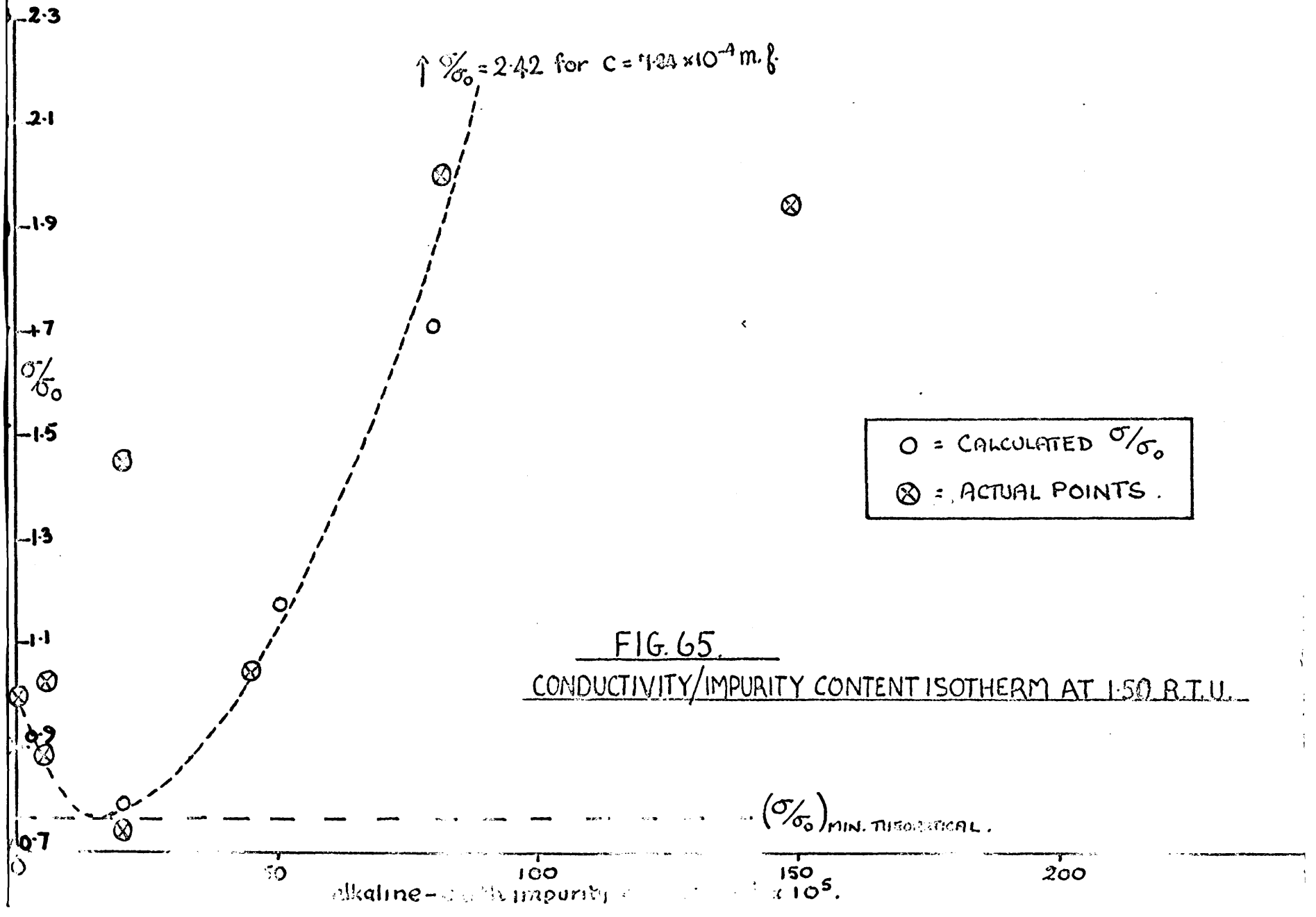

FIG. 65.

CONDUCTIVITY/IMPURITY CONTENT ISOTHERM AT 1·50 R.T.U.

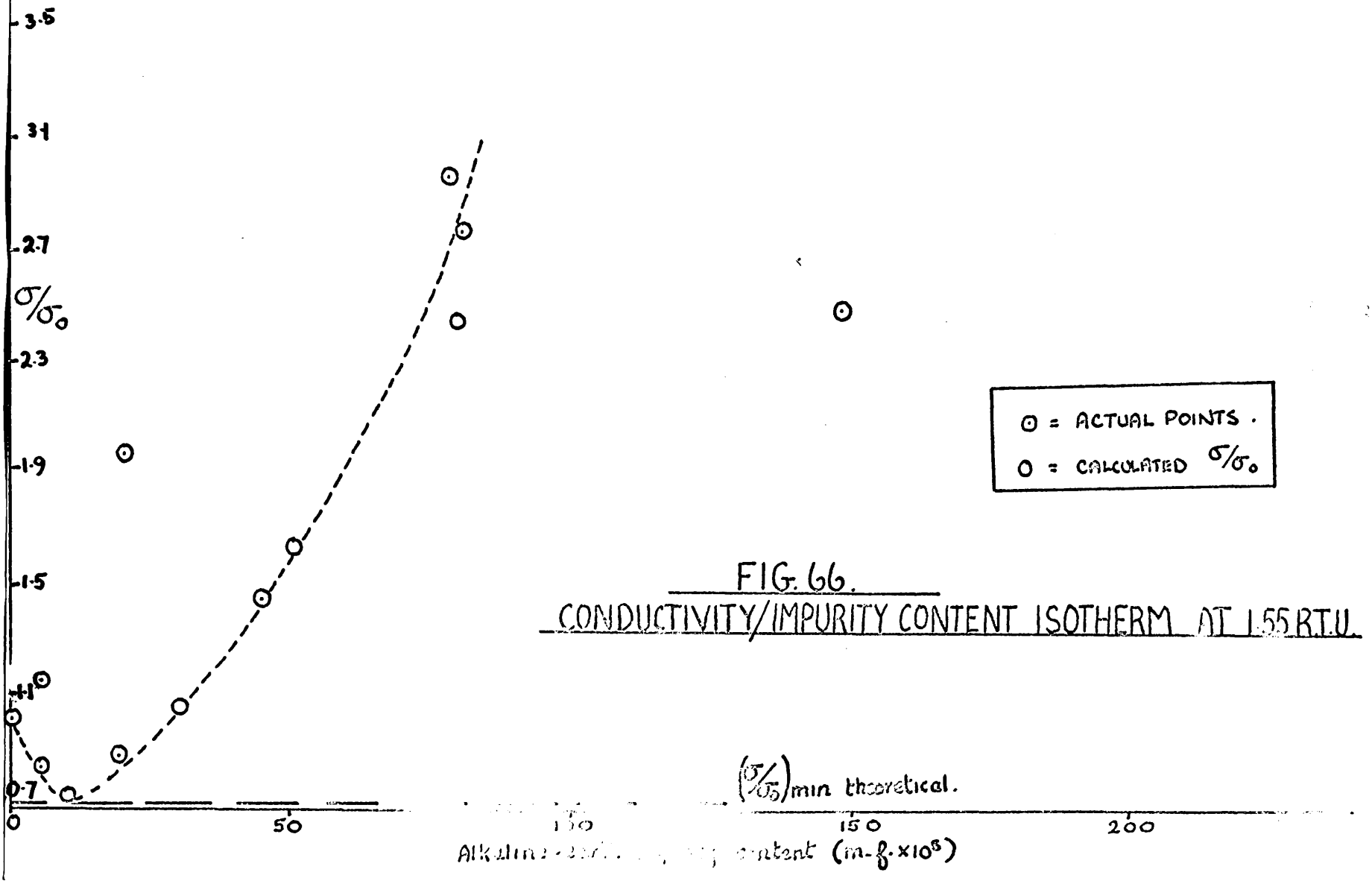

FIG. 66.

CONDUCTIVITY/IMPURITY CONTENT ISOTHERM AT 1.55 R.T.U.

$$\text{i.e. } \sigma/\sigma_o = \left\{\left(\frac{c}{2x_o}\right)^2 + 1\right\}^{\frac{1}{2}} - \frac{c}{2x_o} \cdot \frac{\phi - 1}{\phi + 1} \quad \text{---- (28)}$$

From an examination of the graphs it can be seen that generally there is good agreement between calculated and experimental values of σ/σ_o, though the result at impurity content 1.48×10^{-3} m.f. would seem to be in error. These observations would indicate that there is little or no association at these temperatures[80].

From the magnitude of the values of x_o at 1.55 and 1.50 R.T.U. an estimate of γB, the pre-exponential factor in the thermal vacancy concentration equation (10), can be made. Calculations of γB have been made for NaCl and KCl[15] and they predict that for Schottky vacancies γB is 10^2-10^3 - the value for Frenkel defects is much smaller. Assuming that W the heat of formation of a Schottky defect is 2.00eV, γB for CsI is approximately 3×10^3, which would seem to confirm the existence of Schottky defects in this salt.

4.4(g) CONDUCTIVITY IN RANGE I.

The conductivity of cation impurity-doped crystals, both annealed and unannealed, is summarised in Tables 60 and 61.

TABLE 60.

Conductivity of untreated cation-impurity doped crystals in Range I.

Crystal Type.	Temperature Range (°C).	Impurity Content (m.f. Alkaline-Earth).	σ 2.0 R.T.U. ($ohm^{-1}cm^{-1}$).	E_A(eV).
Melt-grown (Stockbarger)	162-253	-	9.00×10^{-9}	0.61
Melt-grown (Stockbarger)	147-256	5.70×10^{-5}	1.00×10^{-8}	0.42
Solution-grown (H_2SO_4 desiccant)	205-253	-	1.80×10^{-9}	0.79
Solution-grown (H_2SO_4 desiccant)	253-402	-	1.20×10^{-8}	1.09
Solution-grown ($CaCl_2$ desiccant)	203-256	7.84×10^{-4}	1.10×10^{-8}	0.78
Solution-grown ($CaCl_2$ desiccant)	232-315	4.87×10^{-4}	8.80×10^{-9}	1.06

The other untreated cation impurity doped crystals (see Results section) did not show a significant range corresponding to Range I.

TABLE 61.

Conductivity of annealed cation impurity-doped crystals in Range I.

Crystal Type.	Temperature Range (°C).	Impurity Content (m.f. Alkaline-Earth).	$\sigma_{2.0\ R.T.U.}$ ($ohm^{-1}cm^{-1}$).	E_A(eV).
Melt-grown (Stockbarger)	168-265	1.96×10^{-4}	1.00×10^{-8}	0.80
Solution-grown (H_2SO_4 desiccant)	160-315	4.45×10^{-4}	5.00×10^{-8}	curved
Solution-grown (H_2SO_4 desiccant).	203-280	5.20×10^{-5}	5.50×10^{-8}	0.90
Solution-grown (H_2SO_4 desiccant)	224-315	8.10×10^{-4}	2.40×10^{-8}	0.93
Solution-grown (H_2SO_4 desiccant)	< 305	2.10×10^{-4}	-	curved
Solution-grown (H_2SO_4 desiccant)	222-315	5.20×10^{-5}	1.15×10^{-8}	0.85
Solution-grown (H_2SO_4 desiccant)	208-259	1.0×10^{-3}	8.90×10^{-9}	0.43
Solution-grown (H_2SO_4 desiccant)	177-360	1.56×10^{-3}	7.00×10^{-7}	curved
Solution-grown (H_2SO_4 desiccant)	253-302	1.48×10^{-3}	2.60×10^{-8}	0.75
Solution-grown ($CaCl_2$ desiccant)	242-315	7.84×10^{-4}	1.65×10^{-8}	0.93

There was no evidence of any correlation between the conductivity and any of the impurity contents.

Lynch[47] has postulated that the conductivity in this

range is controlled by cation vacancies created by the incorporation of aliovalent impurity in the CsI lattice, the value of U_+ being 0.58eV. However, there was no evidence for this from his diffusion results in this range. In certain cases a 0.60eV range has been observed in this research in the low temperature range, but the most marked example of this range was given by a Lights crystal Fig. 50, which, according to the analysis figures, was by far the purest crystal, containing, in fact, only $1x10^{-6}$ m.f. of Ca^{2+}.

Polarisation effects were investigated in this temperature range and no significant dependence of capacitance upon frequency was found. However, the temperature may be too low to expect polarisation, but if it had been present this would have indicated ionic conductivity[81]. Dielectric loss measurements in this range also showed no evidence of any vacancy complexes, Fig.57.

There was no evidence that this range was due to impurity-created anion vacancies and in any case divalent cation and anion impurities cannot both be soluble[82], although in this case at different temperatures. The results of the conductivity experiments on SO_4^{2-} doped CsI (Figs. 55 - 56) showed that the impurity had no significant effect on the conductivity in this range.

The low temperature range was frequently prefaced by a conductivity range of very low activation energy, (particularly in annealed specimens) and it is thought that this range may be associated with electronic conductivity. It was significant that in cases where this pronounced flat range existed that extrapolation and subtraction of this range from Range I gave conductivities which lay on the extension of the solubility range.

The suggestion that the low temperature conductivity is associated with electronic contributions stemmed from the observation that in certain of the cation impurity-doped solution-grown crystals after annealing, there was evidence of traces of free iodine (or possibly CsI_3), and the conductivity at low temperatures was particularly high in these crystals. The colouration disappeared at approximately 270°C but no iodine was evolved from the crystals. It is possible that some of the impurity remains in the crystal lattice, after the anneal, as M^+ rather than M^{2+}, the larger M^+ ion being more favourable, from the ion size point of view, for the CsI lattice.

i.e. $2MI_2$ (in CsI) $\rightleftharpoons$ 2MI(in CsI) + I_2 ---------- (A)

This would give rise to electronic conduction by the process

$$I^- \overset{e}{\curvearrowright} Ba^{2+} \rightarrow Ba^+ + I \overset{e}{\curvearrowright} Ba^{2+} + I^-$$

It would certainly seem that the free iodine production must be associated with the cation-impurity ions since there was no colouration observed in the pure, annealed crystals.

Annealing in I_2 should drive reation (A) to the left and therefore it might be expected that in the doped crystals subjected to this treatment, evidence of M^{2+} effects in the lattice might be observed. The results of the anneals in iodine vapour did in fact show enhanced conductivity in Range I, Fig. 51. It should be pointed out that this enhancement could be the result of destruction of OH^- ions in the crystal during the anneal[45].

It is suggested that there is a significant contribution from electronic conductivity at low temperatures but there must also be some ionic contribution since σ^- (solubility) + σ^- (proposed electronic) does not account for the observed magnitude of σ^- in all cases. The electronic contribution does not arise from the oxidation of Cs^+ proposed by Ubbelohde et al[49] since the conductivity in this range was usually the smallest in pure Mervyn crystals, though a Mervyn crystal annealed in air did show electronic conductivity at low temperatures, Fig. 48. However, it could arise from small amounts of

$$Cu^+ \longrightarrow Cu^{2+} + e$$
$$\text{or } Fe^{2+} \longrightarrow Fe^{3+} + e \quad \text{in the lattice.}$$

The ionic contribution may be the result of the very small amount of impurity which is soluble at these temperatures or there may possibly be some contribution from boundary effects though the latter should be small in CsI.

4.5. DIFFUSION OF Cs^+ IN UNANNEALED DOPED CRYSTALS, Fig.62.

The experiments were conducted on Ba^{2+}-doped melt-grown crystals, grown by the Stockbarger technique and also on some vacuum-annealed Ba^{2+}-doped solution-grown crystals. The analysis figures for the melt-grown crystals indicate similar alkaline-earth impurity contents $\sim 4.8 \times 10^{-5}$ m.f. (within the limits of errors on analysis). The Cs^+ diffusion results can be used in support of the conductivity results. The scatter in the results did not allow the calculation of activation energies but the results did show a high activation energy range between 250°C and 360°C, which may correspond to solubility Range I (a) observed in the conductivity experiments. Above 360°C there was a decrease in activation energy (c.f. Range I (b)) before the diffusion reached

approximately the pure, intrinsic Cs^+ diffusion line at 451°C. It is possible that these results could be considered to lie on Lynch's Cs^+ diffusion line, but it is regarded as significant that comparison of σ with D, for a section of crystal from the same boule as the crystals used in the diffusion studies showed close agreement. The crystal piece used in the conductivity experiment contained 5.7×10^{-5} m.f. alkaline-earth impurity and the solubility range extended to 372°C and Range I (b) extended to 467°C, Fig. 28. This is compared with 360°C and 451°C respectively for the diffusion experiments. This agreement between the conductivity and diffusion in these crystals suggested that the "impurity regions" observed in the diffusion measurements did in fact correspond to similar regions in the conductivity experiments.

4.6. CONCLUSIONS FROM THE RESULTS.

The results are in general agreement with those of Lynch[47] regarding the ion migration mechanisms. It would appear that Schottky defects are predominant, with movement occurring via vacancies. Both ions make significant contributions to the conductivity above 300°C though the contribution of the cation does not appear to be as large as that predicted by the transport number measurements on CsBr by Laurance[83]. However, Laurance has pointed out that in cases where the transport numbers are not nearly unity or zero, there will be complications associated with preferential growth phenomena at the crystal or compact interfaces which produce considerable scatter in the results.

It is suggested that the values of anion and cation migration activation energies are much higher than Lynch

proposed. Lynch postulated that the low temperature conductivity was associated with cation impurity-induced vacancies with U_+ = 0.58eV. He failed to substantiate this with his diffusion measurements, and also in our diffusion experiments there was no evidence of this low temperature range. We have certainly observed an activation energy of C.60eV, but there is no evidence that this is associated with impurities; in fact the most marked 0.60eV range occurred in a Lights crystal which contained practically no aliovalent cations, Fig. 50.

On the assumption that Range I (b) is associated with the movement of free vacancies created by dissolved cation impurity, the observed activation energies indicate that the value of U_+ is approximately 0.90eV. In the Cs^+ self-diffusion the activation energy was 1.74eV i.e. $U_+ + W/2$, which would lead to a value of W, the heat of formation of a Schottky defect, of about 1.70eV. The values for W in the other caesium halides proposed by Harvey[48] for CsCl (1.96 eV) and Lynch[47] for CsBr and CsI (2.0eV and 1.90eV respectively) are much higher, though these values rely on U_+ being 0.58eV. No theoretical calculations have been made of W for CsCl-type crystals. A simple calculation based on the Jost[5] polarisation considerations is summarised below.

$$E_{Pol} = (1 - 1/\varepsilon)\, e^2/2R \qquad \text{----------} \quad (50)$$

where ε is the dielectric constant (5.65 for CsI)

R is the radius of the vacancy.

E_{Pol} is the polarisation energy.

$$W = W_L - E_{Pol} \qquad \text{----------} \quad (51)$$

where W is the heat of formation of a Schottky defect

W_L is the lattice energy (6.07eV[84] for CsI).

$$\therefore \quad E_{Pol} = e^2/2\,(1 - 1/\varepsilon)(1/R_+ + 1/R_-) \quad \text{---------- (52)}$$

R_+ and R_- are given by 0.9a and 0.6a respectively for the alkali-halides[6] and a is the cation-anion distance.

$$\therefore \quad E_{Pol} = \frac{(4.8029\text{x}10^{-10})^2}{2}\left[1 - \frac{1}{5.65}\right]\left[\frac{10^8}{3.564} + \frac{10^8}{2.376}\right] \text{ ergs/mol.}$$

$$= \frac{(4.8029)^2 \text{ x } 0.823 \text{ x } 7.042 \text{ x } 10^{-13}}{2} \text{ ergs/mol.}$$

$$= 6.690\text{x}10^{-12} \text{ x } 6.2419\text{x}10^{+11} \text{ eV.}$$

$$= 4.17 \text{ eV.}$$

$$\therefore \quad W = (6.07 - 4.17) \text{ eV.}$$

$$= 1.90 \text{ eV.}$$

A similar calculation by Mullen[85] is based on the estimation of W in terms of the elastic and dielectric constants. The solid is regarded as being made up of ions attached to lattice points by harmonic springs.

$$W = W_L + E_{Rel.} \quad \text{---------- (53)}$$

where $E_{Rel.}$ is the change in energy upon relaxation.

For a positive ion vacancy the contribution from electronic polarisabilities is given by

$$E_{Rel.} = \frac{-e^2}{2Kr_o^4}\left[\sum\frac{\alpha_+}{(r_+/r_o)^4} + \sum\frac{\alpha_-}{(r_-/r_o)^4}\right] \quad \text{---- (54)}$$

$$= \frac{-e^2}{2Kr_o^4}\left[9.30\alpha_+ + 13.34\alpha_-\right] \quad \text{---- (55)}$$

Summations of the type shown in equation (54) are given by Jones and Ingham[86].

$$\left.\begin{aligned}\alpha_+ &= 3.34\times10^{-24}\,cm^3\\ \alpha_- &= 6.43\times10^{-24}\,cm^3\end{aligned}\right\}\quad \text{for CsI}^{87}$$

$r_o = 3.96\times10^{-8}\,cm$ (interionic distance)

$K = 5.65.$

There will also be a similar term for the negative ion vacancy.

When the contribution from displacement dipoles is included we have

$$E_{Rel.} = \frac{-11.32e^2}{Kr_o^4}\left[\alpha_+ + \alpha_- + \left(\frac{2e^2}{k_s}\right)\left(1 - 1/K\right)\right] \quad \text{--- (56)}$$

where k_s is the first order spring constant $= 2r_o c_{11}$ and c_{11} (the elastic constant associated with longitudinal vibration along a cube axis) is 2.457×10^{-11} dynes cm^{-2} (c.f. Vallin et al[88]) and k_s is 1.946×10^4 dynes cm^{-1}.

$$\therefore\ E_{Rel.} = -3.435\,eV$$

$$\therefore\ W = (6.07 - 3.435)\,eV$$

$$= 2.63\,eV.$$

The results of these calculations are not in good agreement with our experimental value for W, but more accurate theoretical calculations of the Mott-Littleton[6], Bassani and Fumi[8] and Brauer[10] type are required for NaCl-type crystals before a rigorous comparison can be made.

The assumption that Lynch's 1.37 eV range in I^- diffusion was intrinsic leads to, using our W exp., a value of 0.52 eV for U_- : again this is much higher than that predicted by Lynch. Divalent cation impurities have proved to be very insoluble in the CsI lattice, the "average" enthalpy of solution χ_1 being 1.34 ± 0.22 eV. It is interesting to compare this situation with Harvey's results for CsCl[48]. In that system divalent anion impurities, i.e. SO_4^{2-} appeared to be more soluble than cation impurities, though as has been observed in KCl[30, 89] the SO_4^{2-} ion appeared to occupy two anion sites. Haven[90] had previously suggested that anions might be more soluble in CsCl because of the larger polarisability of the Cs^+ ion. There would be a larger gain in polarisation energy in putting an impurity anion at an anion site than would result for an impurity cation (polarisation energy usually favours solubility). This theory is generally borne out for other alkali-halides where the anion has a higher polarisability, i.e. divalent anion impurity is relatively insoluble. Similarly in CsI where the I^- is more polarisable than the cation we would expect divalent cation impurities to be more soluble. This is borne out by the experimental observations that neither SO_4^{2-} or CO_3^{2-} appear to be soluble in the CsI lattice.

The activation energy for diffusion of Cs^+ in this work was found to be 1.74eV which is to be compared with 1.53eV observed by Lynch. There are only small differences between the magnitude of Lynch's Cs^+ diffusion coefficients and those observed in the present research at higher temperatures, the observed difference in E_A only becoming apparent at low temperatures. The major difference between the crystals used by Lynch and those

used in this work was the purity. Lynch's crystals contained ~0.01% impurity, whereas the "pure" crystals used in the present research were much purer. Impurity effects are expected to be more important at low temperatures and this may account for the lower activation energy observed by Lynch. It may be significant that if a solubility range could be observed in the Cs^+ diffusion it would have an activation energy of about 1.57eV, i.e. $U_+ + \gamma 1/2 = 1.57$. This value is very close to that observed by Lynch, but there is no definite evidence from Lynch's results of the existence of Range I (b) although there may be a slight increase in activation energy above 500°C.

4.7. SUGGESTIONS FOR FUTURE WORK.

The main line of investigation in the present research was directed toward the effects of cation impurities on the conductivity and cation self-diffusion in CsI. It would be of interest to have a detailed study of the effects of anion impurities in this system. Certainly the effects of SO_4^{2-} and to a lesser extent, CO_3^{2-}, were investigated qualitatively in this work, and the conductivity results showed the apparent insolubility of either ion Fig. 55 - 56. However, Lynch[47] has observed effects of S^{2-} doping at low temperatures in CsBr and it may be of interest to investigate the effects of S^{2-}, SO_4^{2-} and CO_3^{2-} in more detail in CsI. In CsI there are large differences between the individual polarisabilities α_+ being $3.34 \times 10^{-24} cm^3$ and α_- being $6.43 \times 10^{-24} cm^3$ and so it would be difficult to observe any solubility of anion impurities[90]. In CsBr there is not a large difference in polarisability between the host ions ($\alpha_+ (Cs^+) = 3.34 \times 10^{-24} cm^3$ and $\alpha_- (Br^-) = 4.16 \times 10^{-24} cm^3$) and so more information regarding the

effects of anion solubility may be obtained from this salt or from CsCl where the cation is the more polarisable , and so a greater gain in polarisation energy would result from substitution of an anion site. Values to date of U_-, the energy for mobility of a negative ion vacancy, depend on estimates of W obtained from self-diffusion studies and the conductivity of cation-doped crystals in the impurity-range[47]. If it were possible to substitutionally incorporate enough divalent negative ions in the lattice, a region of impurity-controlled conductivity, of activation energy U_-, should be observed. Values of U_- so obtained could then be compared with U_- (Calc.) from diffusion measurements.

The problems associated with the surface decrease method for diffusion have already been discussed in the Results section. It was found that crystals which had been polished caused movement of the radioactive deposit over the surface of the crystal thus causing changes in the counting geometry after diffusion. Calculations of diffusion coefficients were made allowing for this, and results for Cs^+ diffusion were obtained which compared favourably with observations made on unpolished solution-grown crystals. It would be of interest, however, to have a comparison of the diffusion coefficients calculated in this way with results obtained by other methods such as microtoming or grinding techniques. It should be stressed that whenever the surface decrease method is used in diffusion, the radioactive tracer should be evaporated on to a cleaved or freshly cut surface of the crystal, in order to obtain the most accurate results.

APPENDIX.

1. Cs-137 DIFFUSION RESULTS.

The count rates observed in the diffusion experiments are given in the following form:

Column A - cpm without absorber, at least 10,000 counts taken.
B - cpm with absorber, at least 5,000 counts taken.
C - cpm background without absorber, 1,500 counts taken.
D - cpm background with absorber, 1,500 counts taken.
E - cpm of standard source, 10,000 counts taken.

Two count rates are recorded in each column for each experiment; the first reading is the count rate before diffusion and the second is the count rate after diffusion. The count rates are uncorrected for background and dead-time losses. The dead-time for the counting equipment was 500 μ sec.

2. Cl-36 DIFFUSION RESULTS.

The count rates observed in these diffusion experiments are given in the following form:

Column A - total count rate (cpm), 10,000 counts taken.
B - background count rate (cpm), 1,500 counts taken.
C - standard source count rate (cpm), 10,000 counts taken.

3. MICROTOMING RESULTS.

The results for the three Mervyn crystals studied are given in the form of a graph of log activity (cpm) versus x^2 (μ^2), Fig. 67.

(A) Mervyn Unannealed Crystals.

$10^3/T(^oA)$.	Time (secs).	A.	B.	C.	D.	E.	Diffusion Coefficient. (cm^2sec^{-1}).
1.733	$1.02x10^5$	1372	184	48	30	18,055	$3.08x10^{-14}$
		1430	194	48	29	18,201	
1.667	$4.17x10^5$	526	78	38	24	1060	$1.50x10^{-12}$
		545	85	34	24	1056	
1.667	$4.17x10^5$	436	70	38	24	1060	$1.00x10^{-13}$
		451	73	34	24	1056	
1.621	$7.23x10^4$	808	115	44	29	17,123	$8.10x10^{-13}$
		823	118	42	28	17,044	
1.621	$7.23x10^4$	720	104	44	29	17,123	$3.70x10^{-12}$
		716	112	42	28	17,044	
1.565	$2.70x10^4$	1900	228	27	23	2204	$3.00x10^{-12}$
		1970	252	27	23	2151	
1.473	$5.40x10^3$	1848	226	41	26	1048	$4.10x10^{-11}$
		1846	233	40	26	1052	
1.473	$5.40x10^3$	1248	163	41	26	1048	$7.10x10^{-12}$
		1297	171	40	26	1052	

$10^3/T(^oA)$.	Time (secs).	A.	B.	C.	D.	E.	Diffusion Coefficient. ($cm^2 sec^{-1}$).
1.464	7.80×10^3	1608	211	45	29	18,142	2.04×10^{-11}
		1619	219	49	29	17,814	
1.464	7.80×10^3	585	88	45	29	18,142	2.10×10^{-10}
		603	97	49	29	17,814	
1.456	7.20×10^3	509	84	28	25	1553	7.30×10^{-11}
		550	90	28	25	1581	
1.447	5.10×10^3	629	85	35	27	17,825	5.51×10^{-11}
		645	102	33	28	17,379	
1.447	5.10×10^3	1681	216	35	27	17,825	6.83×10^{-11}
		1712	233	33	28	17,379	
1.420	3.60×10^3	573	90	27	27	1543	5.80×10^{-11}
		619	98	27	27	1541	
1.414	1.80×10^3	1347	171	42	24	1050	1.50×10^{-10}
		1386	183	41	23	1061	
1.393	3.60×10^3	263	45	26	22	2136	2.40×10^{-10}
		270	52	25	22	2147	

$10^3/T(^oA)$.	Time (secs).	A.	B.	C.	D.	E.	Diffusion Coefficient. (cm^2sec^{-1}).
1.383	$3.60x10^3$	1196	158	24	23	2149	$8.10x10^{-11}$
		1237	170	24	23	2182	
1.383	$3.60x10^3$	667	96	24	23	2149	$3.80x10^{-11}$
		701	103	24	23	2182	
1.383	$3.60x10^3$	1825	231	36	28	17,950	$1.81x10^{-10}$
		1788	257	32	27	17,560	
1.368	$3.60x10^3$	1720	213	55	24	1350	$4.10x10^{-10}$
		1640	228	56	25	1430	
1.368	$3.60x10^3$	1735	218	55	24	1350	$3.00x10^{-10}$
		1659	232	56	25	1430	
1.368	$3.60x10^3$	454	75	27	25	1553	$1.75x10^{-10}$
		471	81	27	25	1569	
1.350	$2.70x10^3$	735	103	28	22	2173	$4.20x10^{-10}$
		745	112	28	22	2173	
1.350	$2.70x10^3$	1012	136	28	22	2173	$4.20x10^{-11}$
		1032	142	28	22	2173	

$10^3/T(^oA)$.	Time (secs).	A.	B.	C.	D.	E.	Diffusion Coefficient. ($cm^2 sec^{-1}$).
1.332	1.80×10^3	342	59	25	22	2153	6.50×10^{-10}
		351	64	25	22	2150	
1.333	1.80×10^3	1244	160	42	25	1733	3.75×10^{-10}
		1231	167	45	23	1772	
1.333	1.80×10^3	1398	173	42	25	1733	1.20×10^{-9}
		1363	189	45	23	1772	
1.290	1.20×10^3	417	66	27	22	2161	5.00×10^{-10}
		418	71	27	22	2119	
1.282	1.20×10^3	1728	208	53	25	2530	2.40×10^{-9}
		1688	222	50	25	2448	
1.383	3.60×10^3	1412	184	36	28	17,950	7.00×10^{-10}
		1370	189	32	27	17,560	
1.715	7.10×10^5	375	60	27	22	2149	1.30×10^{-12}
		369	65	25	22	2129	

(B) Pure, Solution-Grown Crystals (Unpolished).

$10^3/T(^oA)$.	Time (secs).	A.	B.	C.	D.	E.	Diffusion Coefficient. ($cm^2 sec^{-1}$).
1.876	1.38×10^6	1481	152	40	28	4480	1.00×10^{-14}
		1459	154	40	31	4433	
1.754	2.53×10^5	1297	148	41	32	4516	1.30×10^{-13}
		1271	147	39	29	4550	
1.695	8.64×10^4	883	100	40	27	4762	3.51×10^{-13}
		860	98	37	27	4757	
1.610	7.62×10^4	1624	154	40	28	12,983	1.90×10^{-12}
		1541	158	38	28	12,960	
1.610	7.62×10^4	623	77	40	28	12,983	2.70×10^{-12}
		587	78	38	28	12,960	
1.565	7.11×10^4	1063	124	39	29	4502	6.32×10^{-12}
		904	114	37	29	4613	
1.471	1.23×10^4	1116	129	43	29	4371	9.50×10^{-11}
		972	124	37	28	4492	
1.393	3.60×10^3	917	108	40	29	4689	2.93×10^{-10}
		735	99	37	27	4624	

$10^3/T(^oA)$.	Time (secs).	A.	B.	C.	D.	E.	Diffusion Coefficient. ($cm^2 sec^{-1}$).
1.391	3.60×10^3	490	62	36	28	4355	1.63×10^{-10}
		463	63	38	27	4343	
1.355	1.80×10^3	1079	116	39	29	4737	2.68×10^{-10}
		982	108	37	29	4729	
1.355	1.80×10^3	757	98	39	29	4737	1.44×10^{-10}
		710	95	37	29	4729	
1.294	9.00×10^2	961	105	37	27	4479	1.27×10^{-9}
		769	99	38	27	4439	

(C) Pure, Solution-Grown Crystals (Polished).

$10^3/T(^oA)$.	Time (secs).	A.	B.	C.	D.	E.	Diffusion Coefficient ($cm^2 sec^{-1}$).
1.667	4.17×10^5	875	114	38	24	1060	1.70×10^{-12}
		844	119	34	24	1056	
1.522	9.00×10^3	584	82	39	24	1053	2.40×10^{-11}
		623	89	39	24	1037	
1.414	1.80×10^3	444	69	42	24	1050	1.50×10^{-10}
		467	73	41	23	1061	
1.366	1.80×10^3	996	132	34	23	1064	1.30×10^{-10}
		999	140	37	25	1060	

(D) Mervyn Vacuum-Annealed Crystals (Polished).

$10^3/T(^oA)$.	Time (secs).	A.	B.	C.	D.	E.	Diffusion Coefficient ($cm^2 sec^{-1}$).
1.905	2.68×10^6	474	70	26	23	2185	9.50×10^{-14}
		506	76	26	22	2187	
1.686	4.14×10^5	944	127	25	22	2155	1.70×10^{-12}
		1005	134	28	23	2160	
1.527	1.26×10^4	355	58	28	23	2167	1.40×10^{-11}
		400	64	25	22	2150	
1.527	1.26×10^4	744	100	28	23	2167	3.80×10^{-11}
		779	112	25	22	2150	
1.321	1.80×10^3	1432	180	29	24	2171	3.65×10^{-10}
		1241	182	29	24	2133	
1.321	1.80×10^3	1023	137	29	24	2171	4.25×10^{-10}
		946	139	29	24	2133	

(E) Ba^{2+}-Doped, Melt-Grown Crystals (Stockbarger Method).

$10^3/T(^oA)$.	Time (secs).	A.	B.	C.	D.	E.	Diffusion Coefficient ($cm^2 sec^{-1}$).
1.905	2.68×10^6	289	52	26	23	2185	9.93×10^{-14}
		311	54	26	22	2187	
1.720	1.45×10^6	546	71	29	23	-	1.60×10^{-12}
		460	68	29	23	-	
1.720	1.45×10^6	260	44	29	23	-	4.26×10^{-13}
		234	45	29	23	-	
1.715	7.10×10^5	760	102	27	22	2149	2.00×10^{-12}
		729	108	25	22	2129	
1.686	4.14×10^5	623	86	25	22	2155	1.30×10^{-12}
		606	90	28	23	2160	
1.613	7.14×10^4	1144	122	45	30	8733	6.13×10^{-12}
		1055	124	48	31	8659	
1.613	7.14×10^4	1085	112	45	30	8733	1.48×10^{-11}
		956	118	48	31	8659	
1.590	3.60×10^4	302	51	26	23	2147	2.70×10^{-11}
		310	55	27	23	2146	

$10^3/T(^oA)$.	Time (secs).	A.	B.	C.	D.	E.	Diffusion Coefficient ($cm^2 sec^{-1}$).
1.565	2.70×10^4	716	94	27	23	2204	3.00×10^{-11}
		732	103	27	23	2151	
1.548	1.80×10^4	1004	128	27	23	2107	9.98×10^{-12}
		1073	137	27	23	2171	
1.527	1.26×10^4	510	72	28	23	2167	3.90×10^{-11}
		558	79	25	22	2149	
1.456	7.20×10^3	294	52	28	25	1553	9.00×10^{-11}
		327	58	28	25	1581	
1.433	7.20×10^3	604	70	46	31	5519	1.28×10^{-10}
		532	70	45	31	5617	
1.383	3.60×10^3	460	68	24	23	2145	1.00×10^{-10}
		491	74	24	23	2182	
1.368	3.60×10^3	491	78	27	25	1553	1.50×10^{-10}
		511	87	27	25	1569	
1.368	3.60×10^3	539	83	27	25	1553	4.50×10^{-10}
		575	92	27	25	1569	

$10^3/T(^oA)$.	Time (secs).	A.	B.	C.	D.	E.	Diffusion Coefficient ($cm^2 sec^{-1}$).
1.355	3.60×10^3	603	73	45	30	5459	1.59×10^{-9}
		457	73	44	29	5477	
1.355	3.60×10^3	834	95	45	30	5459	5.37×10^{-10}
		702	88	44	29	5477	
1.320	1.80×10^3	908	119	29	24	2183	1.70×10^{-9}
		811	124	29	24	2142	
1.290	1.20×10^3	496	75	27	22	2161	9.60×10^{-10}
		457	78	27	22	2119	

(F) Annealed, Ba^{2}-Doped, Solution-Grown Crystals (Unpolished).

$10^3/T(^oA)$.	Time (secs).	A.	B.	C.	D.	E.	Diffusion Coefficient ($cm^2 sec^{-1}$).
1.869	9.62×10^5	1000	141	39	29	18,069	4.79×10^{-14}
		998	144	35	29	18,100	
1.869	9.62×10^5	1637	208	39	29	18,069	3.62×10^{-14}
		1600	207	35	29	18,100	
1.773	3.45×10^5	931	128	36	29	18,073	3.16×10^{-13}
		980	137	39	29	18,061	
1.773	3.45×10^5	925	124	36	29	18,073	7.42×10^{-13}
		890	125	39	29	18,061	
1.773	3.45×10^5	1223	156	36	29	18,073	5.21×10^{-13}
		1179	157	39	29	18,061	
1.733	1.02×10^5	755	110	48	30	18,055	4.18×10^{-13}
		780	113	48	29	18,201	

$10^3/T(^oA)$.	Time (secs).	A.	B.	C.	D.	E.	Diffusion Coefficient ($cm^2 sec^{-1}$).
1.733	1.02×10^5	1051	146	48	30	18,055	1.85×10^{-13}
		1040	146	48	29	18,201	
1.621	7.23×10^4	669	92	44	29	17,123	2.58×10^{-11}
		618	95	42	28	17,044	
1.621	7.23×10^4	1100	128	44	29	17,123	1.06×10^{-11}
		1004	128	42	28	17,044	

Cl-36 Diffusion Results for Pure Mervyn Crystals.

$10^3/T(^oA)$.	Time (secs).	A.	B.	C.	Diffusion Coefficient ($cm^2 sec^{-1}$).
1.672	9.57×10^4	220	41	2181	2.90×10^{-12}
		211	39	2156	
1.672	9.57×10^4	382	41	2181	1.85×10^{-12}
		369	39	2156	
1.585	4.32×10^4	172	32	1458	3.05×10^{-11}
		162	33	1478	
1.562	7.56×10^4	7576	60	2470	2.75×10^{-11}
		6932	63	2505	
1.530	7.83×10^4	517	51	2507	7.30×10^{-11}
		410	49	2326	
1.530	7.83×10^4	387	51	2503	1.00×10^{-10}
		304	49	2326	
1.495	2.24×10^4	531	32	1482	5.40×10^{-11}
		490	32	1480	

$10^3/T(^oA)$.	Time (secs).	A.	B.	C.	Diffusion Coefficient. (cm^2sec^{-1}).
1.495	$2.24x10^4$	370	32	1482	$2.50x10^{-11}$
		350	32	1480	
1.482	$6.63x10^4$	1125	54	1490	$1.40x10^{-10}$
		902	47	1496	
1.482	$6.63x10^4$	761	54	1490	$1.30x10^{-10}$
		613	47	1496	
1.447	$1.08x10^4$	323	31	1433	$1.90x10^{-10}$
		298	32	1457	
1.447	$1.08x10^4$	462	31	1433	$3.35x10^{-11}$
		448	32	1457	
1.389	$3.60x10^3$	889	39	3299	$4.10x10^{-10}$
		805	38	3245	
1.389	$3.60x10^3$	593	39	3299	$3.95x10^{-10}$
		538	38	3245	

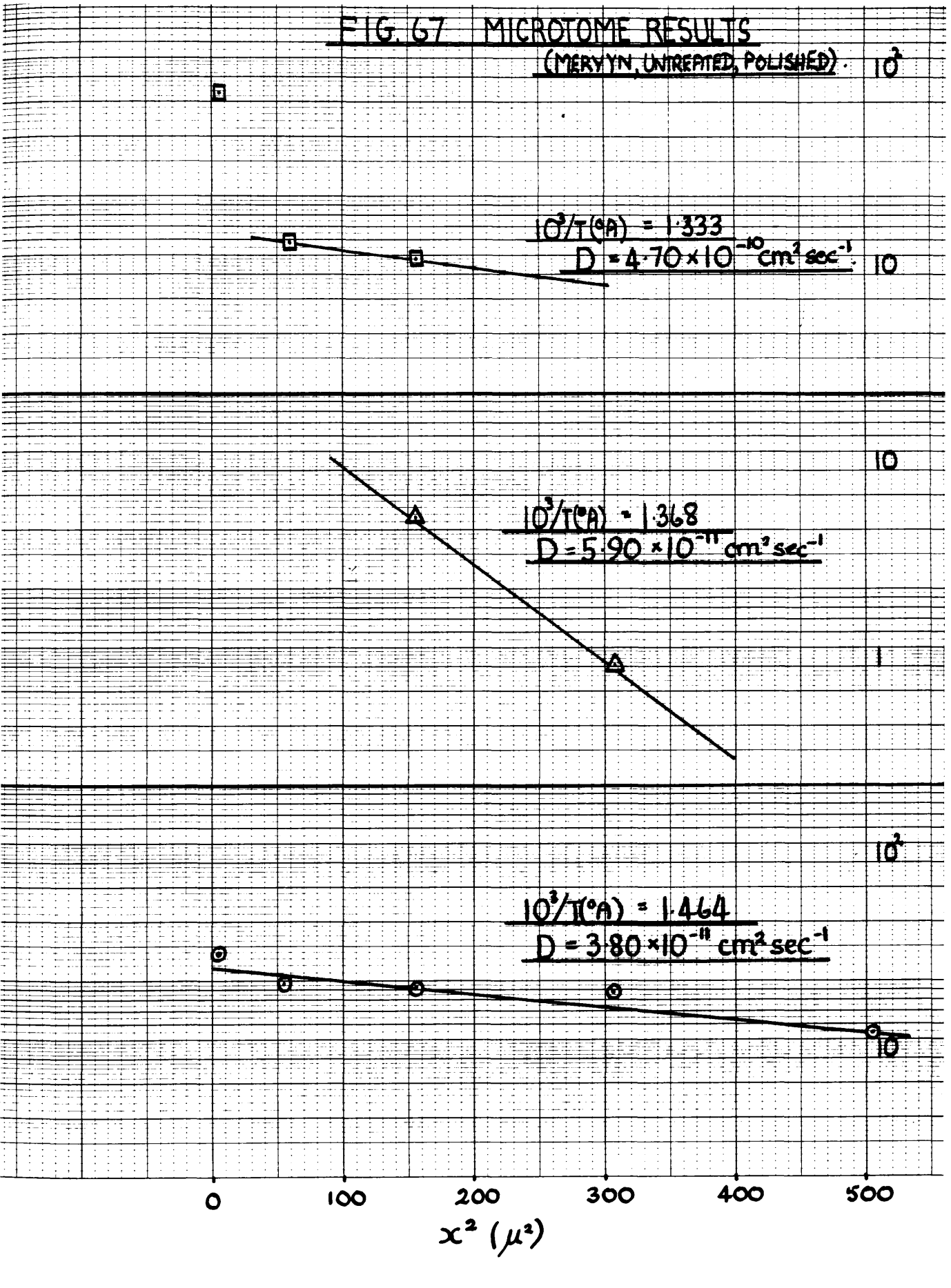
FIG. 67 MICROTOME RESULTS
(MERYYN, UNTREATED, POLISHED)
$10^3/T(°A) = 1.333$
$D = 4.70 \times 10^{-10}\ cm^2\ sec^{-1}$
$10^3/T(°A) = 1.368$
$D = 5.90 \times 10^{-11}\ cm^2\ sec^{-1}$
$10^3/T(°A) = 1.464$
$D = 3.80 \times 10^{-11}\ cm^2\ sec^{-1}$
10^2
10
1
10
10^2
10
0
100
200
300
400
500
$x^2\ (\mu^2)$

REFERENCES.

1.	Frenkel,	Z. Physik., 35, 652, (1926).
2.	Schottky,	Z. Physikal. Chem., 29B, 335, (1935).
3.	Van Bueren,	"Imperfections in Crystals", (North Holland Publishing Company, Amsterdam 1960).
4.	Born and Mayer,	Z. Physik, 75, 1, (1932).
5.	Jost,	J. Chem. Phys., 1, 466, (1933).
6.	Mott and Littleton,	Trans. Faraday Soc., 34, 485, (1938).
7.	Reitz and Gammel,	J. Chem. Phys., 19, 894, (1951).
8.	Bassani and Fumi,	Nuovo Cimento, 11, 274, (1954).
9.	Fumi and Tosi,	Discussions Faraday Soc., 23, 92, (1957).
10.	Brauer,	Z. Naturforsch., 7A, 372, (1952).
11.	Etzel and Maurer,	J. Chem. Phys., 18, 1003, (1950).
12.	Mapother, Crooks and Maurer,	J. Chem. Phys., 18, 1231, (1950).
13.	Kelting and Witt,	Z. Physik., 126, 697, (1949).
14.	Wagner and Hantelmann,	J. Chem. Phys., 18, 72, (1950).
15.	Jacobs and Tompkins,	Quart. Rev., 6, 238, (1952).
16.	Lidiard,	Handbuch der Physik (S. Flugge), Springer-Verlag (Berlin 1957) XX, 246.
17.	Tubandt and Eggert,	Z. Anorg. Chem., 110, 196, (1920).
18.	See, for example, Mott and Gurney,	"Electronic Processes in Ionic Crystals" 2nd Edition (Oxford 1948) p.43.
19.	Compaan and Haven,	Trans. Faraday Soc., 52, 786, (1956).
20.	Van Bueren,	"Imperfections in Crystals" ch. XXIV.
21.	Van Bueren,	ibid ch. III.
22.	Lehovec,	J. Chem. Phys., 21, 1123, (1953).
23.	Eshelby, Newey, Pratt and Lidiard,	Phil. Mag., 3, 75, (1958).

24.	Jost,	Phys. Z., 36, 757, (1935).
25.	Smekal,	Z. Elektrochem., 34, 476, (1928).
26.	Koch and Wagner,	Z. Physikal. Chem., 38B, 295, (1937).
27.	Bean,	PhD. Thesis, University of Illinois, (1952).
28.	Allnatt and Jacobs,	Trans. Faraday Soc., 58, 116, (1962).
29.	Ronge and Wagner,	J. Chem. Phys., 18, 74, (1950).
30.	Gruzensky and Scott,	J. Phys. Chem. Solids, 21, 128, (1961).
31.	Aschner,	PhD. Thesis, University of Illinois, (1954).
32.	Lidiard,	J. Appl. Phys., 33, 414, (1962).
33.	Lidiard,	Discussions Faraday Soc., 31, 263, (1961).
34.	Airoldi and Tosi,	Nuovo Cimento, 8, 584, (1958).
35.	Cook and Dryden,	Australian J. Phys., 13, 260, (1960).
36.	Watkins,	Phys. Rev., 113, 79 and 91 (1959).
37.	Sato,	J. Phys. Soc. Japan., 20, 1008, (1965).
38.	Dreyfus and Nowick,	Phys. Rev., 126, 1367, (1962).
39.	Fischbach and Nowick,	J. Phys. Chem. Solids, 2, 226, (1957).
40.	Hoodless and Thomson,	Phil. Mag., 4, 1131, (1959).
41.	Barr, Hoodless, Morrison and Rudham,	Trans. Faraday Soc., 56, 697, (1960).
42.	Laurance,	Phys. Rev., 120, 57, (1960).
43.	Barr, Morrison and Schroeder,	J. Appl. Phys., 36, 624, (1965).
44.	Fuller,	Phys. Rev., 142, 524, (1966).
45.	Rolfe,	Can. J. Phys., 42, 2195, (1964).
46.	Laurent and Bénard,	J. Phys. Chem. Solids, 3, 7, (1957).
47.	Lynch,	Phys. Rev., 118, 468, (1960).
48.	Harvey,	PhD. Thesis, University of Glasgow, (1965).
49.	Harpur, Moss and Ubbelohde,	Proc. Roy. Soc., A232, 196, (1955).
50.	Harpur and Ubbelohde,	ibid., A232, 310, (1955).

51. Besson, Chauvy and Rossel, Helv. Phys. Acta., 35, 211, (1962).

52. Ecklin, Nadler and Rossel, ibid., 37, 692, (1964).

53. Wells, "Structural Inorganic Chemistry" 3rd edition (Oxford 1962) p. 71.

54. Chemla, Ann. de. Phys., 1, 959, (1956).

55. Debye and Scherrer, Phys. Z., 17, 277, (1916).
ibid., 18, 291, (1916).

56. Standard X-Ray Diffraction Powder Patterns, National Bureau of Standards, Circular 539, 4, 48, (1955).

57. N. Brown. Private Communication.

58. Stockbarger, Rev. Sci. Instr., 7, 133, (1936).

59. "Handbook of Chemistry and Physics", (Chemical Rubber Publishing Company), 43rd edition P.2652, (1961-62).

60. Fick, Pogg. Ann., 94, 59, (1855).

61. Schamp and Katz, Phys. Rev., 94, 828, (1954).

62. Harrison, Morrison and Rudham, Trans. Faraday Soc., 54, 106, (1958).

63. See, for example, Carslaw and Jaeger, "Conduction of Heat in Solids" 2nd edition (Oxford 1959).

64. Lidiard and Tharmalingam, Discussions Faraday Soc., 28, 64, (1959)

65. Jordan and Pochon, Helv. Phys. Acta., 30, 33, (1957).

66. Leymonie and Lacombe, Symposium on Solid State Diffusion, (North Holland Publishing Company Amsterdam 1959) p.37, (1958).

67. Jost, "Diffusion" (Academic Press, New York 1952), p.62.

68. Cook and Duncan, "Modern Radiochemical Practice" (Oxford 1952) p. 79.

69. Shirn, Wajda and Huntington, Acta. Met., 1, 513, (1953).

70. Parry and Dollman, J. Analy. Chem., 36, 1783, (1964).

71. Cullum and Thomas, Analyst., 84, 113, (1959).

72. Allnatt and Jacobs, J. Phys. Chem. Solids, 19 (3/4), 281, (1961).

73.	Haven,	Report of the Conference on Defects in Crystalline Solids, (Bristol 1954), p.261.
74.	Breckenridge,	J. Chem. Phys., 16, 959, (1948). ibid., 18, 913, (1950).
75.	Smith, Jaumot and Arné,	Phys. Rev., 94, 1407 (A7), (1954).
76.	Berkowitz,	J. Appl. Phys., 26, 403, (1955).
77.	Cairns,	PhD. Thesis, University of Glasgow, (1966).
78.	Arai and Mullen,	Phys. Rev., 143, 663, (1966).
79.	Friauf,	J. Appl. Phys., 33, 494, (1962).
80.	See, for example, Kroger,	"Chemistry of Imperfect Crystals" (North Holland Publishing Company p. 637 Amsterdam 1964).
81.	Friauf,	J. Phys. Chem. Solids, 18, 203, (1961). J. Chem. Phys., 22, 1329, (1954).
82.	Lidiard,	J. Phys. Chem. Solids, 6, 298, (1958).
83.	Laurance,	Phys. Rev., 118, 988, (1960).
84.	Tosi,	Solid State Physics, 16, 1, (1964).
85.	Mullen,	Phys. Rev., 143, 658, (1966).
86.	Jones and Ingham,	Proc. Roy. Soc., A107, 636, (1925).
87.	Tessman, Kahn and Schockley,	Phys. Rev., 92, 890, (1953).
88.	Vallin, Beckman and Salama,	J. Appl. Phys., 35, 1222, (1964).
89.	Jacobs and Papiazan,	Phys. Rev., 127, 1567, (1962).
90.	Haven,	Proc. Brit, Ceramic Soc., 1,93, (1964).